NONLINEAR VIBRATIONS OF 3D BEAMS

Stanislav Stoykov

Universidade do Porto
FEUP Faculdade de Engenharia

Universidade do Porto

Faculdade de Engenharia

FEUP

NONLINEAR VIBRATIONS OF 3D BEAMS

Stanislav Stoykov

Dissertation submitted to the Faculty of Engineering of University of Porto

in partial fulfilment of the requirements for the degree of

Doctor of Philosophy

Dissertation Supervisor: Dr. Pedro Leal Ribeiro

Department of Mechanical Engineering, Faculty of Engineering,

University of Porto

May 2012

This work was supported by *Fundação para a Ciência e a Tecnologia*, through the scholarship SFRH/BD/35821/2007.

Keywords: Nonlinear Dynamics, Bifurcation Diagrams, Internal Resonance, Rotating Beams, Floquet's Theory

To my dear Gery

Publications

Several parts of the work done during the PhD studies have been published in journals and presented in conferences.

The work was published (or sent for publication) in the following journals:

- S. Stoykov, P. Ribeiro, Nonlinear forced vibrations and static deformations of 3D beams with rectangular cross section: The influence of warping, shear deformation and longitudinal displacements, *International Journal of Mechanical Sciences* 52 (2010) 1505-1521.

- S. Stoykov, P. Ribeiro, Nonlinear free vibrations of beams in space due to internal resonance, *Journal of Sound and Vibration* 330 (2011) 4574-4595.

- S. Stoykov, P. Ribeiro, Stability of nonlinear periodic steady-state vibrations of 3D beams, *Nonlinear Dynamics* 66 (2011) 335-353.

- S. Stoykov, P. Ribeiro, Vibration analysis of rotating 3D beams by the p-version finite element method, under review.

- S. Stoykov, P. Ribeiro, Nonlinear dynamics of beams with non-symmetrical cross sections, in preparation.

The work was presented in the following conferences:

- S. Stoykov, P. Ribeiro, On the influence of warping, shear and longitudinal displacements on the nonlinear vibrations of beams, *COMPDYN 2009*, 22 – 24 June 2009, Rhodes, Greece.

- S. Stoykov, P. Ribeiro, Vibrations of rotating Timoshenko beams by the p-version finite element method, *ESMC 2009*, 7 – 11 September 2009, Lisbon, Portugal.

- S. Stoykov, P. Ribeiro, Modal interaction in free vibrations of 3D beams, *ECCM 2010*, 16 – 21 May 2010, Paris, France.

- S. Stoykov, P. Ribeiro, Forced vibrations of 3D beams with large amplitudes, *7th International Conference on Numerical Methods and Applications*, 20 – 24 August 2010, Borovetz, Bulgaria.

- S. Stoykov, P. Ribeiro, Response of 3D rotating Timoshenko beams to harmonic excitations, *7th European Nonlinear Dynamics Conference*, 24 – 29 July, 2011, Rome, Italy.

- S. Stoykov, P. Ribeiro, Modal interactions in nonlinear free vibrations of 3D rotating beams, 7th *European Nonlinear Dynamics Conference*, 24 – 29 July, 2011, Rome, Italy.

- S. Stoykov, P. Ribeiro, Internal resonances and modal interactions of nonlinear free and forced vibrations of 3D rotating beams, *7th PhD Seminar on Wind Energy in Europe*, 27 – 28 October 2011, Delft University of Technology, The Netherlands.

- S. Stoykov, P. Ribeiro, Free and forced nonlinear vibrations of 3D beams with non-symmetrical cross section, *ECCOMAS 2012*, 10 – 14 September, 2012, Vienna, Austria (accepted abstract).

The first of all freedoms is the freedom to say everything.

Maurice Blanchot (1907 – 2003)

Preface

I will not say everything, but I will say the most important things. For me, doing a PhD was not only investigating the nonlinear dynamics of beams. It was also travelling from country to another one, meeting different people and cultures, working hard, but also having fun. This time was for me a period, when I grow as a scientist, but also as a person.

I feel like a successful man, because I know that I have great friends who really care for me and for my future. First of all I wish to express my gratitude to Pedro Ribeiro for introducing me in the incredible world of nonlinear dynamics. I am very thankful to him for all the care and help, he gave me. Pedro was not only a supervisor in this period, he was also my friend. I will never forget the jokes and all the humour he used to show me the beautiful life in Portugal. I am looking forward our future meetings.

I wish to thank to *Fundação para a Ciência e a Tecnologia* for giving me the financial support to successfully begin and to finish this work.

Here I want to say thank you to Luisa Sousa and Marcelo Moura from FEUP for helping me to validate my model in the beginning of my studies with Ansys and Abaqus.

Arnaud Lazarus and Olivier Thomas were very kind and helpful for analysing the stability of the solutions.

During my PhD I had the possibility to visit several short training courses. I am very grateful to Fabrizio Vestroni for organising the SICON Events and for giving me full scholarship to attend part of them – in Lyon, Liege and Rome. I also want to thank to CISM Organizers and to Frank Schilder from DTU for giving me a partial scholarship to attend the summer schools in Udine and Copenhagen. Everything I learned and everyone I met on these courses was useful for me and my work.

I am also indebted to my old friend from Sofia University Vassil Tzanov, who is currently doing a PhD at the University of Bristol, for showing me the AUTO software. The endless discussions with you, my friend, about the bifurcations in the life, during the summer schools in Udine and Copenhagen, were unforgettable.

A small part of this PhD was done at TU Delft, The Netherlands. I wish to express my gratitude to Jan Hol for inviting me for this internship. I had luck to meet at TU Delft

Roeland de Breuker and Mostafa Abdalla, the topics we talked about – aeroelasticity and beam models – were very useful to get more information in this areas. To the PhD students Terry Hegberg and Etana Ferede and the Master student Noud Werter, I want to say: Thank you once again for the exchange of knowledge we had!

I had the opportunity to meet Eusebius Doedel in Copenhagen, a great man!

During these four years I met many new friends in Porto. I appreciate all of these friendships. But some of them are really extraordinary (written in the order I met them): Aleksandar Dimitrovski, Marco Basaldella, Ivan da Silva, Rosa Gomez, Arif Ur-Rahman, Julija Vasiljevska, Bea Mora, Miguel Nunes, Sarah Puccia, Rosa Rodriguez, Tiago Palhares, Jakov Krstulovic. Thank you for being my friends!

I also have the best colleagues ever – Hamed Akhavan and Vladimir Stojanovic. I wish you both, good luck in finishing your PhDs.

I wish to say special thanks to my landlady Senhora Carmen da Silva. I appreciate her care of introducing me the Portuguese cuisine and making tea at the moments, when I was ill.

Especially to mention is my first friend in Portugal – Leonardo Bezerra, who I met during my Erasmus period 2005-2006. I was very happy to have you as my guest in Bulgaria last summer and I hope to see you very soon again.

I have three very special Bulgarian friends from my childhood, who inspired my work – the bestman, the best friend and the best pilot. Martin Mitov, he was my most often visitor in Porto, Preslav Vutov, who always held crossed fingers for my thesis and Stoian Petkov, who will fly me from Porto to Sofia for less than 40 minutes on the board of MIG-29.

I have to say my special thanks to my family, for the love and support during the whole time. This PhD wouldn't be possible without their care and education they gave me. I am very grateful to my father, for introducing me in the world of mathematics, from my very early childhood.

Last but not least, I wish to say my very special thanks to my dear fiancée Gery, for all the love, patience and support she has shown me during the whole PhD. Thank you for giving me the inspiration to continue in difficult moments and for being with me all the time.

29 May 2012 Stanislav Stoykov

Abstract

The geometrically nonlinear vibrations of 3D beams are investigated using the *p*-version finite element method. First, beams with rectangular, hence symmetrical, cross sections are considered and then, the model is extended to beams with non-symmetrical cross sections and to beams rotating about a fixed axis.

The beams may vibrate in space, hence they may experience longitudinal, torsional and non-planar bending deformations. After a comparison of different models, a model based on Timoshenko's theory for bending and which assumes that, under torsion, the cross section rotates as a rigid body and is free to warp in the longitudinal direction, as in Saint-Venant's theory, is developed. For beams with rectangular cross sections, an analytical expression for the warping function exists, and it is used, while for beams with asymmetrical cross sections, the warping function is calculated numerically by the boundary element method. The geometric nonlinearity is taken into account by considering Green's nonlinear strain tensor. Isotropic and elastic beams are investigated and generalized Hooke's law is used. Also a model for rotating beams about a fixed axis is developed and the rotation is taken into account in the inertia forces. The equations of motion are derived by the principle of virtual work. The theory employed is valid for moderate rotations of the cross section and displacements, and physical phenomena like internal resonance and change of stability, which arise due to the nonlinearity of the system, can be investigated.

Free and forced vibrations of beams, in the frequency domain, are investigated. The differential equations are discretized into a nonlinear algebraic form by the harmonic balance method and solved by an arc-length continuation method. The stability of the solutions is investigated by Floquet's theory. The variation of the amplitude of vibration with the frequency of vibrations is determined and presented. Couplings between modes are investigated, internal resonances are found and the ensuing multimodal oscillations are described. Some of the couplings discovered lead from planar oscillations to oscillations in the three-dimensional space.

The influence of the speed of rotation on the bending linear modes of vibration is presented. Nonlinear forced vibrations of rotating beams are investigated in the time domain, using direct integration of the equation of motion and considering constant and non-constant speed of rotation. Impulsive type and harmonic external forces are considered.

Resumo

Vibrações de vigas no espaço e em regime geometricamente não linear são investigadas através da versão *p* do método dos elementos finitos. Vigas com secção transversal retangular, logo simétrica, e com fronteiras fixas são consideradas primeiro. Depois, o modelo é estendido a vigas com secções transversais assimétricas e a vigas em rotação em torno de um eixo fixo.

Dado que são consideradas oscilações no espaço tridimensional, as vigas podem experimentar deformação longitudinal (extensão/compressão), torção e flexão em qualquer direção. Após comparação de diferentes modelos, é seleccionado um modelo baseado na teoria de flexão de Timoshenko e que assume que, devido a torção, a secção transversal roda como um corpo rígido e pode empenar livremente no sentido longitudinal, como na teoria de torção de Saint-Venant. Uma expressão analítica para a função de empenamento existe para vigas com secções transversais retangulares e é aqui aplicada. No caso de vigas com secções transversais assimétricas, a função de empenamento é calculada numericamente pelo método de elementos fronteira. Não linearidade do tipo geométrico é considerada através do tensor de deformações de Green. Vigas em materiais isotrópicos e com comportamento linear elástico são investigadas e a lei de Hooke generalizada é adotada. Um modelo para vigas em rotação em torno de um eixo fixo é também desenvolvido, sendo o efeito da rotação tomado em consideração nas forças de inércia. As equações de movimento são obtidas pelo princípio dos trabalhos virtuais. A formulação empregue é válida para rotações da secção transversal e deslocamentos moderados. Fenómenos físicos como ressonâncias internas e mudanças de estabilidade, que surgem devido à não linearidade do sistema, podem ser investigados.

Vibrações de vigas nos regimes livre e forçado são investigadas no domínio da frequência. As equações diferenciais são transformadas em equações algébricas não lineares pelo método de balanceamento dos harmónicos e são resolvidas por um método de continuação. A estabilidade das soluções é investigada aplicando a teoria de Floquet. A variação da amplitude com a frequência das vibrações é determinada. Acoplamentos entre modos de vibração são investigados, ressonâncias internas são encontradas e as consequentes oscilações multi-modais são descritas. Alguns dos acoplamentos fazem com que oscilações num plano se transformem em oscilações no espaço tridimensional.

A influência da velocidade de rotação nos modos lineares de vibração é apresentada. As vibrações forçadas não lineares de vigas em rotação são investigadas no domínio de tempo,

usando a integração direta da equação do movimento, e considerando velocidades de rotação constantes e variáveis. Forças externas impulsivas, isto é, com curta duração, e forças harmónicas são aplicadas.

List of Figures

List of Tables

List of Symbols

Greek symbols

α	Damping factor
β	Damping factor for mass proportional damping
γ	Distribution of the warping along the length of the beam
γ_{xy}	Shear strain
γ_{zx}	Shear strain
Γ	Contour of the cross section
$\delta(y,z)$	Dirac delta function
δ_{ij}	Kronecker delta
δW_V	Virtual work of internal forces
δW_{in}	Virtual work of inertia forces
δW_E	Virtual work of external forces
ε_x	Direct strain
θ_x	Torsion on the reference line
ϑ	Rotation of the beam about the transverse axis z
Θ_{x_i}	Amplitude of i-th harmonic of torsion θ_x
λ	Shear correction factor
λ_i	Characteristic (Floquet) exponents
ν	Poisson's ratio
ξ	Non-dimensional local coordinate
ρ	Density
ρ_n	Floquet multipliers
σ_x	Direct stress
τ_{xy}	Shear stress
τ_{zx}	Shear stress
$\upsilon(y,z)$	Fundamental solution
ϕ_y	Rotation of the cross section about *y* axis
ϕ_z	Rotation of the cross section about *z* axis
ψ	Warping function
ω_i	i-th linear natural frequency
ω_{l_1}	Linear fundamental frequency

ω	Excitation frequency or vibration frequency
Ω	Area of the cross section

Roman symbols

b	Width of the beam
E	Young's modulus
F_i	External force in *i* direction
G	Shear modulus
h	Thickness of the beam
k	Number of harmonics used in HBM
l	Length of the beam
M_i	External moment about *i* axes
N	Number of DOF
p_u	Number of shape functions for longitudinal displacement
p_v	Number of shape functions for transverse, along *y* axis, displacement
p_w	Number of shape functions for transverse, along *z* axis, displacement
p_{θ_x}	Number of shape functions for torsion
p_{ϕ_y}	Number of shape functions for rotation about *y* axis
p_{ϕ_z}	Number of shape functions for rotation about *z* axis
r	Distance between two points
S_0	"Fixed" coordinate system
S_1	"Transport" coordinate system
t_1, t_2	Additional dimensions used to define the L shaped cross section
T	Period of vibration
u	Longitudinal displacement
u_0	Longitudinal displacement on the reference line
v	Transverse displacement along *y* axis
v_0	Transverse displacement on the reference line along y axis
V	Volume of the beam
V_i	Amplitude of i-th harmonic of transverse displacement v_0
V_m	Sum of all amplitudes of the harmonics of v_0
w	Transverse displacement along *z* axis
w_0	Transverse displacement on the reference line along z axis
W_i	Amplitude of i-th harmonic of transverse displacement w_0

W_m	Sum of all amplitudes of the harmonics of w_0
(x_P, y_P, z_P)	Coordinates of point P
(y_c, z_c)	Position of the centroid of the cross section

Vectors and matrices

$\{\alpha_{10}\}$	Angular acceleration vector of the transport coordinate system
$\{\delta d\}$	Virtual displacement vector
$\{\delta q\}$	Disturbance added to the solution
$\{\zeta\}$	Vector of modal coordinates
$\{\psi\}$	Vector of values of the warping function on the nodes of the boundary elements
$\{\psi_n\}$	Vector of values of normal derivative of the warping function on the nodes of the boundary elements
$\left[\omega_j^2\right]$	Diagonal matrix with squares of the linear natural frequencies
$\{\omega_{10}\}$	Angular velocity of the transport coordinate system
$\{a_0\}$, $\{a_{c_i}\}$, $\{a_{s_i}\}$	Vectors of coefficients of Fourier expansion of the disturbance $\{\delta\zeta\}$
$\{a_P\}$	Three dimensional vector of acceleration of point P
$[B]$	Normalized with respect to the mass modal matrix
[CR], $\mathbf{CR_{ij}}$	Matrix due to the acceleration of Coriolis
$[\mathrm{C}^{\mathrm{HBM}}]$, $\mathbf{C_{ij}^{HBM}}$	Damping matrix after application of HBM
$\{d\}$	Vector of displacement components
$\{\mathrm{F}_0\}$	Vector of external forces on the reference line
{F}, $\mathbf{F_i}$	Generalized external forces
$\{\mathrm{F}^{\mathrm{HBM}}\}$	Force vector after application of HBM
$\{\mathcal{F}\}$	Vector of residual forces after application of HBM
[G], $\mathbf{G_{ij}}$	Matrix of influence coefficients defined from the fundamental solution
[H], $\mathbf{H_{ij}}$	Matrix which results from matrix $\widehat{\mathbf{H}}_{\mathbf{ij}}$ and Kronecker delta
$\left[\widehat{\mathrm{H}}\right]$, $\widehat{\mathbf{H}}_{\mathbf{ij}}$	Matrix of influence coefficients defined from the normal derivative of the fundamental solution
[I]	Identity matrix
$\{q\}$, $\boldsymbol{q}$	Vector of generalized coordinates
$\{q_u\}$, $\boldsymbol{q_u}$	Vector of longitudinal generalized coordinates
$\{q_v\}$, $\boldsymbol{q_v}$	Vector of transverse along *y* axis generalized coordinates
$\{q_w\}$, $\boldsymbol{q_w}$	Vector of transverse along *z* axis generalized coordinates

$\{q_\gamma\}$	Vector of generalized coordinates related with warping
$\{q_{\theta_x}\}$, $\boldsymbol{q_{\theta_x}}$	Vector of generalized coordinates related with torsion
$\{q_{\phi_y}\}$, $\boldsymbol{q_{\phi_y}}$	Vector of generalized coordinates related with rotation about *y* axis
$\{q_{\phi_z}\}$, $\boldsymbol{q_{\phi_z}}$	Vector of generalized coordinates related with rotation about *z* axis
$\{\tilde{q}\}$	Disturbed solution
$\{Q\}$, $\boldsymbol{Q_i}$	Vector of coefficients of harmonics of generalized coordinates $\{q\}$
$\{Q_w\}$, $\boldsymbol{Q_{w_i}}$	Vector of coefficients of harmonics of generalized coordinates of $\{q_w\}$
[K], $\mathbf{K_{ij}}$	Stiffness matrix
$[\mathrm{K}^{\mathrm{HBM}}]$, $\mathbf{K_{ij}^{HBM}}$	Stiffness matrix after application of HBM
[M], $\mathbf{M_{ij}}$	Mass matrix
$[\mathrm{M}^{\mathrm{HBM}}]$, $\mathbf{M_{ij}^{HBM}}$	Mass matrix after application of HBM
$[\mathbb{M}_i]$	Matrices used to define stability of the solution
$\vec{n}$	Normal vector
$[N]$	Matrix of shape functions
$[N^u]$	Row vector of longitudinal shape functions
$[N^v]$	Row vector of transverse, along *y*, axis shape functions
$[N^w]$	Row vector of transverse, along *z*, axis shape functions
$[N^\gamma]$	Row vector of shape functions for warping distribution
$\left[N^{\theta_x}\right]$	Row vector of torsional shape functions
$\left[N^{\phi_y}\right]$	Row vector of rotational about *y* axis shape functions
$\left[N^{\phi_z}\right]$	Row vector of rotational about *z* axis shape functions
$[p_0]$, $[p_{c_i}]$, $[p_{s_i}]$	Matrices which results from Fourier expansion of the derivative of the jacobian
{R}, $\mathbf{R_i}$	Vector that is a consequence of the transport acceleration
[T], $\mathbf{T_{ij}}$	Matrix due to the transport acceleration
$\{v_P\}$	Three dimensional vector of velocity of point P
$\{\mathbb{X}\}$	Vector of all coefficients of Fourier expansion of the disturbance $\{\delta\zeta\}$

Some vectors and matrices are presented in two ways: in brackets and in bold without brackets.

Subscripts

0	Denotes components on the reference line
R	Denotes relative components
P	Denotes components of point P
S_0	Denotes vector written with respect to coordinate system S_0
S_1	Denotes vector written with respect to coordinate system S_1
T	Denotes components related with transport coordinate system
C	Denotes components related with Coriolis acceleration
ND	Denotes non-dimensional frequency or speed of rotation

Superscripts

T	Transpose of matrix
HBM	Denotes matrices or vectors which result after application of HBM
i	Denotes the i-the element (used when BEM is applied)
L	Denotes linear component (used to separate the strains from linear and nonlinear)
NL	Denotes nonlinear component (used to separate the strains from linear and nonlinear)

Abbreviations

BEM	Boundary element Method
DOF	Degrees of Freedom
FEM	Finite Element Method
HBM	Harmonic Balance Method

Contents

1

Introduction

1. 1. General Introduction

Beams are structures having one dimension much larger than the other two. Beam models are often used in design, because they can provide valuable insight into the behaviour of the structures with much less effort than more complex models. Beam theories have several engineering applications and are often used to model helicopter rotor blades, wind turbine blades, aircraft wings, robot arms, bridges, etc. The structural modelling of beams can be divided into linear and nonlinear modelling.

Linear systems are those for which the principle of superposition holds. The main modal characteristics of a linear system are its natural frequencies, modal damping ratios and mode shapes. The response of a linear system due to a harmonic excitation is also harmonic and the response frequency is the same as the excitation frequency. In steady-state, the response amplitude is unique and independent on the initial conditions. The study of linear systems is much easier, but they have limited application. In truth, linearity is generally an approximation, because the majority of natural systems are nonlinear.

Nonlinear systems are those for which the principle of superposition does not hold [1. 1]. Several types of nonlinearity exist in mechanical systems, the most common nonlinearities are material, geometrical, inertial, due to body forces or due to friction. The material type of nonlinearity occurs when the stresses are nonlinear functions of strains, for example when a material undergoes plastic behaviour [1. 2], [1. 3]. Geometric nonlinearity is associated with large displacements of solids and results in nonlinear strain-displacement relations [1. 4], [1. 5]. If the large-amplitude vibrations are accompanied by large changes in the curvature, it is necessary to employ a nonlinear

relationship between the curvature and the displacement. Geometric nonlinearity exists also in rigid bodies associated with large displacements and large rotations as, for example, in the case of the pendulum. The nonlinearity due to inertia comes from the kinetic energy, for example, Coriolis or centripetal accelerations can introduce in the system nonlinearity related with the inertia [1. 6]. The nonlinear body forces are mainly magnetic and electric forces. Friction nonlinearity occurs because the friction force is a nonlinear function of the displacement and velocity like Coulomb friction or hysteretic damping. Nonlinearity may appear in the boundary conditions or due to cracks or damage of the structures, as well.

Even in a single degree-of-freedom forced system, the nonlinearity can introduce into the system multiple solutions, jumps, natural frequency shifts, sub-harmonic, super-harmonic and combination resonances, limit cycles, symmetry-breaking and period-multiplying bifurcations, and chaotic motions [1. 7]. In addition to these phenomena, multi degree-of-freedom systems may exhibit modal interactions, resulting in energy exchanges among modes. Hence, nonlinear modelling and analysis is important in the design and optimization of modern structural systems.

Beam structures are often subjected to dynamic loadings that lead to large oscillation amplitudes and, therefore, to vibrations in the geometrically nonlinear regime. To design strategies for prediction and control of large amplitude structural vibrations, one needs to understand their dynamic behaviour, including modal coupling and instabilities.

In this work, geometrically nonlinear vibrations of 3D beams, beams that may deform in three-dimensional space, are studied. In the next sub-sections, a more detailed review of methods for solving nonlinear systems and methods for deriving beam models are given. At the end of the chapter, a sub-section about the organization of the thesis is included.

1. 2. Modelling and solution methodologies in nonlinear dynamics

The first step in the analysis of any structural vibration problem is the formulation of the equation of motion. Structures are continuous systems and, as such systems, they are ideally represented by partial differential equations. There are two different approaches for the derivation of the equation of motion of dynamical problems: vectorial and analytical [1. 8]. The first approach is directly based on Newton's second and third laws,

the second of which famously states that [1. 9] “the rate of change of momentum of a mass is equal to the force acting on it”; the third is the action and reaction law. The vectorial approach applies these laws directly, is based on free body diagrams and is more appropriate for discrete systems, but it has been successfully applied to continuous systems [1. 10], [1. 11]. The approach referred to as analytical mechanics considers the system as a whole rather than its individual components. Generalized coordinates are introduced, which represents a departure from the physical coordinates and the mathematical formulation becomes independent of the set of coordinates. It consists of developing the equation of motion by applying the calculus of variation to kinetic energy and work (and eventually to potential energy), thus it is often referred to as variational approach. This approach is commonly used in formulation of complex mechanical systems and structures. Variational approaches, commonly applied in dynamics, are the principle of virtual work, Hamilton’s principle and Lagrange’s equations [1. 8]. The principle of virtual work states that [1. 9] “if a system, which is in equilibrium under the action of a set of forces, is subjected to a virtual displacement, then the total work done by the forces will be zero”. Virtual displacements are infinitesimal variations from the true position of the system and, to lead to the equations of motion, should be compatible with the constraints of the system. Virtual displacements are not true displacements, because they do not need to really take place and there is no time change associated with them. The principle of virtual work leads to equilibrium equations in the weak form [1. 12], [1. 13] and with appropriate set of shape functions, it can be used to obtain the equation of motion in discretized form, i.e. the equation of motion is directly obtained as a system of ordinary differential equations, instead of, first obtaining the partial differential equation and then discretizing it. The principle of virtual work is rather convenient for the displacement based approach employed in this work, and it is used to obtain the equation of motion.

If the nonlinear partial differential equations are derived, by any of the methods mentioned above, there are two general approaches for treating them. In the first approach, which is the most commonly used in engineering, the partial differential equations and the boundary conditions are discretized by using either a variational or a weighted-residual method [1. 1], [1. 12]. As a result of this approach, a system of nonlinear ordinary differential equations is obtained. In the second approach, the partial

differential equations and the boundary conditions are treated directly - numerically or analytically.

Variational methods employ the calculus of variations. The solution of the partial differential equation is approximated by determination of the extreme or stationary value of a functional (a scalar quantity). In structural dynamics, the functional might be, for example, the total potential energy or the complementary energy of the system. The Ritz method (also known as Rayleigh-Ritz) is the most widely used variational method in structural engineering [1. 1]. Weighted-residual methods begin with the governing partial differential equations and boundary conditions. The solution is approximated by linear combination of independent functions and the methods attempts to minimize the error by set of weight functions. Most common weighted-residual methods include Galerkin, collocation and sub-domain. It should be noted that, there is a close relationship between Galerkin and Ritz methods. If the same interpolation functions are used in both methods, the resulting calculations and approximate solutions are identical [1. 14]. Nevertheless, the methods are different, the Ritz method is variational while Galerkin is not.

In what concerns the second approach, i.e. treating directly the partial differential equations, if the latter are nonlinear, then a perturbation method [1. 15] like the method of multiple scales or the method of averaging can be used. One should note that the perturbation methods may also be used to solve the discretized form of the partial differential equation, i.e. the system of ordinary differential equation.

The finite element method (FEM) [1. 12], [1. 13] was initially based on variational methods [1. 16] and later the weighted-residual methods were also applied with FEM [1. 17]. The *h*-version FEM discretizes the continuous system into sub-domains, i.e. the elements, and uses the displacements on some nodes on the boundary or in the interior of the sub-domains as generalized coordinates. In other words, the *h*-version FEM can be regarded as a piecewise application of a variational or weighted-residual method, but only a small and constant set of trial functions is used for each element, which are the interpolation functions (shape functions), with a corresponding set of undetermined parameters (generalized coordinates). The interpolation functions are usually polynomials, but also they can be trigonometric or other functions. For static problems, the undetermined parameters are constants and for dynamical problems the undetermined parameters are functions of time. Often, Galerkin method is used to approximate the

solution in the sub-domains [1. 12]. In such cases, if the variational principle exists, it is not used directly, even though the two approaches result to identical solutions. An advantage of the variational method is that is provides upper or lower bounds of the solutions, while this information is missing in Galerkin method [1. 14].

Usually the symbol *h* is used to represent the size of the finite elements. Convergence occurs when the size of the largest element is progressively reduced and the mesh is progressively refined, hence the name is *h*-version FEM.

An alternative approach to reduce errors in FEM is based on increasing the number of the shape functions and keeping the mesh constant [1. 13]. Polynomials are often used as shape functions and the polynomial degree of elements is usually denoted by the symbol *p*, hence the name is *p*-version Convergence occurs when the number of the shape functions is progressively increased. The *h*- and *p*- versions are just special applications of the finite element method, which, at least in principle, allows changing the finite element mesh concurrently with increasing the polynomial degree of elements. This general approach is usually called *hp*-version of the finite element method.

The *p*-version FEM has several advantages over the *h*-version [1. 9], [1. 19] the most important ones are:

(i) The *p*-version FEM tends to give accurate results with far fewer degrees of freedom than the *h*-version FEM;

(ii) Simple structures can be modelled using just one element avoiding the assemblage of elements;

(iii) It does not require a change in the mesh to improve the accuracy of the solution.

In this work, a beam structure is modelled using only one *p*-version finite element method with hierarchical shape functions. This method gives the equation of motion as a finite system of coupled nonlinear ordinary differential equations of second order. For comparison purposes, more that one element is used, but the main results are obtained with one element only.

Many methods have been developed to solve nonlinear ordinary differential equations. Possibly the most popular in structural dynamics are of four types: methods that can be grouped under the label “direct integration in the time domain” [1. 20], [1. 21],

perturbation methods [1. 15], the shooting method [1. 7], [1. 22] and the harmonic balance method (HBM) [1. 23], [1. 24]. Each of them has its advantages and disadvantages. Direct time domain integration methods [1. 20], as Newmark, Wilson θ or central differences, prevail particularly in the finite element community and are rather effective for searching the response to particular excitations and with particular initial conditions. Properly used, they have the advantage of leading to accurate solutions in the vast majority of problems. However, even in non-autonomous systems, they require large computational times for computing each steady-state solution and therefore are not good for parametric studies. Perturbation methods, such as multiple scales and averaging, are based on a small parameter and are consequently restricted to weakly nonlinear systems [1. 15]. Using a shooting method, which solves boundary value problems, in free vibration analysis is complex not only because the period of vibration is not known before hand, but also because this method is rather prone to ill conditioning [1. 25], [1. 26]. In this context, the shooting method is based on a numerical time integration scheme, but it can be used with a continuation method for parametric studies. The HBM also has disadvantages, like the fact that the errors may be introduced by the truncation of the Fourier series. Nevertheless, when periodic, hence steady-state, free or forced oscillations, are of interest, the HBM finds its natural application. This method has also several advantages: it is not restricted to small nonlinearities; the solution converges to the exact periodic solution as the number of harmonics increases; the nonlinear equations to be solved are algebraic, not differential; results are attained with a small computational cost; it does not, in most cases, suffer from numerical issues (as ill-conditioning or instability in the algorithm); coupled with a continuation method allows one to straightforwardly carry out parametric studies. Moreover, the HBM provides information which is very easily interpreted, namely one can directly see the shapes of vibration related with each harmonic. The HBM is applicable to systems with simple nonlinearity, like quadratic or cubic, which are the most common mechanical systems. For systems with more complex nonlinearity, the HBM becomes extremely burdensome.

In order to determine how the solutions of a system vary with a certain parameter, as frequency or amplitude of vibration, and to determine bifurcation points and follow the secondary branches from them, one should use continuation schemes which are based on the implicit function theorem. Such methods are predictor-corrector or piece-wise-linear methods [1. 7]. In the predictor-corrector methods, one approximately follows a branch

of solutions, while in the piece-wise-linear methods one exactly follows a linear curve that approximates a branch of solutions. Sequential continuation is the simplest predictor-corrector method which uses directly the parameter of the system as the continuation parameter. A disadvantage of this method is that it cannot pass turning points. The arc-length continuation method used, for example, in [1. 27] – [1. 30], which is based on the method presented in [1. 31], uses the "arc-length" as a continuation parameter and has the ability to pass turning points. The arc-length continuation method is used in this work.

1. 3. Nonlinear normal modes and modal analysis of mechanical systems

The knowledge of the modes of vibration allows one to understand the dynamic characteristics of a structure and can be employed in the prediction of the response to external excitations [1. 32]. Whilst in a linear conservative system, it is possible to define a mode of vibration by its natural frequency and mode shape, which do not change with the vibration amplitude, in a system experiencing geometrically nonlinear vibrations this is not true. In the latter case, periodic, free, oscillations can still be found, but the shape assumed by the system along a vibration period is not constant, the period varies with the vibration amplitude, and the oscillations can significantly deviate from harmonic. A few studies have been carried out on the variation of the shape of vibration and of the vibration period with the vibration amplitude [1. 27], [1. 33], [1. 34].

The definition of mode of vibration in nonlinear systems is not unequivocal and has been a matter of discussion [1. 35]-[1. 39]. Rosenberg [1. 35] suggested that a nonlinear normal mode of a discrete conservative system could be interpreted as a motion where the masses execute periodic, but not necessarily harmonic, vibrations, all masses vibrating with the same period, achieving the maximum amplitude displacement and the static equilibrium points simultaneously, i.e. the system performs a synchronous oscillation. In these conditions, the coordinates of the system are determined by the position of any of the masses, as in linear modes, but the ratio between the vibration amplitudes of any two points is not constant.

Shaw and Pierre [1. 36]-[1. 37] extended Rosenberg's definition for nonlinear normal modes to continuous and damped systems. They defined a nonlinear normal mode as a motion which takes place on a two-dimensional invariant manifold in the phase space. This

manifold has the following properties: it passes through a stable equilibrium point of the system and, at that point, it is tangent to a plane which is an eigenspace of the system linearized about that equilibrium.

The concept of Rosenberg can be extended to continuous systems, by considering an infinite number of infinitesimal masses. Furthermore, it can be extended to non-synchronous, but still periodic oscillations. This extension is appropriate in the presence of internal resonances, i.e. when two or more normal modes interact and the motion is not anymore synchronous – some coordinates may have frequency different than that of the other coordinates. This definition of nonlinear normal mode is considered in the current work.

The normal modes of discrete (or discretized) linear systems are computed by solving eigenvalue problems. In discrete models of nonlinear systems an eigenvalue problem related with steady-state free vibration can also be defined, but the stiffness matrix depends upon the unknown eigenvector. Hence, the eigenvalues and the eigenvectors are, generally, amplitude dependent. It is here considered that these define frequencies and shapes of vibration, which depend on the amplitude of vibration displacement, and which approximately represent the modes of vibration of the nonlinear system. Rather conveniently, these "nonlinear modes" tend to the linear modes when the vibration amplitude decreases.

Due to the variation of the natural frequencies, two or more natural frequencies may become commensurable, creating conditions for the strong interaction of the modes involved. As a result of this phenomenon, known as internal resonance, energy imparted initially to one of the modes involved in the internal resonance will be continuously exchanged among all the modes involved in that internal resonance and multimodal vibration appears [1. 24], [1. 27], [1. 40], [1. 41].

The study of undamped nonlinear free vibrations is important for understanding the system's vibratory response in the nonlinear regime. One reason why the computation and investigation of nonlinear free, undamped oscillations is valuable is that resonances in the forced responses occur in the neighbourhood of these free vibration oscillations [1. 42], this fact is also indicated by many analytical and numerical investigations [1. 23], [1. 24], [1. 38], [1. 40]. Hence, a free vibration study provides information on the dynamic characteristics of the system, information that is of use when the system is

excited by practically any force. During the fundamental resonance of forced vibration, the shape of vibration is identical to that of the neighbouring nonlinear free response; moreover a bifurcation of the free response can considerably affect the resonances of a forced system [1. 43]. Since bifurcations in free vibrations give rise to new types of dynamic behaviour, they have significant effects on the dynamics of forced systems. Hence, the knowledge of the backbone curves, curves that relate the frequency with the vibration amplitude of a particular harmonic or of a particular displacement component, and the bifurcations offers important understanding on the dynamics of the structure. The study of free vibrations of nonlinear systems, with definition of shapes, natural frequencies and bifurcation, is the natural development of studies of normal modes in linear systems.

While the free vibration analysis is essential to understand the dynamic behaviour of structures, the forced vibration response and stability analysis is also of well known importance in engineering application [1. 44]. Forced vibration analysis is directly related with real engineering applications due to presence of external forces. Even though the forced responses occur in the neighbourhood of the free vibration oscillations, stability study is essential [1. 45] since the unstable solutions physically do not exist in the nature.

As pointed out, nonlinearity may introduce chaotic motion in the response of the system. Just a few examples of chaotic motions are given here. Chin and Nayfeh [1. 46], [1. 47] found chaotic motions of planar clamped-hinged beams due to static axial and transverse harmonic excitation. Nayfeh and Pai [1. 48] analysed the nonlinear response of cantilever beam due to base excitations. They showed that motion in one plane may result to motion in both planes and, on certain parameters, to a chaotical motion. Warminski [1. 49], [1. 50] studied chaotic vibrations of parametrically and self-excited systems which arise due to internal resonance. Chaotic motions due to harmonically excited circular plates were investigated by Touzé, Thomas and Amabilli [1. 51], [1. 52]. Chaotic motions due to harmonic forces were also found experimentally. Cusumano and Moon [1. 53] studied experimentally nonlinear vibrations of cantilever beams excited by harmonic force on the clamped boundary. It was shown that planar periodic motions can loose stability and chaotic non-planar motions can appear.

1. 4. Review of beam models

Basically, beam theories can be divided into three groups [1. 1]: (a) Bernoulli-Euler beam theory [1. 54], [1. 55], (b) shear deformable beam theories [1. 56]-[1. 59] (i.e. Timoshenko's theory, third-order shear theory, higher-order shear theories) and (c) three-dimensional beam theories [1. 60]. In the Bernoulli-Euler beam theory, only the axial strain ε_x is taken into account and the cross section perpendicular to the reference axis before deformation is considered to remain plane and perpendicular to the deformed reference line after deformation. In shear deformable beam theories, the shear strains γ_{xy} and γ_{xz}, which are due to out-of-plane warping [1. 61], are considered. In three-dimensional beam theories, both out-of-plane and in-plane warpings are considered. The in-plane warping is due to extension or bending and results in normal strains ε_y and ε_z and shear strain γ_{yz} different from zero, hence the three dimensional stresses are fully accounted. It was validated by Volovoi, Hodges and co-authors [1. 62] that the shear-deformable beam theories are practically equivalent to three-dimensional beam theories for beams of isotropic materials and solid cross sections, thus the Timoshenko shear deformable beam theory is preferred in this work.

One should not confuse 3D beam model with three-dimensional beam theory. The latter was defined above, while the former accounts for a beam that may deform in three-dimensional space, i.e. the beam may experience longitudinal, torsional and non-planar bending deformations. Often, in the literature, the 3D beam model is also called bending-torsional beam model due to couplings between bending and torsional deformations which require the treatment of these deformations together.

The most common cases where bending-torsional coupling may exist in linear 3D beams models are due to anisotropy of the material or due to non-symmetrical properties of the cross sections. Bending-torsion coupling appears in isotropic materials with symmetric cross section with respect to the transverse axes due to the nonlinear terms which arise from the strain-displacement relations.

Klinkel and Govingjee [1. 63] investigated bending-torsion coupling due to anisotropy in elastic properties of the material. The general Saint-Venant torsion theory, which is, under certain assumptions, valid for isotropic materials, was extended to anisotropic materials. For this purpose, three warping functions were developed, associated with two

bending modes and one torsion mode. Ganapathi et al. [1. 64] developed a finite element to analyse sandwich beams including bending and torsion. The convergence of the terms in the warping function was presented and it was shown that for short laminated beams it is important to include, as an additional variable, the distribution of the warping function along the longitudinal axis. The bending-torsion coupling in linear vibrations comes from the interface continuity conditions between layers of the sandwich beams.

Eslimy-Isfahany and Banerjee [1. 65] investigated free and forced vibrations of bending-torsion coupled beams due to non-coincident mass and shear centres. The differential equations of motion were solved analytically. A method focused on the constituent parts of the generalized mass arising from bending and torsional displacements was used. Banerjee and Su [1. 66] applied Hamilton's principle and the dynamic stiffness method to study free vibrations of orthotropic beams whose flexural motions are coupled with torsion. The theory developed can be applied to a wide range of beams, and the authors showed examples for aircraft wings. The coupling of the modes in linear free vibrations is explained by the fact that the cross section of the aircraft wing is not symmetric and the elastic and mass axes do not coincide. More research about bending-torsion coupling in linear vibrations of beams can be found, for example, in [1. 67]-[1. 71].

Crespo da Silva and Zaretzky [1. 72] investigated nonlinear flexural-torsional coupling in inextensional beams neglecting the shear deformation. The method of multiple scales was used to analyse the motion governed by the coupled nonlinear differential equation excited by a periodic force with frequencies near the bending and the torsional natural frequencies. Sharf [1. 73] developed a finite element nonlinear model for bending and torsional vibrations of beams considering Bernoulli-Euler's theory. The warping function was not included. The longitudinal nonlinear terms of second order in the direct strain were neglected, as well as all nonlinear terms in the shear strains. Pai and Palazotto [1. 74] presented a nonlinear curved beam model which accounts for large rotations and displacements. Some effects, like transverse shear stresses, influence of torsional warping on direct strain, extension-bending coupling due to the initial bending curvatures and extension-twisting coupling due to the initial twisting were not considered in the model. Static deformations of beams subjected to different loading and boundary conditions were obtained. Pacoste and Eriksson [1. 75] developed finite elements for 2D and 3D beam analyses. The 3D beam elements are based on Timoshenko type strains and different models were compared in static instability problems. Petrov and Géradin

[1. 76] derived a finite element method for curved and twisted beams based on kinematical hypotheses by the principle of virtual work. The model is formulated for large deformation, and accounts for translational and rotational displacements of the cross-sections, warping of their plane and distortion of their contours. Patel and Ganapathi [1. 77] developed a beam finite element to investigate the nonlinear torsional vibrations of sandwich beams. The transverse displacements were written as a function of the cross sectional rotation by means of cosine and sine functions. The formulation of the element includes a warping function of the cross section and nonlinearity based on the Green's strain definition. The longitudinal terms of second order in the strain expressions were included in the model. The convergence of the natural frequencies, with the number of finite elements and with the number of terms in the warping function, was analysed. Numerical results for nonlinear free vibration of cantilever sandwich beams with different geometrical properties were presented. Cao and Tucker [1. 78] formulated the nonlinear partial differential equations of motion for slender beams using the Cosserat theory and considering flexure along two principal axes, extension, shear and torsion. The nonlinear model was solved using Femlab/Matlab software and the bending-torsion coupling for isotropic materials was presented. Sapountzakis and Dourakopoulos [1. 79]-[1. 80] developed a boundary element method for the nonlinear dynamic analysis of beams of doubly symmetric cross sections. The displacement fields presented follow the Timoshenko's theory, but torsion was not included in the model. Fonseca and Ribeiro [1. 81] presented a *p*-version finite element for geometrically nonlinear vibrations in space of isotropic beams. Bernoulli-Euler's theory was adopted for flexure and Saint-Venant's for torsion, but warping was neglected. The equation of motion was derived by the principle of the virtual work and solved by Newmark's method in time domain. Numerical results were presented and it was shown that convergence is achieved with a small number of degrees of freedom. This work was continued in [1. 82] and the harmonic balance method was applied to investigate nonlinear free vibrations of beams with circular cross section. Internal resonances and coupling between modes were found either in plane bending or in torsion, but 3D vibration due to modal coupling was not described. Variations of bending and torsional shapes of vibration with the respective nonlinear frequencies were presented.

The literature review indicates that in most works the longitudinal nonlinear terms of second order that appear in the strain field were neglected, particularly in non-planar

bending. A Timoshenko model for bending only in one plane, which includes these nonlinear terms, was developed in [1. 83]. These nonlinear terms were also included in only torsional vibrations in [1. 77]. A bending-torsional model, which considers these terms, but only in the shear strains, was presented in [1. 73]. As mentioned above, this model uses Bernoulli-Euler's theory for bending and does not consider warping. A bending-torsional model based on Timoshenko's theory for bending and Saint-Venant's theory for torsion, and which considers all nonlinear terms, was not found in the literature.

In [1. 48] the nonlinear vibration of a cantilever beam subjected to parametric excitations is analysed, using a combination of the methods of multiple scales and Galerkin, unstable planar motion is found and non-planar motion described. An analysis using a similar model and solution methods is carried out in [1. 84], but to investigate non-planar responses of a cantilever beam subjected to lateral harmonic base excitation.

In [1. 53] it was shown experimentally that planar motions can give rise to coupled bending-torsion oscillations even if the bending and torsional modes are uncoupled in the linear model. Under a bifurcation, the planar motion looses stability and non-planar motion occurs. In [1. 85] a simplified two-degree of freedom model was developed to study the former interaction; this study was continued in [1. 86] with a more complete model, and it was found that motions in a plane may loose stability due to a symmetry breaking bifurcation.

Lateral buckling analysis of beams of arbitrary cross section was presented in [1. 87]. The model considers large displacements in both transverse planes and large angles of twist. A flexural-torsional beam model was developed in [1. 88] which takes into account the nonlinear coupling between bending and torsion. The model is applicable for structures loaded in bending and torsion with large displacements, but it was used to predict the post-buckling behaviour of beams with asymmetric sections. This model was extended in [1. 89] where the trigonometric functions which arise from the torsional behaviour of beams were included as additional variables. A geometrically nonlinear finite element model for analysis of composite laminated thin-walled beams including warping deformation was developed in [1. 90]. The influence of the lamina orientation on the structural behaviour was studied.

The beam equation of motion becomes more complicated when instead of one, a set of coupled beams are analysed, such as L shaped beam structures. Planar motions of L shaped beams were studied by Balachandran and Nayfeh [1. 91]. Warminski et al. [1. 92] derived the equation of motion of L shaped beam structure taking into account torsion and bending of both coupled beams. The modal interactions of the coupled beams were investigated.

1. 5. Review of rotating beams

Generally, the motion of a rotating beam is described by a continuous change of its shape due to the elasticity of the beam and by large rotations associated to the rigid body motion. Most of the research of rotating beams, done to date, considers linear bending in one plane: therefore the literature review first addresses this simpler problem. Then, a few works that employed nonlinear models and models that consider rotations of 3D beams are recalled.

Hodges and Rutkowski [1. 93] analysed linear free vibrations, with plane bending, of rotating beams by an *hp*-version finite element method that the authors designed as a "variable-order finite element method". The assumptions of Bernoulli-Euler theory were used and it was considered that the rotation was about a fixed axis in space. Uniform beams with nonzero hub radius, and a tapered beam were investigated. It was demonstrated that a small number or even just one element with many shape functions give better solutions than many elements with a small number of shape functions each. A finite element with four degrees of freedom for rotating Timoshenko beams was presented by Yokoyama [1. 94]. Natural frequencies of flapwise and lagwise vibrations were presented and the influences of rotational speed, hub radius, shear deformation and rotary inertia investigated. Bazoune and Khulief [1. 95] investigated the free linear vibrations of rotating uniform and tapered Timoshenko beams by the finite element method. A setting angle which describes the angle of rotation of the beam about its longitudinal axes was introduced. The effects of rotational speed, hub radius, setting angle and taper parameters on the natural frequencies were investigated and presented for flapwise and lagwise bending vibrations. Linear flapwise bending frequencies of uniform and tapered beams were investigated by Banerjee [1. 96] applying the dynamic stiffness method. Different boundary conditions were considered. The model was

extended by the same author to Timoshenko beams in [1. 97]. Comparisons of natural frequencies for different rotational speeds were presented and the improvements of the model were described. Comparisons of rotating Timoshenko and Bernoulli-Euler beams were shown and discussed. Lin and Hsiao [1. 98] derived the differential equations of rotating Timoshenko beam by the principle of the virtual work. A geometrically nonlinear model was first considered, but it was linearized afterwards. As a result, the static longitudinal displacement, which appears in the equation of motion, is assumed to be known and the system is linear. It is shown that when Coriolis force exists, the axial and transverse vibrations are coupled. The effect of Coriolis force on the natural frequencies of rotating beams with different angular velocities, hub radios and slenderness ratio was investigated. Wang and Wereley [1. 99] developed a spectral finite element method for vibration analysis of rotating tapered beams using a low-degree-of-freedom model. It was shown that a single element is sufficient to capture the dynamic characteristics of a rotating beam. Yardimoglu [1. 100] developed a finite element model for transverse vibrations of tapered Timoshenko beams with rectangular cross section. Tapering functions of breadth and depth were introduced to define the geometry of the beam. Free linear vibrations of rotating tapered beams were also investigated by Banerjee and Jackson [1. 101]. Beams with linearly varying taper in depth and width of the cross section along the length were considered. Gunda et al. [1. 102] developed a *p*-version finite element method for rotating uniform and tapered beams considering Bernoulli-Euler's theory and only transverse displacements in the model. Polynomial functions and Fourier series were used. The obtained results show a good match with the results from different methods and require less degrees of freedom (DOF) than the other methods. Lee and Sheu [1. 103] derived the differential equations of a rotating beam based on Bernoulli-Euler theory considering setting and inclination angles. Like in [1. 98], a geometrically nonlinear model was initially considered, but linearization was implemented. The influence of the setting and inclinations angles on the natural frequencies was discussed. Yoo et al. [1. 104] developed a rotating beam model considering Bernoulli-Euler's theory. The beam cross section is rectangular but with varying thickness and width. Characteristic requirements were specified and the geometric shapes that satisfy these requirements were obtained by an optimization procedure.

Research where nonlinear models were employed is considered now. Pesheck, Pierre and Shaw [1. 105] derived a reduced model for rotating beams using nonlinear normal modes. The authors considered an isotropic, uniform cantilever beam rotating at constant velocity. The beam is constrained to deform in transverse and axial directions and torsion is not considered. Nonlinear axial strain, which causes the axial-transverse coupling, is included in the model. The derived method is able to approximate precisely the nonlinear modes of vibration and to catch internal resonances between two transverse, and between transverse and axial modes with a small number of DOF. Turhan and Bulut [1. 106] investigated the lagwise vibrations of rotating Bernoulli-Euler beams with nonlinear curvature including geometric nonlinearities up to cubic terms. The authors revealed that the rotating speed may change the behaviour from hardening to softening. Younesian and Esmailzadeh [1. 107] analysed nonlinear flapwise vibrations of rotating beams with variable speed. The equation of motion was derived by Hamilton's principle and solved by Galerkin and multiple scales methods. The effect of acceleration and deceleration rates on the vibration amplitude was investigated.

Ambrósio and Nikravesh [1. 108] formulated the equation of motion of a multibody system which undergoes large motions and elasto-plastic deformations. The deformation of the elastic body is related to a corotated configuration, rigidly attached to a point of the body. The capability of this formulation to deal with geometrically nonlinear problems was demonstrated by Ambrósio [1. 109] and the dynamics of rotating beam were studied. The multibody based formulation of flexible and rigid bodies was successfully applied to beams of composite materials by Neto, Ambrósio and Leal [1. 110]. The VABS code, developed by Yu and Hodges [1. 111], was used to define the elasticity matrix.

Chandiramani, Shete and Librescu [1. 112] and [1. 113] presented a higher order model for pretwisted, rotating, laminated composite box-beams using linear theory. The model discards the assumption that transverse shear strains are uniform along the wall thickness and assumes a parabolic variation. The equations of motion were developed by Hamilton's principle and free and forced vibrations were studied using an extended Galerkin method. This theory was compared with the Classical theory and First Order Shear Deformation Theory (FSDT). The roles of pretwist, rotation speed and hub radius were analysed for each theory and significant differences between these theories were shown. Maqueda et al. [1. 114] examined the effect of the centrifugal forces on the

eigenvalue solution by two different finite element formulations: one which assumes that the cross section does not deform in its own plane and remains plane after deformation; and the other which abates this assumption and introduces modes that couple with the deformation of the cross section and the axial and bending deformations. In both formulations, the solution was obtained by determining the static equilibrium configuration of the beam for a given constant value of the angular velocity. Then the equations of motion of a particular static configuration were linearized. It was shown that the model which includes coupling between the deformation modes leads to higher values of the eigenfrequencies. The centrifugal forces also increase the beam stiffness and the frequencies. It was demonstrated that as the effect of the centrifugal forces increase, the effect of the coupled deformation modes decreases and becomes less significant. Bazoune et al. [1. 115] investigated spinning tapered Timoshenko beams considering bending, axial and torsional displacements. Two modal reduction schemes were presented and time responses due to sinusoidal and impulse force compared. Avramov et al. [1. 116] developed a 3D model for beams with arbitrary cross section using Hamilton's principle and considering Bernoulli-Euler's theory. Ozgumus and Kaya [1. 117] developed a bending-torsional model for double tapered beams considering only flapwise bending displacements by Timoshenko's theory. The equations of motion were derived by Hamilton's principle and the Coriolis terms were neglected. The effects of rotational speed, hub radius and taper ratios on the natural frequencies were investigated.

1. 6. Objective and structure of the thesis

The main goal of the thesis is to investigate the dynamics of 3D beams considering geometrical type of nonlinearity. In nonlinear vibrations, multi-harmonic solutions are possible and may result in modal coupling. Thus, one of the objectives is to study free and forced vibrations of clamped-clamped beams, and the interactions between the bending modes in one plane with the bending modes in the other plane and torsion. The asymmetry of the cross section contributes to additional coupling between transverse displacements and torsion, and it is also intended here to study the dynamics of beams with asymmetrical cross sections. A model of rotating cantilever beams is developed and the influence of the speed of rotation on the modes of vibration and on the dynamical behaviour is also investigated.

In Chapter 2, the equation of motion of a 3D beam on isotropic, homogeneous and elastic materials, is developed considering Timoshenko's shear deformable theory for bending and assuming that the cross section rotates as a rigid body and is free to warp in the longitudinal direction, i.e. out-of-plane warping is included, as in Saint-Venant's theory. A Bernoulli-Euler beam model is also developed for comparison purposes. The equation of motion is derived by the principle of virtual work and discretized by the *p*-version finite element method, with hierarchical sets of shape functions.

In Chapter 3, the models presented in Chapter 2 are compared by carrying out static and time domain numerical tests. The influence of: inclusion of the warping function; linearization of the trigonometric terms in strain expressions; approximation of the rotations about the transverse axes by derivatives of the transverse displacements; the longitudinal strains of second order in Green's strain; are pointed out and the most suitable 3D beam model is selected for future investigations.

In Chapter 4, the harmonic balance method is applied to the equation of motion of 3D beams derived in Chapter 2. Two Fourier series expansions are considered, one with only cosine terms, which is appropriate for free vibration analysis and another – with cosine and sine terms – appropriate for forced vibration analysis. A method to determine the stability of the solutions using Floquet's theory and the HBM is included.

In Chapter 5, free and forced vibrations of beams with rectangular cross sections are investigated in the frequency domain. First, free vibrations of 3D beams are examined, coupling between modes is investigated, internal resonances are found and the ensuing multimodal oscillations are described. Some of the couplings discovered lead from planar oscillations to oscillations in the three-dimensional space. Then, bifurcation diagrams and stability of solutions of forced vibrations due to a harmonic force are presented.

In Chapter 6, a model of 3D beams with non-symmetrical cross sections and including geometrical type of nonlinearity is derived. A method for determining the twist centre is presented. An analytical expression for the warping function, most often, does not exists, thus the boundary element method is chosen and presented for evaluating the warping function.

In Chapter 7, the nonlinear dynamics of 3D beams with non-symmetrical cross section is investigated, an L shaped cross section is employed. Linear natural frequencies and the corresponding modes of vibration are presented and the bending-torsional coupling in linear analysis is shown. Free and forced vibrations in the frequency domain are studied, internal resonances are found and the corresponding multi-modal responses are investigated.

In Chapter 8, a model for 3D beams rotating about a fixed axis is derived. The absolute acceleration, which is used to define the inertia forces, is written as a sum of the relative, the transport and Coriolis accelerations and included in the equation of motion by the virtual work of inertia forces.

In Chapter 9, the influence of the speed of rotation on the bending linear modes of vibration is presented. The equation of motion of rotating 3D beam is solved in the time domain, considering constant and non-constant speeds of rotation, under the action of impulsive and harmonic external forces.

Chapter 10 is dedicated to a summary of the conclusions and to suggestions for future work.

References

[1. 1] A. Nayfeh, P. Pai, *Linear and Nonlinear Structural Mechanics*, John Wiley & Sons, Inc., Weinheim, 2004.

[1. 2] M. Kojic, K-J. Bathe, *Inelastic Analysis of Solids and Structures*, Springer, Berlin, 2005.

[1. 3] P. Ribeiro, G. H. M. van der Heijden, Elasto-plastic and geometrically nonlinear vibrations of beams by the *p*-version finite element method, *Journal of Sound and Vibration* 325 (2009) 321–337.

[1. 4] M. Amabili, *Nonlinear Vibrations and Stability of Shells and Plates*, Cambridge University Press, New York, 2008.

[1. 5] Y. C. Fung, *Foundations of Solid Mechanics*, Prentice-Hall, Englewood Cliffs 1965.

[1. 6] G. Kerschen, K. Worden, A. Vakakis, J-C. Golinval, Past, present and future of nonlinear system identification in structural dynamics, *Mechanical Systems and Signal Processing* 20 (2006) 505–592.

[1. 7] A. Nayfeh, B. Balachandran, *Applied Nonlinear Dynamics*, John Wiley & Sons, Inc., Weinheim, 1995.

[1. 8] L. Meirovitch, *Methods of Analytical Dynamics*, Dover Publications, Inc., New York, 2003.

[1. 9] M. Petyt, *Finite Element Vibration Analysis*, Cambridge University Press, Cambridge, 2010.

[1. 10] L. Meirovitch, *Elements of Vibration Analysis*, McGraw-Hill, Inc., Singapore, 1986.

[1. 11] D. Hodges, E. Dowell, *Nonlinear equations of motion for the elastic bending and torsion of twisted nonuniform rotor blades*, NASA Technical Note, 1974.

[1. 12] O. Zienkiewicz, R. Taylor, J. Zhu, *The Finite Element Method: Its Basis and Fundamentals*, Sixth Edition, Oxford, 2005.

[1. 13] B. Szabó, I. Babuška, *Finite Element Analysis*, John Wiley & Sons, New York, 1991.

[1. 14] B. A. Finlayson, L. E. Scriven, The method of weighted residuals – a review, *Applied Mechanics Reviews* 19 (1966) 735-748.

[1. 15] A. Nayfeh, *Perturbation Methods*, Wiley-VCH Verlag GmbH & Co, Weinheim, 2004.

[1. 16] K. K. Gupta, J. L. Meek, A brief history of the beginning of the finite element method, *International Journal for Numerical Methods in Engineering* 39 (1996) 3761-3774.

[1. 17] J. Fish, T. Belytschko, *A First Course in Finite Elements*, John Wiley & Sons Ltd., Chichester, 2007.

[1. 18] P. Ribeiro, *Geometrical Non-linear Vibration of Beams and Plates by the Hierarchical Finite Element Method*, PhD Thesis, University of Southampton, 1998.

[1. 19] P. Ribeiro, Hierarchical finite element analyses of geometrically non-linear vibration of beams and plane frames, *Journal of Sound and Vibration* 246 (2001) 225-244.

[1. 20] K. Bathe, *Finite Element Procedures*, Prentice-Hall, New Jersey 1996.

[1. 21] M. McEwan, J. Wright, J. Cooper, A. Leung, A Combined Modal/Finite Element Analysis Technique for the Dynamic Response of a Non-linear Beam to Harmonic Excitation, *Journal of Sound and Vibration* 243(4) (2001) 601-624.

[1. 22] P. Ribeiro, Non-linear forced vibrations of thin/thick beams and plates by the finite element and shooting methods, *Computers & Structures* 82 (2004) 1413-1423

[1. 23] W. Szemplinska-Stupnicka, *The Behaviour of Nonlinear Vibrating Systems I*, *Fundamental Concepts and Methods: Application to Single-Degree-of-Freedom Systems*, Kluwer Academic Publishers, Dordrecht, 1990.

[1. 24] W. Szemplinska-Stupnicka, *The Behaviour of Nonlinear Vibrating Systems II*, *Advanced Concepts and Applications to Multi-Degree-of-Freedom Systems*, Kluwer Academic Publishers, Dordrecht, 1990.

[1. 25] P. Ribeiro, Nonlinear vibrations of simply-supported plates by the *p*-version finite element method, *Finite Elements in Analysis and Design* 41 (2005) 911–924.

[1. 26] P. Ribeiro, Forced periodic vibrations of laminated composite plates by a *p*-version, first order shear deformation, finite element, *Composites Science and Technology* 66 (2006) 1844–1856

[1. 27] R. Lewandowski, Non-linear free vibration of beams by the finite element and continuation methods, *Journal of Sound and Vibration* 170 (1994) 539-593.

[1. 28] P. Ribeiro, M. Petyt, Non-linear vibrations of beams with internal resonance by the hierarchical finite-element method, *Journal of Sound and Vibration* 224 (1999) 591-624.

[1. 29] P. Ribeiro, M. Petyt, Non-linear free vibration of isotropic plates with internal resonance, *International Journal of Non-Linear Mechanics* 35 (2000) 263-278.

[1. 30] M. Crisfield, A fast incremental/iterative solution procedure that handles "snap-through", *Computers & Structures* 13 (1981) 55-62.

[1. 31] E. Riks, An incremental approach to the solution of snapping and buckling problems, *International Journal of Solids and Structures* 15 (1979) 529-551.

[1. 32] A. Vakakis, *Normal Modes and Localization in Nonlinear Systems*, John Wiley & Sons, New York, 1996.

[1. 33] M. M. Bennouna, R. G. White, The effects of large vibration amplitudes on the fundamental mode shape of a clamped-clamped uniform beam, *Journal of Sound and Vibration* 96 (1984) 309-331.

[1. 34] R. Benamar, M. M. Bennouna, R. G. White, The effects of large vibration amplitudes on the mode shapes and natural frequencies of thin elastic structures. Part I: simply supported and clamped-clamped beams, *Journal of Sound and Vibration* 149 (1991) 179-195.

[1. 35] R. M. Rosenberg, On non-linear vibrations of systems with many degrees of freedom, *Advances Applied Mechanics* 9 (1966) 155-242.

[1. 36] S. W. Shaw, C. Pierre, Normal modes for non-linear vibratory systems, *Journal of Sound and Vibration* 164 (1993) 85–124.

[1. 37] S. W. Shaw, C. Pierre, Normal modes of vibration for non-linear continuous systems, *Journal of Sound and Vibration* 169 (1994) 319–347.

[1. 38] G. Kerschen, M. Peeters, J. C. Golinval, A. Vakakis, Nonlinear normal modes, Part I: A useful framework for the structural dynamicist, *Mechanical Systems and Signal Processing* 23 (2009) 170-194.

[1. 39] M. Peeters, R. Viguie, G. Serandour, G. Kerschen, J. Golinval, Nonlinear normal modes, Part II: Toward a practical computation using numerical continuation techniques, *Mechanical Systems and Signal Processing* 23 (2009) 195-216.

[1. 40] A. Nayfeh, D. Mook, *Nonlinear Oscillations*, John Wiley & Sons, New York, 1995.

[1. 41] A. Manevich, L. Manevitch, *Mechanics of Nonlinear Systems with Internal Resonances*, Imperial College Press, London, 2005.

[1. 42] A. Vakakis, Non-linear Normal Modes (NNMs) and Their Applications in Vibration Theory: an Overview, *Mechanical Systems and Signal Processing* 11 (1997) 3-22.

[1. 43] A. Vakakis, Fundamental and Subharmonic Resonances in a System with a '1-1' Internal Resonance, *Nonlinear Dynamics* 3 (1992) 123-143.

[1. 44] D. Ewins, *Modal Testing: Theory, Practice and Application*, Research Studies Press, Baldock (2000)

[1. 45] R. Seydel, *Practical Bifurcation and Stability Analysis*, Springer-Verlag, New York, 1994.

[1. 46] C. Chin, A. Nayfeh, Three-to-One Internal Resonances in Hinged-Clamped Beams, *Nonlinear Dynamics* 12 (1997) 129–154.

[1. 47] C. Chin, A. Nayfeh, Three-to-One Internal Resonances in Parametrically Excited Hinged-Clamped Beams, *Nonlinear Dynamics* 20 (1999) 131–158.

[1. 48] A. H. Nayfeh, P. F. Pai, Non-linear non-planar parametric responses of an inextensional beam, *International Journal of Non-Linear Mechanics* 24 (1989) 139-158.

[1. 49] J. Warminski, Regular and chaotic vibrations of a parametrically and self-excited system under internal resonance condition, *Meccanica* 40 (2005) 181-202.

[1. 50] J. Warminski, Nonlinear normal modes of coupled self-excited oscillators in regular and chaotic vibration regimes, *Journal of Theoretical and Applied Mechanics* 46 (2008) 693-714.

[1. 51] C. Touzé, O. Thomas, M. Amabili, Forced vibrations of circular plates: From periodic to chaotic motions, *Proceedings of the ASME Design Engineering Technical Conference* 5 (2010) 817-825.

[1. 52] C. Touzé, O. Thomas, M. Amabili, Transition to chaotic vibrations for harmonically forced perfect and imperfect circular plates, *International Journal of Non-Linear Mechanics* 46 (2011) 234–246.

[1. 53] J. Cusumano, F. Moon, Chaotic nonplanar vibrations of the thin elastica, part I: experimental observation of planar instability, *Journal of Sound and Vibration* 179 (1995) 185-208.

[1. 54] I. Sokolnikoff, *Mathematical Theory of Elasticity*, McGraw-Hill, New York, 1956.

[1. 55] M. Attard, Nonlinear theory of non-uniform torsion of thin-walled beams, *Thin-Walled Structures* 4 (1986) 101-134.

[1. 56] S. Timoshenko, J. N. Goodier, *Theory of Elasticity*, McGraw-Hill, New York, 1951.

[1. 57] C. Wang, J. Reddy, K. Lee, *Shear Deformable Beams and Plates*, Elsevier, Oxford, 2000.

[1. 58] J. Hutchinson, Shear coefficients for Timoshenko beam theory, *Journal of Applied Mechanics* 68 (2001) 87-92.

[1. 59] P. Ribeiro, A *p*-version, first order shear deformation, finite element for geometrically non-linear vibration of curved beams, *International Journal for Numerical Methods in Engineering* 61 (2004) 2696-2715.

[1. 60] D. Hodges, *Nonlinear Composite Beam Theory*, American Institute of Aeronautics and Astronautics, Reston, 2006.

[1. 61] G. Wempner, D. Talaslidis, *Mechanics of Solids and Shells. Theory and Application*, CRC Press, Boca Raton, Florida, 2003.

[1. 62] V. Volovoi, D. Hodges, C. Cesnik, B. Popescu, Assessment of Beam Modeling Methods for Rotor Blade Applications, *Mathematical and Computer Modelling* 33 (2001) 1099-1112.

[1. 63] S. Klinkel, S. Govingjee, Anisotropic bending-torsion coupling for warping in a non-linear beam, *Computational Mechanics* 31 (2003) 78-87.

[1. 64] M. Ganapathi, B. Patel, O. Polit, M. Touratier, A C-1 finite element including transverse shear and torsion warping for rectangular sandwich beams, *International Journal for Numerical Methods in Engineering* 45 (1999) 47-75.

[1. 65] S. H. R. Eslimy-Isfahany, J. R. Banerjee, Use of generalized mass in the interpretation of dynamic response of bending-torsion coupled beams, *Journal of Sound and Vibration* 238 (2000) 295-308.

[1. 66] J. Banerjee, H. Su, Free Transverse and Lateral Vibration of Beams with Torsional Coupling, *Journal of Aerospace Engineering* 19 (2006) 13-20.

[1. 67] E. Sapountzakis, V. Mokos, Dynamic analysis of 3-D beam elements including warping and shear deformation effects, *International Journal of Solids and Structures* 43 (2006) 6707-6726.

[1. 68] J. Banerjee, H. Su, Dynamic stiffness formulation and free vibration analysis of a spinning composite beam, *Computers & Structures* 84 (2006) 1208-1214.

[1. 69] M. Kaya, O. Ozgumus, Flexural-torsional-coupled vibration analysis of axially loaded closed-section composite Timoshenko beam by using DTM, *Journal of Sound and Vibration* 306 (2007) 495-506.

[1. 70] E. Sapountzakis, J. Dourakopoulos, Shear deformation effect in flexural-torsional vibrations of beams by BEM, *Acta Mechanica* 203 (2009) 197-221.

[1. 71] J. Lee, S.-E. Kim, Flexural-torsional buckling of thin-walled I-section composites, *Computers & Structures* 79 (2001) 987 – 995.

[1. 72] M. R. M. Crespo da Silva, C. L. Zaretzky, Nonlinear Flexural-Flexural-Torsional Interactions in Beams Including the Effect of Torsional Dynamics. I: Primary Resonance, *Nonlinear Dynamics* 5 (1994) 3-23.

[1. 73] I. Sharf, Geometrically non-linear beam element for dynamic simulation of multibody systems, *International Journal for Numerical Methods in Engineering* 39 (1996) 763-786.

[1. 74] P. Pai, A. Palazotto, Large-deformation analysis of flexible beams, *International Journal of Solids and Structures* 33 (1996) 1335-1353.

[1. 75] C. Pacoste, A. Eriksson, Beam elements in instability problems, *Computer Methods in Applied Mechanics and Engineering* 144 (1997) 163-197.

[1. 76] E. Petrov, M. Géradin, Finite element theory for curved and twisted beams based on exact solutions for three-dimensional solids, Part 1: Beam concept and geometrically exact nonlinear formulation, *Computer Methods in Applied Mechanics and Engineering* 165 (1998) 43-92.

[1. 77] B. Patel, M. Ganapathi, Non-linear torsional vibration and damping analysis of sandwich beams, *Journal of Sound and Vibration* 240 (2001) 385 – 393.

[1. 78] D. Cao, R. Tucker, Nonlinear dynamics of elastic rods using the Cosserat theory: Modelling and simulation, *International Journal of Solids and Structures* 45 (2008) 460-477.

[1. 79] E. Sapountzakis, J. Dourakopoulos, Nonlinear dynamic analysis of Timoshenko beams by BEM. Part I: Theory and numerical implementation, *Nonlinear Dynamics* 58 (2009) 295-306.

[1. 80] E. Sapountzakis, J. Dourakopoulos, Nonlinear dynamic analysis of Timoshenko beams by BEM. Part II: applications and validation, *Nonlinear Dynamics* 58 (2009) 307-318.

[1. 81] J. Fonseca, P. Ribeiro, Beam *p*-version finite element for geometrically non-linear vibrations in space, *Computer Methods in Applied Mechanics and Engineering* 195 (2006) 905-924.

[1. 82] R. Alonso, P. Ribeiro, Flexural and torsional non-linear free vibrations of beams using a p-version finite element, *Computers & Structures* 86 (2008) 1189-1197.

[1. 83] S. Agarwal, A. Chakraborty, S. Gopalakrishnan, Large deformation analysis for anisotropic and inhomogeneous beams using exact linear static solutions, *Composite Structures* 72 (2006) 91-104.

[1. 84] P. F. Pai, A. H. Nayfeh, Non-linear non-planar oscillations of a cantilever beam under lateral base excitations, *International Journal of Non-Linear Mechanics* 25 (1990) 455-414.

[1. 85] J. Cusumano, F. Moon, Chaotic nonplanar vibrations of the thin elastica, part II: derivation and analysis of a low-dimensional model, *Journal of Sound and Vibration* 179 (1995) 209-226.

[1. 86] J. Cusumano, D-C. Lin, Bifurcation and modal interaction in a simplified model of bending torsion vibrations of the thin elastica, *Journal of Vibration and Acoustics* 117 (1995) 30–42.

[1. 87] E. Sapountzakis, J. Dourakopoulos, Flexural-torsional postbuckling analysis of beams of arbitrary cross section, *Acta Mechanica* 209 (2010) 67-84.

[1. 88] F. Mohri, L. Azrar, M. Potier-Ferry, Flexural-torsional post-buckling analysis of thin-walled elements with open sections, *Thin-Walled Structures* 39 (2001) 907-938.

[1. 89] F. Mohri, N. Damil, M. Potier-Ferry, Large torsion finite element model for thin-walled beams, *Computers & Structures* 86 (2008) 671–683.

[1. 90] J. Cardoso, N. Benedito, A. Valido, Finite element analysis of thin-walled composite laminated beams with geometrically nonlinear behavior including warping deformation, *Thin-Walled Structures* 47 (2009) 1363-1372.

[1. 91] B. Balachandran, A. Nayfeh, Nonlinear motions of beam mass structures, *Nonlinear Dynamics* 1 (1990) 39-61.

[1. 92] J. Warminski, M. Cartmell, M. Bochenski, I. Ivanov, Analytical and experimental investigations of an autoparametric beam structure, *Journal of Sound and Vibration* 315 (2008) 486–508.

[1. 93] D. Hodges, M. Rutkowski, Free-Vibration Analysis of Rotating Beams by a Variable-Order Finite-Element Method, *AIAA Journal* 19 (1981) 1459-1466.

[1. 94] T. Yokoyama, Free Vibration Characteristics of Rotating Timoshenko Beams, *International Journal of Mechanical Sciences* 30 (1988) 743-755.

[1. 95] A. Bazoune, Y. Khulief, N. Stephen, Further Results for Modal Characteristics of Rotating Tapered Timoshenko Beams, *Journal of Sound and Vibration* 219 (1999) 157-174.

[1. 96] J. Banerjee, Free Vibration of Centrifugally Stiffened Uniform and Tapered Beams Using the Dynamic Stiffness Method, *Journal of Sound and Vibration* 233 (2000) 857 – 875.

[1. 97] J. Banerjee, Dynamic Stiffness Formulation and Free Vibration Analysis of Centrifugally Stiffened Timoshenko Beams, *Journal of Sound and Vibration* 247 (2001) 97 – 115.

[1. 98] S. Lin, K. Hsiao, Vibration Analysis of a Rotating Timoshenko Beam, *Journal of Sound and Vibration* 240 (2001) 303 – 322.

[1. 99] G. Wang, N. Wereley, Free Vibration Analysis of Rotating Blades with Uniform Tapers, *AIAA Journal* 42 (2004) 2429-2437.

[1. 100] B. Yardimoglu, Vibration analysis of rotating tapered Timoshenko beams by a new finite element model, *Shock and Vibration* 13 (2006) 117 – 126.

[1. 101] J. Banerjee, H. Jackson, Free vibration of rotating tapered beams using the dynamic stiffness method, *Journal of Sound and Vibration* 298 (2006) 1034 – 1054.

[1. 102] J. Gunda, A. Singh, P. Chhabra, R. Ganguli, Free vibration analysis of rotating tapered blades using Fourier-*p* supplement, *Structural Engineering and Mechanics* 27 (2007) 243-257.

[1. 103] S. Lee, J. Sheu, Free Vibrations of a Rotating Inclined Beam, *Journal of Applied Mechanics* 74 (2007) 406 – 414.

[1. 104] H. H. Yoo, J. E. Cho, J. Chung, Modal analysis and shape optimization of rotating cantilever beams, *Journal of Sound and Vibration* 290 (2006) 223-241.

[1. 105] E. Pesheck, C. Pierre, S. Shaw, Modal Reduction of a Nonlinear Rotating Beam Through Nonlinear Normal Modes, *Journal of Vibration and Acoustics* 124 (2002) 229-236.

[1. 106] Ö. Turhan, G. Bulut, On Nonlinear Vibrations of a Rotating Beam, *Journal of Sound and Vibration* 322 (2009) 314-335.

[1. 107] D. Younesian, E. Esmailzadeh, Non-linear Vibration of Variable Speed Rotating Viscoelastic Beams, *Nonlinear Dynamics* 60 (2010) 193-205.

[1. 108] J. Ambrósio, P. Nikravesh, Elasto-plastic deformations in multibody dynamics, *Nonlinear Dynamics* 3 (1992) 85-104.

[1. 109] J. Ambrósio, Dynamics of structures undergoing gross motion and nonlinear deformations: a multibody approach, *Computers & Structures* 59 (1996) 1001-1012.

[1. 110] M. Neto, J. Ambrósio, R. Leal, Composite materials in flexible multibody systems, *Computer Methods in Applied Mechanics and Engineering* 195 (2006) 6860-6873.

[1. 111] W. Yu, D. Hodges, On Timoshenko-like modeling of initially curved and twisted composite beams, *International Journal of Solids and Structures* 39 (2002) 5101–5121.

[1. 112] N.K. Chandiramani, L. Librescu, C.D. Shete, On the free-vibration rotating composite beams using a higher-order shear formulation, *Aerospace Science and Technology* 6 (2002) 545-561.

[1. 113] N. Chandiramani, C. Shete, L. Librescu, Vibration of higher-order-shearable pretwisted rotating composite blades, *International Journal of Mechanical Sciences* 45 (2003) 2017 – 2041.

[1. 114] L. Maqueda, O. Bauchau, A. Shabana, Effect of the Centrifugal Forces on the Finite Element Eigenvalue Solution of a Rotating Blade: a Comparative Study, *Multibody System Dynamics* 19 (2008) 281 – 302.

[1. 115] A. Bazoune, Y. A. Khulief, N. G. Stephen, M. A. Mohiuddin, Dynamic response of spinning tapered Timoshenko beams using modal reduction, *Finite Elements in Analysis and Design* 37 (2001) 199-219.

[1. 116] K. V. Avramov, C. Pierre, N. V. Shyriaieva, Nonlinear Equations of Flexural-Flexural-Torsional Oscillations of Rotating Beams with Arbitrary Cross-Section, *International Applied Mechanics* 44 (2008) 582-589.

[1. 117] O. O. Ozgumus, M. O. Kaya, Energy expressions and free vibration analysis of a rotating double tapered Timoshenko beam featuring bending-torsion coupling, *International Journal of Engineering Science* 45 (2007) 562-586.

2

Models for Beams Vibrating in Space

2. 1. Introduction

In this chapter, two beam models for geometrically nonlinear vibrations in space are presented. Each model is based on a specific beam *p*-version finite element with hierarchical sets of shape functions. The first element follows Timoshenko's theory for flexure, assumes that the cross section rotates as a rigid body and is free to warp in the longitudinal direction, as in Saint-Venants's theory for torsion, i.e. warping is the same for all cross sections. The element is capable of transverse deformations in any plane, longitudinal deformation and cross sectional rotations about three perpendicular reference axes. The second element differs from the first because it assumes Bernoulli-Euler's theory for flexure. It is shown in Chapter 3 that the model based on the second element leads to wrong results when bending is coupled with torsion and because of this it is not developed in detail. Large, rigid body like, motions are not admitted in any of the models presented in this chapter.

The beam under consideration in this chapter is assumed to be of length l and of rectangular cross section with width b and uniform thickness h. The coordinate system is chosen such that the geometric centre of the beam coincides with the origin of the coordinate system (Figure 2. 1). The beam's material is assumed to be elastic, homogeneous and isotropic. The equation of motion derived here is applicable to beams with any symmetrical cross sections, but developed with the appropriate warping function, calculated analytically or numerically.

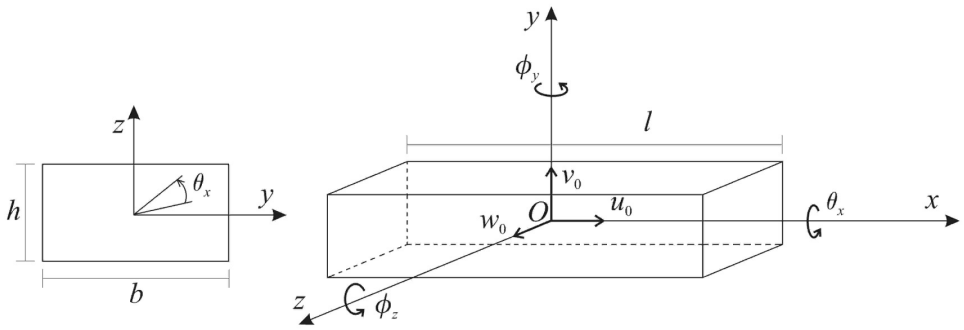

Figure 2. 1. Axes and displacements of the beam element.

2. 2. Equation of motion in the time domain following Timoshenko's and Saint-Venant's theories

The displacement components *u*, *v* and *w* are functions of time and of coordinates *x*, *y* and *z*. The beam model is based on Timoshenko's theory for flexure [2. 1] and Saint-Venant's theory for torsion [2. 2]. By adding the contributions of the corresponding theories, the displacement fields of these models are written as:

$$u(x,y,z,t) = u_0(x,t) - y\,\phi_z(x,t) + z\,\phi_y(x,t) + \psi(y,z)\frac{\partial\theta_x}{\partial x}(x,t),$$

$$v(x,y,z,t) = v_0(x,t) + y\cos\big(\theta_x(x,t)\big) - y - z\sin\big(\theta_x(x,t)\big), \qquad (2.\ 1)$$

$$w(x,y,z,t) = w_0(x,t) + y\sin\big(\theta_x(x,t)\big) + z\cos\big(\theta_x(x,t)\big) - z,$$

where the subscript "0" represents axis *x* (*y* = 0, *z* = 0; *x* contains the cross section centroids of the undeformed beam, that will be often designed as middle line or reference line, in bending it coincides with neutral line) and *t* represents time. *u*, *v* and *w* are, in this order, the displacements along *x*, *y* and *z*; θ_x is the rotation of the cross section about the longitudinal axis *x*; ϕ_y and ϕ_z denote rotations of the cross section about *y* and *z* axes, respectively, from Timoshenko's theory, and $\psi(y,z)$ is the warping function.

It is demonstrated in this paragraph how the displacements in *y* and *z* direction due to torsion are achieved. Since it is assumed that in torsion the cross section rotates as a rigid body and may deform only in the longitudinal direction due to warping, the displacements v and w can be expressed exactly. Let's assume that point $P(y_P,\ z_P)$ is an arbitrary point in the cross section of the beam (Figure 2. 2). After deformation, i.e. rotation of the cross section of θ_x rad, point *P* moves to point *P*' with coordinates

$(y_P + v,\ z_P + w)$. The displacements v and w can be calculated from the initial position of point P - $(y_P,\ z_P)$ and the rotational angle - θ_x. For centre of the coordinate system, is chosen point O, which is unmovable due to rotation (for rectangular cross section, point O is the geometric centre):

$$v = r\cos(\alpha_0 + \theta_x) - r\cos(\alpha_0) = y_P\cos(\theta_x) - z_P\sin(\theta_x) - y_P,$$
$$w = r\sin(\alpha_0 + \theta_x) - r\sin(\alpha_0) = z_P\cos(\theta_x) + y_P\sin(\theta_x) - z_P, \quad (2.\ 2)$$

where α_0 is the angle between the vector $\overrightarrow{OP}$ and the y axis, $r = \sqrt{y_P^2 + z_P^2}$ is the length of $\overrightarrow{OP}$, $\cos(\alpha_0) = y_P/\sqrt{y_P^2 + z_P^2}$ and $\sin(\alpha_0) = z_P/\sqrt{y_P^2 + z_P^2}$.

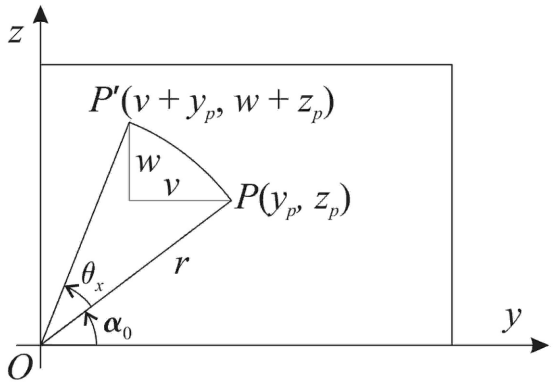

Figure 2. 2. Beam cross section.

It is important to note that the common approximation

$$\sin\big(\theta_x(x,t)\big) \approx \theta_x(x,t) \text{ and } \cos\big(\theta_x(x,t)\big) \approx 1, \quad (2.\ 3)$$

which is only valid for small angles is not applied in equation (2. 1). If we consider only torsion in the displacement fields and the trigonometric terms $\sin\big(\theta_x(x,t)\big)$ and $\cos\big(\theta_x(x,t)\big)$ are also considered, like in (2. 1), then the strain-displacement expressions do not have any trigonometric functions because either they cancel or disappear after applying the basic trigonometric formula

$$\sin\big(\theta_x(x,t)\big)^2 + \cos\big(\theta_x(x,t)\big)^2 = 1. \quad (2.\ 4)$$

The expressions for the strains obtained in this way are more accurate than the expressions that can be obtained if the trigonometric function were approximated by equation (2. 3) directly in equations (2. 1), as is often done. The difference is that in the latter case two spurious terms of second order appear in the shear strains. The inclusion

of these two nonlinear terms in the model gives, inaccurately, smaller torsional displacement. A numerical comparison of the two approaches is shown in Chapter 3. The error becomes more important for beams with height smaller than the width. Hence, in this work the displacements will be expressed using the trigonometric functions as written in equations (2. 1).

In this chapter, only beams with rectangular cross sections, made out of isotropic materials and without external forces acting on the lateral surface in the axial direction are analysed. The warping function employed is the one derived by Sokolnikoff in reference [2. 3] for these conditions, which is the following:

$$\psi(y,z) = yz - \frac{8b^2}{\pi^3}\sum_{n=0}^{\infty}\frac{(-1)^n}{(2n+1)^3}\frac{\sinh(k_n z)}{\cosh(k_n h/2)}\sin(k_n y), \qquad (2.\ 5)$$

$$k_n = \frac{(2n+1)\pi}{b}.$$

The warping function for a beam of square cross section is represented in Figure 2. 3.

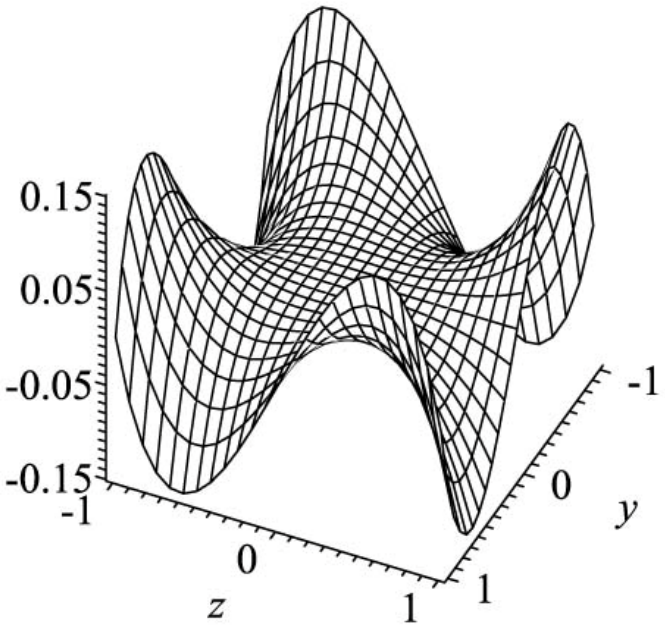

Figure 2. 3.Warping function of square cross section.

Geometrically nonlinear deformation is considered and the axial and shear strains are, at this stage, derived from Green's strain tensor [2. 4] but neglecting the longitudinal terms of second order (2. 6). By using the full Green tensor, it is demonstrated in Chapter 3 that

these terms do not influence the displacement components for moderately large displacements.

$$\varepsilon_x = \frac{\partial u}{\partial x} + \frac{1}{2}\left(\frac{\partial v}{\partial x}\right)^2 + \frac{1}{2}\left(\frac{\partial w}{\partial x}\right)^2,$$

$$\gamma_{zx} = \frac{\partial w}{\partial x} + \frac{\partial u}{\partial z} + \frac{\partial v}{\partial z}\frac{\partial v}{\partial x} + \frac{\partial w}{\partial z}\frac{\partial w}{\partial x}, \tag{2. 6}$$

$$\gamma_{xy} = \frac{\partial u}{\partial y} + \frac{\partial v}{\partial x} + \frac{\partial v}{\partial x}\frac{\partial v}{\partial y} + \frac{\partial w}{\partial x}\frac{\partial w}{\partial y}.$$

Considering the displacements defined in equations (2. 1), the following expressions are obtained for the strains:

$$\varepsilon_x = \frac{\partial u_0}{\partial x} - y\frac{\partial \phi_z}{\partial x} + z\frac{\partial \phi_y}{\partial x} + \psi\frac{\partial^2 \theta_x}{\partial x^2} + \frac{1}{2}\left(\frac{\partial v_0}{\partial x}\right)^2 + \frac{1}{2}\left(\frac{\partial w_0}{\partial x}\right)^2 +$$

$$+\frac{1}{2}y^2\left(\frac{\partial \theta_x}{\partial x}\right)^2 + \frac{1}{2}z^2\left(\frac{\partial \theta_x}{\partial x}\right)^2 - z\frac{\partial v_0}{\partial x}\cos(\theta_x)\frac{\partial \theta_x}{\partial x} + y\frac{\partial w_0}{\partial x}\cos(\theta_x)\frac{\partial \theta_x}{\partial x} - \tag{2. 7}$$

$$-y\frac{\partial v_0}{\partial x}\sin(\theta_x)\frac{\partial \theta_x}{\partial x} - z\frac{\partial w_0}{\partial x}\sin(\theta_x)\frac{\partial \theta_x}{\partial x},$$

$$\gamma_{zx} = \frac{\partial \psi}{\partial z}\frac{\partial \theta_x}{\partial x} + y\frac{\partial \theta_x}{\partial x} + \frac{\partial w_0}{\partial x}\cos(\theta_x) + \phi_y - \frac{\partial v_0}{\partial x}\sin(\theta_x), \tag{2. 8}$$

$$\gamma_{xy} = \frac{\partial \psi}{\partial y}\frac{\partial \theta_x}{\partial x} - z\frac{\partial \theta_x}{\partial x} + \frac{\partial v_0}{\partial x}\cos(\theta_x) - \phi_z + \frac{\partial w_0}{\partial x}\sin(\theta_x). \tag{2. 9}$$

Implementing approximation (2. 3), only at this stage, the following expressions result:

$$\varepsilon_x = \frac{\partial u_0}{\partial x} - y\frac{\partial \phi_z}{\partial x} + z\frac{\partial \phi_y}{\partial x} + \psi\frac{\partial^2 \theta_x}{\partial x^2} + \frac{1}{2}\left(\frac{\partial v_0}{\partial x}\right)^2 + \frac{1}{2}\left(\frac{\partial w_0}{\partial x}\right)^2 +$$

$$+\frac{1}{2}y^2\left(\frac{\partial \theta_x}{\partial x}\right)^2 + \frac{1}{2}z^2\left(\frac{\partial \theta_x}{\partial x}\right)^2 - z\frac{\partial v_0}{\partial x}\frac{\partial \theta_x}{\partial x} + y\frac{\partial w_0}{\partial x}\frac{\partial \theta_x}{\partial x} - \tag{2. 10}$$

$$-y\frac{\partial v_0}{\partial x}\theta_x\frac{\partial \theta_x}{\partial x} - z\frac{\partial w_0}{\partial x}\theta_x\frac{\partial \theta_x}{\partial x},$$

$$\gamma_{zx} = \frac{\partial \psi}{\partial z}\frac{\partial \theta_x}{\partial x} + y\frac{\partial \theta_x}{\partial x} + \frac{\partial w_0}{\partial x} + \phi_y - \frac{\partial v_0}{\partial x}\theta_x, \tag{2. 11}$$

$$\gamma_{xy} = \frac{\partial \psi}{\partial y}\frac{\partial \theta_x}{\partial x} - z\frac{\partial \theta_x}{\partial x} + \frac{\partial v_0}{\partial x} - \phi_z + \frac{\partial w_0}{\partial x}\theta_x. \tag{2. 12}$$

Numerical tests that were carried out in Chapter 3 indicate that the third-order terms that appear in the direct strain (2. 10) are small and do not change the solution. Because of this they are neglected in the remaining part of this work.

It is noted that the displacement field (2. 1) leads to transverse strains ε_y and ε_y and to shear strain γ_{yz} with zero linear parts. Hence, by applying generalized Hooke's law, one would obtain direct stresses σ_y and σ_z, and shear stress τ_{yz}. However, the displacement field (2. 1) does not intend to allow for a proper computation of these strains from the constitutive relations: the only spatial variable most functions depend upon is *x*, as is appropriate in beams, where the dimensions of the cross section are small in comparison with the length. Stresses σ_y and σ_z, and shear stress τ_{yz} will be neglected here, where bending and torsion are of interest. Actually, it was verified in this work, and it was shown for 2D beams in [2. 5], that the inclusion these stresses together with the displacement fields assumed here leads to wrong natural frequencies.

The displacements of the beam neutral axis are expressed in local coordinate system in the form:

$$\{d_0\} = \begin{Bmatrix} u_0(\xi,t) \\ v_0(\xi,t) \\ w_0(\xi,t) \\ \theta_x(\xi,t) \\ \phi_y(\xi,t) \\ \phi_z(\xi,t) \end{Bmatrix} = [N(\xi)]\{q(t)\}, \tag{2. 13}$$

where $\{q(t)\}$ is the vector of generalized coordinates, dependent on time:

$$\{q(t)\} = \begin{Bmatrix} \boldsymbol{q_u}(t) \\ \boldsymbol{q_v}(t) \\ \boldsymbol{q_w}(t) \\ \boldsymbol{q_{\theta_x}}(t) \\ \boldsymbol{q_{\phi_y}}(t) \\ \boldsymbol{q_{\phi_z}}(t) \end{Bmatrix}. \tag{2. 14}$$

The vector $\{q(t)\}$ will be called also vector of generalized displacements, which is widely used in the finite element analysis books. Matrices and vectors are presented in brackets or in bold format. $[N(\xi)]$ is the matrix of shape functions:

$$[N(\xi)] = \begin{bmatrix} \lfloor N^u(\xi) \rfloor & 0 & 0 & 0 & 0 & 0 \\ 0 & \lfloor N^v(\xi) \rfloor & 0 & 0 & 0 & 0 \\ 0 & 0 & \lfloor N^w(\xi) \rfloor & 0 & 0 & 0 \\ 0 & 0 & 0 & \left\lfloor N^{\theta_x}(\xi) \right\rfloor & 0 & 0 \\ 0 & 0 & 0 & 0 & \left\lfloor N^{\phi_y}(\xi) \right\rfloor & 0 \\ 0 & 0 & 0 & 0 & 0 & \left\lfloor N^{\phi_z}(\xi) \right\rfloor \end{bmatrix}. \quad (2.\ 15)$$

$\lfloor N^u(\xi) \rfloor$, $\lfloor N^v(\xi) \rfloor$, $\lfloor N^w(\xi) \rfloor$, $\left\lfloor N^{\theta_x}(\xi) \right\rfloor$, $\left\lfloor N^{\phi_y}(\xi) \right\rfloor$ and $\left\lfloor N^{\phi_z}(\xi) \right\rfloor$ are, in this order, the row vectors of longitudinal, transverse along *y*, transverse along *z*, torsional, rotational about *y* and rotational about *z* shape functions:

$$\begin{aligned} \lfloor N^u(\xi) \rfloor &= \lfloor g_1(\xi) \quad g_2(\xi) \quad \cdots \quad g_{p_u}(\xi) \rfloor, \\ \lfloor N^v(\xi) \rfloor &= \lfloor f_1(\xi) \quad f_2(\xi) \quad \cdots \quad f_{p_v}(\xi) \rfloor, \\ \lfloor N^w(\xi) \rfloor &= \lfloor f_1(\xi) \quad f_2(\xi) \quad \cdots \quad f_{p_w}(\xi) \rfloor, \\ \left\lfloor N^{\theta_x}(\xi) \right\rfloor &= \left\lfloor g_1(\xi) \quad g_2(\xi) \quad \cdots \quad g_{p_{\theta_x}}(\xi) \right\rfloor, \\ \left\lfloor N^{\phi_y}(\xi) \right\rfloor &= \left\lfloor h_1(\xi) \quad h_2(\xi) \quad \cdots \quad h_{p_{\phi_y}}(\xi) \right\rfloor, \\ \left\lfloor N^{\phi_z}(\xi) \right\rfloor &= \left\lfloor h_1(\xi) \quad h_2(\xi) \quad \cdots \quad h_{p_{\phi_z}}(\xi) \right\rfloor, \end{aligned} \quad (2.\ 16)$$

where ξ is a non-dimensional, local coordinate, such that $\xi \in [-1 \ldots 1]$. In the vast majority of the numerical applications carried out in this work, the beams were represented by a single *p*-version finite element. In this case, ξ is given by:

$$\xi = \frac{2x}{l}. \quad (2.\ 17)$$

p_u, p_v, p_w, p_{θ_x}, p_{ϕ_y} and p_{ϕ_z} are the number of shape functions used for each displacement and rotation component in the finite element.

When both boundaries are clamped, the longitudinal and torsional shape functions are, in this work, given by:

$$g_{r-2}(\xi) = \sum_{n=0}^{\mathrm{INT}(r/2)} \frac{(-1)^n (2r-2n-5)!!}{2^n n!\,(r-2n-1)!} \xi^{r-2n-1}, \quad r > 2, \tag{2. 18}$$

the transverse shape functions are given by:

$$f_{r-4}(\xi) = \sum_{n=0}^{\mathrm{INT}(r/2)} \frac{(-1)^n (2r-2n-7)!!}{2^n n!\,(r-2n-1)!} \xi^{r-2n-1}, \quad r > 4, \tag{2. 19}$$

and the shape functions used for the rotations along the transverse axes *y* and *z* are given by:

$$h_{r-3}(\xi) = \sum_{n=0}^{\mathrm{INT}(r/2)} \frac{(-1)^n (2r-2n-5)!!}{2^n n!\,(r-2n-1)!} \xi^{r-2n-1}, \quad r > 3, \tag{2. 20}$$

where $r!! = r(r-2)\ldots(2 \text{ or } 1)$, $0!! = (-1)!! = 1$ and $\mathrm{INT}(r/2)$ denotes the integer part of $r/2$. If only one element is employed, as will be almost always the case, these shape functions satisfy the geometric boundary conditions of clamped-clamped beams (no displacement, no rotation). These shape functions were successfully used in many works, for example [2. 6]-[2. 8]. To analyse beams with different boundary conditions, or to employ more than one finite element, other shape functions, as for example Hermite cubics [2. 9], are added to the finite elements.

A shear correction factor is included in the shear strains associated with bending vibrations. Since, in the present expressions for the shear strains terms related with torsion also appear, we cannot apply, as common, the shear correction factor in Hooke's law. Instead, a square root of the shear correction factor will be applied solely to the bending terms of the shear strains. As a result, the expressions of virtual internal work related with the bending terms will be multiplied by the shear correction factor, and the expressions related with torsion will not contain a shear correction factor. For example, the shear strains γ_{zx} and γ_{xy} from Eqs. (2. 11) and (2. 12) will be replaced by:

$$\begin{aligned} \gamma_{zx} &= \frac{\partial \psi}{\partial z}\frac{\partial \theta_x}{\partial x} + y\frac{\partial \theta_x}{\partial x} + \sqrt{\lambda}\frac{\partial w_0}{\partial x} + \sqrt{\lambda}\phi_y - \sqrt{\lambda}\frac{\partial v_0}{\partial x}\theta_x, \\ \gamma_{xy} &= \frac{\partial \psi}{\partial y}\frac{\partial \theta_x}{\partial x} - z\frac{\partial \theta_x}{\partial x} + \sqrt{\lambda}\frac{\partial v_0}{\partial x} - \sqrt{\lambda}\phi_z + \sqrt{\lambda}\frac{\partial w_0}{\partial x}\theta_x, \end{aligned} \tag{2. 21}$$

where λ is the shear correction factor. According to [2. 10], $\lambda = (5 + 5\nu)/(6 + 5\nu)$ gives appropriate values for beams with rectangular cross section, therefore it will be used in the model; ν is the Poisson's ratio.

The equation of motion is obtained by applying the principle of virtual work [2. 11]:

$$\delta W_V + \delta W_{in} + \delta W_E = 0, \tag{2. 22}$$

where δW_V, δW_{in} and δW_E are the virtual work of internal, inertia and external forces due to a virtual displacement. The weight of the beam is not taken into account. The vector of virtual displacement components will be represented by $\{\delta d\}$ and can be written as:

$$\{\delta d\} = \begin{Bmatrix} \delta u \\ \delta v \\ \delta w \end{Bmatrix}. \tag{2. 23}$$

The virtual works of internal, inertia and external forces are defined as:

$$\delta W_V = -\int_V \{\delta\varepsilon\}^{\mathrm{T}}\{\sigma\}dV = -\{\delta q\}^{\mathrm{T}}[\mathrm{K}(\{q(t)\})]\{q(t)\}, \tag{2. 24}$$

$$\delta W_{in} = -\int_V \rho\{\delta d\}^{\mathrm{T}}\{\ddot{d}\}dV = -\{\delta q\}^{\mathrm{T}}[\mathrm{M}]\{\ddot{q}(t)\}, \tag{2. 25}$$

$$\delta W_E = \int_V \{\delta d_0\}^{\mathrm{T}}\{\mathrm{F}_0\}dV = \{\delta q\}^{\mathrm{T}}\{\mathrm{F}\}, \tag{2. 26}$$

where $\{\delta\varepsilon\}$ represents the virtual strains and $\{\sigma\}$ the stresses, which are related with the strains by Hooke's law:

$$\{\sigma\} = \begin{Bmatrix} \sigma_x \\ \tau_{zx} \\ \tau_{xy} \end{Bmatrix} = \begin{bmatrix} E & 0 & 0 \\ 0 & G & 0 \\ 0 & 0 & G \end{bmatrix} \begin{Bmatrix} \varepsilon_x \\ \gamma_{zx} \\ \gamma_{xy} \end{Bmatrix} = [\mathrm{D}]\{\varepsilon\}, \tag{2. 27}$$

with E - Young's modulus, G - shear modulus, $\{\ddot{d}\}$ – acceleration of a point of the beam, ρ - density of the beam, $\{\mathrm{F}_0\}$ - external forces on the middle line, $\{\mathrm{F}\}$ - generalized external forces, $\{\delta d_0\}$ - virtual displacements on the middle line.

From equation (2. 22) the partial differential equation of motion of the beam is obtained. The geometric boundary conditions for clamped-clamped beams are given here for completeness:

$$u_0(\xi,t)=0,\ \ \xi=-1,\ \ 1,$$

$$v_0(\xi,t)=0,\ \ \xi=-1,\ \ 1,$$

$$\frac{\partial v_0(\xi,t)}{\partial \xi}=0,\ \ \xi=-1,\ \ 1,$$

$$w_0(\xi,t)=0,\ \ \xi=-1,\ \ 1,$$

$$\frac{\partial w_0(\xi,t)}{\partial \xi}=0,\ \ \xi=-1,\ \ 1, \qquad (2.\ 28)$$

$$\theta_x(\xi,t)=0,\ \ \xi=-1,\ \ 1,$$

$$\phi_y(\xi,t)=0,\ \ \xi=-1,\ \ 1,$$

$$\phi_z(\xi,t)=0,\ \ \xi=-1,\ \ 1.$$

The partial differential equation is discretized into a system of ordinary differential equations by the application of the *p*-version FEM. The geometric boundary conditions are satisfied by the shape functions used in the model.

Replacing equations (2. 24) – (2. 26) into (2. 22), the following equation of motion is obtained:

$$[\mathrm{M}]\{\ddot{q}(t)\}+[\mathrm{K}(\{q(t)\})]\{q(t)\}=\{\mathrm{F}(t)\}, \qquad (2.\ 29)$$

where $[\mathrm{M}]$ is the mass matrix, $[\mathrm{K}(\{q(t)\})]$ is the stiffness matrix, which not only depends on the vector of generalized displacements $\{q(t)\}$ but also contains constant terms, and $\{\mathrm{F}(t)\}$ is the vector of generalized external forces. These matrices are given in the following sub-sections. For the sake of simplicity, function arguments are not always represented.

2. 2. 1. Stiffness matrix

The strain vector may be divided by its linear and nonlinear components:

$$\{\varepsilon\} = \{\varepsilon^L\} + \{\varepsilon^{NL}\} = \begin{Bmatrix} \varepsilon_x^L \\ \gamma_{zx}^L \\ \gamma_{xy}^L \end{Bmatrix} + \begin{Bmatrix} \varepsilon_x^{NL} \\ \gamma_{zx}^{NL} \\ \gamma_{xy}^{NL} \end{Bmatrix}, \tag{2. 30}$$

where $\{\varepsilon^L\}$ is the linear part of the strain and $\{\varepsilon^{NL}\}$ is the nonlinear part given by:

$$\varepsilon_x^L = \frac{\partial u_0}{\partial x} - y\frac{\partial \phi_z}{\partial x} + z\frac{\partial \phi_y}{\partial x} + \psi\frac{\partial^2 \theta_x}{\partial x^2}, \tag{2. 31}$$

$$\gamma_{zx}^L = \frac{\partial \psi}{\partial z}\frac{\partial \theta_x}{\partial x} + y\frac{\partial \theta_x}{\partial x} + \sqrt{\lambda}\frac{\partial w_0}{\partial x} + \sqrt{\lambda}\phi_y, \tag{2. 32}$$

$$\gamma_{xy}^L = \frac{\partial \psi}{\partial y}\frac{\partial \theta_x}{\partial x} - z\frac{\partial \theta_x}{\partial x} + \sqrt{\lambda}\frac{\partial v_0}{\partial x} - \sqrt{\lambda}\phi_z, \tag{2. 33}$$

$$\varepsilon_x^{NL} = \frac{1}{2}\left(\frac{\partial v_0}{\partial x}\right)^2 + \frac{1}{2}\left(\frac{\partial w_0}{\partial x}\right)^2 + \frac{1}{2}y^2\left(\frac{\partial \theta_x}{\partial x}\right)^2 + \frac{1}{2}z^2\left(\frac{\partial \theta_x}{\partial x}\right)^2 - \\ -z\frac{\partial v_0}{\partial x}\frac{\partial \theta_x}{\partial x} + y\frac{\partial w_0}{\partial x}\frac{\partial \theta_x}{\partial x}, \tag{2. 34}$$

$$\gamma_{zx}^{NL} = -\sqrt{\lambda}\frac{\partial v_0}{\partial x}\theta_x, \tag{2. 35}$$

$$\gamma_{xy}^{NL} = \sqrt{\lambda}\frac{\partial w_0}{\partial x}\theta_x. \tag{2. 36}$$

From equation (2. 24), the following expression for δW_V is obtained:

$$\delta W_V = -\int_V (\{\delta\varepsilon^L\}^{\mathrm{T}}[\mathrm{D}]\{\varepsilon^L\} + \{\delta\varepsilon^L\}^{\mathrm{T}}[\mathrm{D}]\{\varepsilon^{NL}\} + \{\delta\varepsilon^{NL}\}^{\mathrm{T}}[\mathrm{D}]\{\varepsilon^L\} + \\ +\{\delta\varepsilon^{NL}\}^{\mathrm{T}}[\mathrm{D}]\{\varepsilon^{NL}\})dV = -\{\delta q\}^{\mathrm{T}}[\mathrm{K1}]\{q(t)\} - \{\delta q\}^{\mathrm{T}}[\mathrm{K2}(\{q(t)\})]\{q(t)\} - \\ -\{\delta q\}^{\mathrm{T}}[\mathrm{K3}(\{q(t)\})]\{q(t)\} - \{\delta q\}^{\mathrm{T}}[\mathrm{K4}(\{q(t)\})]\{q(t)\}. \tag{2. 37}$$

In this equation $[\mathrm{K1}]$ is a matrix of constant terms, $[\mathrm{K2}(\{q(t)\})]$ and $[\mathrm{K3}(\{q(t)\})]$ are matrices that depend linearly on the generalized displacements and $[\mathrm{K4}(\{q(t)\})]$ is a matrix that depends quadratically on the generalized displacements. In the equation of motion (2. 29) the constant matrix $[\mathrm{K1}]$ is multiplied by the generalized displacement vector, thus it will be called linear stiffness matrix. From matrices $[\mathrm{K2}(\{q(t)\})]$ and $[\mathrm{K3}(\{q(t)\})]$ arise nonlinear terms of second order in the equation of motion and matrix

$[\mathrm{K4}(\{q(t)\})]$ originates cubic nonlinear terms. These matrices will be called nonlinear stiffness matrices. The total stiffness matrix has the following form:

$$[\mathrm{K}(\{q(t)\})] = [\mathrm{K1}] + [\mathrm{K2}(\{q(t)\})] + [\mathrm{K3}(\{q(t)\})] + [\mathrm{K4}(\{q(t)\})]. \tag{2. 38}$$

2. 2. 1. 1. Linear stiffness matrix [K1]

The linear stiffness matrix [K1] is defined by the following integral:

$$\int_V \{\delta\varepsilon^L\}^{\mathrm{T}}[\mathrm{D}]\{\varepsilon^L\}dV = \int_V \left(E\ \delta\varepsilon_x^L\ \varepsilon_x^L + G\ \delta\gamma_{zx}^L\ \gamma_{zx}^L + G\ \delta\gamma_{xy}^L\ \gamma_{xy}^L\right)dV. \tag{2. 39}$$

The strains that appear in equation (2. 39) may be expressed with shape functions and generalized coordinates. From equations (2. 31) – (2. 33) we have:

$$\varepsilon_x^L = \frac{\partial\lfloor N^u\rfloor}{\partial x}\{q_u\} - y\frac{\partial\lfloor N^{\phi_z}\rfloor}{\partial x}\{q_{\phi_z}\} + z\frac{\partial\lfloor N^{\phi_y}\rfloor}{\partial x}\left\{q_{\phi_y}\right\} + \psi\frac{\partial^2\lfloor N^{\theta_x}\rfloor}{\partial x^2}\{q_{\theta_x}\}, \tag{2. 40}$$

$$\gamma_{zx}^L = \frac{\partial\psi}{\partial z}\frac{\partial\lfloor N^{\theta_x}\rfloor}{\partial x}\{q_{\theta_x}\} + y\frac{\partial\lfloor N^{\theta_x}\rfloor}{\partial x}\{q_{\theta_x}\} + \sqrt{\lambda}\frac{\partial\lfloor N^{w}\rfloor}{\partial x}\{q_w\} + \sqrt{\lambda}\lfloor N^{\phi_y}\rfloor\left\{q_{\phi_y}\right\}, \tag{2. 41}$$

$$\gamma_{xy}^L = \frac{\partial\psi}{\partial y}\frac{\partial\lfloor N^{\theta_x}\rfloor}{\partial x}\{q_{\theta_x}\} - z\frac{\partial\lfloor N^{\theta_x}\rfloor}{\partial x}\{q_{\theta_x}\} + \sqrt{\lambda}\frac{\partial\lfloor N^{v}\rfloor}{\partial x}\{q_v\} - \sqrt{\lambda}\lfloor N^{\phi_z}\rfloor\{q_{\phi_z}\}. \tag{2. 42}$$

Taking variations on equations (2. 40) – (2. 42) we obtain:

$$\begin{aligned}\delta\varepsilon_x^L = {} & \{\delta q_u\}^{\mathrm{T}}\frac{\partial\lfloor N^u\rfloor^{\mathrm{T}}}{\partial x} - y\left\{\delta q_{\phi_z}\right\}^{\mathrm{T}}\frac{\partial\lfloor N^{\phi_z}\rfloor^{\mathrm{T}}}{\partial x} + z\left\{\delta q_{\phi_y}\right\}^{\mathrm{T}}\frac{\partial\lfloor N^{\phi_y}\rfloor^{\mathrm{T}}}{\partial x} + \\ & + \psi\left\{\delta q_{\theta_x}\right\}^{\mathrm{T}}\frac{\partial^2\lfloor N^{\theta_x}\rfloor^{\mathrm{T}}}{\partial x^2},\end{aligned} \tag{2. 43}$$

$$\begin{aligned}\delta\gamma_{zx}^L = {} & \frac{\partial\psi}{\partial z}\left\{\delta q_{\theta_x}\right\}^{\mathrm{T}}\frac{\partial\lfloor N^{\theta_x}\rfloor^{\mathrm{T}}}{\partial x} + y\left\{\delta q_{\theta_x}\right\}^{\mathrm{T}}\frac{\partial\lfloor N^{\theta_x}\rfloor^{\mathrm{T}}}{\partial x} + \sqrt{\lambda}\{\delta q_w\}^{\mathrm{T}}\frac{\partial\lfloor N^{w}\rfloor^{\mathrm{T}}}{\partial x} + \\ & + \sqrt{\lambda}\left\{\delta q_{\phi_y}\right\}^{\mathrm{T}}\lfloor N^{\phi_y}\rfloor^{\mathrm{T}},\end{aligned} \tag{2. 44}$$

$$\delta\gamma_{xy}^{L} = \frac{\partial\psi}{\partial y}\{\delta q_{\theta_x}\}^{\mathrm{T}}\frac{\partial\lfloor N^{\theta_x}\rfloor^{\mathrm{T}}}{\partial x} - z\{\delta q_{\theta_x}\}^{\mathrm{T}}\frac{\partial\lfloor N^{\theta_x}\rfloor^{\mathrm{T}}}{\partial x} + \sqrt{\lambda}\{\delta q_v\}^{\mathrm{T}}\frac{\partial\lfloor N^{v}\rfloor^{\mathrm{T}}}{\partial x} - \\ -\sqrt{\lambda}\{\delta q_{\phi_z}\}^{\mathrm{T}}\lfloor N^{\phi_z}\rfloor^{\mathrm{T}}. \tag{2. 45}$$

The linear stiffness matrix is obtained by replacing expressions (2. 40)-(2. 45) into equation (2. 39). One should note that doing the integration at equation (2. 39) some of the terms become zero due to the cross sectional symmetry properties. Finally, the linear stiffness matrix has the following form:

$$[\mathrm{K1}] = \begin{bmatrix} \mathbf{K1_{11}} & \mathbf{0} & \mathbf{0} & \mathbf{0} & \mathbf{0} & \mathbf{0} \\ \mathbf{0} & \mathbf{K1_{22}} & \mathbf{0} & \mathbf{0} & \mathbf{0} & \mathbf{K1_{26}} \\ \mathbf{0} & \mathbf{0} & \mathbf{K1_{33}} & \mathbf{0} & \mathbf{K1_{35}} & \mathbf{0} \\ \mathbf{0} & \mathbf{0} & \mathbf{0} & \mathbf{K1_{44}} & \mathbf{0} & \mathbf{0} \\ \mathbf{0} & \mathbf{0} & \mathbf{K1_{35}}^{\mathbf{T}} & \mathbf{0} & \mathbf{K1_{55}} & \mathbf{0} \\ \mathbf{0} & \mathbf{K1_{26}}^{\mathbf{T}} & \mathbf{0} & \mathbf{0} & \mathbf{0} & \mathbf{K1_{66}} \end{bmatrix}, \tag{2. 46}$$

where

$$\mathbf{K1_{11}} = E\int_V \frac{d\lfloor N^u\rfloor^{\mathrm{T}}}{dx}\frac{d\lfloor N^u\rfloor}{dx}dV, \tag{2. 47a}$$

$$\mathbf{K1_{22}} = \lambda G\int_V \frac{d\lfloor N^v\rfloor^{\mathrm{T}}}{dx}\frac{d\lfloor N^v\rfloor}{dx}dV, \tag{2. 47b}$$

$$\mathbf{K1_{26}} = -\lambda G\int_V \frac{d\lfloor N^v\rfloor^{\mathrm{T}}}{dx}\lfloor N^{\phi_z}\rfloor dV, \tag{2. 47c}$$

$$\mathbf{K1_{33}} = \lambda G\int_V \frac{d\lfloor N^w\rfloor^{\mathrm{T}}}{dx}\frac{d\lfloor N^w\rfloor}{dx}dV, \tag{2. 47d}$$

$$\mathbf{K1_{35}} = \lambda G\int_V \frac{d\lfloor N^w\rfloor^{\mathrm{T}}}{dx}\lfloor N^{\phi_y}\rfloor dV, \tag{2. 47e}$$

$$\mathbf{K1_{44}} = \int_V \left(E\psi^2\frac{d^2\lfloor N^{\theta_x}\rfloor^{\mathrm{T}}}{dx^2}\frac{d^2\lfloor N^{\theta_x}\rfloor}{dx^2} + G\left(\frac{\partial\psi}{\partial z}+y\right)^2\frac{d\lfloor N^{\theta_x}\rfloor^{\mathrm{T}}}{dx}\frac{d\lfloor N^{\theta_x}\rfloor}{dx} + \right. \\ \left. + G\left(\frac{\partial\psi}{\partial y}-z\right)^2\frac{d\lfloor N^{\theta_x}\rfloor^{\mathrm{T}}}{dx}\frac{d\lfloor N^{\theta_x}\rfloor}{dx}\right)dV, \tag{2. 47f}$$

$$\mathbf{K1_{55}} = \int_V \left(z^2 E \frac{d\lfloor N^{\phi_y} \rfloor^{\mathrm{T}}}{dx} \frac{d\lfloor N^{\phi_y} \rfloor}{dx} + \lambda G \lfloor N^{\phi_y} \rfloor^{\mathrm{T}} \lfloor N^{\phi_y} \rfloor \right) dV, \tag{2. 47g}$$

$$\mathbf{K1_{66}} = \int_V \left(y^2 E \frac{d\lfloor N^{\phi_z} \rfloor^{\mathrm{T}}}{dx} \frac{d\lfloor N^{\phi_z} \rfloor}{dx} + \lambda G \lfloor N^{\phi_z} \rfloor^{\mathrm{T}} \lfloor N^{\phi_z} \rfloor \right) dV. \tag{2. 47h}$$

2. 2. 1. 2. Nonlinear stiffness matrices [K2] and [K3]

The linearly dependent on vector of generalized displacements $\{q(t)\}$ matrix [K2] results from the following integral, which appears in equation (2. 37):

$$\int_V \{\delta\varepsilon^L\}^T [\mathrm{D}] \{\varepsilon^{NL}\} dV = \int_V \left(E\, \delta\varepsilon_x^L\, \varepsilon_x^{NL} + G\, \delta\gamma_{zx}^L\, \gamma_{zx}^{NL} + G\, \delta\gamma_{xy}^L\, \gamma_{xy}^{NL} \right) dV. \tag{2. 48}$$

The nonlinear strains are given in equations (2. 34) - (2. 36) and are expressed by the shape functions and generalized displacements in the following way:

$$\begin{aligned} \varepsilon_x^{NL} = {} & \frac{1}{2} \frac{\partial v_0}{\partial x} \frac{\partial \lfloor N^v \rfloor}{\partial x} \{q_v\} + \frac{1}{2} \frac{\partial w_0}{\partial x} \frac{\partial \lfloor N^w \rfloor}{\partial x} \{q_w\} + \frac{1}{2} y^2 \frac{\partial \theta_x}{\partial x} \frac{\partial \lfloor N^{\theta_x} \rfloor}{\partial x} \{q_{\theta_x}\} + \\ & + \frac{1}{2} z^2 \frac{\partial \theta_x}{\partial x} \frac{\partial \lfloor N^{\theta_x} \rfloor}{\partial x} \{q_{\theta_x}\} - \frac{1}{2} z \frac{\partial v_0}{\partial x} \frac{\partial \lfloor N^{\theta_x} \rfloor}{\partial x} \{q_{\theta_x}\} - \frac{1}{2} z \frac{\partial \theta_x}{\partial x} \frac{\partial \lfloor N^v \rfloor}{\partial x} \{q_v\} + \\ & + \frac{1}{2} y \frac{\partial w_0}{\partial x} \frac{\partial \lfloor N^{\theta_x} \rfloor}{\partial x} \{q_{\theta_x}\} + \frac{1}{2} y \frac{\partial \theta_x}{\partial x} \frac{\partial \lfloor N^w \rfloor}{\partial x} \{q_w\}, \end{aligned} \tag{2. 49}$$

$$\gamma_{zx}^{NL} = -\frac{1}{2} \sqrt{\lambda} \frac{\partial v_0}{\partial x} \lfloor N^{\theta_x} \rfloor \{q_{\theta_x}\} - \frac{1}{2} \sqrt{\lambda} \theta_x \frac{\partial \lfloor N^v \rfloor}{\partial x} \{q_v\}, \tag{2. 50}$$

$$\gamma_{xy}^{NL} = \frac{1}{2} \sqrt{\lambda} \frac{\partial w_0}{\partial x} \lfloor N^{\theta_x} \rfloor \{q_{\theta_x}\} + \frac{1}{2} \sqrt{\lambda} \theta_x \frac{\partial \lfloor N^w \rfloor}{\partial x} \{q_w\}. \tag{2. 51}$$

It can be noticed that terms like $z \frac{\partial v_0}{\partial x} \frac{\partial \theta_x}{\partial x}$, i.e. terms which are quadratic functions of different displacement fields, are written twice multiplied by $1/2$. In each term, different displacements are represented by shape functions and generalized coordinates. This formulation is preferred here because, as will be shown later, will provide useful relation between matrices [K2] and [K3].

The linear virtual strains are presented in equations (2. 43) - (2. 45). The nonlinear matrix [K2] is obtained by replacing the linear virtual strains (2. 43) - (2. 45) and the nonlinear strains (2. 49) - (2. 51) into equation (2. 48). Matrix [K2] has the following form:

$$[\mathrm{K2}(\{q\})] = \begin{bmatrix} \mathbf{0} & \mathbf{K2_{12}} & \mathbf{K2_{13}} & \mathbf{K2_{14}} & \mathbf{0} & \mathbf{0} \\ \mathbf{0} & \mathbf{0} & \mathbf{K2_{23}} & \mathbf{K2_{24}} & \mathbf{0} & \mathbf{0} \\ \mathbf{0} & \mathbf{K2_{32}} & \mathbf{0} & \mathbf{K2_{34}} & \mathbf{0} & \mathbf{0} \\ \mathbf{0} & \mathbf{0} & \mathbf{0} & \mathbf{0} & \mathbf{0} & \mathbf{0} \\ \mathbf{0} & \mathbf{K2_{52}} & \mathbf{0} & \mathbf{K2_{54}} & \mathbf{0} & \mathbf{0} \\ \mathbf{0} & \mathbf{0} & \mathbf{K2_{63}} & \mathbf{K2_{64}} & \mathbf{0} & \mathbf{0} \end{bmatrix}, \tag{2. 52}$$

where

$$\mathbf{K2_{12}}(\boldsymbol{q_v}) = \frac{1}{2}E\int_V \frac{d\lfloor N^u\rfloor^{\mathrm{T}}}{dx}\frac{d\lfloor N^v\rfloor}{dx}\frac{\partial v_0}{\partial x}dV, \tag{2. 53a}$$

$$\mathbf{K2_{13}}(\boldsymbol{q_w}) = \frac{1}{2}E\int_V \frac{d\lfloor N^u\rfloor^{\mathrm{T}}}{dx}\frac{d\lfloor N^w\rfloor}{dx}\frac{\partial w_0}{\partial x}dV, \tag{2. 53b}$$

$$\mathbf{K2_{14}}(\boldsymbol{q_{\theta_x}}) = \frac{1}{2}E\int_V (y^2+z^2)\frac{d\lfloor N^u\rfloor^{\mathrm{T}}}{dx}\frac{d\lfloor N^{\theta_x}\rfloor}{dx}\frac{\partial \theta_x}{\partial x}dV, \tag{2. 53c}$$

$$\mathbf{K2_{23}}(\boldsymbol{q_{\theta_x}}) = \frac{1}{2}\lambda G\int_V \frac{d\lfloor N^v\rfloor^{\mathrm{T}}}{dx}\frac{d\lfloor N^w\rfloor}{dx}\theta_x\, dV, \tag{2. 53d}$$

$$\mathbf{K2_{24}}(\boldsymbol{q_w}) = \frac{1}{2}\lambda G\int_V \frac{d\lfloor N^v\rfloor^{\mathrm{T}}}{dx}\lfloor N^{\theta_x}\rfloor\frac{\partial w_0}{\partial x}dV, \tag{2. 53e}$$

$$\mathbf{K2_{32}}(\boldsymbol{q_{\theta_x}}) = -\frac{1}{2}\lambda G\int_V \frac{d\lfloor N^w\rfloor^{\mathrm{T}}}{\mathrm{d}x}\frac{d\lfloor N^v\rfloor}{dx}\theta_x\, dV, \tag{2. 53f}$$

$$\mathbf{K2_{34}}(\boldsymbol{q_v}) = -\frac{1}{2}\lambda G\int_V \frac{d\lfloor N^w\rfloor^{\mathrm{T}}}{dx}\lfloor N^{\theta_x}\rfloor\frac{\partial v_0}{\partial x}dV, \tag{2. 53g}$$

$$\mathbf{K2_{52}}(\boldsymbol{q_{\theta_x}}) = -\frac{1}{2}E\int_V z^2\frac{d\lfloor N^{\phi_y}\rfloor^{\mathrm{T}}}{dx}\frac{d\lfloor N^v\rfloor}{dx}\frac{\partial \theta_x}{\partial x}dV - \\ -\frac{1}{2}\lambda G\int_V \lfloor N^{\phi_y}\rfloor^{\mathrm{T}}\frac{d\lfloor N^v\rfloor}{dx}\theta_x\, dV, \tag{2. 53h}$$

$$\mathbf{K2_{54}}(\boldsymbol{q_v}) = -\frac{1}{2}E\int_V z^2\frac{d\lfloor N^{\phi_y}\rfloor^{\mathrm{T}}}{dx}\frac{d\lfloor N^{\theta_x}\rfloor}{dx}\frac{\partial v_0}{\partial x}dV - \\ -\frac{1}{2}\lambda G\int_V \lfloor N^{\phi_y}\rfloor^{\mathrm{T}}\lfloor N^{\theta_x}\rfloor\frac{\partial v_0}{\partial x}d\mathrm{V}, \tag{2. 53i}$$

$$\mathbf{K2_{63}}(\boldsymbol{q_{\theta_x}}) = -\frac{1}{2}E\int_V y^2\frac{d\lfloor N^{\phi_z}\rfloor^{\mathrm{T}}}{dx}\frac{d\lfloor N^{w}\rfloor}{dx}\frac{\partial \theta_x}{\partial x}dV - \\ -\frac{1}{2}\lambda G\int_V \lfloor N^{\phi_z}\rfloor^{\mathrm{T}}\frac{d\lfloor N^{w}\rfloor}{dx}\theta_x\,dV, \tag{2. 53j}$$

$$\mathbf{K2_{64}}(\boldsymbol{q_w}) = -\frac{1}{2}E\int_V y^2\frac{d\lfloor N^{\phi_z}\rfloor^{\mathrm{T}}}{dx}\frac{d\lfloor N^{\theta_x}\rfloor}{dx}\frac{\partial w_0}{\partial x}dV - \\ -\frac{1}{2}\lambda G\int_V \lfloor N^{\phi_z}\rfloor^{\mathrm{T}}\lfloor N^{\theta_x}\rfloor\frac{\partial w_0}{\partial x}dV. \tag{2. 53k}$$

The nonlinear matrix [K3] is defined from the following integral:

$$\int_V \{\delta\varepsilon^{NL}\}^{\mathrm{T}}[\mathrm{D}]\{\varepsilon^{L}\}dV = \int_V \left(E\;\delta\varepsilon_x^{NL}\;\varepsilon_x^{L} + G\;\delta\gamma_{zx}^{NL}\;\gamma_{zx}^{L} + G\;\delta\gamma_{xy}^{NL}\;\gamma_{xy}^{L}\right)dV. \tag{2. 54}$$

The linear strains are given in equations (2. 40) – (2. 42) and the virtual nonlinear strains are expressed by the shape functions and generalized displacements in the following way:

$$\delta\varepsilon_x^{NL} = \{\delta q_v\}^{\mathrm{T}}\frac{\partial\lfloor N^{v}\rfloor^{\mathrm{T}}}{\partial x}\frac{\partial v_0}{\partial x} + z^2\{\delta q_{\theta_x}\}^{\mathrm{T}}\frac{\partial\lfloor N^{\theta_x}\rfloor^{\mathrm{T}}}{\partial x}\frac{\partial\theta_x}{\partial x} + \\ +\{\delta q_w\}^{\mathrm{T}}\frac{\partial\lfloor N^{w}\rfloor^{\mathrm{T}}}{\partial x}\frac{\partial w_0}{\partial x} + y^2\{\delta q_{\theta_x}\}^{\mathrm{T}}\frac{\partial\lfloor N^{\theta_x}\rfloor^{\mathrm{T}}}{\partial x}\frac{\partial\theta_x}{\partial x} - \\ -z\{\delta q_v\}^{\mathrm{T}}\frac{\partial\lfloor N^{v}\rfloor^{\mathrm{T}}}{\partial x}\frac{\partial\theta_x}{\partial x} - z\{\delta q_{\theta_x}\}^{\mathrm{T}}\frac{\partial\lfloor N^{\theta_x}\rfloor^{\mathrm{T}}}{\partial x}\frac{\partial v_0}{\partial x} + \\ +y\{\delta q_w\}^{\mathrm{T}}\frac{\partial\lfloor N^{w}\rfloor^{\mathrm{T}}}{\partial x}\frac{\partial\theta_x}{\partial x} + y\{\delta q_{\theta_x}\}^{\mathrm{T}}\frac{\partial\lfloor N^{\theta_x}\rfloor^{\mathrm{T}}}{\partial x}\frac{\partial w_0}{\partial x}, \tag{2. 55}$$

$$\delta\gamma_{zx}^{NL} = -\sqrt{\lambda}\{\delta q_v\}^{\mathrm{T}}\frac{\partial\lfloor N^{v}\rfloor^{\mathrm{T}}}{\partial x}\theta_x - \sqrt{\lambda}\{\delta q_{\theta_x}\}^{\mathrm{T}}\lfloor N^{\theta_x}\rfloor^{\mathrm{T}}\frac{\partial v_0}{\partial x}, \tag{2. 56}$$

$$\delta\gamma_{xy}^{NL} = \sqrt{\lambda}\{\delta q_w\}^{\mathrm{T}} \frac{\partial \lfloor N^w \rfloor^{\mathrm{T}}}{\partial x}\theta_x + \sqrt{\lambda}\{\delta q_{\theta_x}\}^{\mathrm{T}} \lfloor N^{\theta_x} \rfloor^{\mathrm{T}} \frac{\partial w_0}{\partial x}. \tag{2. 57}$$

From the definition of the linear strains (2. 40) – (2. 42) and from the expressions for the virtual nonlinear strains (2. 55) – (2. 57) it can be seen that the matrices [K2] and [K3] are related by:

$$[\mathrm{K3}(\{q(t)\})] = 2\,[\mathrm{K2}(\{q(t)\})]^{\mathrm{T}}. \tag{2. 58}$$

To demonstrate that this relation holds, only one term of the nonlinear matrix [K3] is presented. It is defined from the first terms of (2. 40) and (2. 55) and occupies position (2, 1) in the matrix [K3]:

$$\mathbf{K3_{21}}(\boldsymbol{q_v}) = E\int_V \frac{d\lfloor N^v \rfloor^{\mathrm{T}}}{dx}\frac{d\lfloor N^u \rfloor}{dx}\frac{\partial v_0}{\partial x}dV, \tag{2. 59}$$

and obviously it is true that:

$$\mathbf{K3_{21}}(\boldsymbol{q_v}) = 2\,\mathbf{K2_{12}}(\boldsymbol{q_v})^{\mathrm{T}}. \tag{2. 60}$$

Thus, the relation (2. 58) is true and it will be used in the current work.

2. 2. 1. 3. Nonlinear stiffness matrix [K4]

The nonlinear matrix [K4] is defined using the following integral:

$$\int_V \{\delta\varepsilon^{NL}\}^{\mathrm{T}}[\mathrm{D}]\{\varepsilon^{NL}\}dV = \int_V \left(E\,\delta\varepsilon_x^{NL}\,\varepsilon_x^{NL} + G\,\delta\gamma_{zx}^{NL}\,\gamma_{zx}^{NL} + G\,\delta\gamma_{xy}^{NL}\,\gamma_{xy}^{NL}\right)dV. \tag{2. 61}$$

The nonlinear strains were given in equations (2. 49) – (2. 51) and the virtual nonlinear strains were given in (2. 55) – (2. 57).

The nonlinear matrix [K4] is obtained by replacing the virtual nonlinear strains (2. 55) – (2. 57) and the nonlinear strains (2. 49) – (2. 51) into equation (2. 61). The nonlinear matrix [K4] has the following form:

$$[\mathrm{K4}(\{q\})] = \begin{bmatrix} \mathbf{0} & \mathbf{0} & \mathbf{0} & \mathbf{0} & \mathbf{0} & \mathbf{0} \\ \mathbf{0} & \mathbf{K4_{22}} & \mathbf{0} & \mathbf{K4_{24}} & \mathbf{0} & \mathbf{0} \\ \mathbf{0} & \mathbf{0} & \mathbf{K4_{33}} & \mathbf{K4_{34}} & \mathbf{0} & \mathbf{0} \\ \mathbf{0} & \mathbf{K4_{24}}^{\mathbf{T}} & \mathbf{K4_{34}}^{\mathbf{T}} & \mathbf{K4_{44}} & \mathbf{0} & \mathbf{0} \\ \mathbf{0} & \mathbf{0} & \mathbf{0} & \mathbf{0} & \mathbf{0} & \mathbf{0} \\ \mathbf{0} & \mathbf{0} & \mathbf{0} & \mathbf{0} & \mathbf{0} & \mathbf{0} \end{bmatrix}, \tag{2. 62}$$

where

$$\mathbf{K4_{22}}(\boldsymbol{q_v}, \boldsymbol{q_w}, \boldsymbol{q_{\theta_x}}) = \frac{1}{2}E\int_V \frac{d\lfloor N^v\rfloor^{\mathrm{T}}}{dx}\frac{d\lfloor N^v\rfloor}{dx}\left(\frac{\partial v_0}{\partial x}\right)^2 dV +$$

$$+\frac{1}{2}E\int_V \frac{d\lfloor N^v\rfloor^{\mathrm{T}}}{dx}\frac{d\lfloor N^v\rfloor}{dx}\left(\frac{\partial w_0}{\partial x}\right)^2 dV + \tag{2. 63a}$$

$$+\frac{1}{2}E\int_V (y^2+z^2)\frac{d\lfloor N^v\rfloor^{\mathrm{T}}}{dx}\frac{d\lfloor N^v\rfloor}{dx}\left(\frac{\partial \theta_x}{\partial x}\right)^2 dV,$$

$$\mathbf{K4_{24}}(\boldsymbol{q_v}, \boldsymbol{q_{\theta_x}}) = E\int_V z^2\frac{d\lfloor N^v\rfloor^{\mathrm{T}}}{dx}\frac{d\lfloor N^{\theta_x}\rfloor}{dx}\frac{\partial v_0}{\partial x}\frac{\partial \theta_x}{\partial x}dV +$$

$$+\lambda G\int_V \frac{d\lfloor N^v\rfloor^{\mathrm{T}}}{dx}\lfloor N^{\theta_x}\rfloor\frac{\partial v_0}{\partial x}\theta_x\, dV, \tag{2. 63b}$$

$$\mathbf{K4_{33}}(\boldsymbol{q_v}, \boldsymbol{q_w}, \boldsymbol{q_{\theta_x}}) = \frac{1}{2}E\int_V \frac{d\lfloor N^w\rfloor^{\mathrm{T}}}{dx}\frac{d\lfloor N^w\rfloor}{dx}\left(\frac{\partial v_0}{\partial x}\right)^2 dV +$$

$$+\frac{1}{2}E\int_V \frac{d\lfloor N^w\rfloor^{\mathrm{T}}}{dx}\frac{d\lfloor N^w\rfloor}{dx}\left(\frac{\partial w_0}{\partial x}\right)^2 dV + \tag{2. 63c}$$

$$+\frac{1}{2}E\int_V (y^2+z^2)\frac{d\lfloor N^w\rfloor^{\mathrm{T}}}{dx}\frac{d\lfloor N^w\rfloor}{dx}\left(\frac{\partial \theta_x}{\partial x}\right)^2 dV,$$

$$\mathbf{K4_{34}}(\boldsymbol{q_w}, \boldsymbol{q_{\theta_x}}) = E\int_V y^2\frac{d\lfloor N^w\rfloor^{\mathrm{T}}}{dx}\frac{d\lfloor N^{\theta_x}\rfloor}{dx}\frac{\partial w_0}{\partial x}\frac{\partial \theta_x}{\partial x}dV +$$

$$+\lambda G\int_V \frac{d\lfloor N^w\rfloor^{\mathrm{T}}}{dx}\lfloor N^{\theta_x}\rfloor\frac{\partial w_0}{\partial x}\theta_x\, dV, \tag{2. 63d}$$

$$\mathbf{K4_{44}}(\boldsymbol{q_v}, \boldsymbol{q_w}, \boldsymbol{q_{\theta_x}}) = \frac{1}{2}E\int_V (y^2+z^2)^2 \frac{d\lfloor N^{\theta_x}\rfloor^{\mathrm{T}}}{dx}\frac{d\lfloor N^{\theta_x}\rfloor}{dx}\left(\frac{\partial\theta_x}{\partial x}\right)^2 dV +$$

$$+\frac{1}{2}E\int_V (y^2+z^2)\frac{d\lfloor N^{\theta_x}\rfloor^{\mathrm{T}}}{dx}\frac{d\lfloor N^{\theta_x}\rfloor}{dx}\left(\frac{\partial v_0}{\partial x}\right)^2 dV + \tag{2. 63e}$$

$$+\frac{1}{2}E\int_V (y^2+z^2)\frac{d\lfloor N^{\theta_x}\rfloor^{\mathrm{T}}}{dx}\frac{d\lfloor N^{\theta_x}\rfloor}{dx}\left(\frac{\partial w_0}{\partial x}\right)^2 dV.$$

2. 2. 2. Mass matrix

The mass matrix is defined in equation (2. 25) and can be derived from the following integral:

$$\int_V \rho\{\delta d\}^{\mathrm{T}}\{\ddot{d}\}dV = \rho\int_V (\delta u\,\ddot{u} + \delta v\,\ddot{v} + \delta w\,\ddot{w})dV. \tag{2. 64}$$

The virtual displacements and the accelerations are derived from equation (2. 1):

$$\delta u = \delta u_0 - y\,\delta\phi_z + z\,\delta\phi_y + \psi\,\delta\left(\frac{\partial\theta_x}{\partial x}\right), \tag{2. 65}$$

$$\delta v = \delta v_0 - y\,\delta\theta_x\sin(\theta_x) - z\,\delta\theta_x\cos(\theta_x), \tag{2. 66}$$

$$\delta w = \delta w_0 + y\,\delta\theta_x\cos(\theta_x) - z\,\delta\theta_x\sin(\theta_x), \tag{2. 67}$$

$$\ddot{u} = \ddot{u}_0 - y\,\ddot{\phi}_z + z\,\ddot{\phi}_y + \psi\,\frac{\partial}{\partial x}\ddot{\theta}_x, \tag{2. 68}$$

$$\ddot{v} = \ddot{v}_0 - y\cos(\theta_x)\,\dot{\theta}_x^{\,2} - y\sin(\theta_x)\,\ddot{\theta}_x + z\sin(\theta_x)\,\dot{\theta}_x^{\,2} - z\cos(\theta_x)\,\ddot{\theta}_x, \tag{2. 69}$$

$$\ddot{w} = \ddot{w}_0 - y\sin(\theta_x)\,\dot{\theta}_x^{\,2} + y\cos(\theta_x)\,\ddot{\theta}_x - z\cos(\theta_x)\,\dot{\theta}_x^{\,2} - z\sin(\theta_x)\,\ddot{\theta}_x. \tag{2. 70}$$

The mass matrix is obtained by replacing expressions (2. 65) - (2. 70) into equation (2. 64). It has the following form:

$$[\mathrm{M}] = \begin{bmatrix} \mathbf{M_{11}} & \mathbf{0} & \mathbf{0} & \mathbf{0} & \mathbf{0} & \mathbf{0} \\ \mathbf{0} & \mathbf{M_{22}} & \mathbf{0} & \mathbf{0} & \mathbf{0} & \mathbf{0} \\ \mathbf{0} & \mathbf{0} & \mathbf{M_{33}} & \mathbf{0} & \mathbf{0} & \mathbf{0} \\ \mathbf{0} & \mathbf{0} & \mathbf{0} & \mathbf{M_{44}} & \mathbf{0} & \mathbf{0} \\ \mathbf{0} & \mathbf{0} & \mathbf{0} & \mathbf{0} & \mathbf{M_{55}} & \mathbf{0} \\ \mathbf{0} & \mathbf{0} & \mathbf{0} & \mathbf{0} & \mathbf{0} & \mathbf{M_{66}} \end{bmatrix}, \tag{2. 71}$$

where

$$\mathbf{M_{11}} = \rho \int_V \lfloor N^u \rfloor^{\mathrm{T}} \lfloor N^u \rfloor dV, \tag{2. 72a}$$

$$\mathbf{M_{22}} = \rho \int_V \lfloor N^v \rfloor^{\mathrm{T}} \lfloor N^v \rfloor dV, \tag{2. 72b}$$

$$\mathbf{M_{33}} = \rho \int_V \lfloor N^w \rfloor^{\mathrm{T}} \lfloor N^w \rfloor dV, \tag{2. 72c}$$

$$\mathbf{M_{44}} = \rho \int_V \left(\psi^2 \frac{d\lfloor N^{\theta_x} \rfloor^{\mathrm{T}}}{dx} \frac{d\lfloor N^{\theta_x} \rfloor}{dx} + (y^2 + z^2) \lfloor N^{\theta_x} \rfloor^{\mathrm{T}} \lfloor N^{\theta_x} \rfloor \right) dV, \tag{2. 72d}$$

$$\mathbf{M_{55}} = \rho \int_V z^2 \lfloor N^{\phi_y} \rfloor^{\mathrm{T}} \lfloor N^{\phi_y} \rfloor dV, \tag{2. 72e}$$

$$\mathbf{M_{66}} = \rho \int_V y^2 \lfloor N^{\phi_z} \rfloor^{\mathrm{T}} \lfloor N^{\phi_z} \rfloor dV. \tag{2. 72f}$$

The integrals which present the mass and the stiffness matrices can be calculated by separating the integration over the volume in two parts: integration over the cross sectional area and integration over the length of the element. Transformation into local coordinates is performed.

In the mass and in the stiffness matrices, many of the terms disappear and were not included in the presentation of these matrices. These terms disappear because the integrals become equal to zero due to the integration over the cross sectional area. Such integrals are the integrals which are odd functions of *y* or *z*, i.e. $\int_\Omega y d\Omega = 0$, $\int_\Omega z d\Omega = 0$, $\int_\Omega yz d\Omega = 0$, $\int_\Omega \psi d\Omega = 0$ and others. The vanishing of the integrals is true only for symmetric cross sections. The equation of motion of beams with non-symmetrical cross sections is derived in Chapter 6 and when the cross section is not symmetric, these

integrals are different from zero and introduce more terms in the equation of motion, including coupling of all displacement fields in linear analysis.

2. 2. 3. Vector of generalized external forces

The vector of generalized external forces is defined in equation (2. 26) and may be derived from the following integral:

$$\delta W_E = \int_V \{\delta d_o\}^{\mathrm{T}}\{\mathrm{F}_0\}dV = \tag{2. 73}$$

$$= \int_V \left(\delta u_o F_x + \delta v_o F_y + \delta w_o F_z + \delta\theta_x M_x + \delta\phi_y M_y + \delta\phi_z M_z\right)dV,$$

where

$$\{\mathrm{F}_0(x,t)\} = \begin{Bmatrix} F_x(x,t) \\ F_y(x,t) \\ F_z(x,t) \\ M_x(x,t) \\ M_y(x,t) \\ M_z(x,t) \end{Bmatrix} \tag{2. 74}$$

is the vector of external forces on the middle line, it depends on the position of the applied load on the beam longitudinal axis and on time, and

$$\{\delta d_0\} = \begin{Bmatrix} \delta u_0 \\ \delta v_0 \\ \delta w_0 \\ \delta\theta_x \\ \delta\phi_y \\ \delta\phi_z \end{Bmatrix} \tag{2. 75}$$

is the vector of virtual displacements on the middle line. The vector of generalized external forces has the following form:

$$\{\mathrm{F}(t)\} = \begin{Bmatrix} \mathbf{F}_{\boldsymbol{u_0}}(t) \\ \mathbf{F}_{\boldsymbol{v_0}}(t) \\ \mathbf{F}_{\boldsymbol{w_0}}(t) \\ \mathbf{F}_{\boldsymbol{\theta_x}}(t) \\ \mathbf{F}_{\boldsymbol{\phi_y}}(t) \\ \mathbf{F}_{\boldsymbol{\phi_z}}(t) \end{Bmatrix}, \tag{2. 76}$$

where

$$\mathbf{F}_{\boldsymbol{u_0}} = \int_V \lfloor N^u \rfloor^{\mathrm{T}} F_x \, dV, \tag{2. 77a}$$

$$\mathbf{F}_{\boldsymbol{v_0}} = \int_V \lfloor N^v \rfloor^{\mathrm{T}} F_y \, dV, \tag{2. 77b}$$

$$\mathbf{F}_{\boldsymbol{w_0}} = \int_V \lfloor N^w \rfloor^{\mathrm{T}} F_z \, dV, \tag{2. 77c}$$

$$\mathbf{F}_{\boldsymbol{\theta_x}} = \int_V \left\lfloor N^{\theta_x} \right\rfloor^{\mathrm{T}} M_x \, dV, \tag{2. 77d}$$

$$\mathbf{F}_{\boldsymbol{\phi_y}} = \int_V \left\lfloor N^{\phi_y} \right\rfloor^{\mathrm{T}} M_y \, dV, \tag{2. 77e}$$

$$\mathbf{F}_{\boldsymbol{\phi_z}} = \int_V \left\lfloor N^{\phi_z} \right\rfloor^{\mathrm{T}} M_z \, dV. \tag{2. 77f}$$

2. 3. Equation of motion in the time domain following Bernoulli-Euler's and Saint-Venant's theories

The displacement components for 3D beam models assuming Bernoulli-Euler's theory for bending might be expressed in two ways:

(i) By direct application of Bernoulli-Euler's assumption, in a sense that it uses the derivatives of the transverse displacements as approximations for the rotations about the transverse axes.

(ii) By imposing the assumption that the shear deformation of the middle line (the neutral line in bending) is constrained to zero.

Both assumptions were used in the literature [2. 12]-[2. 17]; here the differences of a model formulated on the first assumption with respect to the Timoshenko based model given in section 2. 2 and the disadvantages when the first assumption is considered in nonlinear analysis are shown.

The same beam from Figure 2. 1 is considered here, with length *l*, and rectangular cross section with width *b* and uniform thickness *h*. The coordinate system is chosen such that the centre of the beam coincides with the origin of the coordinate system. The beam's material is assumed to be elastic, homogeneous and isotropic.

The displacement components *u*, *v* and *w* are functions of time and of coordinates *x*, *y* and *z*. The beam model is based on Bernoulli-Euler's theory for flexure [2. 1] and Saint-Venant's theory for torsion [2. 2]. By adding the contributions of the corresponding theories, taking into account the Bernoulli-Euler's assumption that a plane cross section perpendicular to the reference axis before deformation remains plane and perpendicular to the deformed reference axis after deformation [2. 5], the displacement fields are respectively written as:

$$\begin{aligned} u(x,y,z,t) &= u_0(x,t) - y\frac{\partial v_0(x,t)}{\partial x} - z\frac{\partial w_0(x,t)}{\partial x} + \psi(y,z)\frac{\partial \theta_x(x,t)}{\partial x}, \\ v(x,y,z,t) &= v_0(x,t) + y\cos\big(\theta_x(x,t)\big) - y - z\sin\big(\theta_x(x,t)\big), \\ w(x,y,z,t) &= w_0(x,t) + y\sin\big(\theta_x(x,t)\big) + z\cos\big(\theta_x(x,t)\big) - z, \end{aligned} \tag{2. 78}$$

where, as in the previous section, the subscript "0" represents the neutral axis in pure bending, which coincides with the cross section centroids, ($y = 0$, $z = 0$) and *t* represents time. *u*, *v* and *w* are, in this order, the displacements along *x*, *y* and *z*; θ_x is the rotation about the longitudinal axis and $\psi(y,z)$ is the warping function defined in equation (2. 5). Actually, assumption (i) was used here, the rotations of the cross section about the transverse axes were approximated by the derivatives of the transverse displacements:

$$\begin{aligned} \phi_z(x,t) &= \frac{\partial v_0(x,t)}{\partial x}, \\ \phi_y(x,t) &= -\frac{\partial \mathrm{w}_0(x,t)}{\partial x}. \end{aligned} \tag{2. 79}$$

Considering the strain-displacement relations given in Eq. (2. 6), the following expressions for the strains are obtained:

$$\varepsilon_x = \frac{\partial u_0}{\partial x} - y\frac{\partial^2 v_0}{\partial x^2} - z\frac{\partial^2 w_0}{\partial x^2} + \psi\frac{\partial^2 \theta_x}{\partial x^2} + \frac{1}{2}\left(\frac{\partial v_0}{\partial x}\right)^2 + \frac{1}{2}\left(\frac{\partial w_0}{\partial x}\right)^2 +$$
$$+\frac{1}{2}y^2\left(\frac{\partial \theta_x}{\partial x}\right)^2 + \frac{1}{2}z^2\left(\frac{\partial \theta_x}{\partial x}\right)^2 - z\frac{\partial v_0}{\partial x}\cos(\theta_x)\frac{\partial \theta_x}{\partial x} + y\frac{\partial w_0}{\partial x}\cos(\theta_x)\frac{\partial \theta_x}{\partial x} - \quad (2.\ 80)$$
$$-y\frac{\partial v_0}{\partial x}\sin(\theta_x)\frac{\partial \theta_x}{\partial x} - z\frac{\partial w_0}{\partial x}\sin(\theta_x)\frac{\partial \theta_x}{\partial x},$$

$$\gamma_{zx} = \frac{\partial \psi}{\partial z}\frac{\partial \theta_x}{\partial x} + y\frac{\partial \theta_x}{\partial x} + \frac{\partial w_0}{\partial x}\cos(\theta_x) - \frac{\partial w_0}{\partial x} - \frac{\partial v_0}{\partial x}\sin(\theta_x), \quad (2.\ 81)$$

$$\gamma_{xy} = \frac{\partial \psi}{\partial y}\frac{\partial \theta_x}{\partial x} - z\frac{\partial \theta_x}{\partial x} + \frac{\partial v_0}{\partial x}\cos(\theta_x) - \frac{\partial v_0}{\partial x} + \frac{\partial w_0}{\partial x}\sin(\theta_x). \quad (2.\ 82)$$

Implementing approximation (2. 3), as in the previous section and neglecting the third-order terms in the direct strain, the following expressions result:

$$\varepsilon_x = \frac{\partial u_0}{\partial x} - y\frac{\partial^2 v_0}{\partial x^2} - z\frac{\partial^2 w_0}{\partial x^2} + \psi\frac{\partial^2 \theta_x}{\partial x^2} + \frac{1}{2}\left(\frac{\partial v_0}{\partial x}\right)^2 + \frac{1}{2}\left(\frac{\partial w_0}{\partial x}\right)^2 +$$
$$+\frac{1}{2}y^2\left(\frac{\partial \theta_x}{\partial x}\right)^2 + \frac{1}{2}z^2\left(\frac{\partial \theta_x}{\partial x}\right)^2 - z\frac{\partial v_0}{\partial x}\frac{\partial \theta_x}{\partial x} + y\frac{\partial w_0}{\partial x}\frac{\partial \theta_x}{\partial x}, \quad (2.\ 83)$$

$$\gamma_{zx} = \frac{\partial \psi}{\partial z}\frac{\partial \theta_x}{\partial x} + y\frac{\partial \theta_x}{\partial x} - \frac{\partial v_0}{\partial x}\theta_x, \quad (2.\ 84)$$

$$\gamma_{xy} = \frac{\partial \psi}{\partial y}\frac{\partial \theta_x}{\partial x} - z\frac{\partial \theta_x}{\partial x} + \frac{\partial w_0}{\partial x}\theta_x. \quad (2.\ 85)$$

The middle line displacements are expresses in the local coordinate system by shape functions and generalized coordinates as in (2. 13), using the shape functions defined in (2. 18) – (2. 19). The equation of motion is derived by the principle of virtual work (2. 22) and obtained in a form like (2. 29).

The first two terms in equations (2. 84) and (2. 85) define the shear strains that arise in Saint-Venant's theory for torsion and are zero on the middle line. The remaining terms are due to bending-torsion coupling and are constant along the cross section, causing a contradiction with the Bernoulli-Euler's assumption, that the shear deformation of the middle line is constrained to zero. Actually, Bernoulli-Euler's assumption states that "a

plane cross section perpendicular to the reference axis before deformation remains plane and perpendicular to the deformed reference axis after deformation" and it implies zero shear strain at all, not only on the middle line, but due to torsion the shear strain is zero only on the middle line, thus one should expect that the shear strain will be zero on the middle line for bending-torsional problems. These terms will cause differences in the transverse displacements and twist angles when bending is coupled with torsion, as will be shown in Chapter 3.

Attard [2. 12] imposed a kind of Bernoulli-Euler's assumption to obtain an expression for the longitudinal displacement. As a result, the rotations about the transverse axes were approximated by expressions involving the derivatives of the transverse displacements and the twist angle:

$$u(x,y,z,t) = u_0(x,t) -$$

$$-y\left(\frac{\partial v_0(x,t)}{\partial x}\cos\big(\theta_x(x,t)\big) + \frac{\partial w_0(x,t)}{\partial x}\sin\big(\theta_x(x,t)\big)\right) -$$

$$-z\left(\frac{\partial w_0(x,t)}{\partial x}\cos\big(\theta_x(x,t)\big) - \frac{\partial v_0(x,t)}{\partial x}\sin\big(\theta_x(x,t)\big)\right) + \psi(y,z)\frac{\partial \theta_x}{\partial x}(x,t), \qquad (2.\ 86)$$

$$v(x,y,z,t) = v_0(x,t) + y\cos\big(\theta_x(x,t)\big) - y - z\sin\big(\theta_x(x,t)\big),$$

$$w(x,y,z,t) = w_0(x,t) + y\sin\big(\theta_x(x,t)\big) + z\cos\big(\theta_x(x,t)\big) - z.$$

Using the displacement fields given in (2. 86), the following expression for the shear strains are obtained:

$$\gamma_{zx} = \frac{\partial \psi}{\partial z}\frac{\partial \theta_x}{\partial x} + y\frac{\partial \theta_x}{\partial x}, \qquad (2.\ 87)$$

$$\gamma_{xy} = \frac{\partial \psi}{\partial y}\frac{\partial \theta_x}{\partial x} - z\frac{\partial \theta_x}{\partial x}. \qquad (2.\ 88)$$

These expressions for the shear strains allow shear deformations due to torsion only and do not give additional coupling between torsion and transverse displacements as in (2. 84) and (2. 85).

2. 4. Conclusion

In this chapter, models of isotropic beams with symmetrical cross sections, vibrating in space were presented. The warping function was given for rectangular cross sections. The displacement components of the first model were derived assuming Timoshenko's theory for bending and Saint-Venant's for torsion. The displacements on the middle line were expressed by shape functions and generalized coordinates in local coordinate system applying the *p*-version finite element method. Because the geometry of the beam is regular, only one element was used. The strains were derived from Green's strain tensor, neglecting the longitudinal terms of second order and the stresses were related with the strains by Hooke's law. The equation of motion was derived by the principle of virtual work. As a result a second order ordinary differential equation of motion in time domain was obtained.

The displacement components of a 3D beam model assuming Bernoulli-Euler's theory for bending were also presented. It was shown that the shear strains do not vanish on the middle line if the Bernoulli-Euler's assumption is applied directly into 3D beam models including torsion. Thus, the rotations of the cross section have to be approximated not only by functions of the corresponding derivates of the transverse displacements, but also by the twist angle.

In the next chapter, a comparison between these two models will be presented. Furthermore, there will be discussion about the importance of the warping function, the longitudinal terms of second order and about the approximation of the trigonometric terms. All these comparison will demonstrate that the model presented in Section 2. 2. is the most suitable for 3D beams and this model will be used in the following chapters.

References

[2. 1] C. Wang, J. Reddy, K. Lee, *Shear Deformable Beams and Plates*, Elsevier, Oxford, 2000.

[2. 2] G. Wempner, D. Talaslidis, *Mechanics of Solids and Shells. Theory and Application*, CRC Press, Boca Raton, Florida, 2003.

[2. 3] I. Sokolnikoff, *Mathematical Theory of Elasticity*, McGraw-Hill, New York, 1956.

[2. 4] Y. C. Fung, *Foundations of Solid Mechanics*, Prentice-Hall, Englewood Cliffs 1965.

[2. 5] A. Nayfeh, P. Pai, *Linear and Nonlinear Structural Mechanics*, John Wiley &Sons, Weinheim ,2004.

[2. 6] N. S. Bardell, Free vibration analysis of a flat plate using the hierarchical finite element method, *Journal of Sound and Vibration* 151 (1991) 263-289.

[2. 7] W. Han, and M. Petyt, Geometrically nonlinear vibration analysis of thin, rectangular plates using the hierarchical finite element method - I: The fundamental mode of isotropic plates, *Computers & Structures* 63 (1997) 295-308.

[2. 8] P. Ribeiro, Hierarchical finite element analyses of geometrically non-linear vibration of beams and plane frames, *Journal of Sound and Vibration* 246 (2001) 225-244

[2. 9] O. C. Zienkiewicz, R. L. Taylor, J. Z. Zhu, *The Finite Element Method: Its Basis and Fundamentals*, Sixth edition, Oxford, 2005.

[2. 10] J. Hutchinson, Shear coefficients for Timoshenko beam theory, *Journal of Applied Mechanics* 68 (2001) 87-92.

[2. 11] L. Meirovitch, *Methods of Analytical Dynamics*, Dover Publications Inc., New York, 2003.

[2. 12] M. Attard, Nonlinear theory of non-uniform torsion of thin-walled beams, *Thin-Walled Structures* 4 (1986) 101-134.

[2. 13] F. Mohri, L. Azrar, M. Potier-Ferry, Flexural-torsional post-buckling analysis of thin-walled elements with open sections, *Thin-Walled Structures* 39 (2001) 907-938.

[2. 14] F. Mohri, N. Damil, M. Potier-Ferry, Large torsion finite element model for thin-walled beams, *Computers & Structures* 86 (2008) 671–683.

[2. 15] E. Sapountzakis, J. Dourakopoulos, Flexural-torsional postbuckling analysis of beams of arbitrary cross section, *Acta Mechanica* 209 (2010) 67-84.

[2. 16] S. Klinkel, S. Govingjee, Anisotropic bending-torsion coupling for warping in a non-linear beam, *Computational Mechanics* 31 (2003) 78-87.

[2. 17] I. Sharf, Geometrically non-linear beam element for dynamic simulation of multibody systems, *International Journal for Numerical Methods in Engineering* 39 (1996) 763-786.

3

Comparison and Validation of Beam Models

3. 1. Introduction

In this chapter, the models presented in Chapter 2 are compared. Comparison of the bending natural frequencies with the degrees of freedom for *h*-, *p*- and *hp*-versions of the FEM is also included. The importance of the warping function is analysed for different rectangular cross sections, and it is shown that its consideration can be fundamental to obtain correct results. It is demonstrated that the linearization of the trigonometric functions related with the twist angle, which is usually applied in the displacement field in models based on Saint-Venant's hypothesis, should be done in the strain-displacement relations instead of in the displacement field, also it is shown that the influence of the third-order terms in the direct strain is negligible. Comparisons of the models for 3D beams based on Bernoulli-Euler's and Timoshenko's theories are presented. It is shown that if the rotations about the transverse axes are directly approximated by the respective derivatives of the transverse displacement functions, as is assumed in the model based on Bernoulli-Euler's theory, the additional shear stresses that appear when the bending and torsion motions are coupled, lead to wrong results. Finally, taking into account accuracy and simplicity, the model presented in sub-chapter 2. 2 is chosen and employed to investigate the nonlinear forced vibrations of beams using direct integration of the equations of motion in the time domain. Examples of bending-torsion couplings due to the nonlinear terms are presented in dynamical problems.

The models derived in the previous chapter are applied mostly to clamped-clamped beams with warping free boundary conditions, with the following material properties (aluminium): $E = 7.0^{10}\ \mathrm{N/m^2}$, $\rho = 2778\ \mathrm{kg/m^3}$, $\nu = 0.34$ and different geometrical properties. It is noted that, since we adopted Saint-Venant's hypotheses, the warping

function is equal along the beam axis, including the clamped ends. A discussion on the improvement of the torsional model is given at the end of the chapter.

3. 2. Convergence study

The convergence properties of the models with the number of DOF are analysed in this section. First, the convergence on the computation of the bending linear natural frequencies is presented and the DOF required for convergence in *p*-, *h*- and *hp*-versions of FEM are compared. Also, the convergence on the computation of the torsional linear natural frequencies and the influence of the warping function on these natural frequencies are investigated. Then, the convergence on the computation of displacements due to static loads is analysed, in this case considering geometrical nonlinearity.

3. 2. 1. Bending linear natural frequencies

The error of a FEM approximation can be lowered in three ways:

(i) By generating a sequence of meshes, usually refining a previous mesh, but using the same type of elements in the successive FEM models, i.e., neither changing the number of generalized coordinates nor the shape functions of each element. This FEM approach is designated as the *h*-version FEM.

(ii) By changing the element or elements employed, increasing the number of shape functions and of generalized coordinates in at least some of the elements, but without changing the mesh. This FEM approach is designated as the *p*-version FEM.

(iii) By simultaneously varying the mesh and the number of shape functions of some (at least one) of the finite elements of the mesh. This combination of the previous two is known as *hp*-version FEM.

The *p*-FEM generally gives accurate results with less DOF than the standard *h*-FEM [3. 1]. This advantage is demonstrated in this sub-chapter for the plane bending natural frequencies of Timoshenko clamped-clamped beam with dimensions l = 0.58 m, b = 0.02 m and h = 0.002 m.

The *h*-FEM is defined using the four Hermite cubic functions [3. 2] for each displacement component w_0 and ϕ_y. Each element has 8 DOF. The process of deriving

the mass and the linear stiffness matrices and of assembling the elements is standard and can be found in many books, for example [3. 2]-[3. 4], thus it is not given here. The *p*-FEM presented in sub-chapter 2. 2 is used, but only the mass and linear stiffness matrices related with the bending deformations are considered.

Table 3. 1. Bending linear natural frequencies (rad/s) obtained by *h*-FEM and analytical natural frequencies for Bernoulli-Euler beam.

Elements	2	4	6	10	15	20	Analyt.
DOF	6	14	22	38	58	78	Bernoulli
ω_1	195.8554	193.0514	192.7914	192.7421	192.7365	192.7356	192.7474
ω_2	-	540.5654	532.6710	531.3805	531.2543	531.2343	531.3242
ω_3	-	1074.363	1055.334	1042.567	1041.490	1041.332	1041.608
ω_4	-	-	1792.163	1727.719	1722.028	1721.261	1721.817

Table 3. 2. Bending linear natural frequencies (rad/s) obtained by *p*-FEM.

№ Shape functions	2	4	6	8	10	15	20
DOF	4	8	12	16	20	30	40
ω_1	193.3975	192.7402	192.7357	192.7355	192.7353	192.7352	192.7351
ω_2	542.0568	531.4175	531.2404	531.2391	531.2386	531.2381	531.2378
ω_3	-	1099.197	1043.239	1041.293	1041.271	1041.266	1041.264
ω_4	-	1910.513	1731.917	1721.226	1721.000	1720.991	1720.987

The first four bending natural frequencies obtained by the *h*-FEM with different number of elements, and consequently different number of DOF, are presented in Table 3. 1. The analytical solution of the linear eigenvalue problem, but for Bernoulli-Euler beam, is also included in the table for validation purposes. The same natural frequencies, but obtained by the *p*-FEM using one element and different number of shape functions are presented in Table 3. 2. Convergence with the number of DOF of both, *h* and *p*, FEM is presented in Figure 3. 1. It is clear from the figure that the *p*-FEM requires much less DOF for convergence then the *h*-FEM.

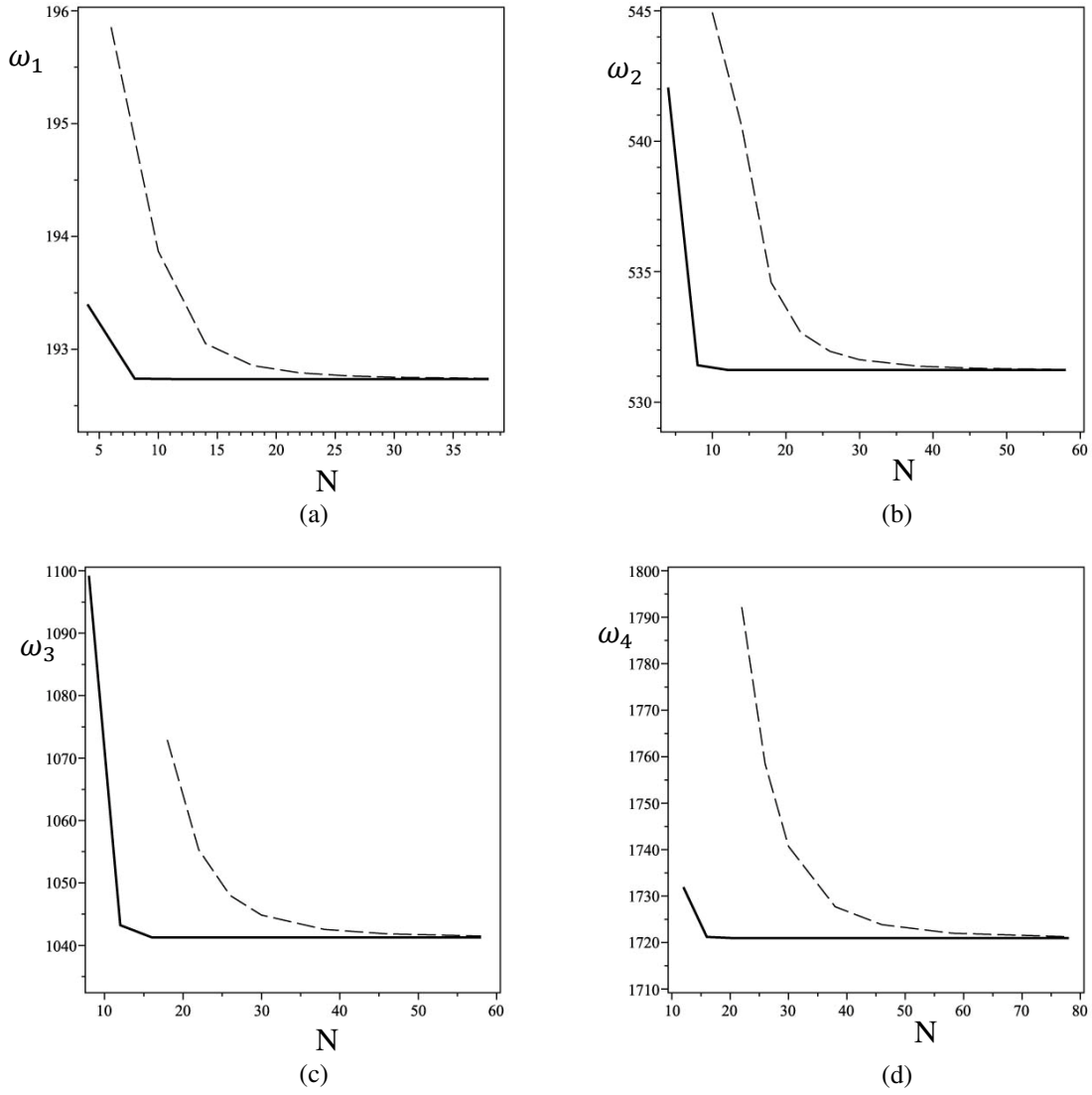

Figure 3. 1. Linear bending natural frequencies (rad/s) plotted as function of the number of DOF of the model, —— *p*-FEM, – – – *h*-FEM. (a) First natural frequency, (b) Second natural frequency, (c) Third natural frequency, (d) Fourth natural frequency.

As a combination of both models, an *hp*-FEM can be developed. The corresponding *hp*-FEM model divides the beam into several elements, each element has the four Hermite cubic shape functions plus additional shape functions which are related with the *p*-FEM. The natural frequencies obtained by the *hp*-FEM with two and three elements are presented in Table 3. 3. It can be seen that for the same number of DOF, but for different number of elements and shape functions, *hp*-FEM gives different natural frequencies. Better results are obtained with less elements and more shape functions, instead of more elements and less shape functions. In the current case, where the beam is initially straight, one element with more shape functions gives convergence with minimum number of DOF. *hp*-FEM is preferred in the cases when the geometry of the structure is more complex and cannot be approximated by a single element. In such structures, a

mesh with minimum number of elements is advised to be defined while for more accurate results the number of shape functions is advised to be increased.

Furthermore, the convergence on the computation of plane bending natural frequencies of beams and beam structures, when Bernoulli-Euler's *p*-version finite elements are employed was analysed in [3. 5]-[3. 7] and a study on the convergence properties of a Timoshenko *p*-version finite element for plane bending was carried out in [3. 8]. The studies published in these references corroborate that accurate beam models with a small number of DOF are achieved using the *p*-version FEM.

Table 3. 3. Bending linear natural frequencies (rad/s) obtained by the *hp*-FEM. The number of *p* shape functions indicates the additional functions added to the four Hermite cubic functions.

№ elements	2 elements	2 elements	2 elements	3 elements	3 elements	3 elements
№ of *p* sh. f.	2 *p* sh. f.	4 *p* sh. f.	6 *p* sh. f.	2 *p* sh. f.	4 *p* sh. f.	6 *p* sh. f.
DOF	14	22	30	22	34	46
ω_1	192.7359	192.7354	192.7353	192.7357	192.7353	192.7352
ω_2	532.0689	531.2292	531.2264	531.2311	531.2266	531.2258
ω_3	1052.763	1041.358	1041.269	1042.559	1041.271	1041.266
ω_4	1747.777	1721.474	1720.961	1728.100	1720.988	1720.953

3. 2. 2. Torsional linear natural frequencies

In this section only the linear torsional natural frequencies are presented and the importance of the warping function is analysed. Both models presented in Chapter 2 adopt the same hypotheses for torsion and hence give equal results when only torsion is analysed, i.e. when the bending displacements are zero.

Table 3. 4 shows the convergence of the torsional natural frequencies with the number of shape functions. The beam analysed has dimensions l = 0.58 m, b = 0.02 m and h = 0.002 m. Only the number of torsional shape functions is presented, because in the linear free vibrations of isotropic beams with symmetrical cross sections the bending, the longitudinal and the torsional motions are uncoupled, i.e. bending and longitudinal displacements do not influence the torsional modes. The warping function is obtained using 25 terms in equation (2. 5) which are enough to obtain convergence on the results

given here. The results are compared with data obtained with Ansys finite element software [3. 9] using *h*-version shell element SHELL281, which has eight nodes with six degrees of freedom at each node. The current results from Ansys are obtained using 2430 elements. The purpose of this shell *h*-version model is to validate the *p*-version model and that is why the very fine mesh was generated in Ansys. It is nevertheless true that close results can also be obtained with fewer shell elements. The shell element is required to provide a reference solution, but we also want to compare the degrees of freedom between beam elements. For this purpose Ansys BEAM189 element, which is a 3D beam element with three nodes and seven degrees of freedom including warping, is used. 30 elements are enough to obtain convergence for the torsional linear natural frequencies. A model with 6 shape functions, i.e. 6 DOF gives very good approximation, at least for the first four torsional linear frequencies. The current model converges to lower values of the natural frequencies in comparison with the shell element, because the warping function is not constrained on the clamped ends. The shell element constrains the longitudinal deformations due to warping on the boundaries, i.e. the beam is stiffer in torsion and consequently the natural frequencies are higher. At the end of the chapter, an improvement of the torsional model is presented by increasing the generalised coordinated and the DOF and the natural frequencies are shown to be in very good agreement with Ansys shell element.

Table 3. 5 presents the torsional natural frequencies of the beam with length l = 0.58 m and different rectangular cross sections. In the first column, an analytical solution for beam with circular cross section is given. The results of the second column are for beam with cross section with the dimensions assumed in Table 3. 4 (b = 0.02 m and h = 0.002 m), but the frequencies were computed without using the warping function and differ significantly from the ones in Table 3. 4. Moreover, the frequencies obtained neglecting the warping function do not change with the dimensions b and h of the cross section of the beam, because in this case the linear mass and stiffness matrices change proportionally when the cross section is changed. In the remaining columns of Table 3. 5, the torsional frequencies are the ones of beams with the same length, but different cross sections and were computed considering the warping function.

Table 3. 4. Torsional natural frequencies (rad/s). The error, presented in brackets, is calculated between the frequencies of the shell element and the ones obtained with the *p*-FEM.

Mode	4 shape functions	6 shape functions	8 shape functions	10 shape functions	Ansys BEAM189	Ansys SHELL281
1	3200.55 (1.65 %)	3200.52 (1.66 %)	3200.52 (1.66 %)	3200.52 (1.66 %)	3310.55	3254.39
2	6409.37 (1.63 %)	6407.38 (1.66 %)	6407.37 (1.66 %)	6407.37 (1.66 %)	6627.50	6515.57
3	10350.8 (5.72 %)	9647.36 (1.46 %)	9627.05 (1.67 %)	9626.85 (1.67 %)	9957.27	9790.33
4	14603.7 (11.6 %)	12959.5 (0.96 %)	12867.4 (1.67 %)	12865.2 (1.68 %)	13306.3	13085.4

Table 3. 5. Torsional natural frequencies (rad/s) of beams with different cross sections with and without using the warping function, 10 shape functions. Analytical solution for beam with circular cross section is included.

Mode	Analytical	Without warping any cross section	With warping b = 0.02 m, h = 0.02 m	With warping b = 0.02 m, h = 0.004 m	With warping b = 0.02 m, h = 0.001 m
1	16608.77	16608.77	15253.68	6091.97	1633.02
2	33217.53	33217.53	30508.30	12194.92	3269.30
3	49826.30	49826.30	45764.82	18319.78	4912.10
4	66435.07	66435.14	61024.22	24477.46	6564.64

The linear torsional mass and stiffness matrices are presented here, in the case when the warping function is neglected. The purpose is to show why the torsional linear frequencies do not change when the cross sectional dimensions are changed.

$$\mathbf{K1_{44}} = G\int_V (y^2+z^2)\frac{d\left\lfloor N^{\theta_x}\right\rfloor^T}{dx}\frac{d\left\lfloor N^{\theta_x}\right\rfloor}{dx}dV = \\ = G\int_\Omega (y^2+z^2)\,d\Omega\int_L \frac{d\left\lfloor N^{\theta_x}\right\rfloor^T}{dx}\frac{d\left\lfloor N^{\theta_x}\right\rfloor}{dx}dL \tag{3. 1}$$

$$\mathbf{M_{44}} = \rho \int_V (y^2 + z^2)\left\lfloor N^{\theta_x} \right\rfloor^T \left\lfloor N^{\theta_x} \right\rfloor dV = \\ = \rho \int_\Omega (y^2 + z^2)\, d\Omega \int_L \left\lfloor N^{\theta_x} \right\rfloor^T \left\lfloor N^{\theta_x} \right\rfloor dL \tag{3. 2}$$

From these definitions of the linear stiffness and mass matrices, it is obvious that changing the dimension of the cross section we change only the value of the integral $\int_\Omega (y^2 + z^2)$ which is common to both matrices. Because of that the natural frequencies are the same for all beams with the same length and material properties and with different cross sections. Obviously, this cannot be true and the results of Table 3. 5 prove it. The frequencies calculated without warping function correspond to the torsional frequencies of a circular beam with the same material properties and length. The frequencies of the beam with square cross section are the closest to the ones of the beam with circular cross section. This follows from the fact that from all rectangles, the square is the closest one to the circle. Table 3. 5 shows that the warping function becomes more important for thinner beams and should not be neglected.

3. 2. 3. Static deformations

Static analyses are performed to study the convergence on the computation of displacements in the nonlinear regime with the number of shape functions. In this section, only data from the model developed in Chapter 2. 2 is presented; later on different models are compared. The dimensions of the beam analysed are 0.02 × 0.02 × 2.0 m. F_z represents the amplitude of an external transverse force in z direction, F_y the amplitude of an external transverse force in y direction, M_x the amplitude of an external moment about the x axis.

Table 3. 6 presents transverse displacements of the order of the beam thickness, due to a static force applied in the middle point of the beam in the z direction. The same number of shape functions is used for the longitudinal and the transverse displacements, and for the rotations about the transverse axes. Four shape functions for each displacement component provide bending displacements that differ, at most, by 0.65% from the ones computed with 12 shape functions used as a reference solution. The absolute error of the displacements calculated using 8 shape functions is below 0.087%, again taking the solutions obtained with 12 shape functions as reference. So we consider that 8 shape

functions provide a very good approximation for the transverse displacements in nonlinear plane bending.

Table 3. 6. Transverse displacements (m) computed with different numbers of shape functions. Force applied and displacement computed in the middle point of the beam. The error, presented in brackets, is computed by using the solution obtained with 12 shape functions as a reference solution.

Number of shape functions	4	6	8	10	12
F_z = 500 N	1.553 10^{-2} (0.45 %)	1.558 10^{-2} (0.13 %)	1.559 10^{-2} (0.06 %)	1.560 10^{-2} (0.0 %)	1.560 10^{-2}
F_z = 800 N	2.041 10^{-2} (0.58 %)	2.050 10^{-2} (0.15 %)	2.052 10^{-2} (0.05 %)	2.053 10^{-2} (0.0 %)	2.053 10^{-2}
F_z = 1000 N	2.296 10^{-2} (0.65 %)	2.306 10^{-2} (0.22 %)	2.309 10^{-2} (0.09 %)	2.310 10^{-2} (0.04 %)	2.311 10^{-2}

Torsions due to a concentrated moment applied in the middle point of the beam and due to a uniformly distributed moment are now analysed. The twist rotations are presented in Tables 3. 7 and 3. 8. It can be noticed that when the moment is distributed, even 4 shape functions give an extremely good approximation, with values that almost do not differ from the ones computed with 25 shape functions (and due to this, it was necessary to use many digits in Table 3. 8). But, if the applied moment is concentrated, much more shape functions are required for convergence. This is explained by the different variation of torsion with the longitudinal coordinate in the two cases and by the shape functions used in the model. The twist angles along the length of the beam, for concentrated and distributed moments, are presented in Figure 3. 2. From these figures it is clear that more shape functions are required to express the distribution of the torsion due to a concentrated moment, Figure 3. 2 (a). Therefore, more shape functions are required for convergence in this case. Considering the balance between computational efficiency and accuracy of the model, 16 shape functions provided a reasonable *p*-element for torsion.

Table 3. 7. Convergence of rotation about the *x* axis (rad) with the number of shape functions. Moment applied in the middle point of the beam. The error, presented in brackets, is computed by using the solution obtained with 25 shape functions as a reference solution.

Number of shape functions	4	8	16	20	25
M_x = 200 Nm	$1.575\ 10^{-1}$ (6.28 %)	$1.636\ 10^{-1}$ (2.65 %)	$1.669\ 10^{-1}$ (0.69 %)	$1.675\ 10^{-1}$ (0.33 %)	$1.6806\ 10^{-1}$
M_x = 400 Nm	$3.150\ 10^{-1}$ (6.28 %)	$3.273\ 10^{-1}$ (2.62 %)	$3.337\ 10^{-1}$ (0.72 %)	$3.351\ 10^{-1}$ (0.30 %)	$3.3612\ 10^{-1}$
M_x = 600 Nm	$4.724\ 10^{-1}$ (6.30 %)	$4.909\ 10^{-1}$ (2.63 %)	$5.006\ 10^{-1}$ (0.71 %)	$5.026\ 10^{-1}$ (0.31 %)	$5.0417\ 10^{-1}$

Table 3. 8. Convergence of rotation about the *x* axis (rad) with the number of shape functions. Distributed moment applied along the length of the beam. The error, presented in brackets, is computed by using the solution obtained with 25 shape functions as a reference solution.

Number of shape functions	4	8	16	25
M_x = 200 Nm/m	$1.7021544\ 10^{-1}$ ($7.05\ 10^{-5}$ %)	$1.7021541\ 10^{-1}$ ($5.29\ 10^{-5}$ %)	$1.7021538\ 10^{-1}$ ($3.52\ 10^{-5}$ %)	$1.7021532\ 10^{-1}$
M_x = 400 Nm/m	$3.4042419\ 10^{-1}$ ($6.76\ 10^{-5}$ %)	$3.4042413\ 10^{-1}$ ($4.99\ 10^{-5}$ %)	$3.4042408\ 10^{-1}$ ($3.53\ 10^{-5}$ %)	$3.4042396\ 10^{-1}$
M_x = 600 Nm/m	$5.1061957\ 10^{-1}$ ($6.85\ 10^{-5}$ %)	$5.1061949\ 10^{-1}$ ($5.29\ 10^{-5}$ %)	$5.1061941\ 10^{-1}$ ($3.72\ 10^{-5}$ %)	$5.1061922\ 10^{-1}$

The relation between the applied moments and the twist angles in Tables 3. 7 and 3. 8 seems to be linear because the nonlinearity in the torsional model is very weak. It comes solely from the direct strain ε_x , since the shear strains γ_{zx} and γ_{xy} are linear when only torsion exists.

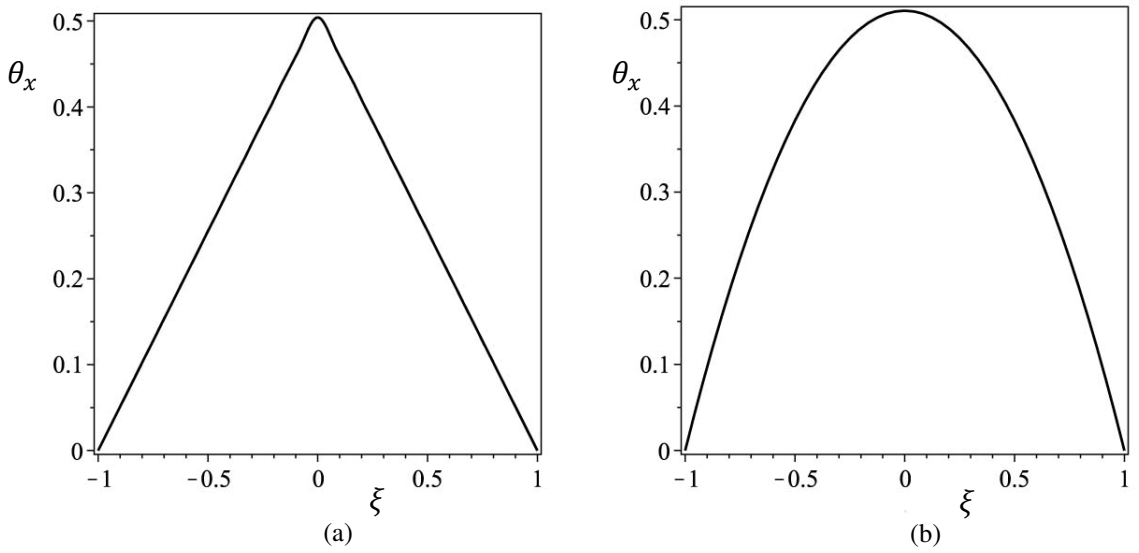

Figure 3. 2. Torsional displacements (rad) of beam with dimensions 0.02 × 0.02 × 2.0 m. (a) Concentrated moment applied in the middle point, M_x= 600 Nm. (b) Distributed moment along the beam length, M_x= 600 Nm/m.

As a result of the convergence studies, it was decided to employ a model with 8 shape functions for bending and longitudinal displacements and 16 shape functions for torsion. In the case of the Timoshenko beam *p*-element, 8 shape function will be used for the rotations about the transverse axes - ϕ_y and ϕ_z. Therefore the total number of degrees of freedom of the complete model is 56. If we analyse only bending in one plane, then the model does not need to include bending in the other plane and torsion and it only has 24 DOF. If we analyse only torsional problems, the model will consider only torsion and the number of DOF will be 16. It is recalled that in the particular case studies of this work only one element is employed for each complete beam. If the geometry of the structure requires more elements and if these are straight beams, the assembling and mapping procedures are not very different from the ones of the common finite element method [3. 7], although a few degrees of freedom do not interfere in the element connection and sub-parametric mapping is common [3. 10].

3. 3. Torsion. Comparison of models adopting the linear approximation of the trigonometric terms in the displacement field and in the strains

In this section the differences that appear if the linear approximation (2. 3) is used in the expressions of displacements (2. 1) or if it is implemented later in the expressions of strains (2. 7) – (2. 9), are presented. Only nonlinear static deformations are considered.

The implementation of approximation (2. 3) in the strain-displacement relations (2. 7) – (2. 9) leads to equations (2. 10) – (2. 12). For completeness, the following equations present the strain-displacement relations that are obtained if the approximation (2. 3) is employed directly in the expressions for the displacements (2. 1) and then the strains are calculated using (2. 6).

$$\varepsilon_x = \frac{\partial u_0}{\partial x} - y\frac{\partial \phi_z}{\partial x} + z\frac{\partial \phi_y}{\partial x} + \psi\frac{\partial^2 \theta_x}{\partial x^2} + \frac{1}{2}\left(\frac{\partial v_0}{\partial x}\right)^2 + \frac{1}{2}\left(\frac{\partial w_0}{\partial x}\right)^2 + \\ + \frac{1}{2}y^2\left(\frac{\partial \theta_x}{\partial x}\right)^2 + \frac{1}{2}z^2\left(\frac{\partial \theta_x}{\partial x}\right)^2 - z\frac{\partial v_0}{\partial x}\frac{\partial \theta_x}{\partial x} + y\frac{\partial w_0}{\partial x}\frac{\partial \theta_x}{\partial x}, \tag{3. 3}$$

$$\gamma_{zx} = \frac{\partial \psi}{\partial z}\frac{\partial \theta_x}{\partial x} + y\frac{\partial \theta_x}{\partial x} + \frac{\partial w_0}{\partial x} + \phi_y - \frac{\partial v_0}{\partial x}\theta_x + z\theta_x\frac{\partial \theta_x}{\partial x}, \tag{3. 4}$$

$$\gamma_{xy} = \frac{\partial \psi}{\partial y}\frac{\partial \theta_x}{\partial x} - z\frac{\partial \theta_x}{\partial x} + \frac{\partial v_0}{\partial x} - \phi_z + \frac{\partial w_0}{\partial x}\theta_x + y\theta_x\frac{\partial \theta_x}{\partial x}. \tag{3. 5}$$

It can be noticed that, in comparison with equations (2. 10) – (2. 12), two terms of second order appear in the expressions of shear strains and the terms of third-order in the expression of direct strain disappear. These two terms of second order significantly change the solution of torsional problems, as is shown in the following examples.

Angles of twist of two beams with different dimensions are presented in the following paragraphs. Each beam is considered to be clamped-clamped. Since the boundary conditions are symmetric and a moment is applied in the centre of the beams, only symmetric shape functions are used for transverse displacements and rotations about the longitudinal axis, and antisymmetric shape functions are used for longitudinal displacement and for rotations around the *y* and *z* axes.

Table 3. 9 gives angles of twist of a cross section of a beam to which moments are applied. The beam cross section is thin, with height equal to 0.002 m, width to 0.02 m and length to 0.58 m. Different moments are applied in the middle point of the beam and the twist angles are measured in the same point. The results are compared with data computed with Ansys software using beam and shell finite elements. The shell element and mesh employed in the previous section are again used here. The same beam, as in the previous section, but with mesh with 100 beam elements is generated to obtain the results. We recall that the two models that result from the displacement fields (2. 1) and

(2. 78) give equal results when only a moment is applied, because both models consider the same theory for torsion and in this case there are no transverse displacements.

Table 3. 9. Rotation about the longitudinal axis θ_x (rad) in the middle of the beam (0.002 × 0.02 × 0.58) with moment applied in the same point.

Moment	Model without the additional second order terms in shear strains, Eqs. (2. 11) and (2. 12)	Model with the additional second order terms in shear strains, Eqs. (3. 4) and (3. 5)	Ansys BEAM189	Ansys SHELL281
M_x = 0.5 Nm	0.0541	0.0517	0.0519	0.0542
M_x = 1 Nm	0.108	0.094	0.104	0.108
M_x = 3 Nm	0.324	0.197	0.311	0.324
M_x = 5 Nm	0.537	0.259	0.517	0.538

Torsion of a beam with square cross section (height – 0.02 m, width – 0.02 m, length - 2.0 m) was also analysed. The results are presented in Table 3. 10.

These examples show that inclusion of the two second order terms in the shear strains decreases the twist angle. The difference becomes significant for larger rotations. These terms are related only with torsion and do not appear if the torsion strains are developed considering no further approximations than that the projection of the cross sections on the (y, z) plane rotates as a rigid body. Therefore, these results corroborate that the linear approximation (2. 3) should only be done after the strains are calculated. The results of the model without the additional second order terms in the shear strains in Table 3. 9 are closer to the results obtained by shell element while the results of the same model in Table 3. 10 are closer to the ones obtained by beam element. This can be explained by the fact that in the first case the beam is very thin, hence similar to a shell, while in the second case the beam cross section is square and the shell finite element is not very adequate. Again, the relation between the applied moment and the twist angles seems to be linear when the model without the additional second order terms in the shear strains is employed, because of the weak nonlinear terms in torsion. This weak nonlinearity is not a result of further (other than the initial assumptions) approximations or simplifications; meaning that the pure torsional behaviour of the present beams is close to linear when the rotations are moderate.

Table 3. 10. Rotation about the longitudinal axis θ_x (rad) in the middle of the beam (0.02 × 0.02 × 2.0) with moment applied in the same point.

Moment	Model without the additional second order terms in shear strains, Eqs. (2. 11) and (2. 12)	Model with the additional second order terms in shear strains, Eqs. (3. 4) and (3. 5)	Ansys BEAM189	Ansys SHELL281
M_x = 50 Nm	0.0417	0.0416	0.0419	0.0431
M_x = 100 Nm	0.0833	0.0829	0.0838	0.0862
M_x = 200 Nm	0.167	0.163	0.168	0.172
M_x = 500 Nm	0.417	0.376	0.419	0.430

3. 4. Comparison of models including and neglecting the third-order terms in the direct strain

A model including the third-order terms in the direct strain (2. 10) was developed and compared with the model neglecting them, presented in Chapter 2. 2. The respective stiffness matrices are not given here because, as shown in the tables below, their influence on the beam's displacements is very weak and they are not used in the numerical results in the next chapters. The inclusion of these terms adjoins nonlinearities of order three, four and five in the equation of motion. Static deformations of clamped-clamped beams with different cross sections are compared. A point force on the middle of the beam is applied, thus only symmetrical shape functions for the transverse and torsional displacement and antisymmetrical shape functions for the longitudinal displacement and rotations along the transverse axes are used. Because of the high nonlinearity, only 5 shape functions for each displacement component are used, this number of shape functions, which is smaller than the one employed in the previous examples, is adequate for the purposes here, since it provides an accurate enough model and the differences between results with or without the additional nonlinear terms should be of the same order if more or less shape functions are used. Because the third-order terms in the direct stain (2. 10) present bending-torsional coupling, these terms will be different from zero when the transverse and the torsional displacements are not zero. Thus, the applied force will be such that excites all displacement components.

Tables 3. 11 – 3. 13 present the transverse and torsional displacements of beam with dimensions b = 0.02 m, l = 2.0 m and three different thicknesses, h = 0.02 m, h = 0.01 m and h = 0.002 m, respectively, due to a combined load applied on the middle of the beam. The difference between both models is very small, thus the third-order terms can be neglected to avoid having nonlinearity higher than cubic. The errors shown in the tables are the absolute values of the errors computed by considering the model with third-order terms as reference.

Table 3. 11. Transverse displacements (v_0 and w_0) and rotation about the x axis (θ_x) in the middle of the beam for models including and neglecting the third-order terms in the direct strain, beam dimensions b = 0.02 m, h = 0.02 m, l = 2.0 m. A combined force is applied in the middle of the beam.

F_y = 1000 N F_z = 1000 N M_x = 600 Nm	Model neglecting the third-order terms	Model including the third-order terms	Error (%)
Displacement v_0 (m)	0.018758	0.018845	0.46
Displacement w_0 (m)	0.018758	0.018752	0.03
Rotation θ_x (rad)	0.476348	0.476825	0.10

Table 3. 12. Transverse displacements (v_0 and w_0) and rotation about the x axis (θ_x) in the middle of the beam for models including and neglecting the third-order terms in the direct strain, beam dimensions b = 0.02 m, h = 0.01 m, l = 2.0 m. A combined force is applied in the middle of the beam.

F_y = 1000 N F_z = 500 N M_x = 100 Nm	Model neglecting the third-order terms	Model including the third-order terms	Error (%)
Displacement v_0 (m)	0.028787	0.028840	0.18
Displacement w_0 (m)	0.017862	0.017826	0.20
Rotation θ_x (rad)	0.379950	0.381563	0.42

Table 3. 13. Transverse displacements (v_0 and w_0) and rotation about the x axis (θ_x) in the middle of the beam for models including and neglecting the third-order terms in the direct strain, beam dimensions b = 0.02 m, h = 0.002 m, l = 2.0 m. A combined force is applied in the middle of the beam.

F_y = 10 N F_z = -10 N M_x = 0.3 Nm	Model neglecting the third-order terms	Model including the third-order terms	Error (%)
Displacement v_0 (m)	0.003944	0.003945	0.03
Displacement w_0 (m)	-0.013808	-0.013807	0.01
Rotation θ_x (rad)	0.119827	0.119926	0.08

3. 5. Bending-torsion couplings in beams. Comparison between 3D beam models assuming Timoshenko's and Bernoulli-Euler's theories

In the previous sections the nonlinear torsional model was verified by carrying out comparisons with data computed using Ansys. The nonlinear planar bending parts of the *p*-version models based on Bernoulli-Euler and Timoshenko theories, which were implemented in the context of this particular work, were verified by comparison with data published by McEwan et al. on a thin beam [3. 11]. Both *p*-models provided accurate displacements in plane bending. Furthermore, and in an agreement with previous publications [3. 6] - [3. 8], [3. 12], both models required a small number of degrees of freedom, with an expected advantage in this respect of the Bernoulli-Euler model.

In this section, the models that arise from displacement fields (2. 1) and (2. 78) are compared in static cases that simultaneously involve bending and torsion. A beam with dimensions l = 2.0 m, b = 0.02 m and h = 0.02 m is considered. The beam is long, so the differences between the bending deflections of models based on Bernoulli-Euler and Timoshenko theories are expected to be very small. Two transverse forces, in y and z directions, and a moment are applied in the middle of the beam. To avoid convergence problems, first a force with small amplitude is applied, and then the force amplitude is increased step by step till its final value. For each step, the previous solution is used as a prediction of the new one. For the sake of simplicity, the model that results from

equations (2. 1) will be called Model 1 and the model that results from equations (2. 78) will be called Model 2.

Figure 3. 3 presents the displacements obtained from static transverse forces of 1200 N and a moment of 120 Nm applied in the middle point of the beam. The results show that both models give very close results for bending (a), but the results for torsion are completely different (b). In picture (c) the rotation about the transverse axis *y* and the derivative of the transverse displacement w_0 are plotted. The rotation about the transverse axis *y* is considered to be equal to the derivative of the transverse displacement w_0 in Model 2, while Model 1 assumes that they are different and this difference increases when bending couples with torsion. Both rotations about the transverse axes are plotted on picture (d). Due to the twist angle, these rotations are also different, even though the beam cross section is square and both transverse forces are equal.

In the next example, Figure 3. 4, the applied transverse forces remain the same but the moment is increased to 350 Nm. The bending displacement obtained from Model 2 becomes smaller and different than the same displacement computed using Model 1 (a), while the twist angle becomes closer to the one of Model 1 (b). The differences between the rotation about the transverse axis and the corresponding derivative of the transverse displacement increase (c) and the differences between the two rotations about the transverse axes also increase (d).

As we mentioned before, if only a twisting moment is applied on the beam, both models give the same results since both are based upon the same hypothesis regarding torsion. It was also verified that both models give very close results if only a transverse force – a plane bending situation – is applied, which is expected since the beam is thin in comparison with its length.

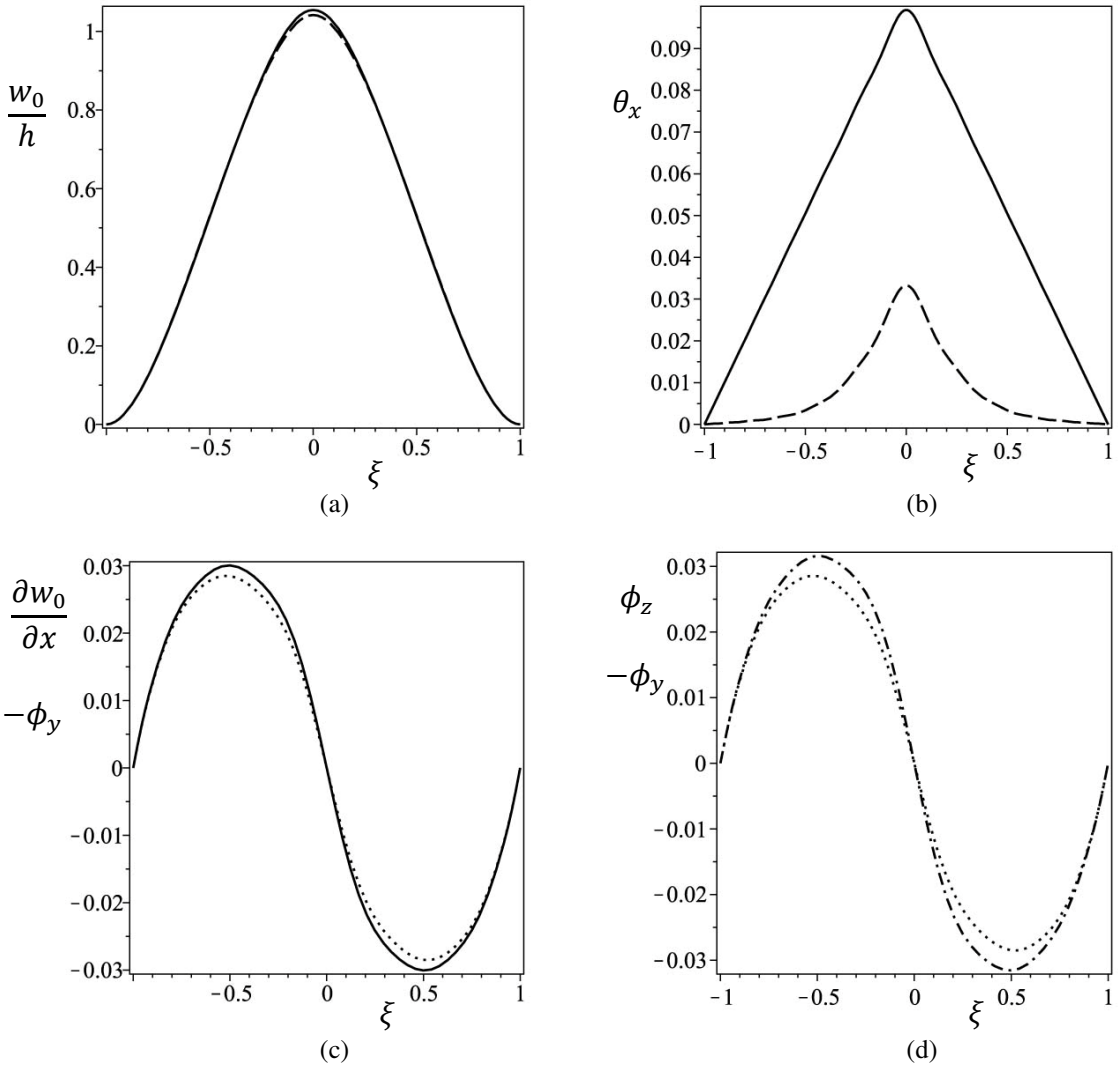

Figure 3. 3. Comparison of transverse displacement (dimensionless) and rotations about longitudinal and about transverse axes (rad) in the middle line of the beam, due to a force applied in the middle point, computed using both models: $F_y = F_z = 1200$ N, $M_x = 120$ Nm. (a) — w_0 from Model 1, --- w_0 from Model 2; (b) — θ_x from Model 1, --- θ_x from Model 2; (c) — $\partial w_0/\partial x$ from Model 1, ⋯ $(-\phi_y)$ from Model 1; (d) -·-·- ϕ_z from Model 1, ⋯ $(-\phi_y)$ from Model 1.

Differences of the type discussed above become bigger if we increase the moment. Figure 3. 5 plots the same displacements but the applied moment is increased to 500 Nm. The bending displacement of Model 2 becomes smaller than the one in Model 1 (a), but both models give very close results for the twist angles (b). The differences between the rotation about the transverse axis and the corresponding derivative of the transverse displacement increase (c) and the differences between the two rotations about the transverse axes also become bigger than in the previous example (d).

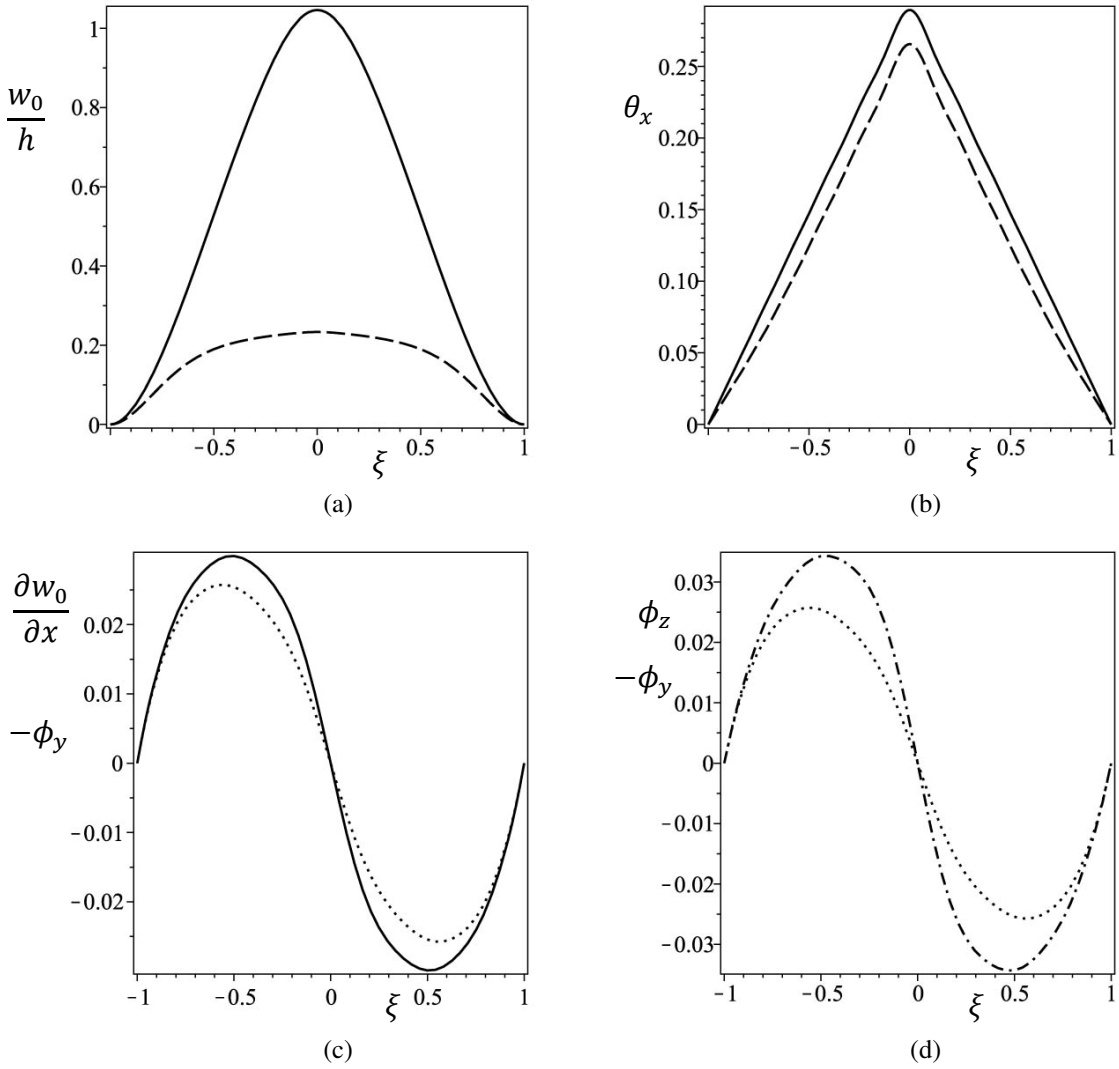

Figure 3. 4. Comparison of transverse displacement (dimensionless) and rotations about longitudinal and about transverse axes (rad) in the middle line of the beam, due to a force applied in the middle point, computed using both models: F_y = F_z = 1200 N, M_x = 350 Nm. (a) — w_0 from Model 1, --- w_0 from Model 2; (b) — θ_x from Model 1, --- θ_x from Model 2; (c) — $\partial w_0/\partial x$ from Model 1, ⋯ $(-\phi_y)$ from Model 1; (d) -·-·- ϕ_z from Model 1, ⋯ $(-\phi_y)$ from Model 1.

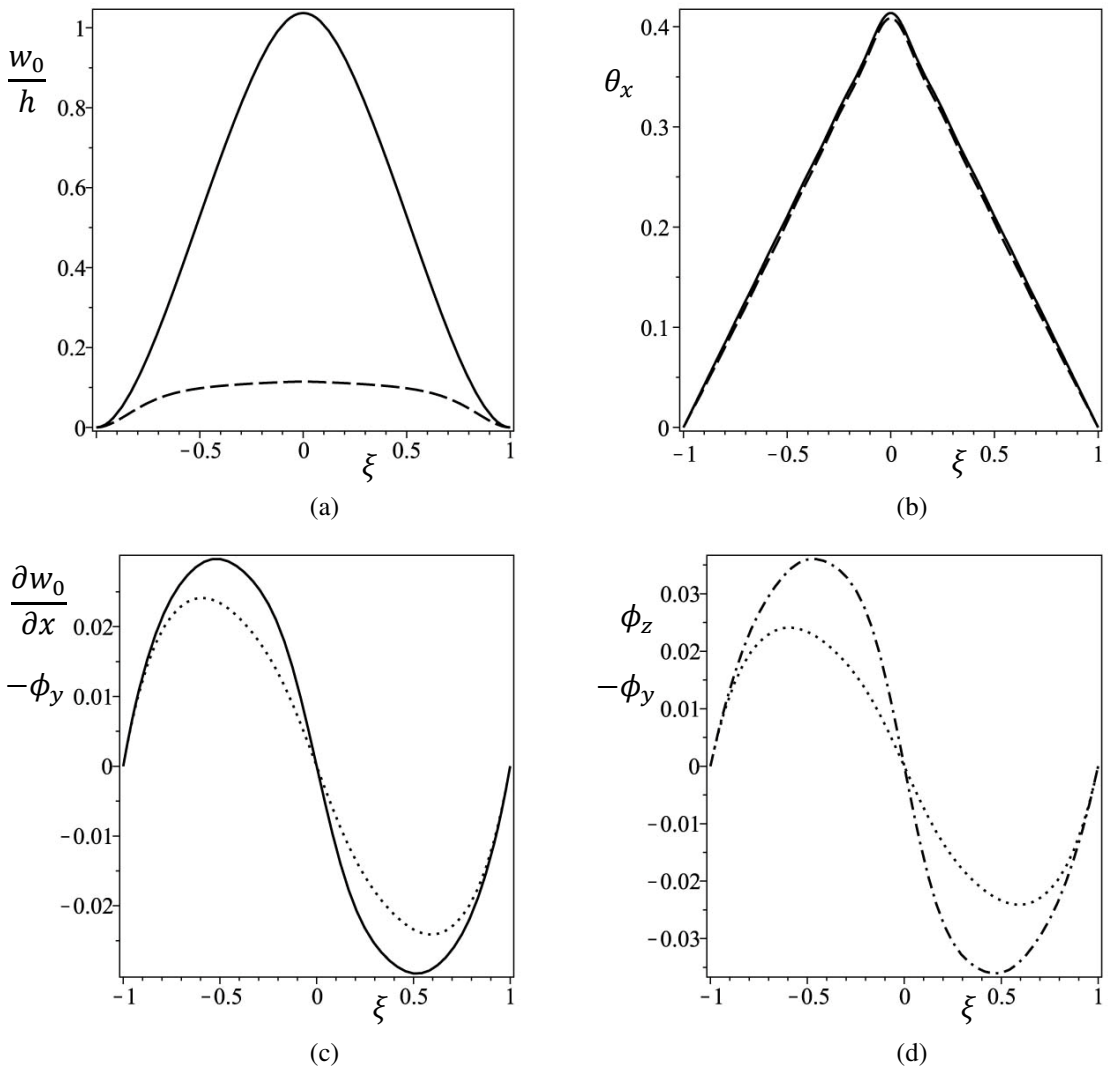

Figure 3. 5. Comparison of transverse displacement (dimensionless) and rotations about longitudinal and about transverse axes (rad) in the middle line of the beam, due to a force applied in the middle point, computed using both models: $F_y = F_z$ = 1200 N, M_x = 500 Nm. (a) — w_0 from Model 1, --- w_0 from Model 2; (b) — θ_x from Model 1, --- θ_x from Model 2; (c) — $\partial w_0/\partial x$ from Model 1, ⋯ $(-\phi_y)$ from Model 1; (d) -·-·- ϕ_z from Model 1, ⋯ $(-\phi_y)$ from Model 1.

On the other hand the examples on Figures 3. 3, 3. 4 and 3. 5 show that Model 2 gives very different results from Model 1 when torsion is coupled with bending. This is explained by the fact that the rotations about the transverse axes are significantly influenced not only by the transverse forces but also by the applied moment. Thus, these rotations cannot be directly approximated by the derivatives of the transverse displacements in the way it was done in Model 2. In fact, the transverse displacements v_0 and w_0 remain equal – and therefore so do their derivatives – since the beam cross section is square and the transverse forces are equal, while the rotations about the original transverse axes are different (pictures (d) on Figures 3. 3, 3. 4 and 3. 5).

It was also verified, using Ansys software and the beam and shell elements employed in previous sections, that, in the case of bending-torsion coupling, the rotations along the transverse axes are different, even in the case of beams with square cross section and equal transverse forces. An example of the differences between both rotations, ϕ_y and ϕ_z, is presented in Table 3. 14.

In the former examples, a beam with square cross section was chosen and equal transverse forces were applied, in order to show that the rotations about the original transverse axes are not equal in absolute value while the transverse displacements remain equal and their derivatives also. The same disadvantages appear when Model 2 is used for thinner beams and different forces.

Table 3. 14. Transverse displacements (v_0 and w_0) and rotation about x (θ_x) in the middle of the beam and maximum values of rotations about the transverse axes (ϕ_y and ϕ_z), are compared with results based on Ansys software, using beam and shell elements. A combined force is applied in the middle of the beam.

F_y = 1200 N F_z = 1200 N M_x = 300 Nm	Model 1	Ansys BEAM189	Ansys SHELL281
Displacement v_0 (m)	0.021	0.021	-
Displacement w_0 (m)	0.021	0.021	0.021
Rotation θ_x (rad)	0.289	0.293	0.300
Max value of ϕ_y (rad)	0.026	0.029	0.026
Max value of ϕ_z (rad)	0.034	0.031	0.035

These disadvantages of Model 2 come from the nonlinear terms in the shear strains in equations (2. 84) – (2. 85). Numerical tests were performed and it was verified that a model without the nonlinear terms in the shear strains gives results in accordance with the results from Model 1. The assumption behind Model 2 - that lines perpendicular to the middle line remain perpendicular during bending - implies that the shear deformation on the middle line is constrained to zero (the shear deformation is zero at all, and in particular case on the middle line). The shear deformation due to torsion is also zero on the middle line. Thus, the shear deformation should be zero on the middle line for bending-torsional couplings. However, this is not true in Model 2 due to the nonlinear terms of the shear strain (2. 84) – (2. 85), which are different from zero on the middle

line when bending is coupled with torsion. Attard [3. 13] imposed this condition - zero shear deformation on the middle line - to obtain an expression for the longitudinal displacement. As a result, the rotations along the transverse axes were approximated by the derivatives of the transverse displacements and twist angle (2. 86). This expression gives shear strains which have only linear part and involve only θ_x – equations (2. 87) and (2. 88). If one wants to develop a 3D beam model based on Bernoulli-Euler's theory for bending, the displacements field (2. 86) should be considered instead of the commonly used (2. 78).

3. 6. Evaluation of the importance of the longitudinal nonlinear terms of second order

Model 1, which considers displacement fields (2. 1), is now employed to investigate the influence of the second order terms of the longitudinal displacement. For that purpose, we carry out computations considering all nonlinear terms of second order in Green's strain field given by:

$$\varepsilon_x = \frac{\partial u}{\partial x} + \frac{1}{2}\left(\frac{\partial u}{\partial x}\right)^2 + \frac{1}{2}\left(\frac{\partial v}{\partial x}\right)^2 + \frac{1}{2}\left(\frac{\partial w}{\partial x}\right)^2,$$

$$\gamma_{zx} = \frac{\partial w}{\partial x} + \frac{\partial u}{\partial z} + \frac{\partial u}{\partial z}\frac{\partial u}{\partial x} + \frac{\partial v}{\partial z}\frac{\partial v}{\partial x} + \frac{\partial w}{\partial z}\frac{\partial w}{\partial x}, \tag{3. 6}$$

$$\gamma_{xy} = \frac{\partial u}{\partial y} + \frac{\partial v}{\partial x} + \frac{\partial u}{\partial x}\frac{\partial u}{\partial y} + \frac{\partial v}{\partial x}\frac{\partial v}{\partial y} + \frac{\partial w}{\partial x}\frac{\partial w}{\partial y},$$

and compare the results with the model presented in sub-chapter 2. 2, which is based on the strain-displacements relations given by equations (2. 6). Here 5 symmetric shape functions are used for transverse displacements and rotations about the longitudinal axis, and 5 antisymmetric shape functions are used for longitudinal displacement and for rotations about the *y* and *z* axes. As in section 3. 4, this number of shape functions, even though it is smaller than the one employed in the previous examples, is adequate for our purposes here, since it provides an accurate enough model and the differences between results with or without the additional nonlinear terms should be of the same order if more or less shape functions are used.

Table 3. 15 presents the displacements in the middle of the beam due to a combined force applied in the same point. The beam is clamped-clamped and with the following dimensions: b = 0.02 m, h = 0.02 m, l = 2.0 m. The longitudinal displacements computed with and without longitudinal nonlinear terms of second order are plotted on Figure 3. 6.

Table 3. 15. Comparison of models including and neglecting the second order terms on the longitudinal displacements. Force applied in the middle of the beam, displacements measured in the same point. The error is calculated using as a reference the results from the model including these terms.

F_y = 1000 N F_z = 1000 N M_x = 300 Nm	Model including the quadratic terms of longitudinal displacement, Eq. (3. 6)	Model neglecting the quadratic terms of longitudinal displacement, Eq. (2. 6)	Error %
Displacement v_0 (m)	0.019210	0.019234	0.1256
Displacement w_0 (m)	0.019210	0.019234	0.1256
Rotation θ_x (rad)	0.242081	0.242270	0.0781

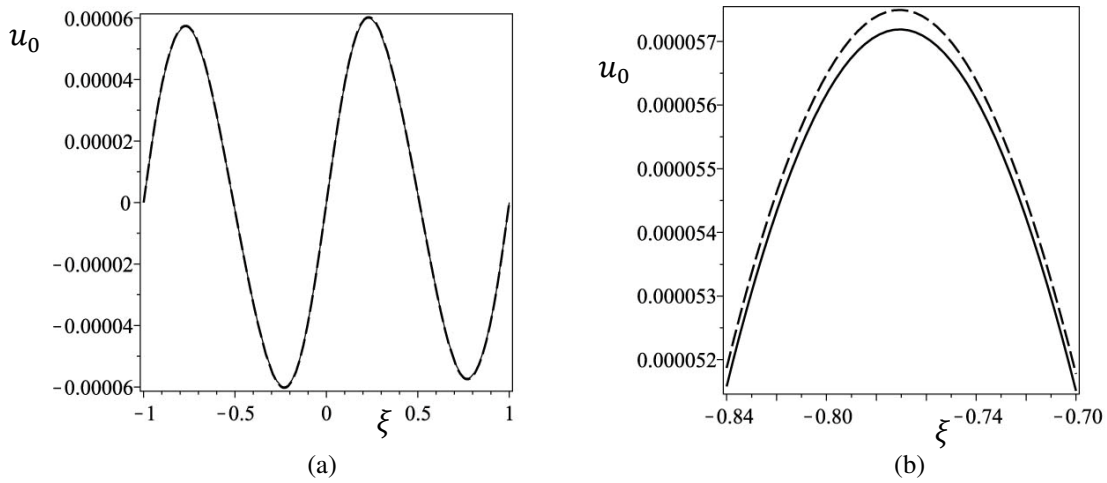

Figure 3. 6. Comparison of longitudinal displacements (m) of a clamped-clamped beam, computed with models including and neglecting the second order terms on longitudinal displacement in the strains. Line – model including these terms, dash – model neglecting these terms. (a) full length of the beam, (b) a section of the beam.

These and other tests that were carried out, but are not included here, indicate that in the presence of combined bending and torsion it is reasonable to neglect second order terms of longitudinal displacements. It can be noticed that the model including all nonlinear terms gives smaller results than the other model. This is explained by the inclusion of more terms of second order, which increase the stiffness of the beam model (a hardening spring effect) and lead to smaller displacements.

3. 7. Dynamic response

The dynamic response of beams to harmonic excitations is investigated in this section, with particular attention to bending-torsion coupling. Considering the above comparisons, Model 1, i.e. the model that results from displacement fields (2. 1), is employed. Still as a consequence of the previous analysis, warping function (2. 5) is included in the model, the linearization of the trigonometric functions is implemented only in the strain expressions, the terms of second order on the longitudinal displacement component are neglected and the terms of third-order in the direct strain are also neglected. As occurred above, the total number of DOF is 56.

First, in order to further validate the model here derived and respective codes, the dynamic responses are compared with ones published in [3. 14]. A clamped-free beam with dimensions: b = 0.06 m, h = 0.04 m, l = 1.0 m and material properties: $E = 7\,10^{10}$ N/m^2, $\rho = 2730$ kg/m^3, $\nu = 0.32$ is considered. Two distributed transverse forces are applied: $F_y = F_z = 2000 \sin\left(\pi \frac{\xi+1}{2}\right) \sin(8 \text{ x } 207.0236\, t)$. The transverse forces are the same as in [3. 14] but transformed for a local variable ξ in the interval [-1, 1]. The initial displacements and velocities are zero. The three displacements and the three rotations on the free end of the beam are plotted in Figure 3. 7.

The graphics in Figure 3. 7 are the same as the ones obtained by Cosserat theory in [3. 14]. The torsion and the rotations along the transverse axes appear with the opposite signs because of the different orientations of the coordinate systems chosen in this work and in [3. 14].

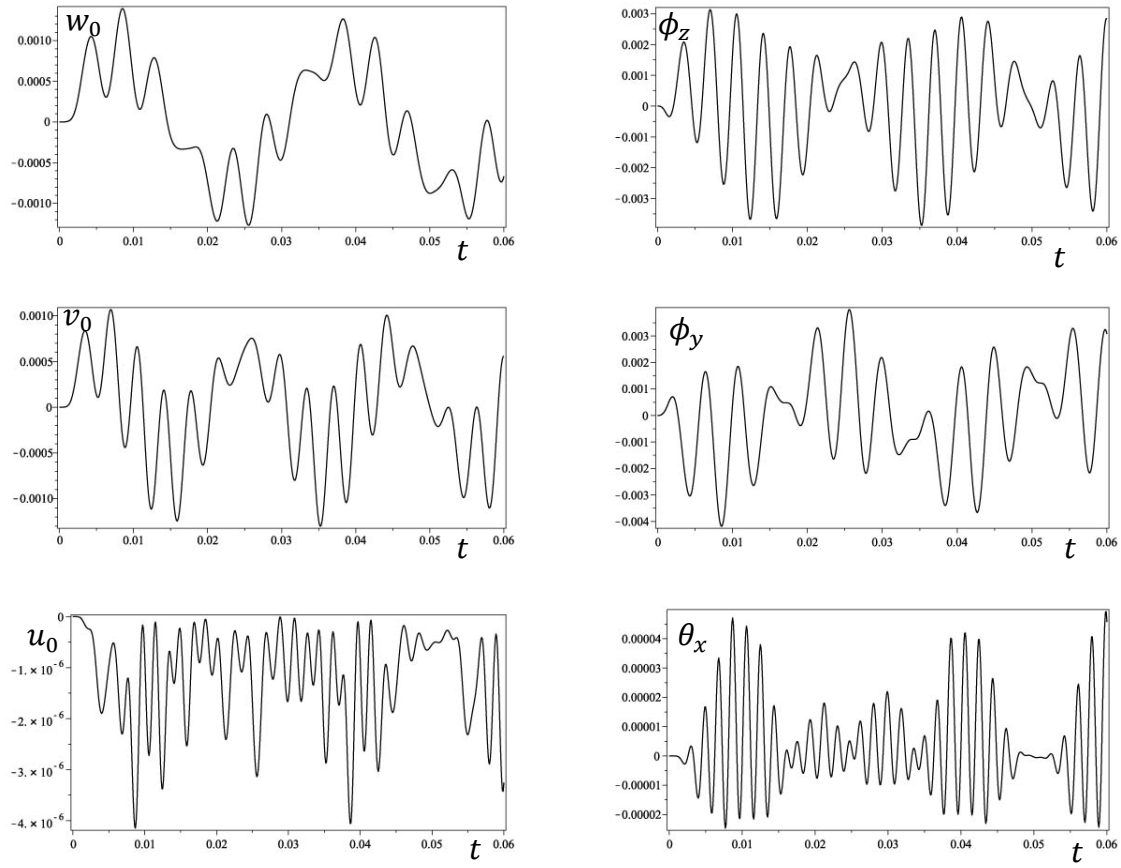

Figure. 3. 7. Dynamic responses of clamped-free beam at the free end under harmonic distributed forces. w_0, v_0 and u_0 are given in meters, while ϕ_z, ϕ_y and θ_x are given in radians.

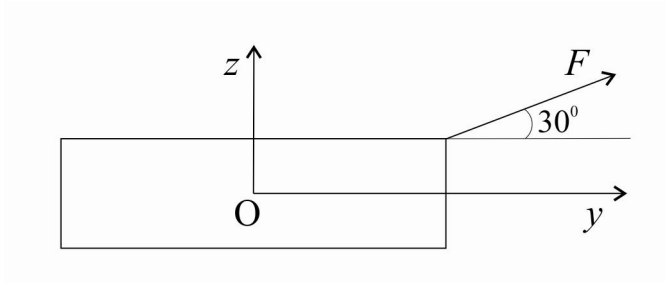

Figure 3. 8. Combined excitation.

As another example, an inclined point force is applied to a beam with dimensions: b = 0.02 m, h = 0.002 m, l = 0.58 m and with the material properties employed in the previous sections. The point force is applied at the edge of the middle cross section (x = 0) as shown in Figure 3. 8, and zero initial displacements and velocities are considered. Three different force amplitudes are chosen in order to show the effect of nonlinear bending-torsional coupling due to large displacements. The excitation frequency is $\omega = 202$ rad/s, which is 1.05 times the beam's natural frequency of flexure in the Oxz

plane. A damping matrix equal to 0.0001 times the linear stiffness matrix is used. Figure 3. 9 shows the steady state time responses for two periods of vibration, phase plots and Fourier spectra of the two transverse displacements and of the twist angle. The applied force is $F = 0.02\sin(212\,t)$ N. The amplitude of the force is small and the regime is linear, therefore there is no coupling between transverse displacement and twist. Also because the regime is linear, all displacements are harmonic functions of time, the projection of trajectories on phase planes are ellipses and only the first harmonic appears in the Fourier spectra.

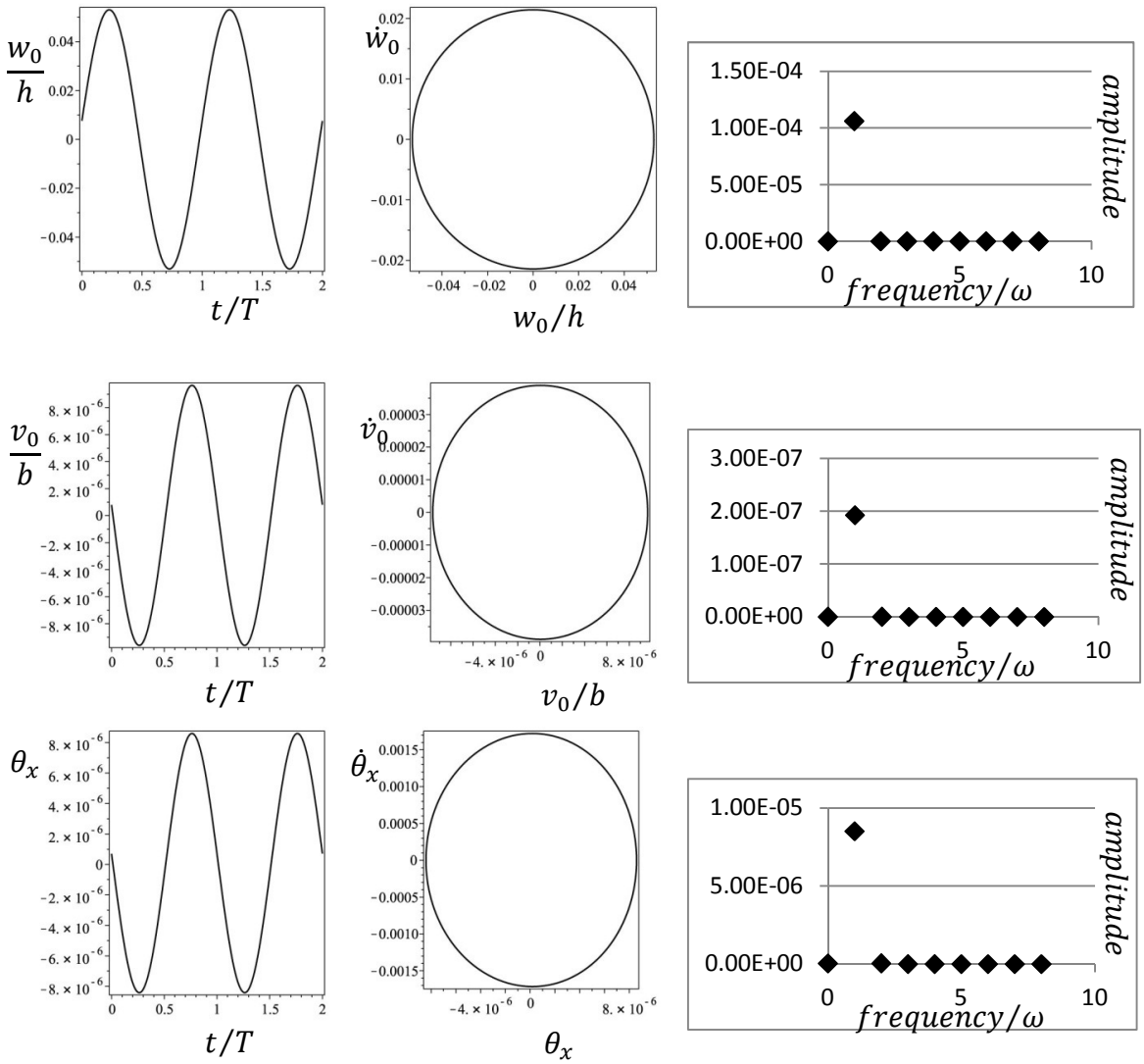

Figure 3. 9. Steady state time response plots, phase plots and Fourier spectra for beam with dimensions: 0.002 × 0.02 × 0.58. Force: $F = 0.02\sin(202t)$ N applied in the middle of the beam (x = 0). t – time, T – period of vibration.

The amplitude of the applied force is increased to 3 N and the ensuing steady state time responses, phase plots and Fourier spectra are shown in Figure 3. 10. The transverse displacement in the z direction is about the thickness of the beam, hence the nonlinear

terms are important and twist changes its symmetry properties due to the bending-torsion coupling which arises at these larger displacements. A constant term and the second harmonic appear in torsion.

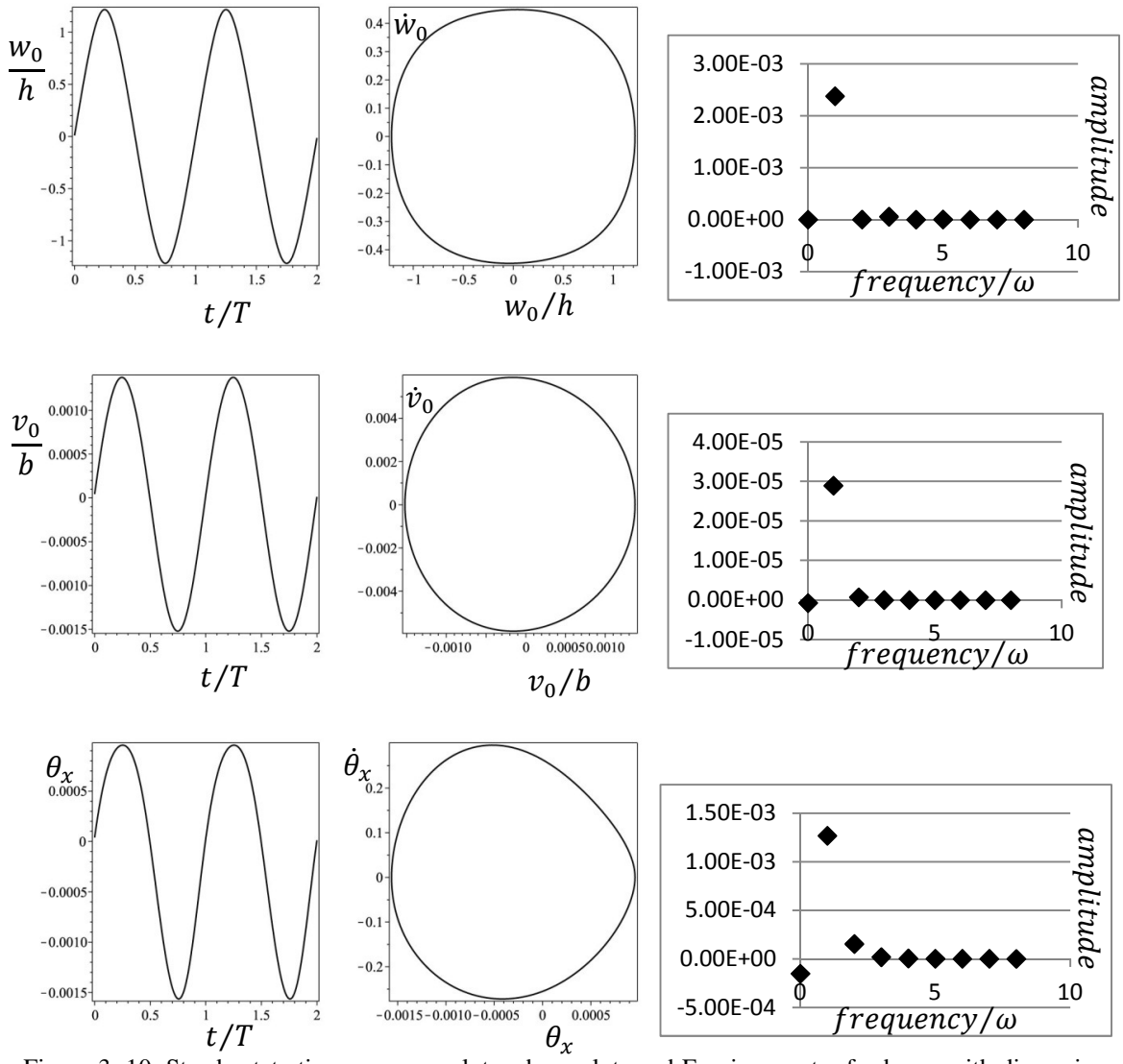

Figure 3. 10. Steady state time response plots, phase plots and Fourier spectra for beam with dimensions: 0.002 × 0.02 × 0.58. Force: $F = 3\sin(202t)$ N applied in the middle of the beam (x = 0). t – time, T – period of vibration.

In the last example, Figure 3. 11, the force amplitude is increased to 15 N and the transverse displacement in the z direction is about twice the thickness of the beam. The constant term and the second harmonic appear, alongside the main harmonic, in the Fourier spectra of all displacement components, but in particular in the w_0 displacement and in the angle of twist. Hence, none of the displacement components experiments symmetric oscillations about a zero equilibrium point. If we apply a force only in one bending plane or only a twisting moment, generally – as occurred in numerical tests using this model – the nonlinear response remains symmetric about zero. However, when

the force simultaneously excites bending and torsion, the response becomes non-symmetric due to coupling between bending and torsional terms.

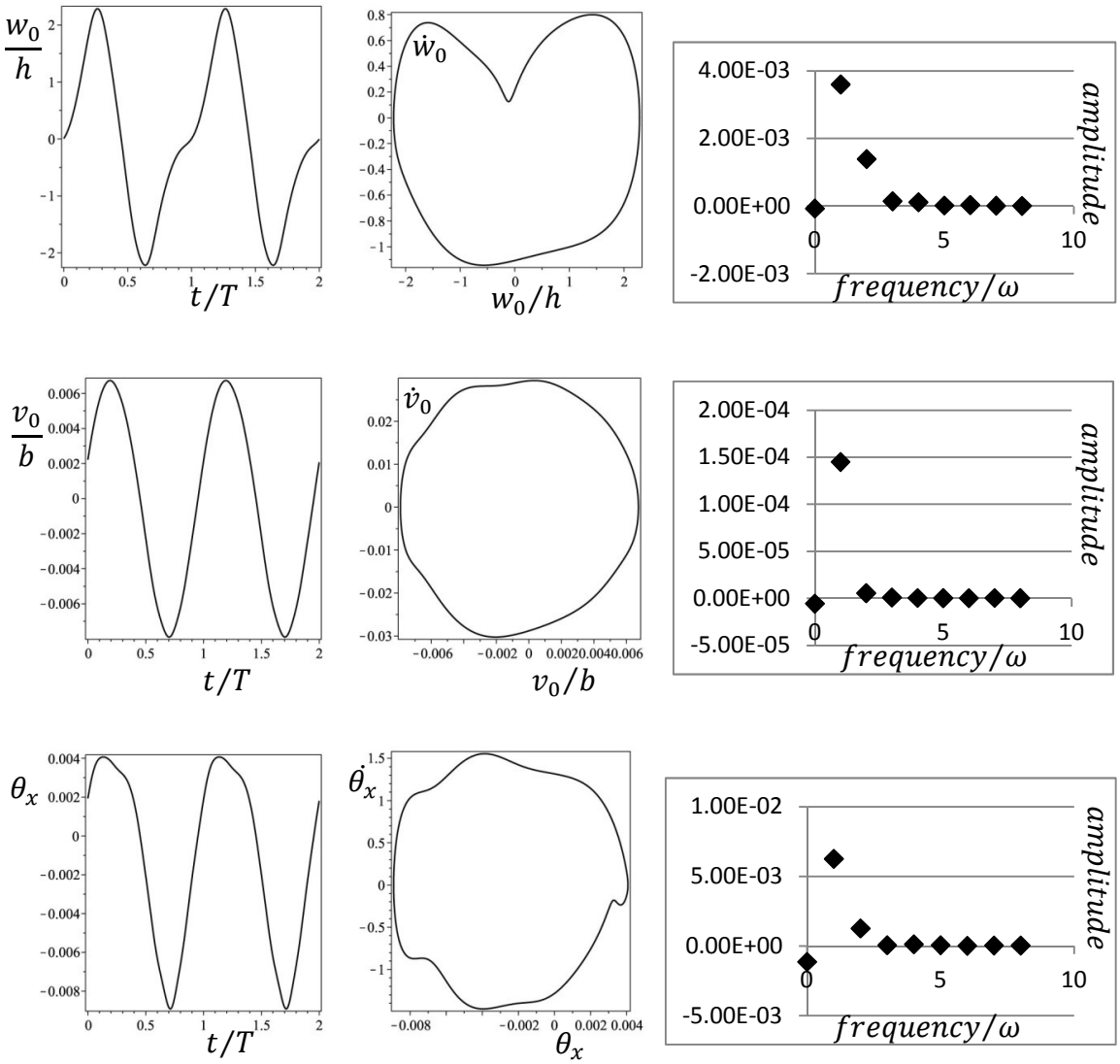

Figure 3. 11. Steady state time response plots, phase plots and Fourier spectra for beam with dimensions: 0.002 × 0.02 × 0.58. Force: $F = 15\sin(202t)$ N applied in the middle of the beam (x = 0). t – time, T – period of vibration.

3. 8. On the improvement of the torsional model

In this sub-chapter, the effect of torsion in the longitudinal displacement, presented in Chapter 2, is changed to a more general form. With this improvement the boundary conditions are more accurately respected and, as a result, the linear natural frequencies in torsion are closer to the ones obtained with Ansys using shell elements.

The same beam as in Chapter 2 with rectangular cross section and with elastic, homogeneous and isotropic materials is considered. The displacement field, only for torsion, is presented as [3. 15]:

$$u(x,y,z,t) = \psi(y,z)\,\gamma(x,t),$$
$$v(x,y,z,t) = y\cos\big(\theta_x(x,t)\big) - y - z\sin\big(\theta_x(x,t)\big), \tag{3. 7}$$
$$w(x,y,z,t) = y\sin\big(\theta_x(x,t)\big) + z\cos\big(\theta_x(x,t)\big) - z,$$

where the displacement components *u*, *v* and *w* represent the longitudinal, transverse along *y* and transverse along *z* axes, as in Chapter 2, ψ is the warping function, defined in equation (2. 5). An additional function is included in the model - $\gamma(x,t)$ - and the longitudinal displacement due to warping is written as $\psi(y,z)\,\gamma(x,t)$. The new function $\gamma(x,t)$ represents the distribution of the warping along the length of the beam. This formulation respects more accurately the boundary conditions. On a clamped boundary, the longitudinal displacement must be zero, hence there can be no cross-sectional warping and this is easy to impose by appropriately choosing the shape functions for $\gamma(x,t)$. On the other hand, in the previous formulations the longitudinal displacement originated by warping is given by $\psi(y,z)\frac{\partial\theta_x(x,t)}{\partial x}$ and cannot be zero at the clamped boundaries. In fact, $\frac{\partial\theta_x(x,t)}{\partial x}$ must be different from zero because torque due to shear stresses exists on the clamped boundaries and it is related with $\frac{\partial\theta_x(x,t)}{\partial x}$

The linear strains due to displacement field (3. 7) are given by:

$$\varepsilon_x = \psi\,\frac{\partial\gamma}{\partial x}, \tag{3. 8}$$

$$\gamma_{zx} = y\frac{\partial\theta_x}{\partial x} + \frac{\partial\psi}{\partial z}\gamma, \tag{3. 9}$$

$$\gamma_{xy} = -z\frac{\partial\theta_x}{\partial x} + \frac{\partial\psi}{\partial y}\gamma. \tag{3. 10}$$

The unknown functions along the reference axis $\theta_x(x,t)$ and $\gamma(x,t)$ are expressed by shape functions and generalised coordinates in the local coordinate system:

$$\begin{Bmatrix}\theta_x(\xi,t)\\ \gamma(\xi,t)\end{Bmatrix}=\begin{bmatrix}\lfloor N^{\theta_x}(\xi)\rfloor & 0\\ 0 & \lfloor N^{\gamma}(\xi)\rfloor\end{bmatrix}\begin{Bmatrix}q_{\theta_x}(t)\\ q_{\gamma}(t)\end{Bmatrix}. \tag{3. 11}$$

The shape functions, used for both unknown functions $\theta_x(x,t)$ and $\gamma(x,t)$, in this model will be the same as the ones used for θ_x in Chapter 2 – the set of functions $\{g\}$ given in equation (2. 18). This set of shape functions satisfies the boundary conditions and it is appropriate for γ.

Using the principle of virtual work as in Chapter 2, the linear stiffness and the mass matrices are expressed by:

$$[\mathrm{K1}]=\begin{bmatrix}\mathbf{K1_{11}} & \mathbf{K1_{12}}\\ \mathbf{K1_{12}^{T}} & \mathbf{K1_{22}}\end{bmatrix}, \tag{3. 12}$$

where

$$\mathbf{K1_{11}}=G\int_V (y^2+z^2)\frac{\partial\lfloor N^{\theta_x}\rfloor^{\mathrm{T}}}{\partial x}\frac{\partial\lfloor N^{\theta_x}\rfloor}{\partial x}\,dV, \tag{3. 13a}$$

$$\mathbf{K1_{12}}=G\int_V \left(y\frac{\partial\psi}{\partial z}-z\frac{\partial\psi}{\partial y}\right)\frac{\partial\lfloor N^{\theta_x}\rfloor^{\mathrm{T}}}{\partial x}\lfloor N^{\gamma}\rfloor\,dV, \tag{3. 13b}$$

$$\mathbf{K1_{22}}=\int_V \left(E\,\psi^2\frac{\partial\lfloor N^{\gamma}\rfloor^{\mathrm{T}}}{\partial x}\frac{\partial\lfloor N^{\gamma}\rfloor}{\partial x}+G\left(\left(\frac{\partial\psi}{\partial z}\right)^2+\left(\frac{\partial\psi}{\partial y}\right)^2\right)\lfloor N^{\gamma}\rfloor^{\mathrm{T}}\lfloor N^{\gamma}\rfloor\right)dV, \tag{3. 13c}$$

and

$$[\mathrm{M}]=\begin{bmatrix}\mathbf{M_{11}} & \mathbf{0}\\ \mathbf{0} & \mathbf{M_{22}}\end{bmatrix}, \tag{3. 14}$$

where

$$\mathbf{M_{11}}=\rho\int_V (y^2+z^2)\left\lfloor N^{\theta_x}\right\rfloor^{\mathrm{T}}\left\lfloor N^{\theta_x}\right\rfloor dV \tag{3. 15a}$$

$$\mathbf{M_{22}}=\rho\int_V \psi^2\,\lfloor N^{\gamma}\rfloor^{\mathrm{T}}\lfloor N^{\gamma}\rfloor dV. \tag{3. 15b}$$

The linear natural frequencies of a beam with dimensions b = 0.02 m, h = 0.002 and l = 0.58 are analysed as a demonstrative example of this improved model for torsion. The material properties are the same as the ones previously used. Table 3. 16 presents the linear natural frequencies calculated with different number of shape functions (the same shape functions are used for each function θ_x and γ).

Table 3. 16. Linear natural frequencies for torsion. The error is calculated between results of Ansys and the model using 25 shape functions.

6 shape functions	10 shape functions	14 shape functions	20 shape functions	25 shape functions	Ansys Shell281	Error %
3355.4797	3272.5704	3256.2519	3253.1791	3253.0861	3254.39	0.0399
6648.7696	6538.7095	6516.5568	6512.7147	6512.6191	6515.57	0.0453
9952.9521	9840.9109	9794.3547	9785.2885	9785.0093	9790.33	0.0544
13225.4373	13124.5308	13084.3464	13076.8222	13076.6305	13085.37	0.0668
71207.3776	16555.5924	16409.0915	16394.2124	16393.7472	16407.30	0.0826
-	19974.1734	19754.6603	19742.8452	19742.5562	19762.63	0.1016

It is obvious that many shape functions are required in order to obtain convergence in the linear frequencies. In Figures 3. 12 and 3. 13, the shapes of θ_x and γ at the first and second linear vibration modes are presented. A large number of shape functions are needed because of the shape of $\gamma(x,t)$, i.e. because of the distribution of warping along the length of the beam. The results are better than the model where $\psi(y,z)\frac{\partial\theta_x(x,t)}{\partial x}$ is used for the longitudinal displacement, which, for the same beam, leads to the linear natural frequencies of vibration presented in Table 3. 4.

The linear mode shapes confirm that many shape functions are required to obtain the functions on Figure 3. 12 (b) and Figure 3. 13 (b) with the shape function set $\{g\}$ defined in (2 18). Thus, the convergence of natural frequencies for torsion now requires more shape functions. Furthermore, with this torsional formulation, not only the shape functions are increased, but also the displacement field has more variables.

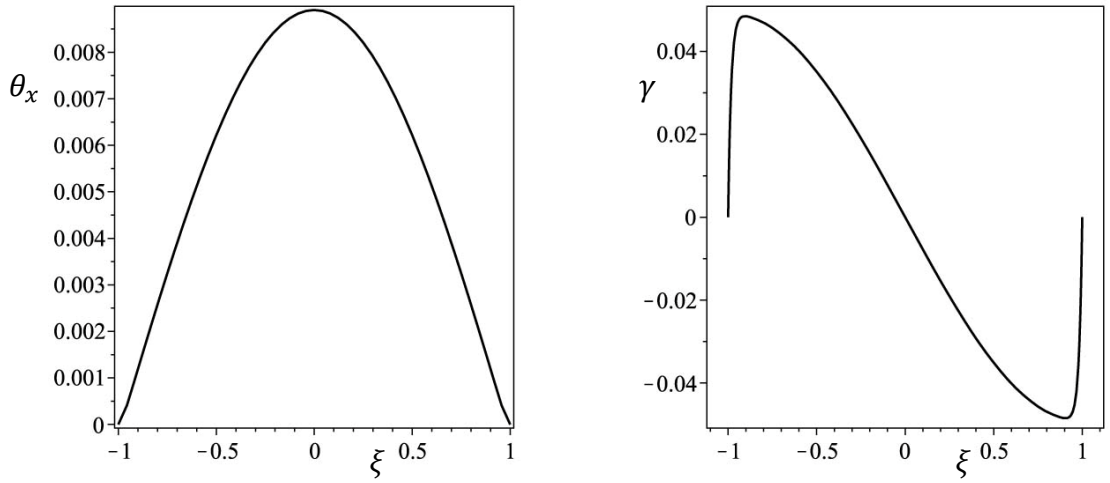

(a) (b)

Figure 3. 12. Shapes of (a) θ_x and (b) γ, at the first linear mode of vibration in torsion.

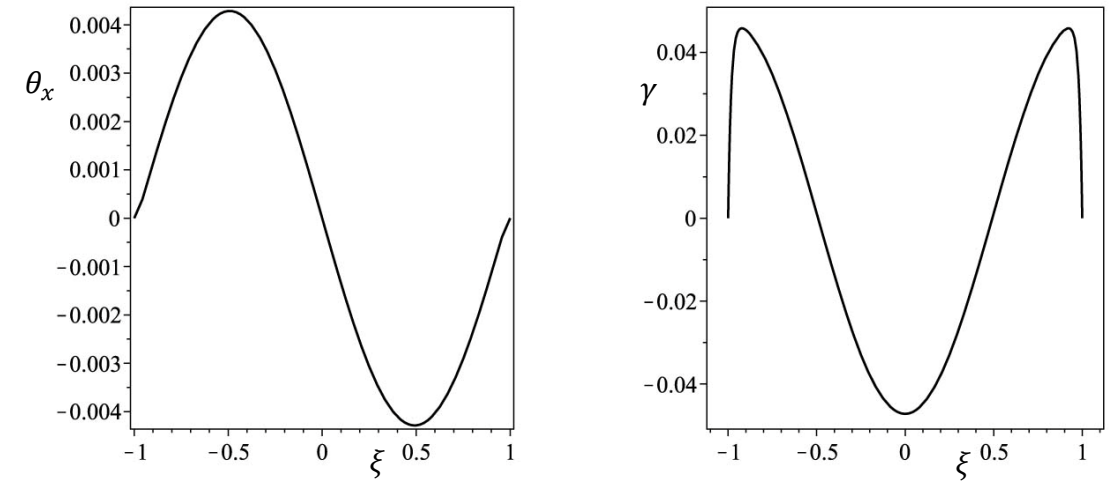

(a) (b)

Figure 3. 13. Shapes of (a) θ_x and (b) γ, at the second linear mode of vibration in torsion.

3. 9. Conclusion

P-version finite elements for geometrically nonlinear vibrations of 3D beams with rectangular cross section, which were presented in Chapter 2, were compared. The effects of the warping function, longitudinal displacements of second order and shear deformations were analysed, with a particular emphasis on deformations where torsion and bending are coupled. An improvement of the torsional model was presented, which due to the clamped boundary conditions requires more shape functions. The results show

that to have a correct and efficient model for nonlinear bending-torsion vibrations of beams, one should consider that:

(i) The warping function is very important to analyse torsion of beams with rectangular cross section, especially when the width of the beam is different from the height;

(ii) If applied, the linearization of the trigonometric terms ($\sin(\theta_x)$ and $\cos(\theta_x)$) which arise from twist of the transverse cross sections, should be implemented only in the strain expressions, not in the displacement field;

(iii) The third order terms in the direct strain which appear as nonlinear terms of order three, four and five in the stiffness matrix can be neglected (this was verified for displacement amplitudes until twice the beam thickness of clamped-clamped beams);

(iv) The common approximation of the rotations along the transverse axes used in Bernoulli-Euler's theory for bending of 2D beams should not be directly combined with Saint-Venant's theory in 3D beams. The rotations have to be approximated by expressions that involve both derivatives of transverse displacements and torsion;

(v) The longitudinal displacements of second order can be neglected, since they almost do not change the results (this was verified for displacement amplitudes until twice the beam thickness). This simplifies the model, significantly reducing the terms in the nonlinear matrices;

(vi) It is also recalled that, at least in the cases addressed, the nonlinear terms due to torsion alone are rather weak;

(vii) The improvement of the torsional model by including an additional function, which represents the distribution of the warping along the length, requires more shape functions and increases significantly the DOF.

(viii) The *p*-version element based on Timoshenko's and Saint-Venant's theories is accurate and employs a reduced number of degrees of freedom;

Considering these conclusions, taking into account that the future model should be accurate but with relatively few DOF, the investigations of the rest of the current work will continue with the model presented in Chapter 2. 2.

References

[3. 1] B. A. Szabó, I. Babuska, *Finite Element Analysis*, John Wiley & Sons, New York, 1991.

[3. 2] O. C. Zienkiewicz, R. L. Taylor, J. Z. Zhu, *The Finite Element Method: Its Basis and Fundamentals*, Sixth edition, Oxford, 2005.

[3. 3] M. Petyt, *Introduction to Finite Element Vibration Analysis*, Cambridge University Press, Cambridge, 2010.

[3. 4] L. Meirovitch, *Elements of Vibration Analysis*, McGraw-Hill Inc., Singapore, 1986.

[3. 5] J. Fonseca, P. Ribeiro, Beam *p*-version finite element for geometrically non-linear vibrations in space, *Computer Methods in Applied Mechanics and Engineering* 195 (2006) 905-924.

[3. 6] P. Ribeiro, M. Petyt, Non-linear vibrations of beams with internal resonance by the hierarchical finite-element method, *Journal of Sound and Vibration* 224 (1999) 591-624.

[3. 7] P. Ribeiro, Hierarchical finite element analyses of geometrically non-linear vibration of beams and plane frames, *Journal of Sound and Vibration* 246 (2001) 225-244.

[3. 8] P. Ribeiro, A *p*-version, first order shear deformation, finite element for geometrically non-linear vibration of curved beams, *International Journal for Numerical Methods in Engineering* 61 (2004) 2696-2715.

[3. 9] ANSYS Workbench User's Guide, 2009.

[3. 10] K. Bathe, *Finite Element Procedures*, Prentice-Hall, New Jersey 1996.

[3. 11] M. McEwan, J. Wright, J. Cooper, A. Leung, A Combined Modal/Finite Element Analysis Technique for the Dynamic Response of a Non-linear Beam to Harmonic Excitation, *Journal of Sound and Vibration* 243 (2001) 601-624.

[3. 12] P. Ribeiro, Non-linear forced vibrations of thin/thick beams and plates by the finite element and shooting methods, *Computers & Structures* 82 (2004) 1413-1423

[3. 13] M. Attard, Nonlinear theory of non-uniform torsion of thin-walled beams, *Thin-Walled Structures* 4 (1986) 101-134.

[3. 14] D. Cao, R. Tucker, Nonlinear dynamics of elastic rods using the Cosserat theory: Modelling and simulation, *International Journal of Solids and Structures* 45 (2008) 460-477.

[3. 15] M. Ganapathi, B. Patel, O. Polit, M. Touratier, A C-1 finite element including transverse shear and torsion warping for rectangular sandwich beams, *International Journal for Numerical Methods in Engineering* 45 (1999) 47-75.

4

Frequency Domain Equations of Motion and Determination of Stability by Harmonic Balance Method

4. 1. Introduction

In this chapter, the implementation of the Harmonic Balance Method (HBM) to the differential equation of motion, developed in Chapter 2, is presented. The vibrations are considered to be periodic, thus the displacement vector is expanded in Fourier series. Free and forced vibrations are analyzed in the next chapters, thus two different expansions are presented here. In the case of free vibration analysis, in the absence of damping, the cosine terms can be the only terms considered in the Fourier series. While in the case of forced vibration analysis, when a mass proportional damping is introduced, and the velocity is included in the equation of motion, cosine and sine terms have to be used in the Fourier series. In the last section, a method to determine the stability of the solutions using the HBM is presented.

The HBM can be applied either to the beam's equation of motion developed in Chapter 2 for symmetrical cross sections or to the beam's equation of motion developed in Chapter 6 for non-symmetrical cross sections. In this chapter, the equation of motion of symmetrical cross sections is considered for the application of HBM, but the same assumptions are valid for the equation of motion derived in Chapter 6. Since the equation of motion of non-symmetrical cross sections has more terms then the one of symmetrical cross sections, the resulting algebraic equation after the application of the HBM will have more terms, but they can be derived in a similar way as the ones for symmetrical cross sections presented here.

4. 2. Reduced form of the equation of motion

The equation of motion of 3D beams with rectangular cross sections, considering Timoshenko's theory for bending and Saint-Venant's theory for torsion, was developed in Chapter 2. It has the form:

$$[\mathrm{M}]\{\ddot{q}(t)\} + [\mathrm{K1}]\{q(t)\} + [\mathrm{K2}(\{q(t)\})]\{q(t)\} + 2\,[\mathrm{K2}(\{q(t)\})]^{\mathrm{T}}\{q(t)\} + \\ +[\mathrm{K4}(\{q(t)\})]\{q(t)\} = \{\mathrm{F}(t)\}, \tag{4. 1}$$

where $[\mathrm{M}]$ is the mass matrix defined in sub-chapter 2. 2. 2, $[\mathrm{K1}]$ is the linear stiffness matrix (i.e. matrix of constant terms, but called linear because it leads to linear terms in the equation of motion) defined in equation (2. 46) and $[\mathrm{K2}(\{q(t)\})]$ and $[\mathrm{K4}(\{q(t)\})]$ are the nonlinear stiffness matrices defined in equations (2. 52) and (2. 62) respectively. Equation (2. 58), which relates matrices $[\mathrm{K2}(\{q(t)\})]$ and $[\mathrm{K3}(\{q(t)\})]$, was used.

The longitudinal inertia has a small influence in the problem at hand [4. 1] and is neglected; the vector $\boldsymbol{q_u}(t)$ is eliminated from the equation of motion without neglecting it. In these conditions, the vector of generalized longitudinal displacements, $\boldsymbol{q_u}(t)$, is given by:

$$\boldsymbol{q_u}(t) = -\mathbf{K1_{11}}^{-1}\,\mathbf{K2_{12}}\big(\boldsymbol{q_v}(t)\big)\,\boldsymbol{q_v}(t) - \\ -\mathbf{K1_{11}}^{-1}\,\mathbf{K2_{13}}\big(\boldsymbol{q_w}(t)\big)\,\boldsymbol{q_w}(t) - \mathbf{K1_{11}}^{-1}\,\mathbf{K2_{14}}\left(\boldsymbol{q_{\theta_x}}(t)\right)\,\boldsymbol{q_{\theta_x}}(t) + \\ +\mathbf{K1_{11}}^{-1}\,\mathbf{F_{u_0}}(t), \tag{4. 2}$$

where $\mathbf{F_{u_0}}(t)$ is the generalized external force vector applied in longitudinal direction on the middle line.

The reduced equation of motion has the following form:

$$\begin{bmatrix} \mathbf{M_{22}} & \mathbf{0} & \mathbf{0} & \mathbf{0} & \mathbf{0} \\ \mathbf{0} & \mathbf{M_{33}} & \mathbf{0} & \mathbf{0} & \mathbf{0} \\ \mathbf{0} & \mathbf{0} & \mathbf{M_{44}} & \mathbf{0} & \mathbf{0} \\ \mathbf{0} & \mathbf{0} & \mathbf{0} & \mathbf{M_{55}} & \mathbf{0} \\ \mathbf{0} & \mathbf{0} & \mathbf{0} & \mathbf{0} & \mathbf{M_{66}} \end{bmatrix} \begin{Bmatrix} \ddot{q}_v \\ \ddot{q}_w \\ \ddot{q}_{\theta_x} \\ \ddot{q}_{\phi_y} \\ \ddot{q}_{\phi_z} \end{Bmatrix} + \begin{bmatrix} \mathbf{K1_{22}} & \mathbf{0} & \mathbf{0} & \mathbf{0} & \mathbf{K1_{26}} \\ \mathbf{0} & \mathbf{K1_{33}} & \mathbf{0} & \mathbf{K1_{35}} & \mathbf{0} \\ \mathbf{0} & \mathbf{0} & \mathbf{K1_{44}} & \mathbf{0} & \mathbf{0} \\ \mathbf{0} & \mathbf{K1_{35}}^{\mathrm{T}} & \mathbf{0} & \mathbf{K1_{55}} & \mathbf{0} \\ \mathbf{K1_{26}}^{\mathrm{T}} & \mathbf{0} & \mathbf{0} & \mathbf{0} & \mathbf{K1_{66}} \end{bmatrix} \begin{Bmatrix} q_v \\ q_w \\ q_{\theta_x} \\ q_{\phi_y} \\ q_{\phi_z} \end{Bmatrix} +$$

$$+ \begin{bmatrix} \mathbf{0} & \mathbf{K2_{23}}(q_{\theta_x}) & \mathbf{K2_{24}}(q_w) & \mathbf{0} & \mathbf{0} \\ \mathbf{K2_{32}}(q_{\theta_x}) & \mathbf{0} & \mathbf{K2_{34}}(q_v) & \mathbf{0} & \mathbf{0} \\ \mathbf{0} & \mathbf{0} & \mathbf{0} & \mathbf{0} & \mathbf{0} \\ \mathbf{K2_{52}}(q_{\theta_x}) & \mathbf{0} & \mathbf{K2_{54}}(q_v) & \mathbf{0} & \mathbf{0} \\ \mathbf{0} & \mathbf{K2_{63}}(q_{\theta_x}) & \mathbf{K2_{64}}(q_w) & \mathbf{0} & \mathbf{0} \end{bmatrix} \begin{Bmatrix} q_v \\ q_w \\ q_{\theta_x} \\ q_{\phi_y} \\ q_{\phi_z} \end{Bmatrix} +$$

$$+2 \begin{bmatrix} \mathbf{0} & \mathbf{K2_{32}}^{\mathrm{T}}(q_{\theta_x}) & \mathbf{0} & \mathbf{K2_{52}}^{\mathrm{T}}(q_{\theta_x}) & \mathbf{0} \\ \mathbf{K2_{23}}^{\mathrm{T}}(q_{\theta_x}) & \mathbf{0} & \mathbf{0} & \mathbf{0} & \mathbf{K2_{63}}^{\mathrm{T}}(q_{\theta_x}) \\ \mathbf{K2_{24}}^{\mathrm{T}}(q_w) & \mathbf{K2_{34}}^{\mathrm{T}}(q_v) & \mathbf{0} & \mathbf{K2_{54}}^{\mathrm{T}}(q_v) & \mathbf{K2_{64}}^{\mathrm{T}}(q_w) \\ \mathbf{0} & \mathbf{0} & \mathbf{0} & \mathbf{0} & \mathbf{0} \\ \mathbf{0} & \mathbf{0} & \mathbf{0} & \mathbf{0} & \mathbf{0} \end{bmatrix} \begin{Bmatrix} q_v \\ q_w \\ q_{\theta_x} \\ q_{\phi_y} \\ q_{\phi_z} \end{Bmatrix} +$$

$$+ \begin{bmatrix} \mathbf{K5_{22}}(q_v, q_w, q_{\theta_x}) & \mathbf{K5_{23}}(q_v, q_w) & \mathbf{K5_{24}}(q_v, q_{\theta_x}) & \mathbf{0} & \mathbf{0} \\ \mathbf{K5_{32}}(q_v, q_w) & \mathbf{K5_{33}}(q_v, q_w, q_{\theta_x}) & \mathbf{K5_{34}}(q_w, q_{\theta_x}) & \mathbf{0} & \mathbf{0} \\ \mathbf{K5_{42}}(q_v, q_{\theta_x}) & \mathbf{K5_{43}}(q_w, q_{\theta_x}) & \mathbf{K5_{44}}(q_v, q_w, q_{\theta_x}) & \mathbf{0} & \mathbf{0} \\ \mathbf{0} & \mathbf{0} & \mathbf{0} & \mathbf{0} & \mathbf{0} \\ \mathbf{0} & \mathbf{0} & \mathbf{0} & \mathbf{0} & \mathbf{0} \end{bmatrix} \begin{Bmatrix} q_v \\ q_w \\ q_{\theta_x} \\ q_{\phi_y} \\ q_{\phi_z} \end{Bmatrix} = \tag{4. 3}$$

$$= \begin{Bmatrix} \mathbf{F}_{v_0} - 2\,\mathbf{K2_{12}}(q_v)^{\mathrm{T}}\,\mathbf{K1_{11}}^{-1}\,\mathbf{F}_{u_0} \\ \mathbf{F}_{w_0} - 2\,\mathbf{K2_{13}}(q_w)^{\mathrm{T}}\,\mathbf{K1_{11}}^{-1}\,\mathbf{F}_{u_0} \\ \mathbf{F}_{\theta_x} - 2\,\mathbf{K2_{14}}(q_{\theta_x})^{\mathrm{T}}\,\mathbf{K1_{11}}^{-1}\,\mathbf{F}_{u_0} \\ \mathbf{F}_{\phi_y} \\ \mathbf{F}_{\phi_z} \end{Bmatrix}$$

By eliminating the longitudinal displacement $\boldsymbol{q_u}(t)$ from the equation of motion, the external force in longitudinal direction appears in the components of the force vector related with the transverse external force and the moment about the *x* axis, because of couplings induced by nonlinear terms. In the rest part of the chapter, the function arguments will not be always represented.

The sub-matrices $\mathbf{K5_{ij}}$ are given by:

$$\mathbf{K5_{ij}} = \mathbf{K4_{ij}} - 2\,\mathbf{K2_{1i}}^{\mathrm{T}}\,\mathbf{K1_{11}}^{-1}\,\mathbf{K2_{1j}}, \qquad i, j = 2, 3, 4. \tag{4. 4}$$

Sub-matrices $\mathbf{M_{ij}}$, $\mathbf{K1_{ij}}$, $\mathbf{K2_{ij}}$ and $\mathbf{K4_{ij}}$ are defined in sub-chapter 2. 2. Matrix [K5] in equation (4. 3) is defined from the sub-matrices of the matrices [K2] and [K4] due to the elimination of vector $\boldsymbol{q_u}(t)$. Matrix [K5] is quadratically dependent on vector $\{q(t)\}$ and

since the sub-matrices $\mathbf{K4}_{ij}$ are defined as a sum of more than one matrix, these matrices become dependent on two or three components of the vector $\{q(t)\}$. The mass matrix, the stiffness matrix of constant terms and the linearly dependent on $\{q(t)\}$ stiffness matrices in equation (4. 3) are the same as the ones in equation (4. 1) but without the terms related with the longitudinal displacement.

Neglecting the longitudinal inertia reduces the DOF of the system. It is recalled that the longitudinal displacement $\boldsymbol{q_u}$ is not neglected from the equation of motion and it can be calculated using equation (4. 2), i.e. the longitudinal displacement is expressed as a quadratic function of the transverse displacements $\boldsymbol{q_v}$ and $\boldsymbol{q_w}$ and of torsion $\boldsymbol{q_{\theta_x}}$. As a result, this approximation not only reduces the DOF, but also gives better approximation of the longitudinal displacement when Fourier transformation is applied. Because the longitudinal displacement is a quadratic function of the other displacements, its expansion in Fourier series contains harmonics twice of higher order than the other displacements. As will be shown in the next chapter, higher harmonics of the longitudinal displacements are important for accurate results.

4. 3. Harmonic Balance Method for free vibration analysis.

Periodic (hence steady-state) free oscillations are of interest, so the generalized displacements are given by a truncated Fourier series, with the constant term, even and odd harmonics, i.e., the generalized displacements are written as:

$$\begin{Bmatrix} \boldsymbol{q_v}(t) \\ \boldsymbol{q_w}(t) \\ \boldsymbol{q_{\theta_x}}(t) \\ \boldsymbol{q_{\phi_y}}(t) \\ \boldsymbol{q_{\phi_z}}(t) \end{Bmatrix} = \frac{1}{2}\begin{Bmatrix} \boldsymbol{Q_{v_0}} \\ \boldsymbol{Q_{w_0}} \\ \boldsymbol{Q_{\theta_{x_0}}} \\ \boldsymbol{Q_{\phi_{y_0}}} \\ \boldsymbol{Q_{\phi_{z_0}}} \end{Bmatrix} + \sum_{i=1}^{k} \begin{Bmatrix} \boldsymbol{Q_{v_i}} \\ \boldsymbol{Q_{w_i}} \\ \boldsymbol{Q_{\theta_{x_i}}} \\ \boldsymbol{Q_{\phi_{y_i}}} \\ \boldsymbol{Q_{\phi_{z_i}}} \end{Bmatrix} \cos(i\omega t), \tag{4. 5}$$

where k is the number of harmonics used in the Fourier series. A series with even harmonics and the constant term was selected, instead of the often used series with odd harmonics only (see for example [4. 2]-[4. 5]), because of two reasons: (1) unlike in planar vibrations, the equations of motion in space present both quadratic and cubic nonlinear terms, even after neglecting the longitudinal inertia; (2) we will be also interested in finding symmetry breaking bifurcations of planar vibration modes,

bifurcations which lead to the excitation of even harmonics. One should note that the sine terms are not included in the Fourier series. They are not excited in the main branch because damping is not considered in free vibration analysis and only the vector of generalized coordinates and its second derivative appear in the equation of motion. This formulation reduces the DOF but has disadvantage that 1:1 internal resonances cannot be discovered. Nevertheless, 1:1 internal resonances are studies in forced vibrations analysis where sine terms are included in the Fourier series.

The new unknowns are the coefficients of the harmonics, which can be written in vector form as:

$$\{Q\} = \begin{Bmatrix} \boldsymbol{Q_v} \\ \boldsymbol{Q_w} \\ \boldsymbol{Q_{\theta_x}} \\ \boldsymbol{Q_{\phi_y}} \\ \boldsymbol{Q_{\phi_z}} \end{Bmatrix}, \tag{4. 6}$$

where, for example in the case $k = 5$, $\boldsymbol{Q_w}$ is expressed by:

$$\boldsymbol{Q_w} = \begin{Bmatrix} \boldsymbol{Q_{w_0}} \\ \boldsymbol{Q_{w_1}} \\ \boldsymbol{Q_{w_2}} \\ \boldsymbol{Q_{w_3}} \\ \boldsymbol{Q_{w_4}} \\ \boldsymbol{Q_{w_5}} \end{Bmatrix}, \tag{4. 7}$$

and the dimension of each sub-vector $\boldsymbol{Q_{w_i}}$ is the number of shape functions used for w_0, i.e. p_w. It results from the former assumptions that the unknown vector $\{Q\}$ does not depend on time. The longitudinal displacement can be recovered from equations (4. 5) and (4. 2).

The time dependent generalised coordinates are replaced by their Fourier expansion, equation (4. 5), inserted in the equation of motion (4. 3) and the HBM [4. 6]-[4. 7] is employed. The resulting equation of motion in the frequency domain is of the form (in the absence of the external force):

$$\begin{aligned} \{\mathcal{F}(\{Q\}, \omega)\} = (-\omega^2\,[\mathrm{M}^{\mathrm{HBM}}] + [\mathrm{K1}^{\mathrm{HBM}}] + [\mathrm{K2}^{\mathrm{HBM}}(\{Q\})] + \\ +2\,[\mathrm{K2}^{\mathrm{HBM}}(\{Q\})]^{\mathrm{T}} + [\mathrm{K5}^{\mathrm{HBM}}(\{Q\})])\{Q\} = \{0\}, \end{aligned} \tag{4. 8}$$

where $[\mathrm{M}^{\mathrm{HBM}}]$ represents the mass matrix which is created from matrices $\mathbf{M_{ij}}$ of equation (4. 3), $[\mathrm{K1}^{\mathrm{HBM}}]$ is the stiffness matrix of constant terms which results from matrices $\mathbf{K1}_{ij}$ of equation (4. 3), $[\mathrm{K2}^{\mathrm{HBM}}(\{Q\})]$ is the stiffness matrix which depends linearly on the coefficients of the harmonics, it is created from matrices $\mathbf{K2}_{ij}$ of equation (4. 3), and $[\mathrm{K5}^{\mathrm{HBM}}(\{Q\})]$ is the stiffness matrix which depends quadratically on the coefficients of harmonics, it results from matrices $\mathbf{K5}_{ij}$ of equation (4. 3). The structure of these matrices after the HBM is implemented is presented in the next sub-sections for the case $k = 5$, i.e. when harmonics till fifth order are used in equation (4. 5). In this case, the longitudinal displacement, obtained from equation (4. 2) is expressed with harmonics up to the tenth. The total number of degrees of freedom of the frequency domain model is $\mathrm{N} = (1 + k)\left(p_v + p_w + p_{\theta_x} + p_{\phi_y} + p_{\phi_z}\right)$.

4. 3. 1. Stiffness matrix after application of the HBM

4. 3. 1. 1. Linear stiffness matrix $[\mathrm{K1}^{\mathrm{HBM}}]$

The complete linear stiffness matrix of the time domain equation of motion was presented in Chapter 2 in equation (2.46). After neglecting the longitudinal displacement, its structure is given in equation (4. 3), with the sub-matrices given by equations (2. 47b) – (2. 47h). Assuming harmonics up to fifth order in equation (4. 5), the linear stiffness matrix $[\mathrm{K1}^{\mathrm{HBM}}]$ becomes:

$$[\mathrm{K1}^{\mathrm{HBM}}] = \begin{bmatrix} \mathbf{K1_{22}^{HBM}} & \mathbf{0} & \mathbf{0} & \mathbf{0} & \mathbf{K1_{26}^{HBM}} \\ \mathbf{0} & \mathbf{K1_{33}^{HBM}} & \mathbf{0} & \mathbf{K1_{35}^{HBM}} & \mathbf{0} \\ \mathbf{0} & \mathbf{0} & \mathbf{K1_{44}^{HBM}} & \mathbf{0} & \mathbf{0} \\ \mathbf{0} & \mathbf{K1_{35}^{HBM^T}} & \mathbf{0} & \mathbf{K1_{55}^{HBM}} & \mathbf{0} \\ \mathbf{K1_{26}^{HBM^T}} & \mathbf{0} & \mathbf{0} & \mathbf{0} & \mathbf{K1_{66}^{HBM}} \end{bmatrix}, \tag{4. 9}$$

where, for example, the sub-matrix $\mathbf{K1_{22}^{HBM}}$ is expressed as:

$$\mathbf{K1_{22}^{HBM}} = \begin{bmatrix} \frac{1}{2}\,\mathbf{K1_{22}} & \mathbf{0} & \mathbf{0} & \mathbf{0} & \mathbf{0} & \mathbf{0} \\ \mathbf{0} & \mathbf{K1_{22}} & \mathbf{0} & \mathbf{0} & \mathbf{0} & \mathbf{0} \\ \mathbf{0} & \mathbf{0} & \mathbf{K1_{22}} & \mathbf{0} & \mathbf{0} & \mathbf{0} \\ \mathbf{0} & \mathbf{0} & \mathbf{0} & \mathbf{K1_{22}} & \mathbf{0} & \mathbf{0} \\ \mathbf{0} & \mathbf{0} & \mathbf{0} & \mathbf{0} & \mathbf{K1_{22}} & \mathbf{0} \\ \mathbf{0} & \mathbf{0} & \mathbf{0} & \mathbf{0} & \mathbf{0} & \mathbf{K1_{22}} \end{bmatrix}. \tag{4. 10}$$

The rest of the sub-matrices in equation (4. 9) have the same structure as sub-matrix $\mathbf{K1}_{\mathbf{22}}^{\mathbf{HBM}}$ in equation (4. 10), but using the corresponding sub-matrices defined in equations (2. 47b) – (2. 47h).

4. 3. 1. 2. Nonlinear stiffness matrix $[\mathrm{K2}^{\mathrm{HBM}}(\{Q\})]$

The linearly dependent on the vector of coefficients of harmonics $\{Q\}$ matrix $[\mathrm{K2}^{\mathrm{HBM}}(\{Q\})]$, which results from replacing equation (4. 5) into (4. 3), has the following form:

$$[\mathrm{K2}^{\mathrm{HBM}}(\{Q\})] = \begin{bmatrix} \mathbf{0} & \mathbf{K2}_{\mathbf{23}}^{\mathbf{HBM}}(\boldsymbol{Q}_{\theta_x}) & \mathbf{K2}_{\mathbf{24}}^{\mathbf{HBM}}(\boldsymbol{Q}_w) & \mathbf{0} & \mathbf{0} \\ \mathbf{K2}_{\mathbf{32}}^{\mathbf{HBM}}(\boldsymbol{Q}_{\theta_x}) & \mathbf{0} & \mathbf{K2}_{\mathbf{34}}^{\mathbf{HBM}}(\boldsymbol{Q}_v) & \mathbf{0} & \mathbf{0} \\ \mathbf{0} & \mathbf{0} & \mathbf{0} & \mathbf{0} & \mathbf{0} \\ \mathbf{K2}_{\mathbf{52}}^{\mathbf{HBM}}(\boldsymbol{Q}_{\theta_x}) & \mathbf{0} & \mathbf{K2}_{\mathbf{54}}^{\mathbf{HBM}}(\boldsymbol{Q}_v) & \mathbf{0} & \mathbf{0} \\ \mathbf{0} & \mathbf{K2}_{\mathbf{63}}^{\mathbf{HBM}}(\boldsymbol{Q}_{\theta_x}) & \mathbf{K2}_{\mathbf{64}}^{\mathbf{HBM}}(\boldsymbol{Q}_w) & \mathbf{0} & \mathbf{0} \end{bmatrix}, \tag{4. 11}$$

where each of the sub-matrices is constructed as a sum of matrices that are linearly dependent on the coefficients of the harmonics written in equation (4. 5), similar to the matrices presented in equations (2. 53d) – (2. 53k). The difference is that now these matrices depend on the coefficients of the harmonics instead of the generalised coordinates. For example, the sub-matrix $\mathbf{K2}_{\mathbf{24}}^{\mathbf{HBM}}(\boldsymbol{Q}_w)$ is expressed as:

$$\mathbf{K2}_{\mathbf{24}}^{\mathbf{HBM}}(\boldsymbol{Q}_w) = \frac{1}{2}\begin{bmatrix} \frac{1}{2}\mathbf{K2}_{24}(\boldsymbol{Q}_{w_0}) & \mathbf{K2}_{24}(\boldsymbol{Q}_{w_1}) & \mathbf{K2}_{24}(\boldsymbol{Q}_{w_2}) \\ \mathbf{K2}_{24}(\boldsymbol{Q}_{w_1}) & \mathbf{K2}_{24}(\boldsymbol{Q}_{w_0}) + \mathbf{K2}_{24}(\boldsymbol{Q}_{w_2}) & \mathbf{K2}_{24}(\boldsymbol{Q}_{w_1}) + \mathbf{K2}_{24}(\boldsymbol{Q}_{w_3}) \\ \mathbf{K2}_{24}(\boldsymbol{Q}_{w_2}) & \mathbf{K2}_{24}(\boldsymbol{Q}_{w_1}) + \mathbf{K2}_{24}(\boldsymbol{Q}_{w_3}) & \mathbf{K2}_{24}(\boldsymbol{Q}_{w_0}) + \mathbf{K2}_{24}(\boldsymbol{Q}_{w_4}) \\ \mathbf{K2}_{24}(\boldsymbol{Q}_{w_3}) & \mathbf{K2}_{24}(\boldsymbol{Q}_{w_2}) + \mathbf{K2}_{24}(\boldsymbol{Q}_{w_4}) & \mathbf{K2}_{24}(\boldsymbol{Q}_{w_1}) + \mathbf{K2}_{24}(\boldsymbol{Q}_{w_5}) \\ \mathbf{K2}_{24}(\boldsymbol{Q}_{w_4}) & \mathbf{K2}_{24}(\boldsymbol{Q}_{w_3}) + \mathbf{K2}_{24}(\boldsymbol{Q}_{w_5}) & \mathbf{K2}_{24}(\boldsymbol{Q}_{w_2}) \\ \mathbf{K2}_{24}(\boldsymbol{Q}_{w_5}) & \mathbf{K2}_{24}(\boldsymbol{Q}_{w_4}) & \mathbf{K2}_{24}(\boldsymbol{Q}_{w_3}) \end{bmatrix}$$

$$\begin{bmatrix} \mathbf{K2}_{24}(\boldsymbol{Q}_{w_3}) & \mathbf{K2}_{24}(\boldsymbol{Q}_{w_4}) & \mathbf{K2}_{24}(\boldsymbol{Q}_{w_5}) \\ \mathbf{K2}_{24}(\boldsymbol{Q}_{w_2}) + \mathbf{K2}_{24}(\boldsymbol{Q}_{w_4}) & \mathbf{K2}_{24}(\boldsymbol{Q}_{w_3}) + \mathbf{K2}_{24}(\boldsymbol{Q}_{w_5}) & \mathbf{K2}_{24}(\boldsymbol{Q}_{w_4}) \\ \mathbf{K2}_{24}(\boldsymbol{Q}_{w_1}) + \mathbf{K2}_{24}(\boldsymbol{Q}_{w_5}) & \mathbf{K2}_{24}(\boldsymbol{Q}_{w_2}) & \mathbf{K2}_{24}(\boldsymbol{Q}_{w_3}) \\ \mathbf{K2}_{24}(\boldsymbol{Q}_{w_0}) & \mathbf{K2}_{24}(\boldsymbol{Q}_{w_1}) & \mathbf{K2}_{24}(\boldsymbol{Q}_{w_2}) \\ \mathbf{K2}_{24}(\boldsymbol{Q}_{w_1}) & \mathbf{K2}_{24}(\boldsymbol{Q}_{w_0}) & \mathbf{K2}_{24}(\boldsymbol{Q}_{w_1}) \\ \mathbf{K2}_{24}(\boldsymbol{Q}_{w_2}) & \mathbf{K2}_{24}(\boldsymbol{Q}_{w_1}) & \mathbf{K2}_{24}(\boldsymbol{Q}_{w_0}) \end{bmatrix}, \tag{4. 12}$$

where

$$\mathbf{K2_{24}}(\boldsymbol{Q_{w_i}}) = \frac{1}{2}\lambda G \int_V \frac{d\lfloor N^v \rfloor^{\mathrm{T}}}{dx} \lfloor N^{\theta_x} \rfloor \left(\frac{d\lfloor N^w \rfloor}{dx} \{Q_{w_i}\} \right) dV \tag{4. 13}$$

comes from the definition of $\mathbf{K2_{24}}$ in equation (2. 53e). The term $\frac{d\lfloor N^w \rfloor}{dx}\{Q_{w_i}\}$ is a scalar.

4. 3. 1. 3. Nonlinear stiffness matrix $[\mathrm{K5}^{\mathrm{HBM}}(\{Q\})]$

The matrix $[\mathrm{K5}^{\mathrm{HBM}}(\{Q\})]$, which results from replacing equation (4. 5) into (4. 3), and depends quadratically on the vector of coefficients of harmonics $\{Q\}$, has the following form:

$$[\mathrm{K5}^{\mathrm{HBM}}(\{Q\})] =$$

$$= \begin{bmatrix} \mathbf{K5_{22}^{HBM}}(\boldsymbol{Q_v}, \boldsymbol{Q_w}, \boldsymbol{Q_{\theta_x}}) & \mathbf{K5_{23}^{HBM}}(\boldsymbol{Q_v}, \boldsymbol{Q_w}) & \mathbf{K5_{24}^{HBM}}(\boldsymbol{Q_v}, \boldsymbol{Q_{\theta_x}}) & \mathbf{0} & \mathbf{0} \\ \mathbf{K5_{32}^{HBM}}(\boldsymbol{Q_v}, \boldsymbol{Q_w}) & \mathbf{K5_{33}^{HBM}}(\boldsymbol{Q_v}, \boldsymbol{Q_w}, \boldsymbol{Q_{\theta_x}}) & \mathbf{K5_{34}^{HBM}}(\boldsymbol{Q_w}, \boldsymbol{Q_{\theta_x}}) & \mathbf{0} & \mathbf{0} \\ \mathbf{K5_{42}^{HBM}}(\boldsymbol{Q_v}, \boldsymbol{Q_{\theta_x}}) & \mathbf{K5_{43}^{HBM}}(\boldsymbol{Q_w}, \boldsymbol{Q_{\theta_x}}) & \mathbf{K5_{44}^{HBM}}(\boldsymbol{Q_v}, \boldsymbol{Q_w}, \boldsymbol{Q_{\theta_x}}) & \mathbf{0} & \mathbf{0} \\ \mathbf{0} & \mathbf{0} & \mathbf{0} & \mathbf{0} & \mathbf{0} \\ \mathbf{0} & \mathbf{0} & \mathbf{0} & \mathbf{0} & \mathbf{0} \end{bmatrix}, \tag{4. 14}$$

where each of these sub-matrices has the form given in equation (4. 4), i.e. it is constructed as a sum of matrices, quadratically dependent on the coefficients of the harmonics from equation (4. 5). For example, the sub-matrix $\mathbf{K5_{33}^{HBM}}(\boldsymbol{Q_v}, \boldsymbol{Q_w}, \boldsymbol{Q_{\theta_x}})$, considering (2. 63c) and (4. 4) is a sum of matrices which depend quadratically on $\boldsymbol{Q_v}$, $\boldsymbol{Q_w}$ and $\boldsymbol{Q_{\theta_x}}$ and may be written in the following way:

$$\mathbf{K5_{33}^{HBM}}(\boldsymbol{Q_v}, \boldsymbol{Q_w}, \boldsymbol{Q_{\theta_x}}) = \mathbf{K4_{33}^{HBM}}(\boldsymbol{Q_v}) + \mathbf{K4_{33}^{HBM}}(\boldsymbol{Q_w}) + \mathbf{K4_{33}^{HBM}}(\boldsymbol{Q_{\theta_x}}) - \\ -2\,\mathbf{K4_{33}^{HBM^*}}(\boldsymbol{Q_w}) \tag{4. 15}$$

where, for example,

$$\mathbf{K4_{33}^{HBM}}(\mathbf{Q_w}) = \frac{1}{4}\begin{bmatrix} \mathbf{A_{11}} & \mathbf{A_{12}} & \mathbf{A_{13}} & \mathbf{A_{14}} & \mathbf{A_{15}} & \mathbf{A_{16}} \\ \mathbf{A_{12}}^{\mathrm{T}} & \mathbf{A_{22}} & \mathbf{A_{23}} & \mathbf{A_{24}} & \mathbf{A_{25}} & \mathbf{A_{26}} \\ \mathbf{A_{13}}^{\mathrm{T}} & \mathbf{A_{23}}^{\mathrm{T}} & \mathbf{A_{33}} & \mathbf{A_{34}} & \mathbf{A_{35}} & \mathbf{A_{36}} \\ \mathbf{A_{14}}^{\mathrm{T}} & \mathbf{A_{24}}^{\mathrm{T}} & \mathbf{A_{34}}^{\mathrm{T}} & \mathbf{A_{44}} & \mathbf{A_{45}} & \mathbf{A_{46}} \\ \mathbf{A_{15}}^{\mathrm{T}} & \mathbf{A_{25}}^{\mathrm{T}} & \mathbf{A_{35}}^{\mathrm{T}} & \mathbf{A_{45}}^{\mathrm{T}} & \mathbf{A_{55}} & \mathbf{A_{56}} \\ \mathbf{A_{16}}^{\mathrm{T}} & \mathbf{A_{26}}^{\mathrm{T}} & \mathbf{A_{36}}^{\mathrm{T}} & \mathbf{A_{46}}^{\mathrm{T}} & \mathbf{A_{56}}^{\mathrm{T}} & \mathbf{A_{66}} \end{bmatrix}, \tag{4. 16}$$

where the sub-matrices $\mathbf{A_{ij}}$ are given in Appendix A.

4. 3. 2. Mass matrix after application of the HBM

The mass matrix of the equation of motion was presented in Chapter 2 in equation (2. 71) and after neglecting the longitudinal displacement its structure is given in equation (4. 3), where the sub-matrices are given by equations (2. 72b) – (2. 72f). Assuming harmonics up to fifth order in equation (4. 5), the mass matrix $[\mathrm{M}^{\mathrm{HBM}}]$ becomes:

$$[\mathrm{M}^{\mathrm{HBM}}] = \begin{bmatrix} \mathbf{M}_{22}^{\mathbf{HBM}} & \mathbf{0} & \mathbf{0} & \mathbf{0} & \mathbf{0} \\ \mathbf{0} & \mathbf{M}_{33}^{\mathbf{HBM}} & \mathbf{0} & \mathbf{0} & \mathbf{0} \\ \mathbf{0} & \mathbf{0} & \mathbf{M}_{44}^{\mathbf{HBM}} & \mathbf{0} & \mathbf{0} \\ \mathbf{0} & \mathbf{0} & \mathbf{0} & \mathbf{M}_{55}^{\mathbf{HBM}} & \mathbf{0} \\ \mathbf{0} & \mathbf{0} & \mathbf{0} & \mathbf{0} & \mathbf{M}_{66}^{\mathbf{HBM}} \end{bmatrix}, \tag{4. 17}$$

where, for example, the sub-matrix $\mathbf{M}_{22}^{\mathbf{HBM}}$ is expressed as:

$$\mathbf{M}_{22}^{\mathbf{HBM}} = \begin{bmatrix} \mathbf{0} & \mathbf{0} & \mathbf{0} & \mathbf{0} & \mathbf{0} & \mathbf{0} \\ \mathbf{0} & \mathbf{M}_{22} & \mathbf{0} & \mathbf{0} & \mathbf{0} & \mathbf{0} \\ \mathbf{0} & \mathbf{0} & \mathbf{4\,M}_{22} & \mathbf{0} & \mathbf{0} & \mathbf{0} \\ \mathbf{0} & \mathbf{0} & \mathbf{0} & \mathbf{9\,M}_{22} & \mathbf{0} & \mathbf{0} \\ \mathbf{0} & \mathbf{0} & \mathbf{0} & \mathbf{0} & \mathbf{16\,M}_{22} & \mathbf{0} \\ \mathbf{0} & \mathbf{0} & \mathbf{0} & \mathbf{0} & \mathbf{0} & \mathbf{25\,M}_{22} \end{bmatrix}. \tag{4. 18}$$

The rest of the sub-matrices in equation (4. 17) have the same structure as the sub-matrix $\mathbf{M}_{22}^{\mathbf{HBM}}$ in equation (4. 18), but using the corresponding sub-matrices defined in equations (2. 72b) – (2. 72f).

4. 4. Harmonic Balance Method for forced vibration analysis.

Periodic oscillations due to external harmonic excitations are of interest in this sub-chapter and damping is introduced in the equation of motion. The latter, can be written in the following form:

$$[\mathrm{M}]\{\ddot{q}(t)\} + \frac{\beta}{\omega}[\mathrm{M}]\{\dot{q}(t)\} + [\mathrm{K1}]\{q(t)\} + [\mathrm{KNL}(\{q(t)\})]\{q(t)\} = \{\mathrm{F}\}\cos(\omega t), \tag{4. 19}$$

where the nonlinear stiffness matrix $[\mathrm{KNL}(\{q(t)\})]$ is defined as:

$$[\mathrm{KNL}(\{q(t)\})] = [\mathrm{K2}(\{q(t)\})] + 2\,[\mathrm{K2}(\{q(t)\})]^{\mathrm{T}} + [\mathrm{K5}(\{q(t)\})]. \tag{4. 20}$$

The mass matrix $[\mathrm{M}]$, the linear stiffness matrix $[\mathrm{K1}]$ and the nonlinear stiffness matrices $[\mathrm{K2}(\{q(t)\})]$ and $[\mathrm{K5}(\{q(t)\})]$ have the form given in equation (4. 3), i.e. the

longitudinal inertia is neglected and the matrix $[\mathrm{K5}(\{q(t)\})]$ is defined in equation (4. 4) A damping proportional to the mass matrix and dependent on the frequency of vibration is inserted into the equation of motion [4. 8]. It depends also on damping factor α which can be estimated from experiments:

$$\beta = \alpha\, \omega_{l_1}^2, \tag{4. 21}$$

where ω_{l_1} presents the fundamental linear frequency. The excitation frequency is represented by ω. This kind of damping, dependent on the excitation frequency, is preferred for bifurcation analysis, because after application of HBM only the square of the vibration frequency will appear in the algebraic equation.

The generalised displacements are expressed in Fourier series. Here, both sine and cosine terms are required due to the introduced damping which is related with the velocity, i.e. the generalized displacements are now written as:

$$\begin{Bmatrix} \boldsymbol{q_v}(t) \\ \boldsymbol{q_w}(t) \\ \boldsymbol{q_{\theta_x}}(t) \\ \boldsymbol{q_{\phi_y}}(t) \\ \boldsymbol{q_{\phi_z}}(t) \end{Bmatrix} = \frac{1}{2}\begin{Bmatrix} \boldsymbol{Q_{v_0}} \\ \boldsymbol{Q_{w_0}} \\ \boldsymbol{Q_{\theta_{x_0}}} \\ \boldsymbol{Q_{\phi_{y_0}}} \\ \boldsymbol{Q_{\phi_{z_0}}} \end{Bmatrix} + \sum_{i=1}^{k}\left(\begin{Bmatrix} \boldsymbol{Q_{v_{c_i}}} \\ \boldsymbol{Q_{w_{c_i}}} \\ \boldsymbol{Q_{\theta_{x_{c_i}}}} \\ \boldsymbol{Q_{\phi_{y_{c_i}}}} \\ \boldsymbol{Q_{\phi_{z_{c_i}}}} \end{Bmatrix} \cos(i\omega t) + \begin{Bmatrix} \boldsymbol{Q_{v_{s_i}}} \\ \boldsymbol{Q_{w_{s_i}}} \\ \boldsymbol{Q_{\theta_{x_{s_i}}}} \\ \boldsymbol{Q_{\phi_{y_{s_i}}}} \\ \boldsymbol{Q_{\phi_{z_{s_i}}}} \end{Bmatrix} \sin(i\omega t) \right), \tag{4. 22}$$

The new unknowns are the coefficients of the harmonics and can be written in vector form as:

$$\{Q\} = \begin{Bmatrix} \boldsymbol{Q_v} \\ \boldsymbol{Q_w} \\ \boldsymbol{Q_{\theta_x}} \\ \boldsymbol{Q_{\phi_y}} \\ \boldsymbol{Q_{\phi_z}} \end{Bmatrix} \tag{4. 23}$$

where, considering harmonics up to third order, for example $\boldsymbol{Q_w}$ is expressed by:

$$\boldsymbol{Q_w} = \begin{Bmatrix} \boldsymbol{Q_{w_0}} \\ \boldsymbol{Q_{w_{c_1}}} \\ \boldsymbol{Q_{w_{s_1}}} \\ \boldsymbol{Q_{w_{c_2}}} \\ \boldsymbol{Q_{w_{s_2}}} \\ \boldsymbol{Q_{w_{c_3}}} \\ \boldsymbol{Q_{w_{s_3}}} \end{Bmatrix} \tag{4. 24}$$

and the dimension of each sub-vector $\boldsymbol{Q_{w_i}}$ is the number of shape functions used for w_0, i.e. p_w. The unknown vector $\{Q\}$ does not contain the longitudinal displacement since it was eliminated from the equation of motion, as explained in the beginning, it can be expressed as a quadratic function of the other displacements by equation (4. 2).

The time dependent generalised coordinates are replaced by their Fourier expansion, equation (4. 22), inserted in the equation of motion (4. 19) and the HBM [4. 6]-[4. 7] is employed. The resulting equation of motion in the frequency domain is of the form:

$$\begin{aligned} \{\mathcal{F}(\{Q\},\omega)\} = (-\omega^2\,[\mathrm{M}^{\mathrm{HBM}}] + [\mathrm{C}^{\mathrm{HBM}}] + [\mathrm{K1}^{\mathrm{HBM}}] + [\mathrm{K2}^{\mathrm{HBM}}(\{Q\})] + \\ +2\,[\mathrm{K2}^{\mathrm{HBM}}(\{Q\})]^{\mathrm{T}} + [\mathrm{K5}^{\mathrm{HBM}}(\{Q\})])\{Q\} - \{\mathrm{F}^{\mathrm{HBM}}\} = \{0\}, \end{aligned} \tag{4. 25}$$

where $[\mathrm{M}^{\mathrm{HBM}}]$ represents the mass matrix which is created from the matrices $\mathbf{M_{ij}}$ of equation (4. 3), $[\mathrm{C}^{\mathrm{HBM}}]$ is the damping matrix, which is a function of $\beta[\mathrm{M}^{\mathrm{HBM}}]$, $[\mathrm{K1}^{\mathrm{HBM}}]$ is the stiffness matrix of constant terms, which is created using matrices $\mathbf{K1_{ij}}$ from equation (4. 3), $[\mathrm{K2}^{\mathrm{HBM}}(\{Q\})]$ is the stiffness matrix which depends linearly on the coefficients of the harmonics, it is created from matrices $\mathbf{K2_{ij}}$ of equation (4. 3), and $[\mathrm{K5}^{\mathrm{HBM}}(\{Q\})]$ is the stiffness matrix which depends quadratically on the coefficients of harmonics, it results from matrices $\mathbf{K5_{ij}}$ of equation (4. 3). The structure of these matrices after the HBM is implemented is presented in the next sub-sections for the case k = 3, i.e. when harmonics till third order are used in equation (4. 22). The total number of degrees of freedom of the frequency domain model is now $\mathrm{N} = (1 + 2k)\left(p_v + p_w + p_{\theta_x} + p_{\phi_y} + p_{\phi_z}\right)$ where p_v, p_w, p_{θ_x}, p_{ϕ_y} and p_{ϕ_z} are the number of shape functions used for each displacement in the model and k is the order of harmonics used in the Fourier series.

4. 4. 1. Stiffness matrix after application of the HBM

4. 4. 1. 1. Linear stiffness matrix $[\mathrm{K1}^{\mathrm{HBM}}]$

The linear stiffness matrix of the dynamic equation of motion is given in equation (4. 3), where the sub-matrices are among equations (2. 47b) – (2. 47h) from Chapter 2. Assuming harmonics up to third order in equation (4. 22), the linear stiffness matrix $[\mathrm{K1}^{\mathrm{HBM}}]$ becomes:

$$[\mathrm{K1}^{\mathrm{HBM}}] = \begin{bmatrix} \mathbf{K1_{22}^{HBM}} & \mathbf{0} & \mathbf{0} & \mathbf{0} & \mathbf{K1_{26}^{HBM}} \\ \mathbf{0} & \mathbf{K1_{33}^{HBM}} & \mathbf{0} & \mathbf{K1_{35}^{HBM}} & \mathbf{0} \\ \mathbf{0} & \mathbf{0} & \mathbf{K1_{44}^{HBM}} & \mathbf{0} & \mathbf{0} \\ \mathbf{0} & \mathbf{K1_{35}^{HBM^T}} & \mathbf{0} & \mathbf{K1_{55}^{HBM}} & \mathbf{0} \\ \mathbf{K1_{26}^{HBM^T}} & \mathbf{0} & \mathbf{0} & \mathbf{0} & \mathbf{K1_{66}^{HBM}} \end{bmatrix}, \tag{4. 26}$$

where for example $\mathbf{K1_{22}^{HBM}}$ is expressed as:

$$\mathbf{K1_{22}^{HBM}} = \begin{bmatrix} \frac{1}{2}\,\mathbf{K1_{22}} & \mathbf{0} & \mathbf{0} & \mathbf{0} & \mathbf{0} & \mathbf{0} & \mathbf{0} \\ \mathbf{0} & \mathbf{K1_{22}} & \mathbf{0} & \mathbf{0} & \mathbf{0} & \mathbf{0} & \mathbf{0} \\ \mathbf{0} & \mathbf{0} & \mathbf{K1_{22}} & \mathbf{0} & \mathbf{0} & \mathbf{0} & \mathbf{0} \\ \mathbf{0} & \mathbf{0} & \mathbf{0} & \mathbf{K1_{22}} & \mathbf{0} & \mathbf{0} & \mathbf{0} \\ \mathbf{0} & \mathbf{0} & \mathbf{0} & \mathbf{0} & \mathbf{K1_{22}} & \mathbf{0} & \mathbf{0} \\ \mathbf{0} & \mathbf{0} & \mathbf{0} & \mathbf{0} & \mathbf{0} & \mathbf{K1_{22}} & \mathbf{0} \\ \mathbf{0} & \mathbf{0} & \mathbf{0} & \mathbf{0} & \mathbf{0} & \mathbf{0} & \mathbf{K1_{22}} \end{bmatrix}. \tag{4. 27}$$

The structure of the sub-matrix defined in equation (4. 27) is very similar to the one defined in equation (4. 10), but now it has seven rows and seven columns, instead of six. The rest of the sub-matrices in equation (4. 26) have the same structure as the sub-matrix $\mathbf{K1_{22}^{HBM}}$ in equation (4. 27), but using the corresponding sub-matrices defined in equations (2. 47b) – (2. 47h).

4. 4. 1. 2. Nonlinear stiffness matrix $[\mathrm{K2}^{\mathrm{HBM}}(\{Q\})]$

The linearly dependent on the vector of coefficients of harmonics $\{Q\}$ matrix $[\mathrm{K2}^{\mathrm{HBM}}(\{Q\})]$, which results from replacing equation (4. 22) into (4. 19), has the following form:

$$[\mathrm{K2}^{\mathrm{HBM}}(\{Q\})] = \begin{bmatrix} \mathbf{0} & \mathbf{K2}_{\mathbf{23}}^{\mathbf{HBM}}(\boldsymbol{Q}_{\theta_x}) & \mathbf{K2}_{\mathbf{24}}^{\mathbf{HBM}}(\boldsymbol{Q}_w) & \mathbf{0} & \mathbf{0} \\ \mathbf{K2}_{\mathbf{32}}^{\mathbf{HBM}}(\boldsymbol{Q}_{\theta_x}) & \mathbf{0} & \mathbf{K2}_{\mathbf{34}}^{\mathbf{HBM}}(\boldsymbol{Q}_v) & \mathbf{0} & \mathbf{0} \\ \mathbf{0} & \mathbf{0} & \mathbf{0} & \mathbf{0} & \mathbf{0} \\ \mathbf{K2}_{\mathbf{52}}^{\mathbf{HBM}}(\boldsymbol{Q}_{\theta_x}) & \mathbf{0} & \mathbf{K2}_{\mathbf{54}}^{\mathbf{HBM}}(\boldsymbol{Q}_v) & \mathbf{0} & \mathbf{0} \\ \mathbf{0} & \mathbf{K2}_{\mathbf{63}}^{\mathbf{HBM}}(\boldsymbol{Q}_{\theta_x}) & \mathbf{K2}_{\mathbf{64}}^{\mathbf{HBM}}(\boldsymbol{Q}_w) & \mathbf{0} & \mathbf{0} \end{bmatrix}, \tag{4. 28}$$

where each of these sub-matrices are linearly dependent on the coefficients of the harmonics written in equation (4. 22). They are similar to the matrices, given in equations (2. 53d) – (2. 52k). For example, the sub-matrix $\mathbf{K2}_{\mathbf{24}}^{\mathbf{HBM}}(\boldsymbol{Q}_w)$ is expressed as:

$$\mathbf{K2}_{\mathbf{24}}^{\mathbf{HBM}}(\boldsymbol{Q}_w) = \frac{1}{2}\begin{bmatrix} \frac{\mathbf{1}}{\mathbf{2}}\mathbf{K2}_{\mathbf{24}}(\boldsymbol{Q}_{w_0}) & \mathbf{K2}_{\mathbf{24}}(\boldsymbol{Q}_{w_1}) & \mathbf{K2}_{\mathbf{24}}(\boldsymbol{Q}_{w_2}) \\ \mathbf{K2}_{\mathbf{24}}(\boldsymbol{Q}_{w_1}) & \mathbf{K2}_{\mathbf{24}}(\boldsymbol{Q}_{w_0}) + \mathbf{K2}_{\mathbf{24}}(\boldsymbol{Q}_{w_3}) & \mathbf{K2}_{\mathbf{24}}(\boldsymbol{Q}_{w_4}) \\ \mathbf{K2}_{\mathbf{24}}(\boldsymbol{Q}_{w_2}) & \mathbf{K2}_{\mathbf{24}}(\boldsymbol{Q}_{w_4}) & \mathbf{K2}_{\mathbf{24}}(\boldsymbol{Q}_{w_0}) - \mathbf{K2}_{\mathbf{24}}(\boldsymbol{Q}_{w_3}) \\ \mathbf{K2}_{\mathbf{24}}(\boldsymbol{Q}_{w_3}) & \mathbf{K2}_{\mathbf{24}}(\boldsymbol{Q}_{w_1}) + \mathbf{K2}_{\mathbf{24}}(\boldsymbol{Q}_{w_5}) & -\mathbf{K2}_{\mathbf{24}}(\boldsymbol{Q}_{w_2}) + \mathbf{K2}_{\mathbf{24}}(\boldsymbol{Q}_{w_6}) \\ \mathbf{K2}_{\mathbf{24}}(\boldsymbol{Q}_{w_4}) & \mathbf{K2}_{\mathbf{24}}(\boldsymbol{Q}_{w_2}) + \mathbf{K2}_{\mathbf{24}}(\boldsymbol{Q}_{w_6}) & \mathbf{K2}_{\mathbf{24}}(\boldsymbol{Q}_{w_1}) - \mathbf{K2}_{\mathbf{24}}(\boldsymbol{Q}_{w_5}) \\ \mathbf{K2}_{\mathbf{24}}(\boldsymbol{Q}_{w_5}) & \mathbf{K2}_{\mathbf{24}}(\boldsymbol{Q}_{w_3}) & -\mathbf{K2}_{\mathbf{24}}(\boldsymbol{Q}_{w_4}) \\ \mathbf{K2}_{\mathbf{24}}(\boldsymbol{Q}_{w_6}) & \mathbf{K2}_{\mathbf{24}}(\boldsymbol{Q}_{w_4}) & \mathbf{K2}_{\mathbf{24}}(\boldsymbol{Q}_{w_3}) \end{bmatrix} \tag{4. 29}$$

$$\begin{bmatrix} \mathbf{K2}_{\mathbf{24}}(\boldsymbol{Q}_{w_3}) & \mathbf{K2}_{\mathbf{24}}(\boldsymbol{Q}_{w_4}) & \mathbf{K2}_{\mathbf{24}}(\boldsymbol{Q}_{w_5}) & \mathbf{K2}_{\mathbf{24}}(\boldsymbol{Q}_{w_6}) \\ \mathbf{K2}_{\mathbf{24}}(\boldsymbol{Q}_{w_1}) + \mathbf{K2}_{\mathbf{24}}(\boldsymbol{Q}_{w_5}) & \mathbf{K2}_{\mathbf{24}}(\boldsymbol{Q}_{w_2}) + \mathbf{K2}_{\mathbf{24}}(\boldsymbol{Q}_{w_6}) & \mathbf{K2}_{\mathbf{24}}(\boldsymbol{Q}_{w_3}) & \mathbf{K2}_{\mathbf{24}}(\boldsymbol{Q}_{w_4}) \\ -\mathbf{K2}_{\mathbf{24}}(\boldsymbol{Q}_{w_2}) + \mathbf{K2}_{\mathbf{24}}(\boldsymbol{Q}_{w_6}) & \mathbf{K2}_{\mathbf{24}}(\boldsymbol{Q}_{w_1}) - \mathbf{K2}_{\mathbf{24}}(\boldsymbol{Q}_{w_5}) & -\mathbf{K2}_{\mathbf{24}}(\boldsymbol{Q}_{w_4}) & \mathbf{K2}_{\mathbf{24}}(\boldsymbol{Q}_{w_3}) \\ \mathbf{K2}_{\mathbf{24}}(\boldsymbol{Q}_{w_0}) & \mathbf{0} & \mathbf{K2}_{\mathbf{24}}(\boldsymbol{Q}_{w_1}) & \mathbf{K2}_{\mathbf{24}}(\boldsymbol{Q}_{w_2}) \\ \mathbf{0} & \mathbf{K2}_{\mathbf{24}}(\boldsymbol{Q}_{w_0}) & -\mathbf{K2}_{\mathbf{24}}(\boldsymbol{Q}_{w_2}) & \mathbf{K2}_{\mathbf{24}}(\boldsymbol{Q}_{w_1}) \\ \mathbf{K2}_{\mathbf{24}}(\boldsymbol{Q}_{w_1}) & -\mathbf{K2}_{\mathbf{24}}(\boldsymbol{Q}_{w_2}) & \mathbf{K2}_{\mathbf{24}}(\boldsymbol{Q}_{w_0}) & \mathbf{0} \\ \mathbf{K2}_{\mathbf{24}}(\boldsymbol{Q}_{w_2}) & \mathbf{K2}_{\mathbf{24}}(\boldsymbol{Q}_{w_1}) & \mathbf{0} & \mathbf{K2}_{\mathbf{24}}(\boldsymbol{Q}_{w_0}) \end{bmatrix},$$

where $\mathbf{K2}_{\mathbf{24}}(\boldsymbol{Q}_{w_i})$ was defined in equation (4. 13).

4. 4. 1. 3. Nonlinear stiffness matrix $[\mathrm{K5}^{\mathrm{HBM}}(\{Q\})]$

The matrix $[\mathrm{K5}^{\mathrm{HBM}}(\{Q\})]$ results from replacing equation (4. 22) into (4. 19), it depends quadratically on the vector of coefficients of harmonics $\{Q\}$ and it has the following form:

$$[\mathrm{K5}^{\mathrm{HBM}}(\{Q\})] =$$

$$= \begin{bmatrix} \mathbf{K5_{22}^{HBM}}(\boldsymbol{Q_v}, \boldsymbol{Q_w}, \boldsymbol{Q_{\theta_x}}) & \mathbf{K5_{23}^{HBM}}(\boldsymbol{Q_v}, \boldsymbol{Q_w}) & \mathbf{K5_{24}^{HBM}}(\boldsymbol{Q_v}, \boldsymbol{Q_{\theta_x}}) & \mathbf{0} & \mathbf{0} \\ \mathbf{K5_{32}^{HBM}}(\boldsymbol{Q_v}, \boldsymbol{Q_w}) & \mathbf{K5_{33}^{HBM}}(\boldsymbol{Q_v}, \boldsymbol{Q_w}, \boldsymbol{Q_{\theta_x}}) & \mathbf{K5_{34}^{HBM}}(\boldsymbol{Q_w}, \boldsymbol{Q_{\theta_x}}) & \mathbf{0} & \mathbf{0} \\ \mathbf{K5_{42}^{HBM}}(\boldsymbol{Q_v}, \boldsymbol{Q_{\theta_x}}) & \mathbf{K5_{43}^{HBM}}(\boldsymbol{Q_w}, \boldsymbol{Q_{\theta_x}}) & \mathbf{K5_{44}^{HBM}}(\boldsymbol{Q_v}, \boldsymbol{Q_w}, \boldsymbol{Q_{\theta_x}}) & \mathbf{0} & \mathbf{0} \\ \mathbf{0} & \mathbf{0} & \mathbf{0} & \mathbf{0} & \mathbf{0} \\ \mathbf{0} & \mathbf{0} & \mathbf{0} & \mathbf{0} & \mathbf{0} \end{bmatrix}, \tag{4. 30}$$

where each of these sub-matrices has the form given in equation (4. 4), i.e. it is constructed as a sum of matrices, quadratically dependent on the coefficients of the harmonics from equation (4. 22). For example, the sub-matrix $\mathbf{K5_{33}^{HBM}}(\boldsymbol{Q_v}, \boldsymbol{Q_w}, \boldsymbol{Q_{\theta_x}})$, considering (2. 63c) and (4. 4) is a sum matrices which depend quadratically on $\boldsymbol{Q_v}$, $\boldsymbol{Q_w}$ and $\boldsymbol{Q_{\theta_x}}$ and may be written in the way as in equation (4. 15). For example, $\mathbf{K4_{33}^{HBM}}(\boldsymbol{Q_w})$ has the following form:

$$\mathbf{K4_{33}^{HBM}}(\boldsymbol{Q_w}) = \frac{1}{4}\begin{bmatrix} \mathbf{A_{11}} & \mathbf{A_{12}} & \mathbf{A_{13}} & \mathbf{A_{14}} & \mathbf{A_{15}} & \mathbf{A_{16}} & \mathbf{A_{17}} \\ \mathbf{A_{12}}^{\mathrm{T}} & \mathbf{A_{22}} & \mathbf{A_{23}} & \mathbf{A_{24}} & \mathbf{A_{25}} & \mathbf{A_{26}} & \mathbf{A_{27}} \\ \mathbf{A_{13}}^{\mathrm{T}} & \mathbf{A_{23}}^{\mathrm{T}} & \mathbf{A_{33}} & \mathbf{A_{34}} & \mathbf{A_{35}} & \mathbf{A_{36}} & \mathbf{A_{37}} \\ \mathbf{A_{14}}^{\mathrm{T}} & \mathbf{A_{24}}^{\mathrm{T}} & \mathbf{A_{34}}^{\mathrm{T}} & \mathbf{A_{44}} & \mathbf{A_{45}} & \mathbf{A_{46}} & \mathbf{A_{47}} \\ \mathbf{A_{15}}^{\mathrm{T}} & \mathbf{A_{25}}^{\mathrm{T}} & \mathbf{A_{35}}^{\mathrm{T}} & \mathbf{A_{45}}^{\mathrm{T}} & \mathbf{A_{55}} & \mathbf{A_{56}} & \mathbf{A_{57}} \\ \mathbf{A_{16}}^{\mathrm{T}} & \mathbf{A_{26}}^{\mathrm{T}} & \mathbf{A_{36}}^{\mathrm{T}} & \mathbf{A_{46}}^{\mathrm{T}} & \mathbf{A_{56}}^{\mathrm{T}} & \mathbf{A_{66}} & \mathbf{A_{67}} \\ \mathbf{A_{17}}^{\mathrm{T}} & \mathbf{A_{27}}^{\mathrm{T}} & \mathbf{A_{37}}^{\mathrm{T}} & \mathbf{A_{47}}^{\mathrm{T}} & \mathbf{A_{57}}^{\mathrm{T}} & \mathbf{A_{67}}^{\mathrm{T}} & \mathbf{A_{77}} \end{bmatrix}, \tag{4. 31}$$

where the sub-matrices $\mathbf{A_{ij}}$ are defined in Appendix B.

4. 4. 2. Damping matrix after application of the HBM

A mass proportional and frequency dependent damping was introduced into the equation of motion (4. 19). Replacing equation (4. 22) into equation (4. 19), considering harmonics up to third order and implementing the HBM, the damping matrix has the following form:

$$[\mathrm{C}^{\mathrm{HBM}}] = \begin{bmatrix} \mathbf{C_{22}^{HBM}} & \mathbf{0} & \mathbf{0} & \mathbf{0} & \mathbf{0} \\ \mathbf{0} & \mathbf{C_{33}^{HBM}} & \mathbf{0} & \mathbf{0} & \mathbf{0} \\ \mathbf{0} & \mathbf{0} & \mathbf{C_{44}^{HBM}} & \mathbf{0} & \mathbf{0} \\ \mathbf{0} & \mathbf{0} & \mathbf{0} & \mathbf{C_{55}^{HBM}} & \mathbf{0} \\ \mathbf{0} & \mathbf{0} & \mathbf{0} & \mathbf{0} & \mathbf{C_{66}^{HBM}} \end{bmatrix}, \tag{4. 32}$$

where, for example $\mathbf{C_{22}^{HBM}}$ is written as:

$$\mathbf{C_{22}^{HBM}} = \beta \begin{bmatrix} \mathbf{0} & \mathbf{0} & \mathbf{0} & \mathbf{0} & \mathbf{0} & \mathbf{0} & \mathbf{0} \\ \mathbf{0} & \mathbf{0} & \mathbf{M_{22}} & \mathbf{0} & \mathbf{0} & \mathbf{0} & \mathbf{0} \\ \mathbf{0} & \mathbf{-M_{22}} & \mathbf{0} & \mathbf{0} & \mathbf{0} & \mathbf{0} & \mathbf{0} \\ \mathbf{0} & \mathbf{0} & \mathbf{0} & \mathbf{0} & \mathbf{2\,M_{22}} & \mathbf{0} & \mathbf{0} \\ \mathbf{0} & \mathbf{0} & \mathbf{0} & \mathbf{-2\,M_{22}} & \mathbf{0} & \mathbf{0} & \mathbf{0} \\ \mathbf{0} & \mathbf{0} & \mathbf{0} & \mathbf{0} & \mathbf{0} & \mathbf{0} & \mathbf{3\,M_{22}} \\ \mathbf{0} & \mathbf{0} & \mathbf{0} & \mathbf{0} & \mathbf{0} & \mathbf{-3\,M_{22}} & \mathbf{0} \end{bmatrix}. \tag{4. 33}$$

4. 4. 3. Mass matrix after application of the HBM

Assuming harmonics up to third order in equation (4. 22), the mass matrix $[\mathrm{M}^{\mathrm{HBM}}]$ becomes:

$$[\mathrm{M}^{\mathrm{HBM}}] = \begin{bmatrix} \mathbf{M_{22}^{HBM}} & \mathbf{0} & \mathbf{0} & \mathbf{0} & \mathbf{0} \\ \mathbf{0} & \mathbf{M_{33}^{HBM}} & \mathbf{0} & \mathbf{0} & \mathbf{0} \\ \mathbf{0} & \mathbf{0} & \mathbf{M_{44}^{HBM}} & \mathbf{0} & \mathbf{0} \\ \mathbf{0} & \mathbf{0} & \mathbf{0} & \mathbf{M_{55}^{HBM}} & \mathbf{0} \\ \mathbf{0} & \mathbf{0} & \mathbf{0} & \mathbf{0} & \mathbf{M_{66}^{HBM}} \end{bmatrix}, \tag{4. 34}$$

where, for example, $\mathbf{M_{22}^{HBM}}$ is expressed as:

$$\mathbf{M_{22}^{HBM}} = \begin{bmatrix} \mathbf{0} & \mathbf{0} & \mathbf{0} & \mathbf{0} & \mathbf{0} & \mathbf{0} & \mathbf{0} \\ \mathbf{0} & \mathbf{M_{22}} & \mathbf{0} & \mathbf{0} & \mathbf{0} & \mathbf{0} & \mathbf{0} \\ \mathbf{0} & \mathbf{0} & \mathbf{M_{22}} & \mathbf{0} & \mathbf{0} & \mathbf{0} & \mathbf{0} \\ \mathbf{0} & \mathbf{0} & \mathbf{0} & \mathbf{4\,M_{22}} & \mathbf{0} & \mathbf{0} & \mathbf{0} \\ \mathbf{0} & \mathbf{0} & \mathbf{0} & \mathbf{0} & \mathbf{4\,M_{22}} & \mathbf{0} & \mathbf{0} \\ \mathbf{0} & \mathbf{0} & \mathbf{0} & \mathbf{0} & \mathbf{0} & \mathbf{9\,M_{22}} & \mathbf{0} \\ \mathbf{0} & \mathbf{0} & \mathbf{0} & \mathbf{0} & \mathbf{0} & \mathbf{0} & \mathbf{9\,M_{22}} \end{bmatrix}. \tag{4. 35}$$

4. 4. 4. External force vector after application of the HBM

The vector of generalized external forces was defined in Chapter 2, equation (2. 76) and in the case of neglecting the longitudinal inertia is written in equation (4. 3). External forces in longitudinal direction are not considered and vibrations due to harmonic forces are investigated, i.e. the external force vector has the following form:

$$\{\mathrm{F}(t)\} = \begin{Bmatrix} \mathbf{F}_{v_0} \\ \mathbf{F}_{w_0} \\ \mathbf{F}_{\theta_x} \\ \mathbf{F}_{\phi_y} \\ \mathbf{F}_{\phi_z} \end{Bmatrix} \cos(\omega t). \tag{4. 36}$$

After application of the HBM, the external force vector becomes:

$$\{\mathrm{F}^{\mathrm{HBM}}\} = \begin{Bmatrix} \mathbf{F}_{v_0}^{\mathbf{HBM}} \\ \mathbf{F}_{w_0}^{\mathbf{HBM}} \\ \mathbf{F}_{\theta_x}^{\mathbf{HBM}} \\ \mathbf{F}_{\phi_y}^{\mathbf{HBM}} \\ \mathbf{F}_{\phi_z}^{\mathbf{HBM}} \end{Bmatrix}, \tag{4. 37}$$

where, for example $\mathbf{F}_{w_0}^{\mathbf{HBM}}$ has the following form:

$$\mathbf{F}_{w_0}^{\mathbf{HBM}} = \begin{Bmatrix} \mathbf{0} \\ \mathbf{F}_{w_0} \\ \mathbf{0} \\ \mathbf{0} \\ \mathbf{0} \\ \mathbf{0} \\ \mathbf{0} \end{Bmatrix}, \tag{4. 38}$$

where $\mathbf{F}_{w_0}$ is the vector of the generalized external force in transverse direction z defined in (2. 77c).

4. 5. Stability of the solutions

The determination of the stability of dynamical system is of primary interest in engineering applications because only stable solutions exist in nature. In a nonlinear system more than a single solution may appear but some of the solutions may be unstable. Moreover, the fact that an unstable solution is found indicates that other solution(s) exist which can lead to significant changes of the system response.

First, two definitions of stability, known as Lyapunov and Poincaré stability, are given.

A solution $u(t)$ is said to be Lyapunov stable if, given a small number $\varepsilon > 0$, there exists a number $\delta = \delta(\varepsilon) > 0$ such that any other solution $v(t)$ for which $\|u - v\| < \delta$ at time $t = t_0$ satisfies $\|u - v\| < \varepsilon$ for all $t > t_0$ [4. 9].

A solution $u(t)$ is said to be Poincaré stable if, given a small number $\varepsilon > 0$, there exists a number $\delta = \delta(\varepsilon) > 0$ such that any other solution $v(t)$ for which $\|u(t=0) - v(t=\tau)\| < \delta$ for some τ, then there exists t_1 and t_2 for which $\|u(t_1) - v(t_2)\| < \varepsilon$ [4. 9].

The definition of Lyapunov is appropriate for equilibrium solutions but it is restrictive for dynamical solutions. For example, a periodic solution of nonlinear system, according to the definition of Lyapunov, can be unstable, while according to definition of Poincaré it is stable. Two periodic solutions which are "close" to each other for some $t = t_0$ but with different amplitudes, will generally have different fundamental frequencies, since in nonlinear systems the natural frequency of vibration is dependent on the amplitude of vibration. This will result in different periods and after certain time they will be "far" from each other which, considering Lyapunov's definition of stability, means that the solution is unstable. Nevertheless, the same solution can be stable in terms of Poincaré's definition, it means that the orbits of both solutions are "close". Thus, one should use Poincaré stability for dynamical solutions. However, these concepts do not provide any explicit schemes for determining the stability of periodic solutions, thus explicit scheme is here presented based on Floquet's theory.

The local stability of a steady-state periodic solution (4. 22) of equation (4. 19) is studied by adding a small disturbance [4. 6]:

$$\{\tilde{q}(t)\} = \{q(t)\} + \{\delta q(t)\}. \tag{4. 39}$$

The evolution of the variation of the disturbed solution $\{\tilde{q}(t)\}$ is examined. If $\{\delta q(t)\}$ goes to zero with time, then $\{q(t)\}$ is stable, if it grows then $\{q(t)\}$ is unstable.

Substituting (4. 39) into (4. 19), expanding the nonlinear terms by Taylor series around $\{q(t)\}$ and keeping only linear terms in the disturbance, the following equation is obtained:

$$[\mathrm{M}]\{\delta\ddot{q}(t)\} + \frac{\beta}{\omega}[\mathrm{M}]\{\delta\dot{q}(t)\} + [\mathrm{K1}]\{\delta q(t)\} + \\ + \frac{\partial([\mathrm{KNL}(\{q(t)\})]\{q(t)\})}{\partial\{q(t)\}}\{\delta q(t)\} = \{0\}. \tag{4. 40}$$

Matrix $\frac{\partial([\mathrm{KNL}(\{q(t)\})]\{q(t)\})}{\partial\{q(t)\}}$ depends linearly and quadratically on vector $\{q(t)\}$, therefore, it is a periodic matrix. With $\{q(t)\}$ given by equation (4. 22), assuming that harmonics up to third order are considered, $\frac{\partial([\mathrm{KNL}(\{q(t)\})]\{q(t)\})}{\partial\{q(t)\}}$ can be expressed in a Fourier series with harmonics till sixth order:

$$\frac{\partial([\mathrm{KNL}(\{q(t)\})]\{q(t)\})}{\partial\{q(t)\}} = [\mathrm{p_0}] + \sum_{i=1}^{6}\left([\mathrm{p_{c_i}}]\cos(i\omega t) + [\mathrm{p_{s_i}}]\sin(i\omega t)\right). \tag{4. 41}$$

The Fourier coefficients $[\mathrm{p_0}]$, $[\mathrm{p_{c_i}}]$, $[\mathrm{p_{s_i}}]$, i=1, 2, ..., 6 are matrices which depend linearly and quadratically of vector $\{q(t)\}$. Since the vector $\{q(t)\}$ is expressed with harmonics up to third order in equation (4. 22), the expression (4. 41) with harmonics up to sixth order is exact.

The modal coordinates of the linear system are given by:

$$\{\delta q(t)\} = [\mathrm{B}]\{\delta\zeta(t)\} \tag{4. 42}$$

where [B] is the normalized modal matrix, so that the matrix of modal masses is the identity matrix. All eigenvectors which arise from the linear eigenvalue problem are included in the modal matrix [B]. Using the modal coordinates, multiplying equation (4. 40) by $[\mathrm{B}]^{\mathrm{T}}$ the following system is obtained:

$$\begin{aligned}&\{\delta\ddot{\zeta}(t)\} + \frac{\beta}{\omega}\{\delta\dot{\zeta}(t)\} + [\omega_j^2]\{\delta\zeta(t)\} + \\ &+[\mathrm{B}]\left([\mathrm{p_0}] + \sum_{i=1}^{6}\left([\mathrm{p_{c_i}}]\cos(i\omega t) + [\mathrm{p_{s_i}}]\sin(i\omega t)\right)\right)[\mathrm{B}]^{\mathrm{T}}\{\delta\zeta(t)\} = \{0\}.\end{aligned} \tag{4. 43}$$

where $[\omega_j^2]$ is a diagonal matrix with squares of the linear natural frequencies on its diagonal elements. The transformation into modal coordinates is preferred here to avoid numerical errors in the stability analysis from calculation the inverse of the mass matrix.

In the computations presented in the current work, the disturbance $\{\delta\zeta(t)\}$ is expressed with harmonics up to sixth order. It is assumed to have the form:

$$\{\delta\zeta(t)\} = e^{\lambda}\left(\frac{1}{2}\{a_0\} + \sum_{i=1}^{6}\left(\{a_{c_i}\}\cos(i\omega t) + \{a_{s_i}\}\sin(i\omega t)\right)\right), \tag{4. 44}$$

where λ are the characteristic exponents. Inserting equation (4. 44) into equation (4. 43) and applying the HBM, the following system is obtained:

$$(\lambda^2\,[\mathbb{M}_2] + \lambda\,[\mathbb{M}_1] + [\mathbb{M}_0])\{\mathbb{X}\} = \{0\}, \tag{4. 45}$$

where

$$\{\mathbb{X}\} = \begin{Bmatrix} \boldsymbol{a_0} \\ \boldsymbol{a_{c_1}} \\ \boldsymbol{a_{s_1}} \\ \vdots \\ \boldsymbol{a_{c_6}} \\ \boldsymbol{a_{s_6}} \end{Bmatrix}. \tag{4. 46}$$

Since the disturbance, equation (4. 44), is expressed by a constant term and harmonics up to sixth order, the number of elements in the rows and the columns of matrices $[\mathbb{M}_0]$, $[\mathbb{M}_1]$ and $[\mathbb{M}_2]$ is $13\left(p_v + p_w + p_{\theta_x} + p_{\phi_y} + p_{\phi_z}\right)$. For simplicity, the matrix $[\mathbb{M}_0]$ is presented as a sum of two matrices:

$$[\mathbb{M}_0] = [\mathbb{M}\mathbb{L}_0] + [\mathbb{M}\mathbb{N}\mathbb{L}_0], \tag{4. 47}$$

where $[\mathbb{M}\mathbb{L}_0]$ is matrix of constant terms and $[\mathbb{M}\mathbb{N}\mathbb{L}_0]$ is matrix that depends on vector $\{q(t)\}$ and is constituted by combinations of sub-matrices $[\mathrm{p}_0]$, $[\mathrm{p}_{c_i}]$, $[\mathrm{p}_{s_i}]$, i=1, 2, ..., 6. These sub-matrices are defined in equation (4. 41) and they depend linearly and quadratically of vector $\{q(t)\}$. They are computed analytically using symbolic manipulation. The matrices $[\mathbb{M}\mathbb{L}_0]$ and $[\mathbb{M}\mathbb{N}\mathbb{L}_0]$ have the following form:

$$[\mathbb{M}\mathbb{L}_0] = \begin{bmatrix} 1/2\,[\omega_j^2] & \cdots & & & 0 \\ \vdots & [\omega_j^2] - \omega^2[\mathrm{I}] & \beta[\mathrm{I}] & & \vdots \\ & -\beta[\mathrm{I}] & [\omega_j^2] - \omega^2[\mathrm{I}] & & \\ & & & \ddots & \\ 0 & \cdots & & [\omega_j^2] - 36\omega^2[\mathrm{I}] & 6\beta[\mathrm{I}] \\ & & & -6\beta[\mathrm{I}] & [\omega_j^2] - 36\omega^2[\mathrm{I}] \end{bmatrix} \tag{4. 48}$$

$$[\mathbb{MNL}_0] = \begin{bmatrix} \frac{1}{2}\mathbf{p_0} & \frac{1}{2}\mathbf{p_{c_1}} & \frac{1}{2}\mathbf{p_{s_1}} & \frac{1}{2}\mathbf{p_{c_2}} & \frac{1}{2}\mathbf{p_{s_2}} & \cdots \\ & \mathbf{p_0} + \frac{1}{2}\mathbf{p_{s_1}} & \frac{1}{2}\mathbf{p_{s_2}} & \frac{1}{2}\mathbf{p_{c_1}} + \frac{1}{2}\mathbf{p_{c_3}} & \frac{1}{2}\mathbf{p_{s_1}} + \frac{1}{2}\mathbf{p_{s_3}} & \cdots \\ & & \mathbf{p_0} - \frac{1}{2}\mathbf{p_{c_2}} & -\frac{1}{2}\mathbf{p_{s_1}} + \frac{1}{2}\mathbf{p_{s_3}} & \frac{1}{2}\mathbf{p_{c_1}} - \frac{1}{2}\mathbf{p_{c_3}} & \cdots \\ & & & \mathbf{p_0} + \frac{1}{2}\mathbf{p_{c_4}} & \frac{1}{2}\mathbf{p_{s_4}} & \cdots \\ & \text{SYM} & & & \mathbf{p_0} - \frac{1}{2}\mathbf{p_{c_4}} & \cdots \\ & & & & & \ddots \end{bmatrix} \tag{4. 49}$$

The matrices $[\mathbb{M}_1]$ and $[\mathbb{M}_2]$ have the following form:

$$[\mathbb{M}_1] = \begin{bmatrix} 1/2\,\beta[\mathrm{I}] & \cdots & & 0 \\ \vdots & \beta[\mathrm{I}] & 2\omega[\mathrm{I}] & \vdots \\ & -2\omega[\mathrm{I}] & \beta[\mathrm{I}] & \\ & & \ddots & \\ 0 & \cdots & \beta[\mathrm{I}] & 12\omega[\mathrm{I}] \\ & & -12\omega[\mathrm{I}] & \beta[\mathrm{I}] \end{bmatrix}, \tag{4. 50}$$

$$[\mathbb{M}_2] = \begin{bmatrix} 1/2\,[\mathrm{I}] & \cdots & 0 \\ \vdots & [\mathrm{I}] & \vdots \\ & [\mathrm{I}] & \\ & \ddots & \\ & [\mathrm{I}] & \\ 0 & \cdots & [\mathrm{I}] \end{bmatrix}, \tag{4. 51}$$

where $\left[\omega_j^2\right]$ is a diagonal matrix with squares of the linear natural frequencies on its diagonal elements, [I] is the identity matrix, ω is the excitation frequency, β is the damping factor defined in equation (4. 21). Matrix $[\mathbb{MNL}_0]$ is symmetric. The full form of the matrices is given in Appendix C.

Equation (4. 45) can be transformed to the following eigenvalue problem:

$$\begin{bmatrix} \mathbf{0} & \mathbf{I} \\ -\mathbb{M}_{\mathbf{2}}{}^{-1}\mathbb{M}_{\mathbf{0}} & -\mathbb{M}_{\mathbf{2}}{}^{-1}\mathbb{M}_{\mathbf{1}} \end{bmatrix} \begin{Bmatrix} \mathbb{X} \\ \mathbb{Y} \end{Bmatrix} = \lambda \begin{Bmatrix} \mathbb{X} \\ \mathbb{Y} \end{Bmatrix}, \tag{4. 52}$$

where $\{\mathbb{Y}\} = \lambda\{\mathbb{X}\}$.

Equation (4. 52) has $2(2H+1)$N eigenvalues, where H is the number of harmonics used for the disturbance (4. 44), i.e. H = 6, and N is the number of degrees of freedom of the time domain equation (4. 19), i.e. $\mathrm{N} = p_v + p_w + p_{\theta_x} + p_{\phi_y} + p_{\phi_z}$.

The dimension of the system presented by equation (4. 43) is N and so the Floquet multipliers are 2N, because equation (4. 43) presents a system of second order ordinary differential equations. The Floquet multipliers are the eigenvalues of the monodromy matrix [4. 9].

Since the solution of the disturbance was assumed in the form (4. 44), the eigenvalues λ_n of the eigenvalue problem (4. 52) are the Floquet exponents. They are related with the Floquet multipliers ρ_n by [4. 9]:

$$\rho_n = e^{\lambda_n T}, \tag{4. 53}$$

or

$$\lambda_n = \frac{1}{T}\ln \rho_n + i\frac{2\pi k}{T}, \quad k \in \mathbb{Z}, \tag{4. 54}$$

where T is the period of vibration and $i = \sqrt{-1}$.

The eigenvalue problem (4. 52) gives $2(2H+1)$N eigenvalues. The 2N Floquet exponents, which are necessary to define the stability of the solution, have to be selected among all $2(2H+1)$N eigenvalues. The method proposed in [4. 10], [4. 11] is used here to select the Floquet exponents.

In the infinite eigenvalue problem (4. 52), i.e. when infinite number of harmonics are used in equation (4. 44), there are 2N families of solutions and 2N eigenvectors are independent – one from each family [4. 10]. In the truncated problem, $2(2H+1)$N eigenvectors of (4. 52) are computed and the 2N with the most symmetric shape are selected. The corresponding eigenvalues are the Floquet exponents. The proposed method is numerical, so its accuracy depends on the number of shape functions used in the model, equation (2. 13), the number of harmonics used for the solution, equation (4. 22), and the number of harmonics used for the disturbance, equation (4. 44). A numerical algorithm DEVCRG developed in Fortran [4. 12] and included in IMSL libraries is used to solve the non-symmetric eigenvalue problem (4. 52).

The solution is unstable, if

$$\mathrm{Re}(\lambda_n) > 0 \tag{4. 55}$$

for any eigenvalue λ_n of (4. 52). In the stability boundary

$$\mathrm{Re}(\lambda_n) = 0. \tag{4. 56}$$

Stability of a periodic solution may be lost in the following three ways:

- A real eigenvalue satisfies (4. 56), i.e. the eigenvalue is zero.
- A complex eigenvalue satisfies (4. 56), i.e. the eigenvalue is imaginary
- Two complex conjugate eigenvalues satisfy (4. 56), i.e. there are two imaginary eigenvalues with opposite signs.

In the first case the instability is due to transcritical, saddle node or symmetry breaking bifurcations. In the second case the instability is due to a period doubling. In the third case the instability is due to secondary Hopf or Neimark bifurcation [4. 9].

4. 6. Conclusion

In this chapter, the resulting algebraic equations of motion, after application of the harmonic balance method, of free and forced vibrations of beams were presented. In the free vibration analysis, only cosine terms were considered and the HBM was applied to Fourier series expansion using the constant term and even and odd harmonics till fifth order. In the forced vibration analysis, a damping matrix was considered and sine terms were included in Fourier series. The HBM was applied considering a constant term and even and odd harmonics till third order. A method to study the stability of the solutions was presented, based on Floquet's theory but considering the HBM.

References

[4. 1] P. Ribeiro, Hierarchical finite element analyses of geometrically non-linear vibration of beams and plane frames, *Journal of Sound and Vibration* 246 (2001) 225-244.

[4. 2] M. M. Bennouna, R. G. White, The effects of large vibration amplitudes on the fundamental mode shape of a clamped-clamped uniform beam, *Journal of Sound and Vibration* 96 (1984) 309-331.

[4. 3] R. Benamar, M. M. Bennouna, R. G. White, The effects of large vibration amplitudes on the mode shapes and natural frequencies of thin elastic structures. Part I: simply supported and clamped-clamped beams, *Journal of Sound and Vibration* 149 (1991) 179-195.

[4. 4] R. Lewandowski, Non-linear free vibration of beams by the finite element and continuation methods, *Journal of Sound and Vibration* 170 (1994) 539-593.

[4. 5] P. Ribeiro, M. Petyt, Non-linear vibration of beams with internal resonance by the hierarchical finite-element method, *Journal of Sound and Vibration* 224 (1999) 591-624.

[4. 6] W. Szemplinska-Stupnicka, *The Behaviour of Nonlinear Vibrating Systems*, Kluwer Academic Publishers, Dordrecht, 1990.

[4. 7] P. Ribeiro, M. Petyt, Non-linear free vibration of isotropic plates with internal resonance, *International Journal of Non-Linear Mechanics* 35 (2000) 263-278.

[4. 8] M. Petyt, *Introduction to Finite Element Vibration Analysis*. Cambridge, Cambridge University Press, 1990.

[4. 9] A. Nayfeh, B. Balachandran, *Applied Nonlinear Dynamics: Analytical, Computational and Experimental Methods*, New York, 1995.

[4. 10] A. Lazarus, O. Thomas, A harmonic-based method for computing the stability of periodic solutions of dynamical systems, *Comptes Rendus Mecanique* 338 (2010) 510–517.

[4. 11] O. Thomas, A. Lazarus, C. Touzé, A harmonic-based method for computing the stability of periodic oscillations of non-linear structural systems, *Proceedings of the ASME 2010 International Design Engineering Technical Conferences & Computers and Information in Engineering Conference*, August 15-18, 2010, Montreal, Canada.

[4. 12] W. Press, B. Flannery, S. Teukolsky, W. Vetterling, *Numerical Recipes in Fortran 77 : The Art of Scientific Computing*, Cambridge University Press, Cambridge, 1986.

5

Free and Forced Vibration Analysis in the Frequency Domain

5. 1. Introduction

In this chapter, free and forced vibrations of beams with rectangular cross sections are investigated in the frequency domain. The 3D beam equation of motion, developed in sub-chapter 2. 2, is used here and the harmonic balance method, presented in Chapter 4, is employed to convert the nonlinear system of differential equations into a nonlinear algebraic system. The later is solved by a continuation method and the results are presented as frequency-amplitude diagrams. First, the importance of including higher harmonics for the longitudinal displacement and the advantage of removing it, but not neglecting, are shown. Then, free vibrations of 3D beams are examined, coupling between modes is investigated, internal resonances are found and the ensuing multimodal oscillations are described. Some of the couplings discovered lead from planar oscillations to oscillations in the three-dimensional space. Bifurcation diagrams and stability of solution of forced vibrations due to a harmonic force are presented in the last section.

The frequency domain equation of motion (4. 8) or (4. 25) is solved by the arc-length continuation method used, for example, in [5. 1]-[5. 4], which is based on the method presented in [5. 5] and has the ability to pass turning points. The method imposes a constraint equation and is composed of two main loops: in the external loop a predictor to the solution is defined and in the internal loop this predictor is corrected employing Newton's method, which converges to the solution quadratically.

The term “backbone curve” designates a curve that relates the frequency with the vibration amplitude at a certain point. “Backbone curves” are presented by plotting the amplitude of a particular harmonic or of a particular displacement component in the vertical axis and plotting the frequency of vibration in the horizontal axis. The designation “main branch” indicates a branch that contains a solution that simultaneously obeys the following: occurs at zero vibration amplitude, corresponding to a linear mode shape; occurs at a linear natural frequency or at a sub-harmonic of a linear natural frequency. A “secondary branch” is one that bifurcates from a main branch.

5. 2. Influence of the higher harmonics of the longitudinal displacement

The equation of motion, based on Timoshenko’s theory for bending and Saint-Venant’s for torsion, was derived in sub-chapter 2. 2. The longitudinal inertia was neglected in sub-chapter 4. 2, the equation of motion which results from eliminating but not neglecting the longitudinal displacement was given in equation (4. 3) and the longitudinal displacement can be calculated from equation (4. 2). Periodic steady-state responses of the beam were considered and the harmonic balance method was implemented in Chapter 4. In this sub-chapter, the backbone curves, which result from models including and neglecting the longitudinal inertia, are compared.

Harmonics up to third order are considered in the Fourier series and the harmonic balance method is implemented to two equations of motion:

1) the equation of motion including the longitudinal inertia (2. 29) and

2) the equation of motion neglecting the longitudinal inertia (4. 3).

Neglecting the longitudinal inertia, the longitudinal displacement becomes a quadratic function of the transverse displacements and torsion – equation (4. 2), and if harmonics up to third are considered, the longitudinal displacement is given by an expression with harmonics up to sixth order in the Fourier expansion.

Figure 5. 1 shows the backbone curves of the non-zero harmonics of the transverse displacement $w_0(x,t)$ of models including and neglecting the longitudinal inertia. It is obvious that the higher harmonics of the longitudinal displacement are important for correct approximation of the third harmonic of the transverse displacement w_0 – Figure

5. 1 (b) and for the total displacement – Figure 5. 1 (c). Furthermore, it was numerically verified that there is no visible difference between the backbone curves obtained by considering the longitudinal inertia in the equation of motion but expressing the longitudinal displacement with harmonics up to sixth order and expressing the other displacements with harmonics up to third order, and the backbone curves obtained by neglecting the longitudinal inertia and expressing the rest of displacements with harmonics up to third order.

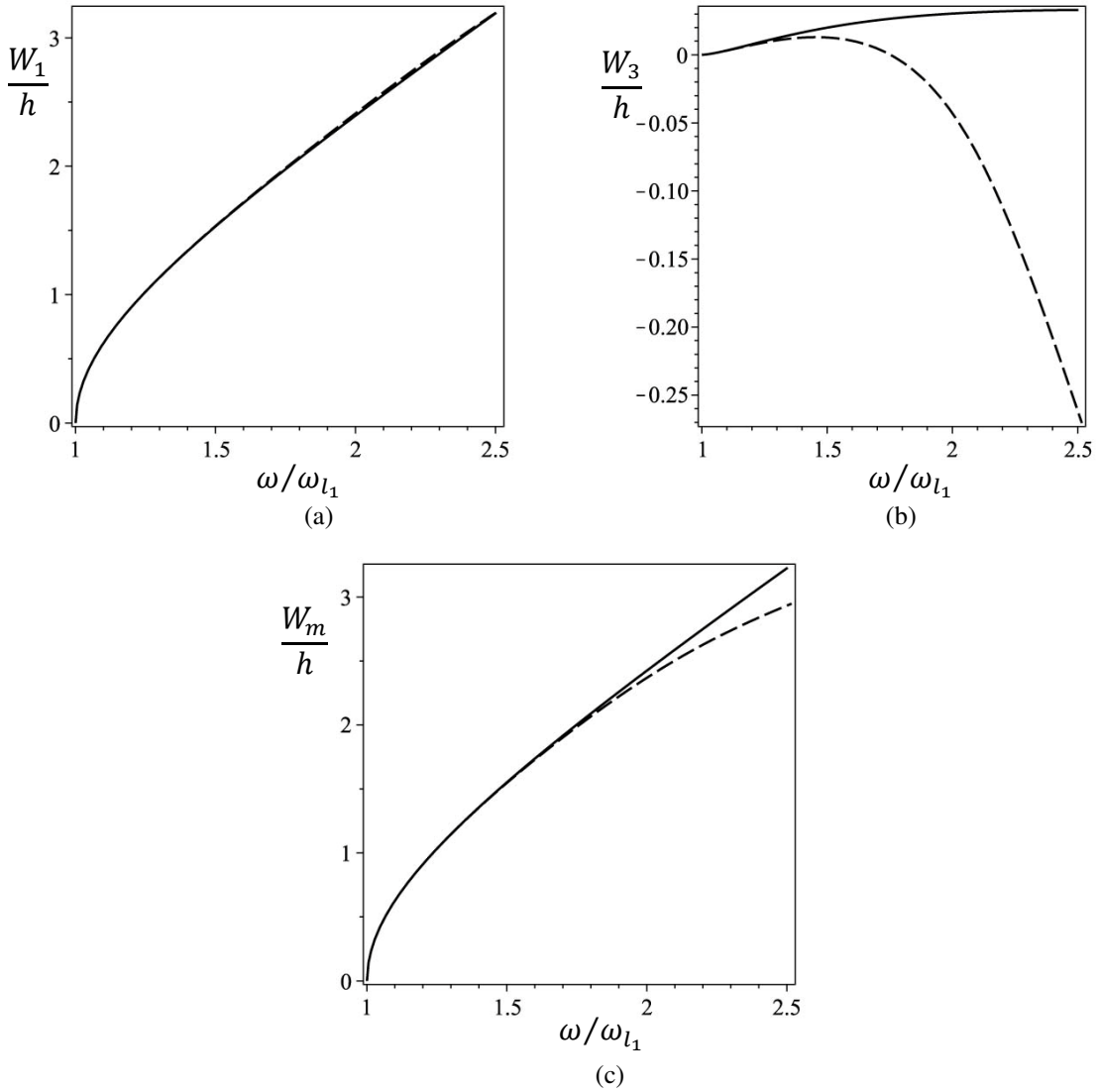

Figure 5. 1. First main branch of bending in plane *xz* using harmonics until the third ($k = 3$); amplitudes of: (a) first harmonic, (b) third harmonic, (c) total displacement. The amplitudes are calculated in the middle of the beam. ── model including the longitudinal inertia, - - - - model neglecting the longitudinal inertia.

The amplitudes presented in Figure 5. 1 are given by:

$$W_1(\xi) = \lfloor \mathrm{N}^{\mathrm{w}}(\xi) \rfloor \{Q_{w_1}\},$$

$$W_3(\xi) = \lfloor \mathrm{N}^{\mathrm{w}}(\xi) \rfloor \{Q_{w_3}\},$$

$$W_m(\xi) = \frac{1}{2} W_0(\xi) + \sum_{i=1}^{k} W_i(\xi), \tag{5. 1}$$

where *k* is the number of harmonics and, in the figure, $\xi = 0$, i.e. the middle of the beam. In the examples that follow, the amplitudes of the constant terms and of the harmonics' displacement components will be calculated using formulas similar to (5. 1) but with the corresponding displacements, shape functions and coefficients. In the example of Figure 5. 1, the constant term and the even harmonics of the Fourier expansion of w_0 were not excited and remain zero. One should observe that w_0 defines the amplitude on the middle line of the transverse displacement in direction *z*, while W_0 presents the constant term of w_0 from Fourier series.

Taking into account the results presented in Figure 5. 1 and noting that by eliminating the longitudinal displacement from the equation of motion the DOF are significantly decreased, the future results will be developed from the equation of motion (4. 3) given in Chapter 4, and different number of harmonics will be considered.

5. 3. Free vibrations of 3D beams

Free modes of vibration of a beam and their coupling are studied. In most of the ensuing analysis, clamped-clamped boundaries are considered. In particular, but without loss of generality, the model derived in this section was applied to beams with the following material properties: $E = 7.0 \times 10.0^{10}$ N m^{-2}, $\rho = 2778$ kg m^{-3}, $\nu = 0.34$ (aluminium). The geometric properties are: $l = 0.58$ m, $b = 0.02$ m and $h = 0.0075$ m.

5. 3. 1. Analysis of convergence

Following the convergence studies on the number of shape functions carried out in Chapter 3, which were complemented by a swift convergence study carried out in the framework of the present chapter, models with ten longitudinal shape functions and seven shape functions for each of the other displacement components ($p_u = 10$, $p_v =$

$p_w = p_{\theta_x} = p_{\phi_y} = p_{\phi_z} = 7$) will be used. To investigate the convergence with the number of harmonics, solutions were computed with different numbers of harmonics and two cases are presented here. In the first case, harmonics till third order are used in equation (4. 5) and in the second case, six terms are employed, i.e. the constant term and harmonics until the fifth.

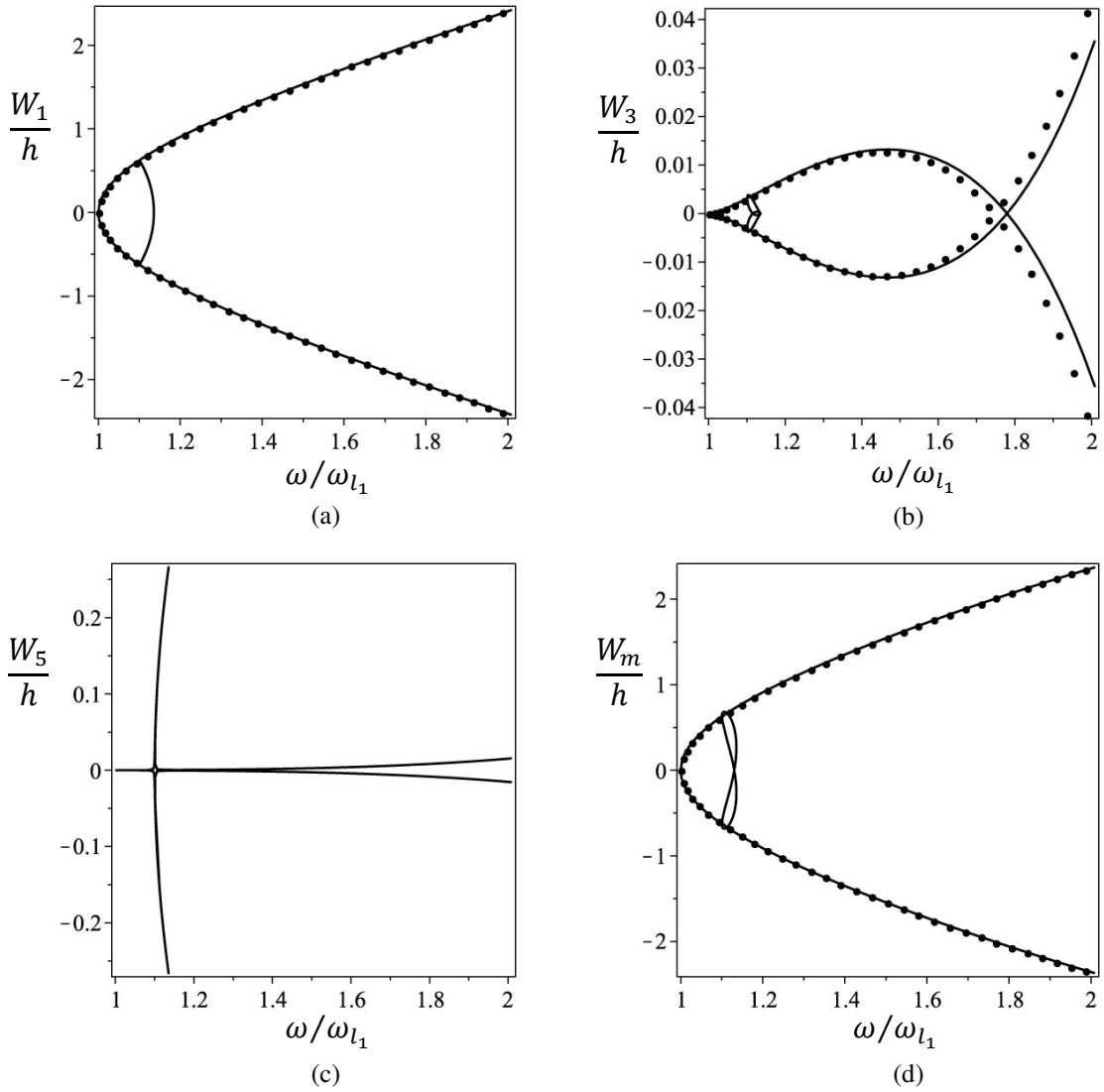

Figure 5. 2. First main branch of bending in plane *xz*, ─ model using harmonics till fifth order (k = 5), • • • model using harmonics till third order (k = 3); amplitudes of: (a) first harmonic, (b) third harmonic, (c) fifth harmonic, (d) total displacement. The amplitudes are calculated in the middle of the beam (ξ = 0).

A comparison of the first main branch of the beam that starts at the first linear bending vibration mode in plane *xz*, computed with different number of harmonics is presented in Figure 5. 2. The constant term and the even harmonics in equation (4. 5) are not excited in this main branch. Also, all the terms which are not related with the transverse displacement w_0 in equation (4. 6) are zero. Figure 5. 2 presents the amplitudes of the

first and the third harmonics of the displacement component along z, as well as the total amplitude in the middle of the beam, computed using different number of harmonics; it also presents the amplitude of the fifth harmonic computed with the second Fourier expansion.

Figure 5. 2 (a), (b) and (d) indicate that, with the Fourier expansion that employs harmonics up to third order, most of the backbone curve is computed with quite good accuracy. However, a turning point and solutions which relate the positive with the negative parts of the bifurcation diagrams can only be found if the fifth harmonic is included. Furthermore, the third harmonic amplitude slightly changes if the fifth harmonic is also present in the Fourier series. Consequently, harmonics up to fifth order will be used in the following analysis. The turning point, bifurcation points and the internal resonances that appear in this example are discussed in detail in the next section.

5. 3. 2. Bifurcation diagrams and internal resonances

As a result of the convergence studies, all harmonics till fifth and a constant term will be employed in the ensuing tests, and the model uses 10 shape functions for the longitudinal displacement and 7 for each of the other displacement components. Hence, the total number of degrees of freedom in the frequency domain is 210.

The continuation method was started twice at the first linear bending mode, first with very small positive amplitude and then with very small negative amplitude. One turning and several bifurcation points were discovered on the first main branch. Figure 5. 3 presents all the bifurcation points found until $\omega/\omega_{l_1} \cong 2$ and the secondary branches that start from them. Only the first harmonic is plotted in this bifurcation diagram, other harmonics are addressed later. Since the main branch continues from positive to negative amplitude of vibration and the opposite, both main branches – starting with positive and negative amplitudes of the first mode – are presented. As a result, the turning and bifurcation points appear in pairs: for each point in the “positive” branch there is another at the same frequency but on the “negative” branch. In the first harmonic, the bifurcation points number 1 and 1’, respectively of the “positive” and the “negative” branches, coincide.

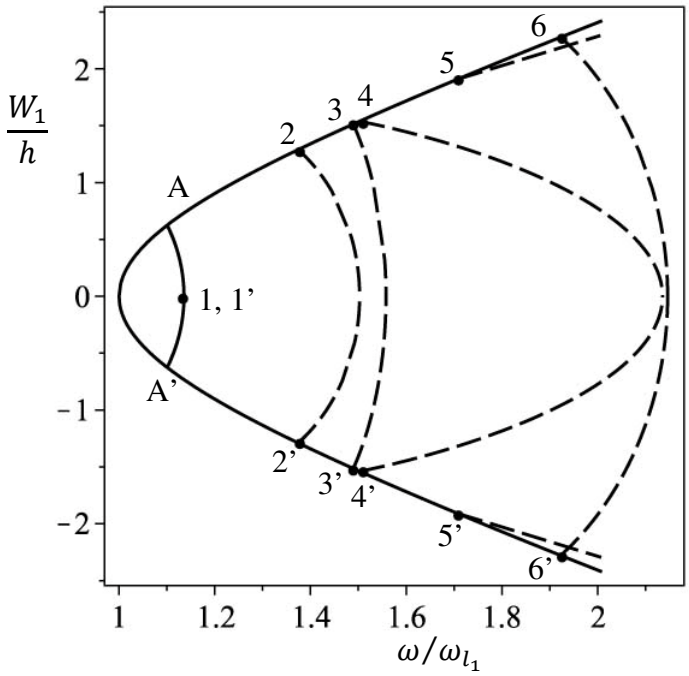

Figure 5. 3. Bifurcation diagram that starts on the first linear mode in bending, first harmonic. ─ first main branch, - - - secondary branches, • bifurcation points (numbered), A, A' – indicate turning points, $\xi = 0$.

5. 3. 2. 1. Oscillations in one plane

The free vibrations of clamped-clamped beams in one plane were previously investigated in [5. 2], using as well a *p*-version finite element. However, only odd harmonics were employed and Bernoulli-Euler theory was followed. Thus, the part of the present analysis that is devoted to planar vibrations differs from the one of [5. 2] in the facts that Timoshenko theory is adopted for bending and that symmetry breaking bifurcations leading to secondary branches can now be studied, because a constant term and even harmonics are considered. Moreover, it will be verified here that point A on Figure 5. 3 is actually a turning point and not other type of bifurcation, as though in [5. 2]. Finally, and more important than the former aspects, is the fact that bifurcations that lead to non-planar vibrations can be, and are, investigated with the present model. The next section is devoted to those bifurcations and to the resulting vibrations in space.

Figure 5. 4 presents the first part of the backbone curve $\left(1 \leq \omega/\omega_{l_1} \leq 1.2\right)$. Starting at the linear solution and following the main branch with positive amplitude, the amplitudes of the first and third harmonics increase until $\omega/\omega_{l_1} \cong 1.098$ and start to decrease after $\omega/\omega_{l_1} \cong 1.098$; at the later frequency the amplitude of the fifth harmonic increases. The increment of the fifth harmonic near frequency value $\omega/\omega_{l_1} \cong 1.1$ is due to 1:5 internal resonance between first and third bending modes. It is underlined that this is still the first

main branch: there is no change of the jacobian sign and the modes related with the first and third harmonics are the same (although with small variation of natural frequencies and shapes).

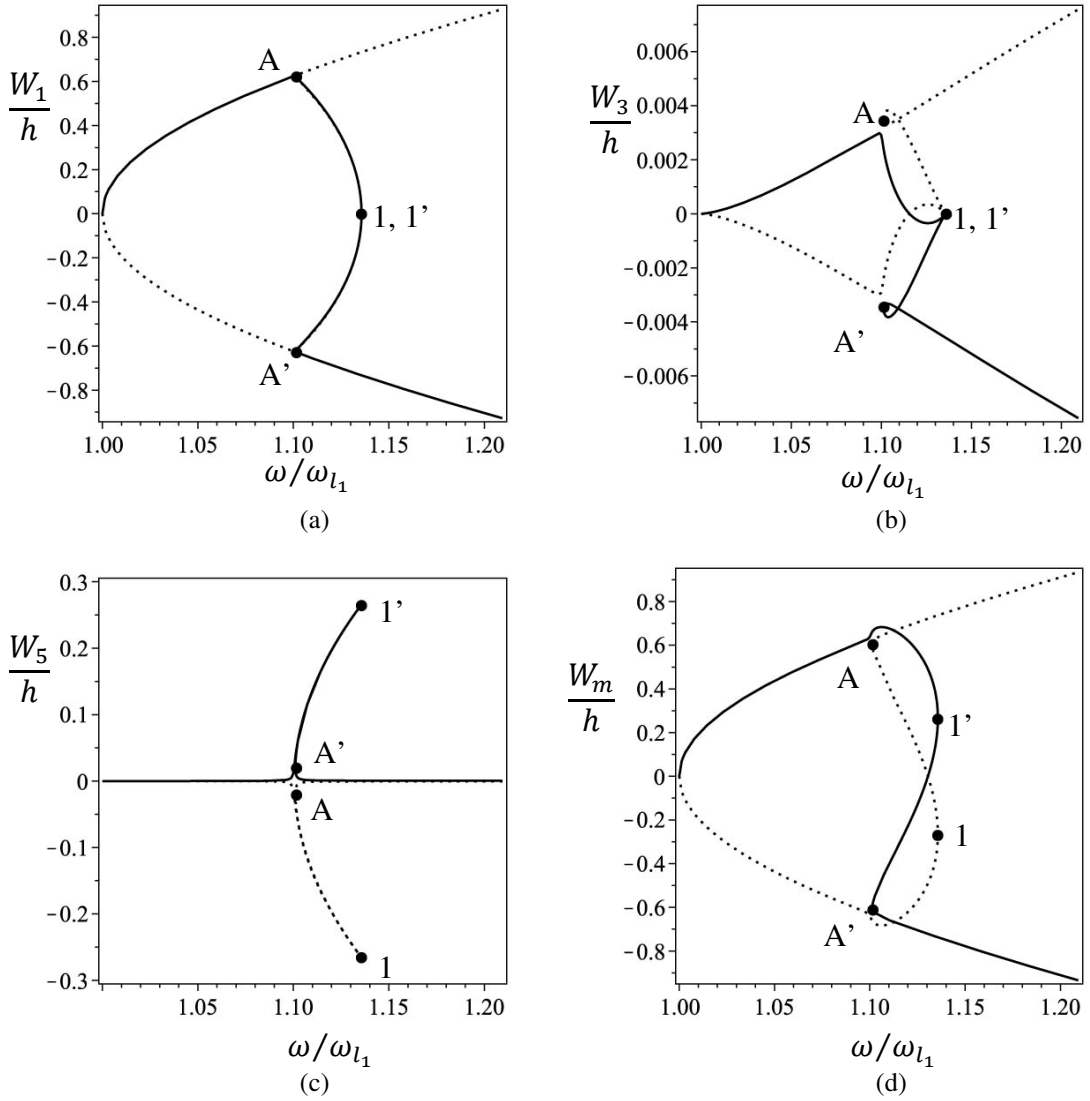

Figure 5. 4. First main branch of bending in plane *xz*: ─ bifurcation diagram obtained using the first mode with positive amplitude, · · · bifurcation diagram obtained using the first mode with negative amplitude, 1 and 1' – bifurcation points; A, A' – turning points: (a) first harmonic, (b) third harmonic, (c) fifth harmonic, (d) total displacement, $\xi = 0$.

The fifth harmonic increases till a bifurcation point (point 1') is reached at $\omega/\omega_{l_1} \cong 1.136$. The first and third harmonic at this bifurcation point are zero. Continuing after the bifurcation point, but still following the same branch, the fifth harmonic decreases and the first and third harmonics' amplitudes become negative; then a turning point is found at $\omega/\omega_{l_1} \cong 1.101$. Curiously, at this stage we return to an oscillation in the first and third harmonics only, continuing the initial hardening spring part of the main branch.

From the bifurcation point 1' (and likewise, from point 1) begins another main branch which is, in this model, related only with the fifth harmonic and the third mode of vibration. This branch is not shown in Figure 5. 4, but can be seen in [5. 2], where the shapes of vibration and the backbone curves of this second main branch are presented.

The turning points $\omega/\omega_{l_1} \cong 1.101$, represented by letters A and A' in the figures, were also found in [5. 2] but taken to be bifurcation points due to the form of the curve. The bifurcation and turning points designations used here follow the definition in [5. 6], which states that a point $(\{Q_0\}, \omega_0)$ is a bifurcation point if the following conditions are satisfied:

(1a) $\{\mathcal{F}(\{Q_0\},\ \omega_0)\} = \{0\}$,

(2a) $\operatorname{rank} \frac{\partial\{\mathcal{F}(\{Q_0\}, \omega_0)\}}{\partial\{Q\}} = \mathrm{N} - 1$,

(3a) $\frac{\partial\{\mathcal{F}(\{Q_0\}, \omega_0)\}}{\partial\omega} \in \operatorname{range} \frac{\partial\{\mathcal{F}(\{Q_0\}, \omega_0)\}}{\partial\{Q\}}$,

i. e. $\operatorname{rank} \left(\frac{\partial\{\mathcal{F}(\{Q_0\}, \omega_0)\}}{\partial\{Q\}} \middle| \frac{\partial\{\mathcal{F}(\{Q_0\}, \omega_0)\}}{\partial\omega}\right) = \mathrm{N} - 1$,

(4a) Exactly two branches of stationary solutions intersect with two distinct tangents.

Still agreeing to [5. 6], a point $(\{Q_0\}, \omega_0)$ is a turning point if the following conditions are satisfied:

(1b) $\{\mathcal{F}(\{Q_0\},\ \omega_0)\} = \{0\}$,

(2b) $\operatorname{rank} \frac{\partial\{\mathcal{F}(\{Q_0\}, \omega_0)\}}{\partial\{Q\}} = \mathrm{N} - 1$,

(3b) $\frac{\partial\{\mathcal{F}(\{Q_0\}, \omega_0)\}}{\partial\omega} \notin \operatorname{range} \frac{\partial\{\mathcal{F}(\{Q_0\}, \omega_0)\}}{\partial\{Q\}}$,

i. e. $\operatorname{rank} \left(\frac{\partial\{\mathcal{F}(\{Q_0\}, \omega_0)\}}{\partial\{Q\}} \middle| \frac{\partial\{\mathcal{F}(\{Q_0\}, \omega_0)\}}{\partial\omega}\right) = \mathrm{N}$,

(4b) There is a parameterization $\{Q(\sigma)\},\ \omega(\sigma)$ with $\{Q(\sigma_0)\} = \{Q_0\},\ \omega(\sigma_0) = \omega_0$ and $\frac{\mathrm{d}^2\omega}{\mathrm{d}\sigma^2}(\sigma_0) \neq 0$.

Vector $\{\mathcal{F}(\{Q\},\ \omega)\}$ is defined in equation (4. 8). Condition (4b) in the turning point definition was not checked as it is defined, i.e. the existence of such a parameterization

was not verified. This condition prevents a point from not being a hysteresis point [5. 6] and was checked graphically: Figure 5. 4 shows that points A and A' are not hysteresis points. The satisfaction of condition (3b) for turning points, proves that points A and A' are not bifurcation points. The dimension of vector $\{\mathcal{F}(\{Q\}, \omega)\}$ is N, previously defined.

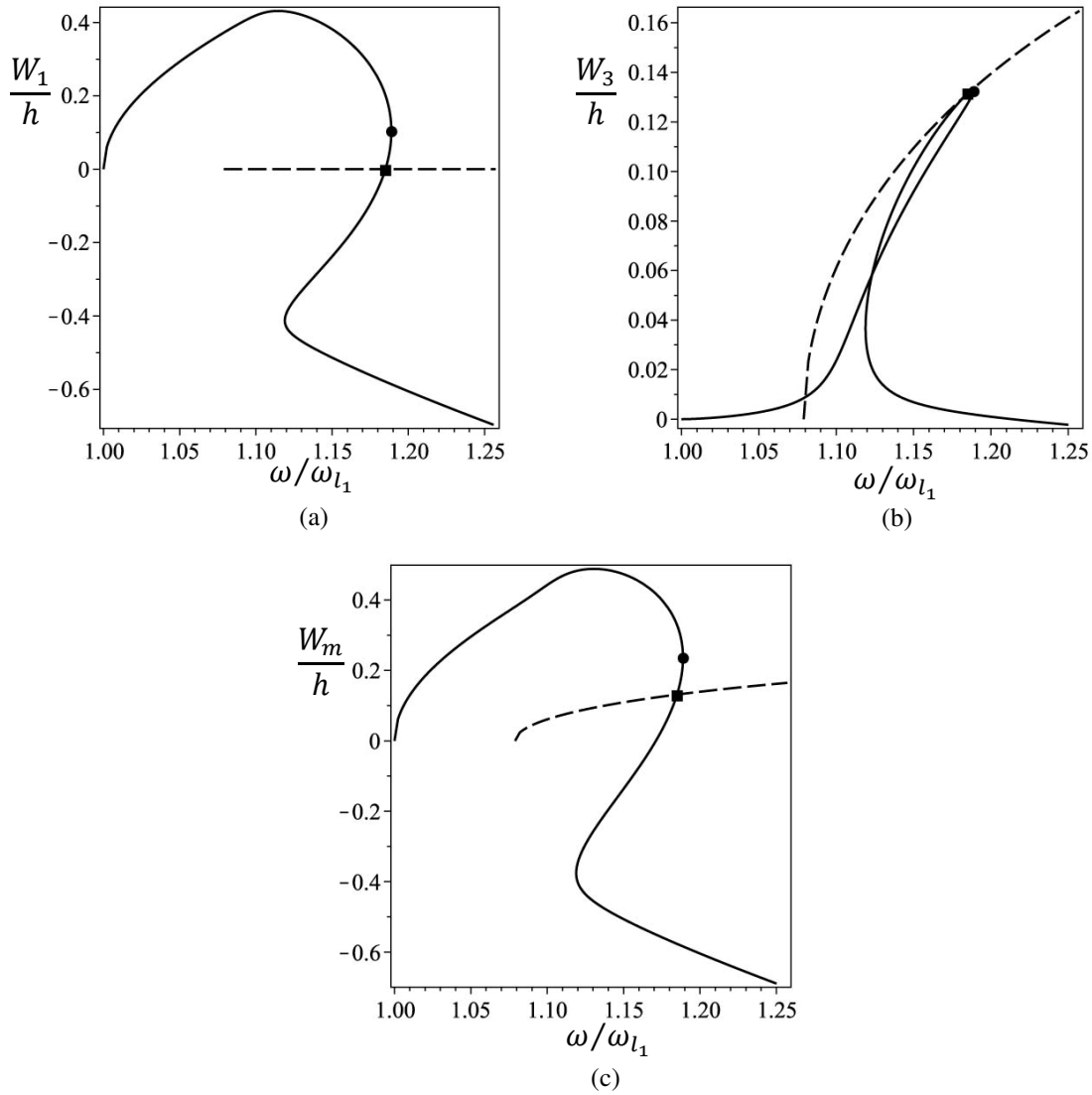

Figure 5. 5. ── first and - - - - second main branches of bending in plane *xz* of hinged-clamed beam using harmonics till third order (k = 3); amplitudes of: (a) first harmonic, (b) third harmonic, (c) total displacement. The amplitudes are calculated in the middle of the beam (ξ = 0), ● – turning point, ■ – bifurcation point.

It is noted that in the paragraphs above definitions that correspond to equilibrium solutions were applied with the justification that, after application of the HBM, we are dealing with an algebraic system: time is not explicit in the equations of motion or in the results. Naturally, all our "equilibrium solutions" are in fact periodic oscillations that can be recovered using equations of the form of equation (4. 5).

To further validate the present model, a test on a hinged-clamped beam was carried out and the results verified to agree with the ones of Lewandowski [5. 1]. The interest in this case, results from the fact that a turning point similar to the one presented in Figure 5. 4 was found. In the case of the hinged-clamped beam a secondary branch relating main branches was not found in the frequencies analysed and the main branches are directly related by a bifurcation point. The bifurcation diagrams of the amplitudes of the first and the third harmonics and the total amplitude of vibration are shown in Figure 5. 5. The third harmonic increases at frequency $\omega/\omega_{l_1} \cong 1.1$ due to 1:3 internal resonance between the first and second modes [5. 7].

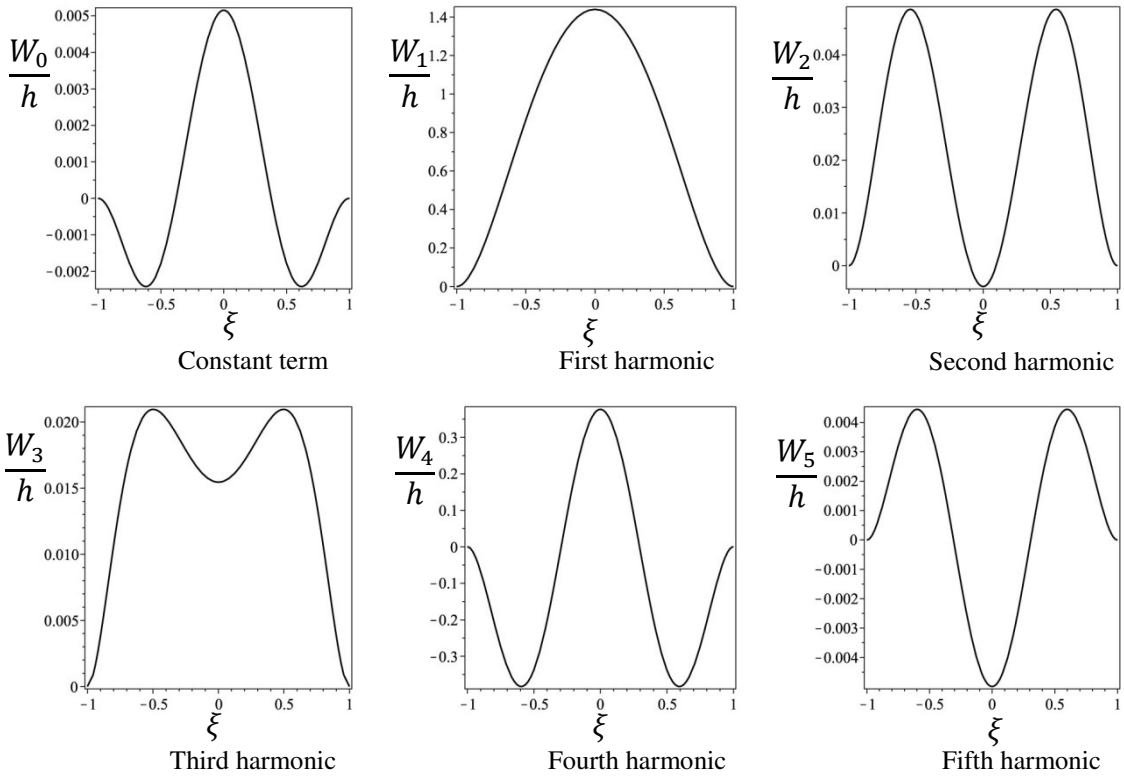

Figure 5. 6. Shapes of the harmonics at point $\omega/\omega_{l_1} = 1.60$ of the positive part of the secondary branch that starts from bifurcation point 4.

Returning to the clamped-clamped beam example, at the fourth and fifth bifurcation points (Figure 5. 3), secondary branches appear where all harmonics and the constant term in w_0 are present. These bifurcation points and the secondary branches were not found in [5. 1]-[5. 2] because only odd harmonics were considered in those references. In these secondary branches the vibration remains in one plane and it is not coupled with torsion. The shapes of the all harmonics at a certain point on the secondary branch that starts at the bifurcation point 4 are presented in Figure 5. 6. Figure 5. 7 shows the time

history and the projection on a phase plane defined by the transverse displacement and velocity at the middle of the beam for the same point of the secondary branch. The oscillation on the secondary branch is asymmetric: the projection on the phase plane lost symmetry with respect to the vertical axis due to the even harmonics that appear in the transverse displacement w_0.

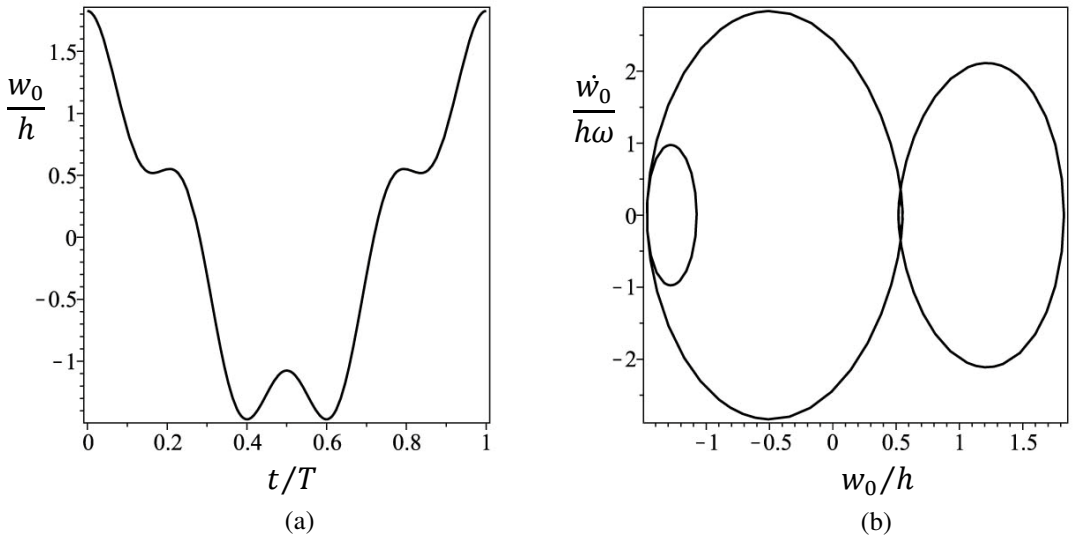

Figure 5. 7. Time history (a) and phase plot (b) defined by transverse displacement and velocity at the middle of the beam (ξ = 0), solution at $\omega/\omega_{l_1} = 1.60$ of the positive part of the secondary branch that starts from bifurcation point 4, T – period of vibration.

The secondary branch that starts on point 4 relates to another main branch (not shown) where vibrations in the third mode and fourth harmonic occur. On the other hand, a connection between the secondary branch that starts on point 5 and another main branch was not found. Similar secondary branches, i.e., branches that are related with odd and even harmonics and that apparently do not lead to a main branch, have been found in plates [5. 8].

These results confirm that although the nonlinearity is cubic in pure bending, even harmonics can appear in the solution due to symmetry breaking bifurcations.

5. 3. 2. 2. Oscillations in space

We will now see in more detail the second bifurcation point (Figure 5. 3) and the secondary and second main branches related with it. This bifurcation point occurs approximately at $\omega/\omega_{l_1} = 1.37$. The ratio between the nonlinear bending fundamental frequency in *xz* plane and the linear bending fundamental frequency in *xy* plane is

approximately 2. Therefore, a 1:2 internal resonance occurs and the first mode of w_0 (bending in plane *xz*) couples with the first mode of v_0 (bending in plane *xy*), which is related with the second harmonic. The bifurcation diagrams of the first, third and fifth harmonics of the displacement in the *z* direction, i.e. w_0, are presented in Figure 5. 8. The other harmonics of the displacement w_0 and the constant term are zero.

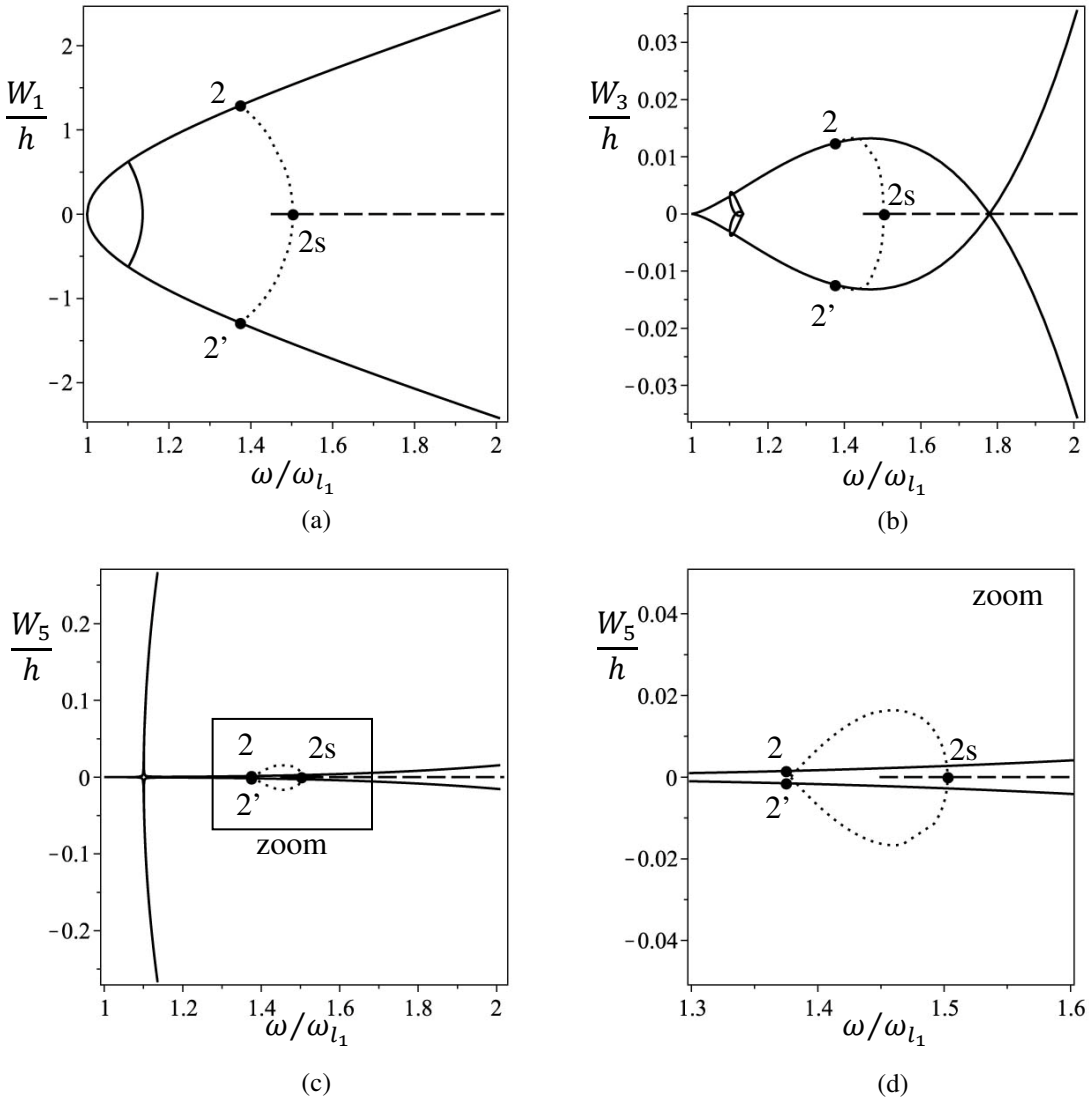

Figure 5. 8. Bifurcation diagrams of bending in the *xz* plane (displacement w_0) with a secondary branch found at point $\omega/\omega_{l_1} = 1.37$. — first main branch, · · · secondary branch, - - - second main branch. (a) first harmonic of w_0, (b) third harmonic of w_0, (c) fifth harmonic of w_0, (d) zoomed area of (c), $\xi = 0$. Points 2, 2' – the same bifurcation points as in Figure 5. 3; point 2s – bifurcation point which relates the secondary branch with the second main branch.

In the secondary branch, the displacement in the *y* direction, v_0, is excited and the two transverse displacements - v_0 and w_0 - become coupled. Due to the bending-torsional coupling, torsion also occurs. As an example, the shapes of the harmonics of the two transverse displacements and torsion at $\omega/\omega_{l_1} = 1.45$, from the positive part of the

secondary branch are presented in Figure 5. 9. Only the harmonics different from zero are shown.

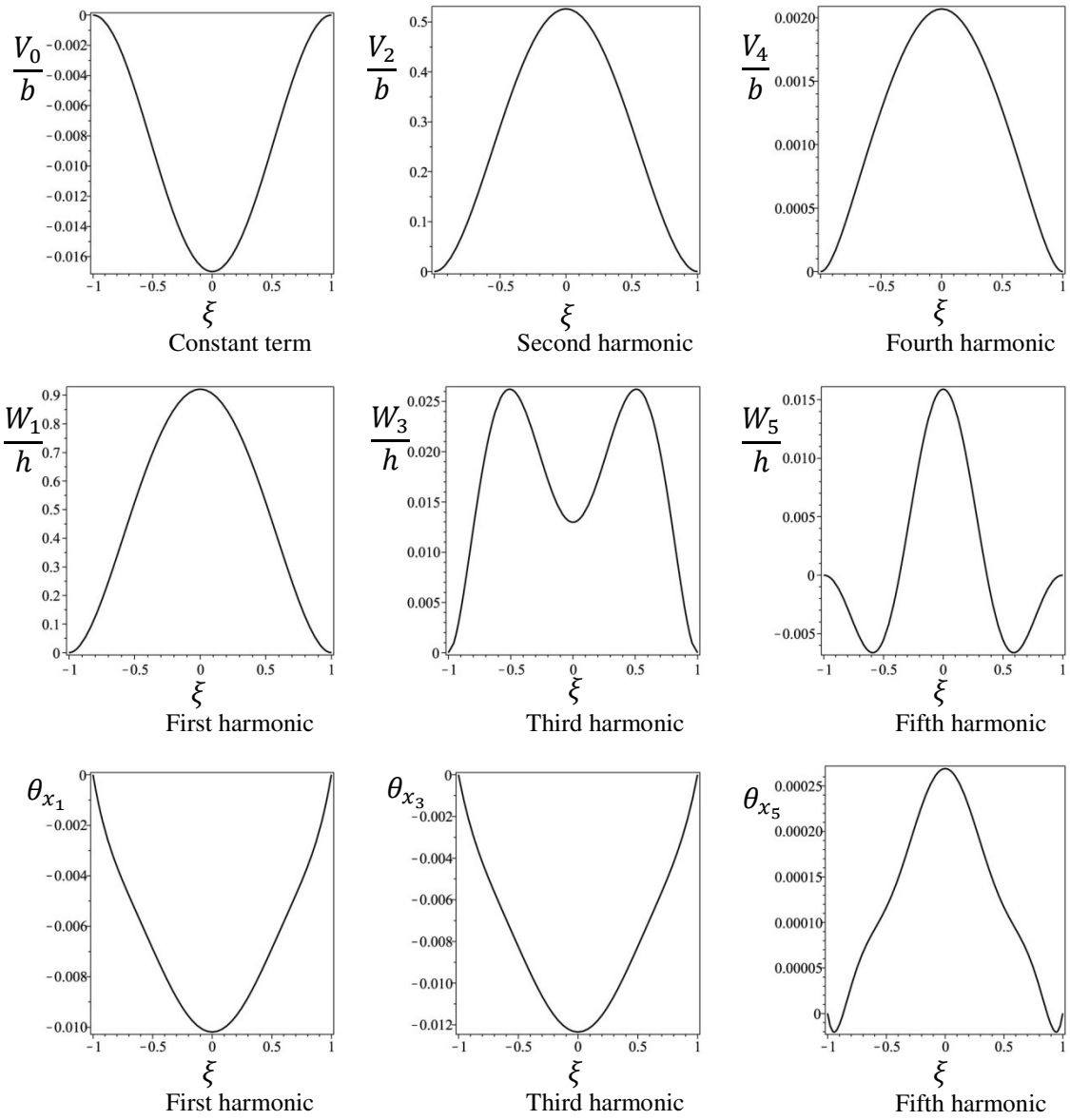

Figure 5. 9. Shapes of the non-zero harmonics at point $\omega/\omega_{l_1} = 1.45$ of the positive part of the secondary branch that starts at the second bifurcation point.

Starting from the bifurcation point number 2 found for bending in *xz* and following the secondary branch, the amplitude of the transverse displacement w_0 decreases while the amplitude of the transverse displacement v_0 increases (Figures 5. 8 and 5. 10). The secondary branch crosses another main branch when the amplitude of w_0 becomes zero. In the latter main branch the beam vibrates only in one plane, but now the plane is *xy* and the vibration is related with displacement v_0. With the model employed, only the second

harmonic is excited in this main branch and it has a shape similar to the one of the first linear mode.

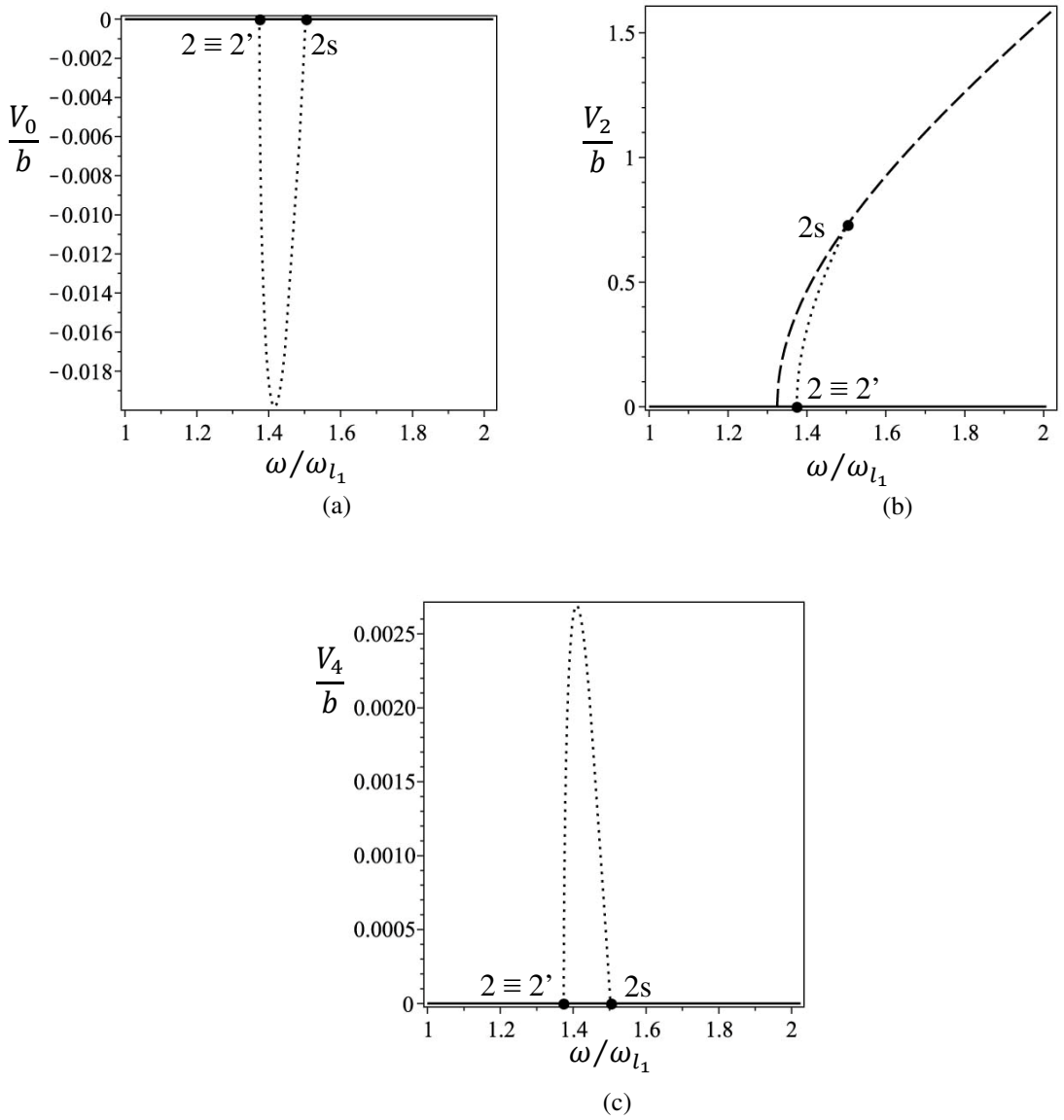

Figure 5. 10. Bifurcation diagrams of bending in the *xy* plane (displacement v_0) computed at $\xi = 0$, — first main branch, · · · secondary branch, - - - second main branch. (a) constant term of v_0, (b) second harmonic of v_0, (c) fourth harmonic of v_0. The first main and the second main branches of the constant term and the fourth harmonic have zero amplitude. Points 2 and 2' are the same bifurcation points as in Figure 5. 3; point 2s is a bifurcation point that relates the secondary branch with the second main branch.

Torsion only appears in the secondary branch – as shown in Figures 5. 9 and 5. 11 – and is due to the bending-torsional coupling. It should be noted that following the secondary branches that originate on the two bifurcation points, one in the positive main branch (point 2) and the other one in the negative main branch (point 2'), both secondary branches have harmonics of v_0 with the same amplitudes, but opposite amplitudes in torsion.

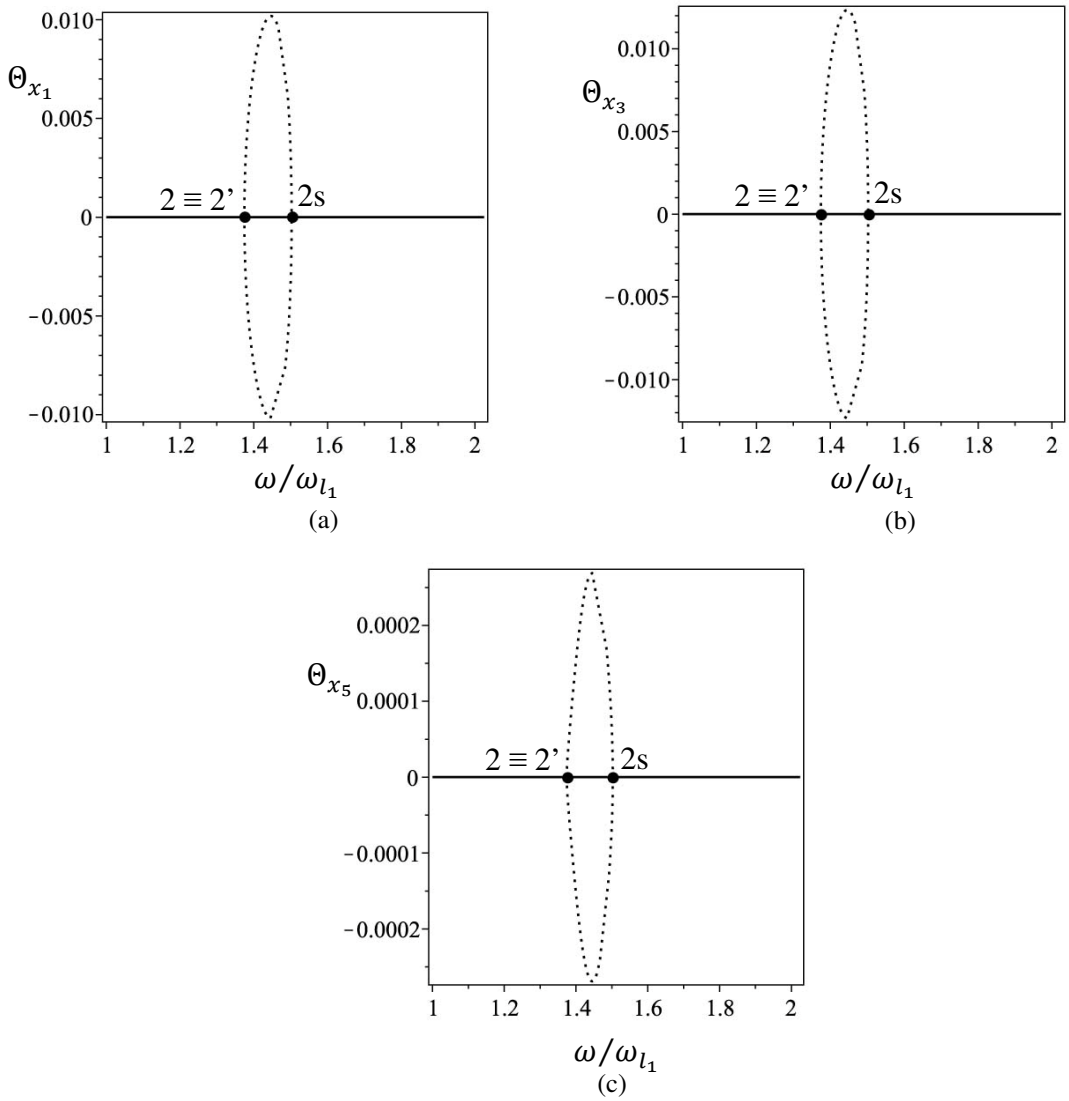

Figure 5. 11. Bifurcation diagrams of torsion θ_x: ─ first main branch, · · · secondary branch, - - - second main branch. (a) first harmonic of θ_x, (b) third harmonic of θ_x, (c) fifth harmonic of θ_x, $\xi = 0$. Points 2 and 2' are the same bifurcation points as in Figure 5. 3; point 2s is the bifurcation point that relates the secondary branch with the second main branch.

From the third bifurcation point on Figure 5. 3 also results a branch of solutions where vibrations occur in space. At this point the nonlinear fundamental frequency of bending in *xz* plane becomes one fifth of the second frequency of bending in *xy* plane, i.e. a 1:5 internal resonance, which couples modes similar to the first linear mode in the *xz* plane and to the second linear mode in the *xy* plane, occurs. Due to the nonlinearity, other harmonics appear in the secondary branch and they attain much smaller vibration amplitudes. In this secondary branch, the first, the third and the fifth harmonics of v_0 are excited and coupled with the first, the third and the fifth harmonics of w_0 and the constant term and the second and the fourth harmonics of θ_x. This secondary branch

leads to a second main branch, where the beam vibrates in the second bending mode in plane *xy* and in the fifth harmonic.

The sixth bifurcation point also leads to vibrations in space due to a 1:4 internal resonance which relates the first nonlinear frequency of bending in *xz* plane with, again, the second nonlinear frequency of bending in *xy* plane. In the secondary branch, even harmonics and the constant term in v_0 are excited and, consequently, so is torsion. This secondary branch connects with a second main branch, which is related with the second bending mode in plane *xy* (displacement v_0) and with the fourth harmonic.

Finally, variations in time of the beam centroidal line are presented in Figures 5. 12 and 5. 13. Figure 5. 12 presents the vibration of the beam for half period of vibration at point $\omega/\omega_{l_1} = 1.485$ on the secondary branch that starts at the second bifurcation point. The leading harmonics of this branch are the first harmonic of w_0, related with the first mode of w_0, and the second harmonic of v_0 related with the first mode of v_0. The other half of the period of vibration follows the same displacements but in the opposite order. In Figure 5. 13 a quarter period of vibration at point $\omega/\omega_{l_1} = 1.55$ from the secondary branch that stems from the third bifurcation point is presented. The leading harmonics on this branch are the first harmonic in w_0, related with the first mode of w_0, and the fifth harmonic of v_0 related with the second mode of v_0. The second quarter of the period of vibration is the same but with negative part in the *xz* plane and the second half period follows the first half but in the opposite way. Both figures clearly show that these vibrations occur in three-dimensional space.

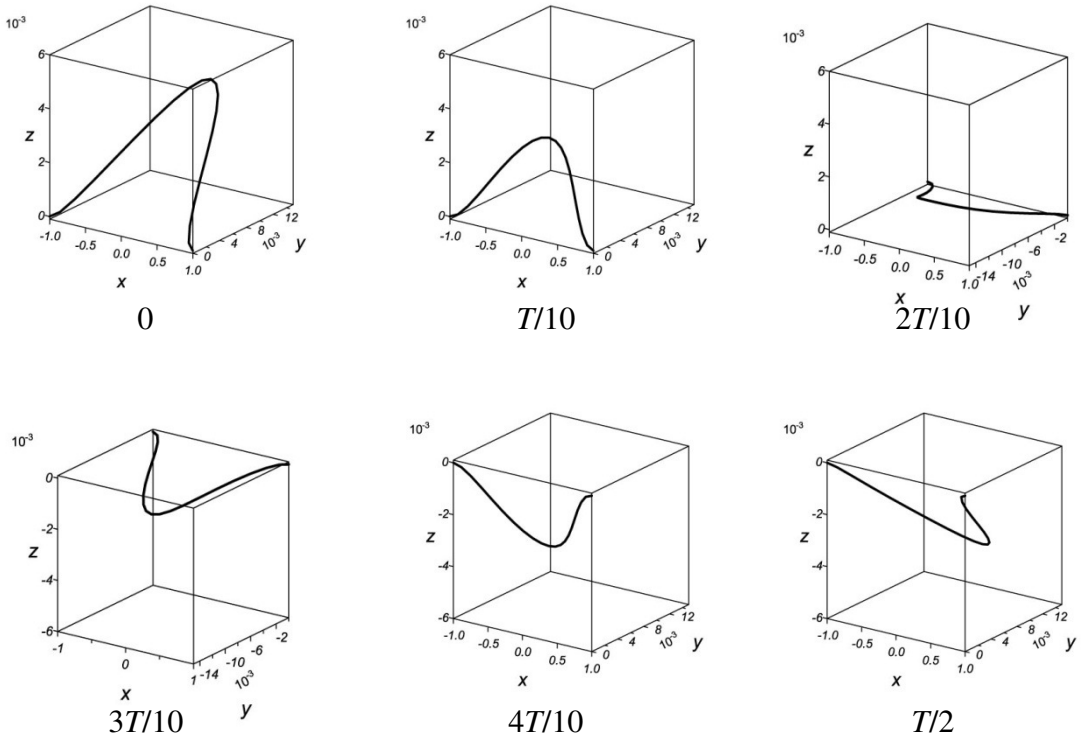

Figure 5. 12. Half period of vibration of the beam at point $\omega/\omega_{l_1} = 1.485$ from the secondary branch of the second bifurcation point. T – period of vibration. The displacements in y and z are calculated in meters while the longitudinal axis is presented in the local coordinates.

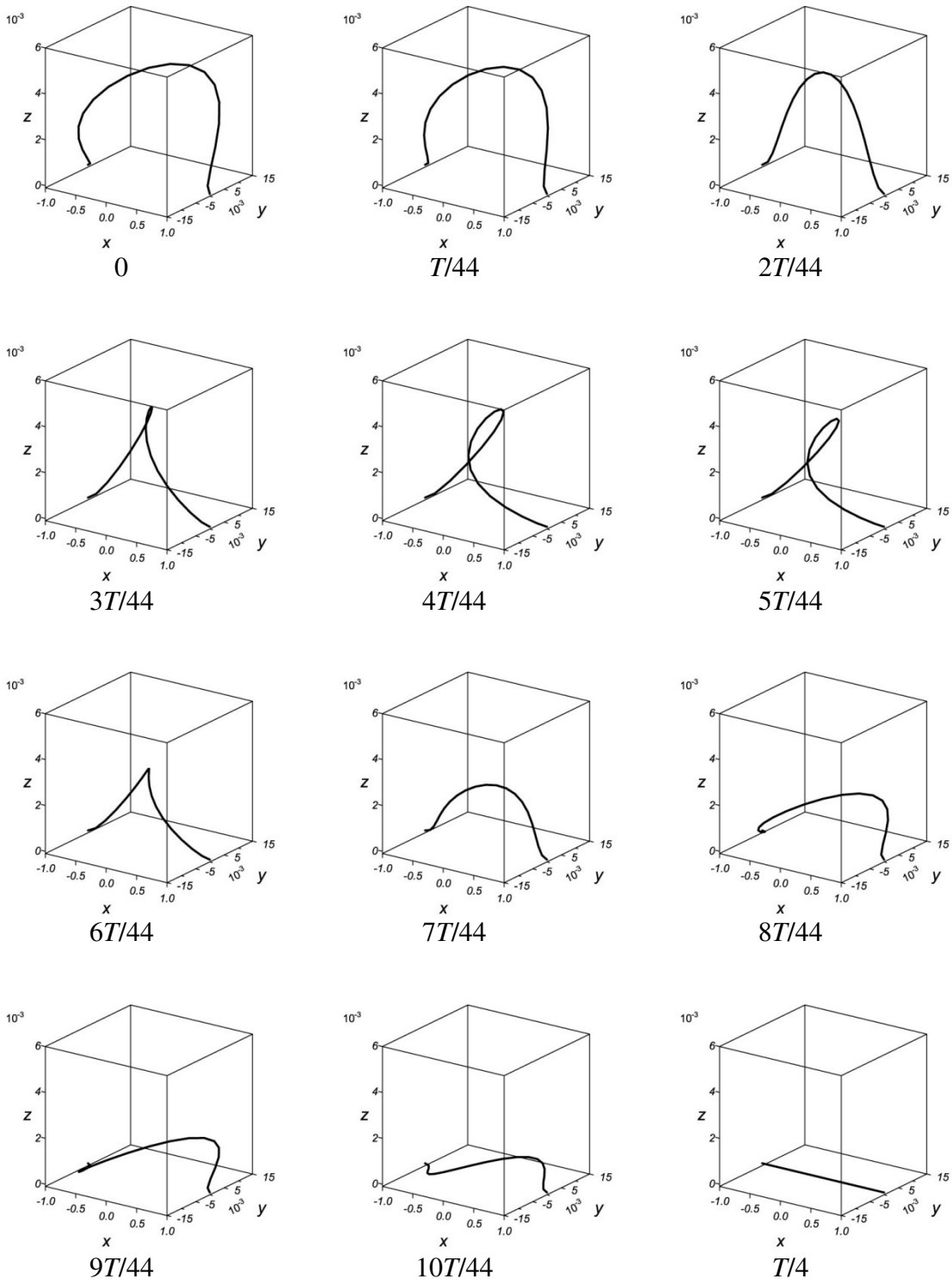

Figure 5. 13. Quarter period of vibration of the beam at point $\omega/\omega_{\iota_1} = 1.55$ from the secondary branch of the third bifurcation point. T – period of vibration. The displacements y and z are calculated in metres while the longitudinal axis is presented in the local coordinates.

5. 4. Forced vibrations of 3D beams

Considering the convergence study presented for static deformations of 3D beams in Chapter 3, the convergence study for bending of beams in the frequency domain presented in [5. 2] and the results presented in previous sub-section, a model with the same number of shape functions, i.e. with 10 longitudinal shape functions and 7 shape functions for the bending displacements, torsion and rotation about both transverse axes, is used. Furthermore, it was verified that a model with more shape functions converges to the same results in forced vibrations.

First, the model derived in the previous chapter is partially validated using existing results for planar vibrations of clamped-clamped beams. The model is compared with results obtained by experimental means [5. 9] and numerically using shooting method [5. 10]. The beam is excited by a point harmonic force of amplitude 0.134 N applied in transverse direction z. The geometrical and material properties of the beam from [5. 10] are implemented here, i.e. l = 0.406 m, b = 0.02 m and h = 0.002 m and $E = 7.172\ 10^{10}$ N m^{-2}, $\rho = 2800$ kg m^{-3}, $\nu = 0.33$. The comparison is presented on Figure 5. 14. The presented results are for an undamped beam, in accordance with the results obtained by the shooting method [5. 10]. The results are in very good agreement with the ones from shooting method and fairly good with the experimental ones.

The model is now applied to clamped-clamped beams with the following material properties (aluminium): $E = 7.0\ 10^{10}\ N$ m^{-2}, $\rho = 2778$ kg m^{-3}, $\nu = 0.34$. The geometric properties are: l = 0.58 m, b = 0.02 m and h = 0.015 m. Damping is calculated by equation (4. 21), with $\alpha = 0.01$. For comparison purposes, beams with different thicknesses and lengths will also be analysed.

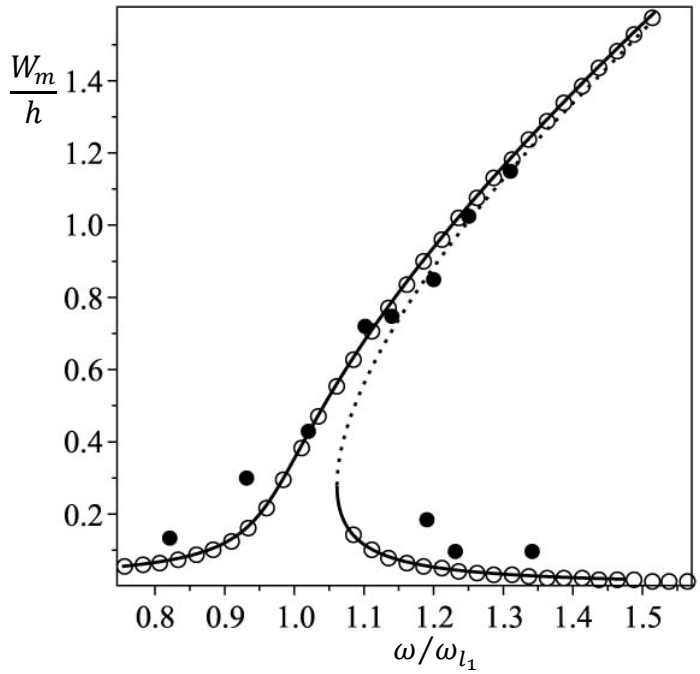

Figure 5. 14. Transverse displacement w_0 of the beam for transverse force amplitude 0.134 N, ξ = 0. ● – experimental results, ○ – numerical by shooting method, ── stable solutions from current model, ····· unstable solutions from current model.

An inclined harmonic force with amplitude of 50 N is applied at the edge of the middle cross section (x = 0), as shown in Figure 5. 15, in order to excite all displacement components and cause vibration in space. The applied force is symmetric about plane x = 0 and we will only analyse oscillations that are symmetric about this plane. Thus, we can reduce the above model using only symmetric or non-symmetric shape functions, according to which displacement the shape functions are related to. A model with 5 anti-symmetric shape functions for longitudinal displacement, 4 symmetric shape functions for both transverse and the torsional displacements and 4 anti-symmetric shape functions for both rotations along the transverse axes is applied in the tests. The same model is used in the rest of the examples, since only forces, symmetric with respect to plane x = 0, are applied.

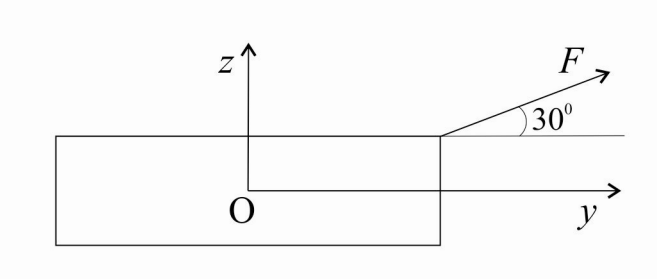

Figure 5. 15. Inclined excitation.

Figures 5. 16 – 5. 18 show the variation of the amplitude of each harmonic, i.e. of the constant term, first, second and third harmonics, of the two transverse displacements and torsion. For example, the amplitude of the first harmonic of transverse displacement w_0 is calculated by:

$$W_1 = \sqrt{{W_{c_1}}^2 + {W_{s_1}}^2} \tag{5. 2}$$

where W_{c_1} and W_{s_1} are the amplitudes of the cosine and sine terms of the first harmonic of w_0. These amplitudes are computed at a particular ξ using:

$$\begin{aligned} W_{c_1}(\xi) &= \lfloor \mathrm{N^w}(\xi) \rfloor \left\{ Q_{w_{c_1}} \right\}, \\ W_{s_1}(\xi) &= \lfloor \mathrm{N^w}(\xi) \rfloor \left\{ Q_{w_{s_1}} \right\}. \end{aligned} \tag{5. 3}$$

In all the examples, the amplitudes of the constant terms and of the harmonics' displacement components are calculated using formulas similar to (5. 2) and (5. 3) but with corresponding displacements, shape functions and coefficients.

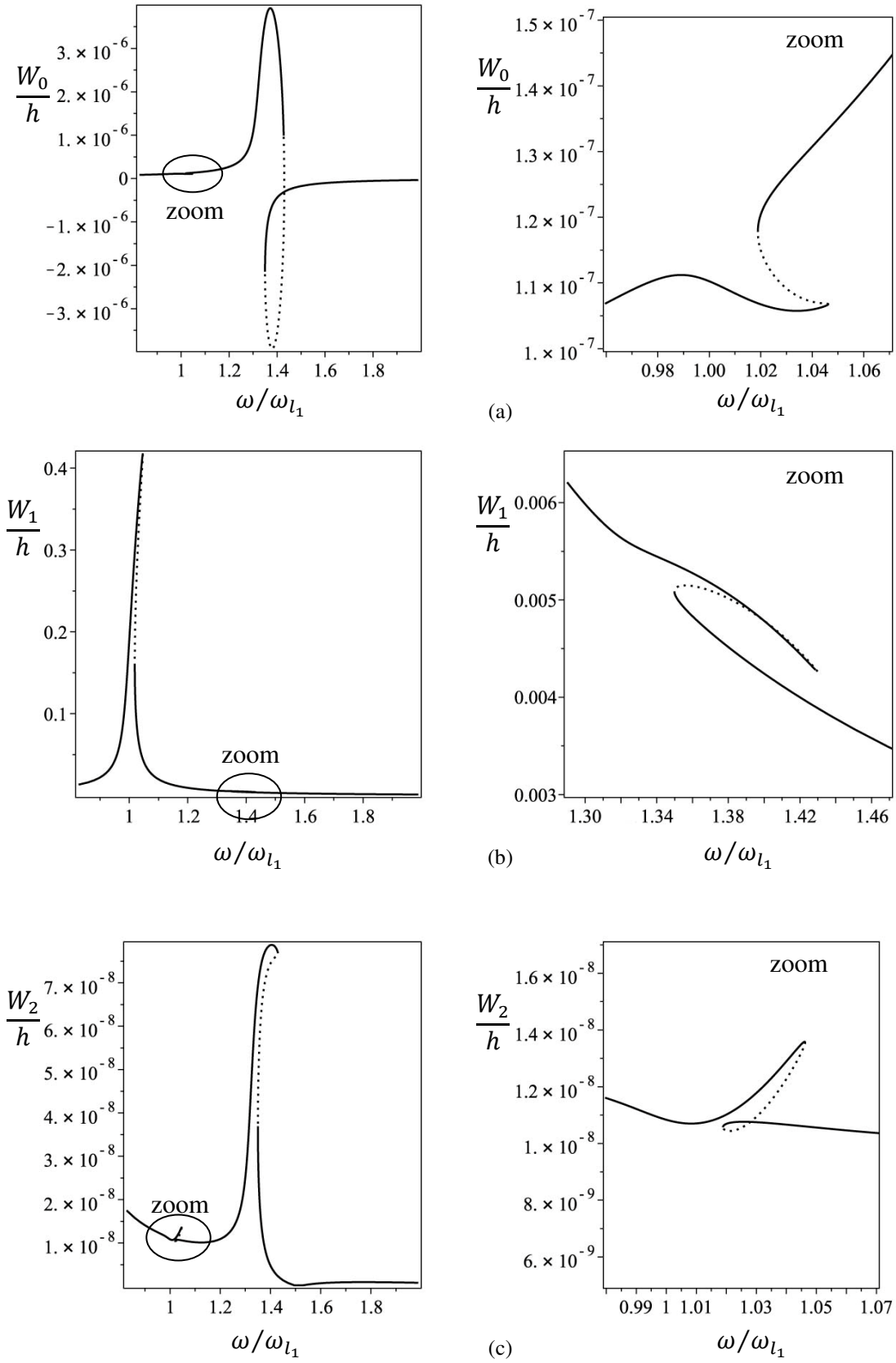

Figure 5. 16. Continues on the next page.

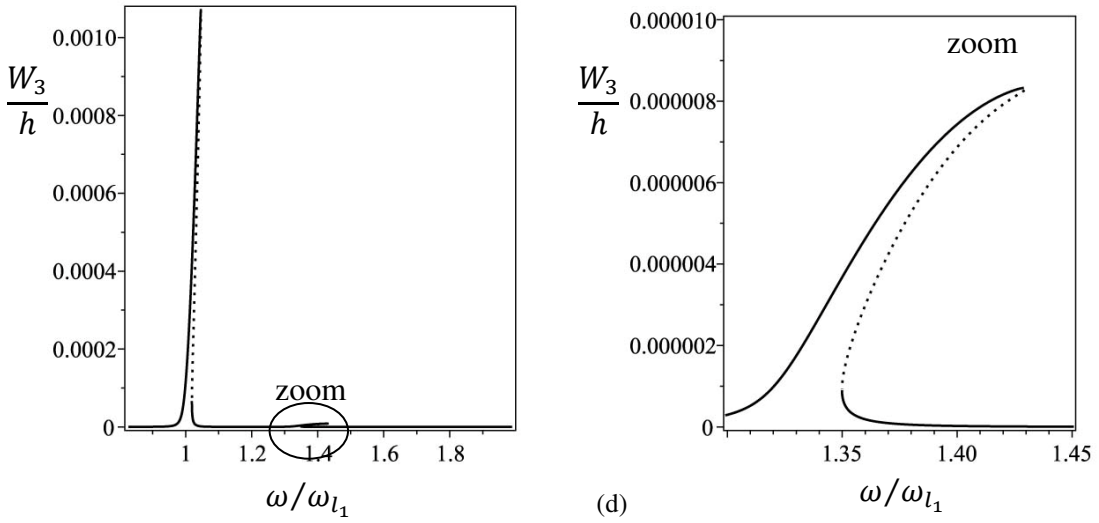

Figure 5. 16. Transverse displacement w_0 as function of the excitation frequency for force amplitude 50 N, ξ = 0. (a) W_0 – amplitude of the constant term, (b) W_1 – amplitude of the first harmonic, (c) W_2 – amplitude of the second harmonic, (d) W_3 – amplitude of the third harmonic. Line – stable solution, dots – unstable solution.

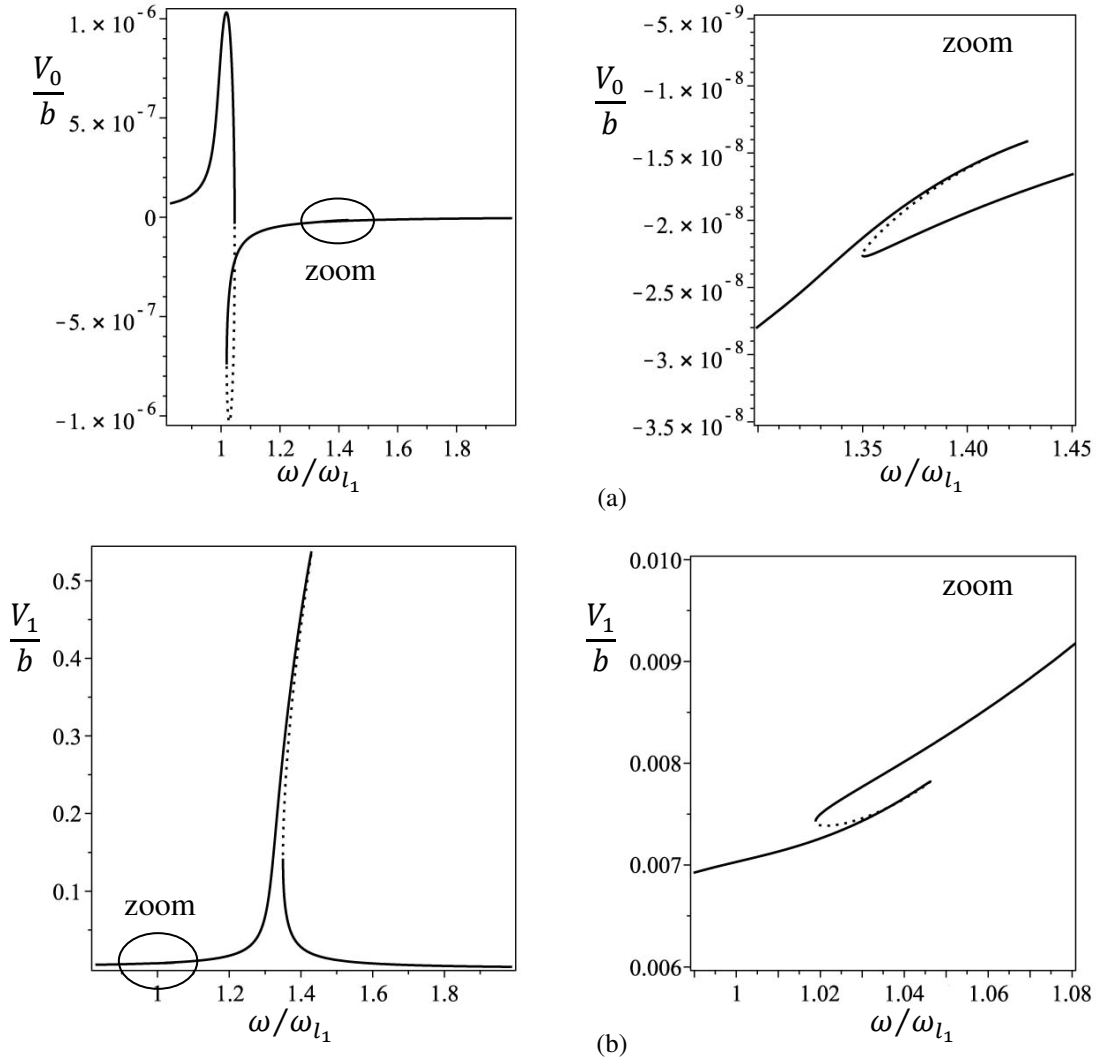

Figure 5. 17. Continues on the next page.

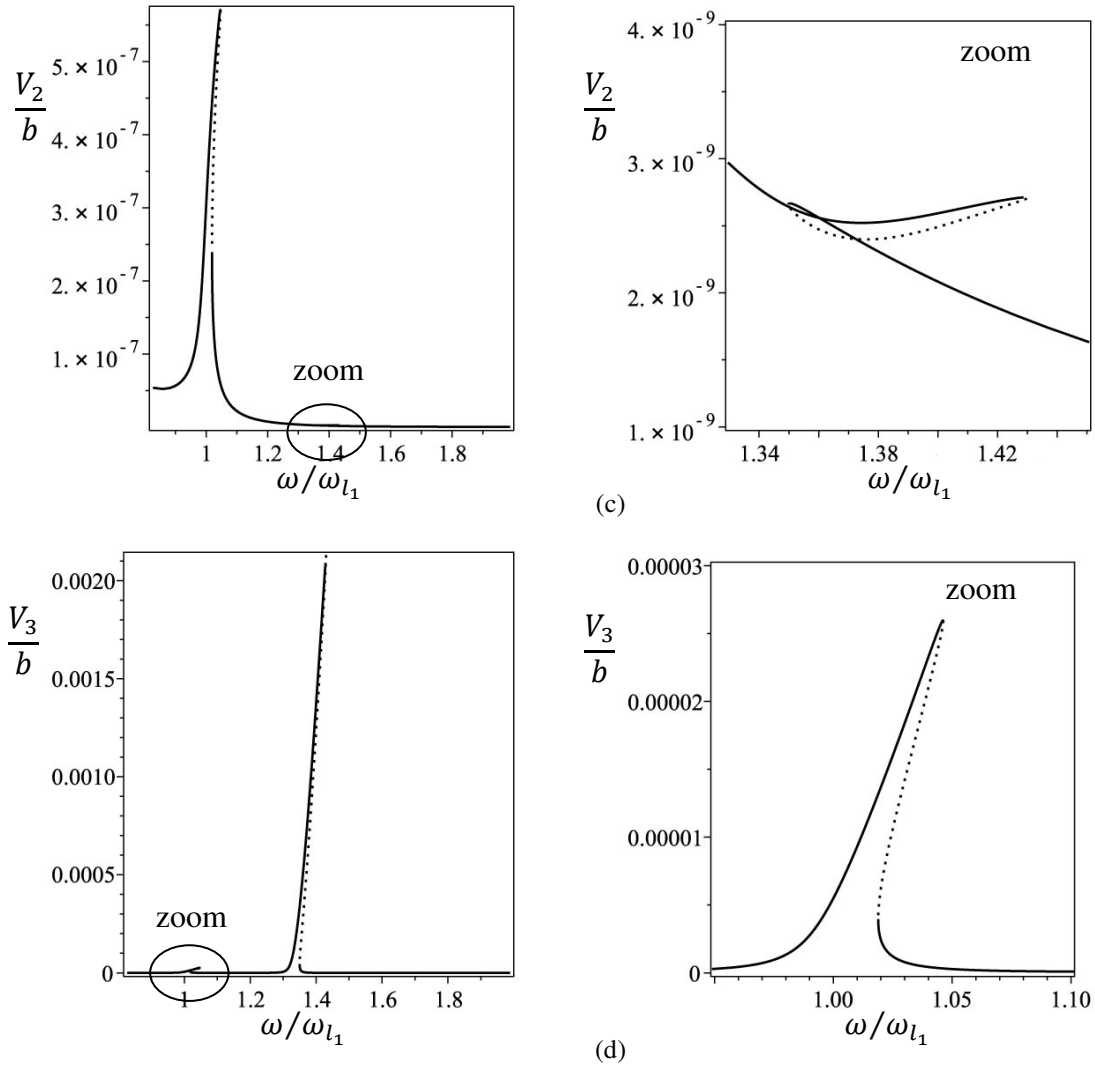

Figure 5. 17. Transverse displacement v_0 as function of the excitation frequency for force amplitude 50 N, $\xi = 0$. (a) V_0 – amplitude of the constant term, (b) V_1 – amplitude of the first harmonic, (c) V_2 – amplitude of the second harmonic, (d) V_3 – amplitude of the third harmonic. Line – stable solution, dots – unstable solution.

The longitudinal axis of Figures 5. 16 – 5. 18 is non-dimensional, since the excitation frequency is divided by the fundamental frequency which is the first linear frequency of bending in *xz* plane, $\omega_{w_{l_1}} = 1445.14$ rad/s. The first linear frequency in the other bending plane is, for this beam, $\omega_{v_{l_1}} = 1926.33$ rad/s, or $\omega_{v_{l_1}} = 1.33\,\omega_{w_{l_1}}$. As expected, the main harmonics of this response are the first harmonics of both transverse displacements (Figure 5. 16 (b) and Figure 5. 17 (b)). Increasing the frequency of vibration, the amplitude of vibration increases till a turning point is reached at $\omega/\omega_{l_1} = 1.05$. Near ω_{l_1} the amplitude of vibration increases mainly in the transverse direction *z*, while vibration also occurs in the other plane but its amplitude remains small. Hence, for frequencies close to the first linear bending mode in plane *xz* (related with displacement

component w_0) the vibration is mainly in plane *xz* (Figure 5. 19 (a)), even if the force excites the beam in space. Torsion also exists, but it is very small because the beam is much stiffer in torsion (Figure 5. 18). This is reflected in the first linear frequency in torsion, which is 14665.07 rad/s, i.e. 10 times the fundamental frequency.

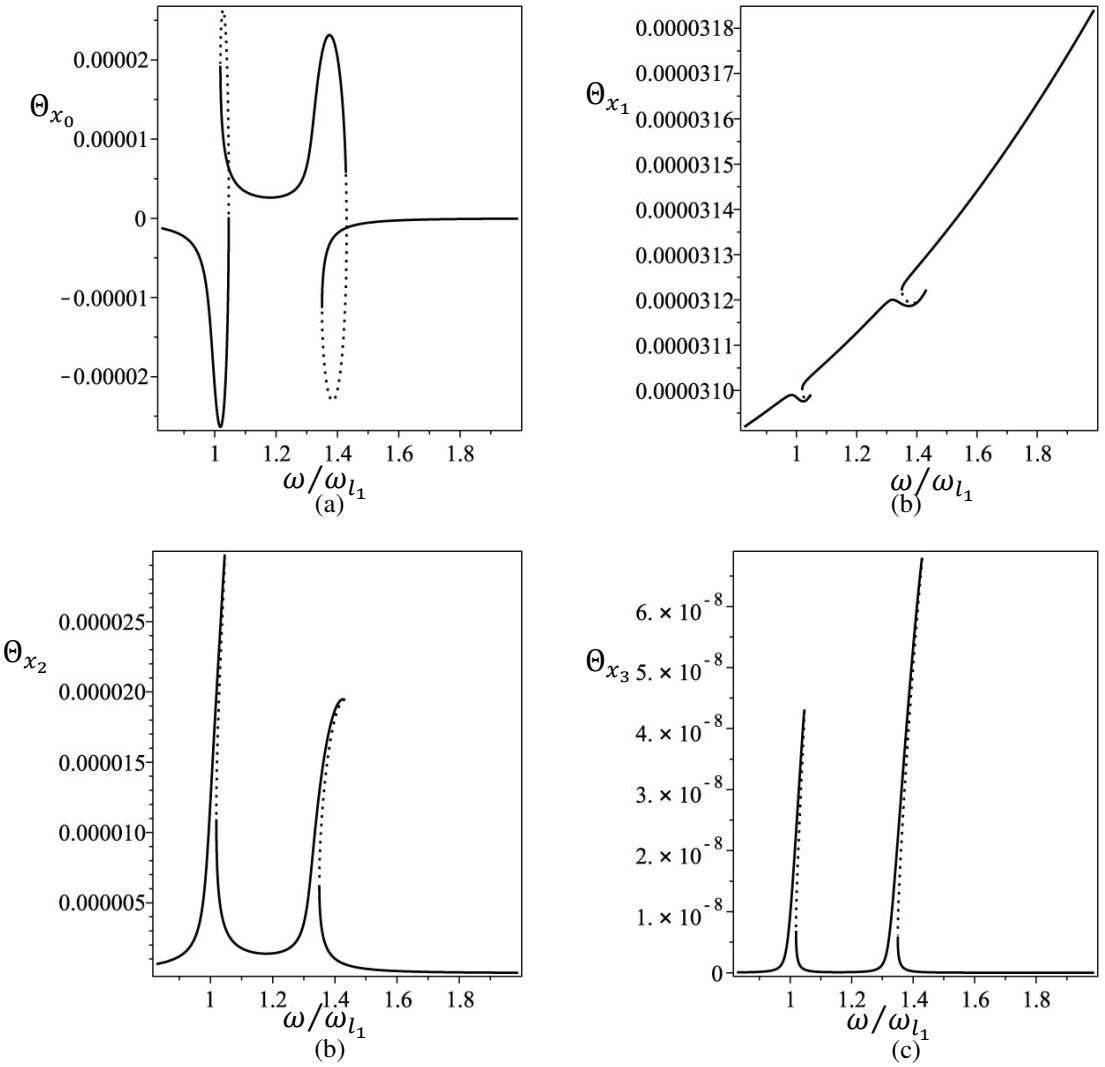

Figure 5. 18. Torsion θ_x as function of the excitation frequency for force amplitude 50 N, $\xi = 0$. (a) Θ_{x_0} – amplitude of the constant term, (b) Θ_{x_1} – amplitude of the first harmonic, (c) Θ_{x_2} – amplitude of the second harmonic, (d) Θ_{x_3} – amplitude of the third harmonic. Line – stable solution, dots – unstable solution.

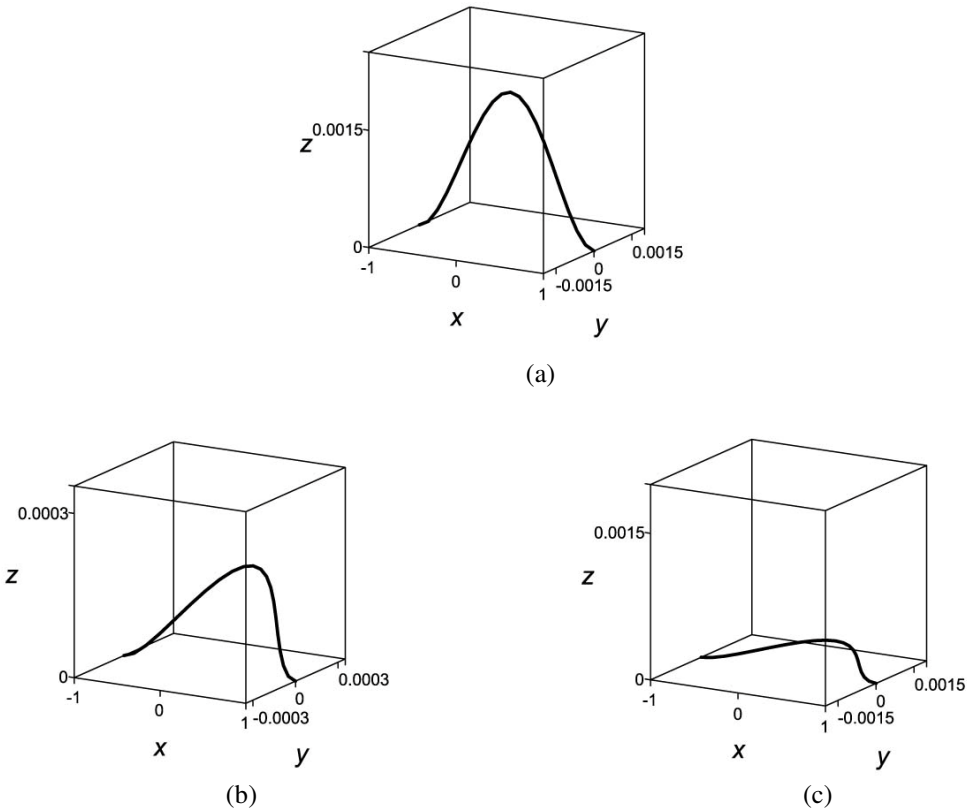

Figure 5. 19. 3D shape of vibration assumed by the beam at t = 0 s for different excitation frequencies. (a) $\omega/\omega_{l_1} = 1.04$, (b) $\omega/\omega_{l_1} = 1.18$, (c) $\omega/\omega_{l_1} = 1.31$.

After the turning point, an unstable region of solutions exists where the amplitude of bending in *xz* plane decreases. There is a region in which both transverse amplitudes are small and more or less equal. In this region the vibration is clearly in 3D space but with small amplitude (Figure 5. 19 (b)), because the frequency of excitation is not close to any natural frequency of vibration. The amplitude starts to increase when the frequency approaches the first linear frequency of bending in plane *xy* (mainly related with displacement v_0). For frequencies close to this value, the vibration is again mainly in one plane, but this is now plane *xy* (Figure 5. 19 (c)).

In the next example, a beam with the same material properties and with dimensions h = 0.02 m, b = 0.02 m and l = 2.0 m is analysed. Since the beam cross section is square, the natural frequencies of bending in planes *xz* and *yz* are the same, and changes on the stability status and shape of vibration can appear due to 1:1 internal resonance between the two bending oscillations. A transverse force of 6 N is applied in the middle of the beam only in transverse direction *z*. The variation of the amplitude of the first harmonic of transverse displacement in *z*, W_1, is presented in Figure 5. 20. Increasing the excitation

frequency, a real characteristic exponent becomes greater than zero (corresponding to a real Floquet multiplier leaving the unit circle through +1) and a bifurcation similar to a supercritical pitchfork bifurcation of a static equilibrium solution, which gives rise to one unstable and two stable branches, is observed. The system of equations (4. 25) is a system of algebraic equations which are typical for static problems, but the solution is not a static solution, it is a periodic solution, obtained from equation (4. 22). Thus, following the definition of bifurcation points of periodic solutions given in [5. 11], the bifurcation point is a supercritical symmetry-breaking bifurcation point. It results in a pair of stable asymmetric solutions and one unstable symmetric solution. The asymmetry is due to even harmonics and a constant term which appear in Fourier spectra for the torsional displacement. The unstable branch remain in one plane, the *xz* plane where the force is applied, while the stable branches present motions of the beam in space, even though the applied force is only in one plane. The latter motions are not symmetric about plane *xy*, unlike the stable oscillation before the bifurcation point.

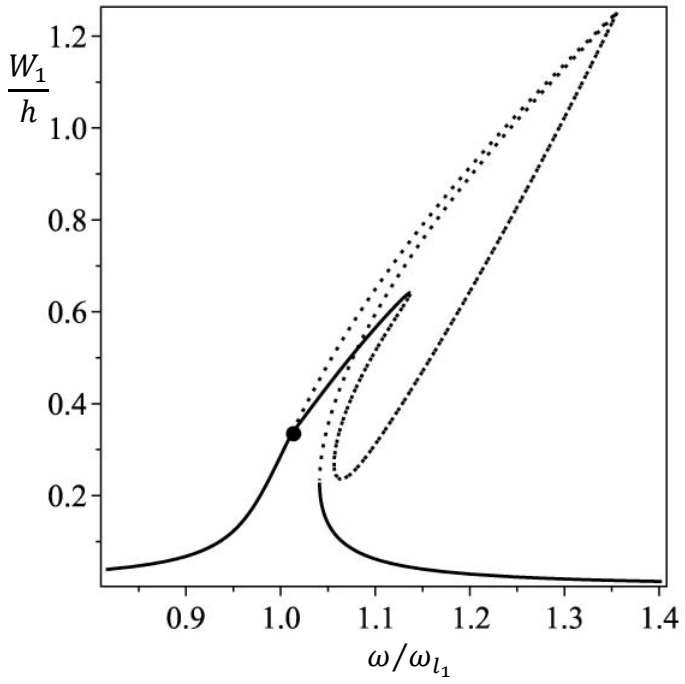

Figure 5. 20. First harmonic of w_0 for beam with square cross section; ── stable solution, --- unstable solution, ● – symmetry-breaking bifurcation point.

Both stable branches coincide in Figure 5. 20 since the first harmonics of vibration in *z*, W_1, have equal amplitudes. The turning points in this figure, where a stable and an unstable branch coalesce correspond to cyclic-fold bifurcations of the periodic oscillations [5. 11]. The symmetry-breaking bifurcation point in Figure 5. 20 is due to

1:1 internal resonance between the fundamental frequencies in both transverse displacements. Similar bifurcation points, but called pitchfork bifurcations, since in the 'vibration amplitude-frequency' diagram the bifurcation looks like a pitchfork, and the corresponding branches were presented for strings in [5. 12].

The two stable branches, which arise from the bifurcation point, can be better seen on Figure 5. 21, where the variations of the amplitudes of the vectors related with the cosine and sine terms of the first harmonic of transverse displacement in *y*, V_{c_1} and V_{s_1}, with the frequency of excitation are plotted. Both branches have the same amplitudes but with different signs for the cosine and sine terms. It results into two different vibrations with the same amplitude for the first harmonic of v_0 but with different phases. After the bifurcation point, when the amplitude of V_{c_1} becomes positive and starts to increase, the amplitude of V_{s_1} is negative and starts to decrease. After the first turning point, both amplitudes are positive. Torsion also occurs in the secondary branches where the vibration is in space, due to a bending-torsional coupling. Torsion angles are very small and are presented on Figure 5. 22. Phase plots relating the torsional angle with the respective angular velocity for points of the two stable asymmetric solutions are shown on Figure 5. 23, where the asymmetry can be clearly seen.

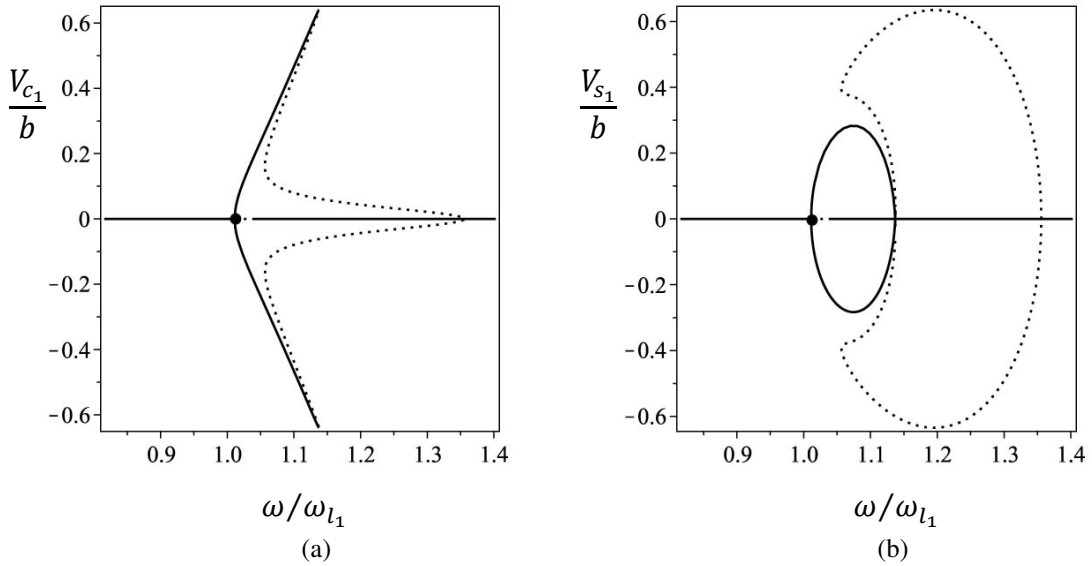

Figure 5. 21. Cosine (a) and sine (b) terms of first harmonic of v_0, as a function of frequency, in beam with square cross section; ── stable solution, --- unstable solution, ● – symmetry-breaking bifurcation point.

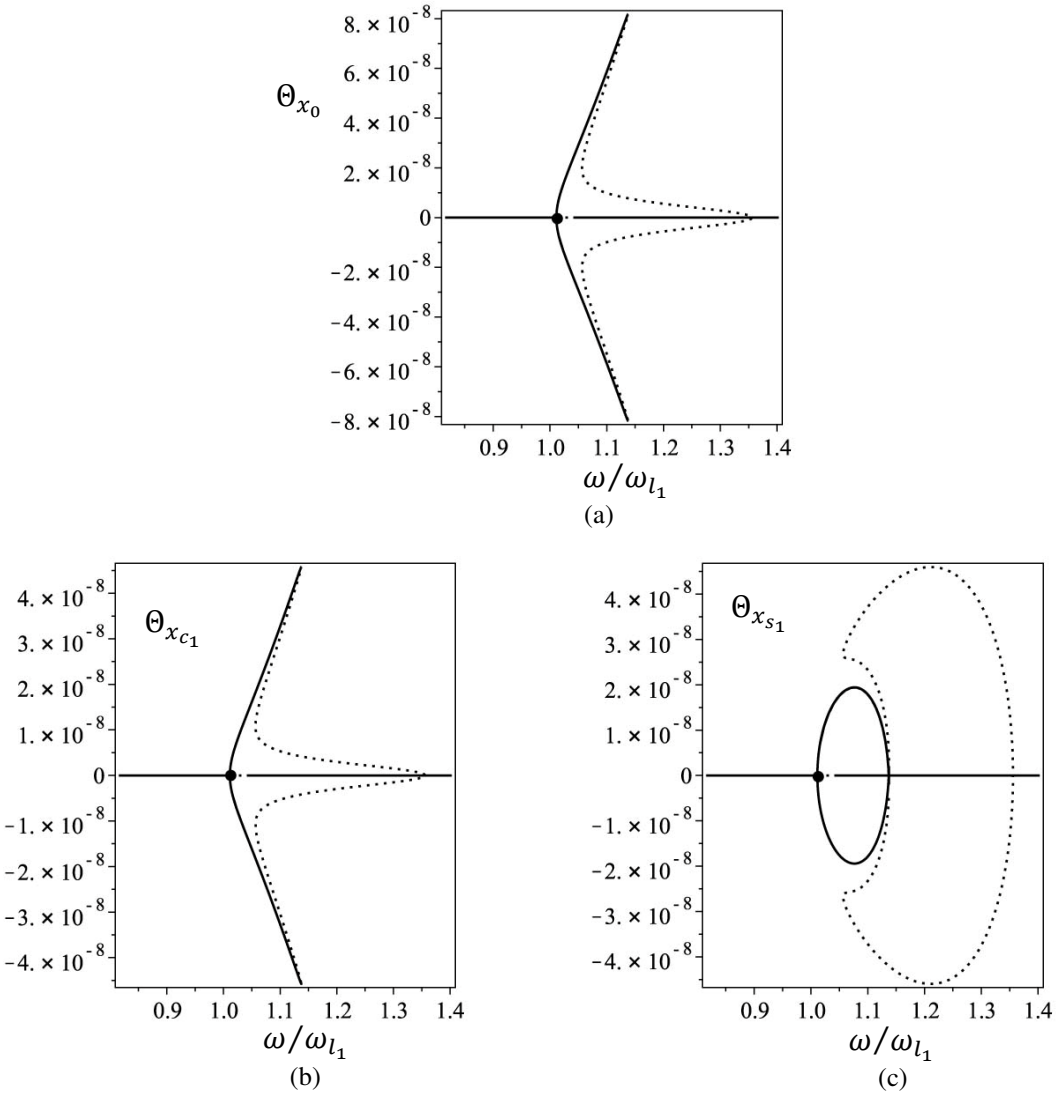

Figure 5. 22. Constant term (a), cosine (b) and sine (c) terms of first harmonic of θ_x, as a function of frequency, in beam with square cross section; ── stable solution, --- unstable solution, ● – symmetry-breaking bifurcation point.

Finally, the bifurcation diagrams and the stability of the solutions of the same problem, are compared and validated with AUTO [5. 13]. AUTO is a software for continuation and bifurcation problems in ordinary differential equations. In order to run the current model, written as system of ordinary differential equations of second order in (4. 19), the systems has to be written like an autonomous system of first order ordinary differential equations. First the system is transformed into a non-autonomous system of first order ordinary differential equations, increasing twice the degrees of freedom. Then, the resulting system is transformed into autonomous system of first order ordinary differential equations by adding two additional equations. These equations are result of adding a nonlinear oscillator with the required periodic force as one of its solution

components [5. 13]. The new unknown vector $\{\hat{q}\}$ contains the vector of generalized coordinates $\{q(t)\}$, its velocity $\{\dot{q}(t)\}$ and the solutions of the nonlinear oscillator, i.e. cosine and sine functions related with the required frequency of excitation.

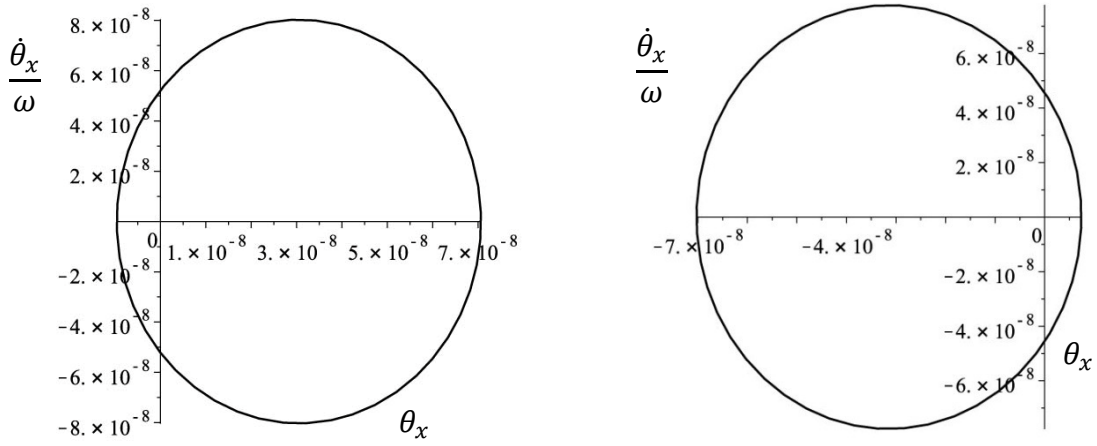

Figure 5. 23. Phase plots of torsion θ_x at $\omega/\omega_{l_1} = 1.1$ of (a) asymmetric stable branch with positive $\Theta_{x_{c_1}}$; (b) asymmetric stable branch with negative $\Theta_{x_{c_1}}$.

The results obtained by AUTO are presented in Figure 5. 24. Figure 5. 24 (a) presents the maximum value of w_0 versus the non-dimensional frequency of vibration. AUTO does not implement HBM for periodic solutions, thus the harmonics of the periodic solution are not obtained directly as solution of the system. The results of Figure 5. 24 (a) are slightly higher than the ones of Figure 5. 20 because the latter figure plots only the first harmonic while the former figure plots the maximum value of w_0. Figure 5. 24 (b) presents the maximum value of v_0 versus the non-dimensional frequency of vibration. It is pointed out again that the stable branches which arise from the bifurcation point are two, but on Figure 5. 24 they coincide because the two branches have the same amplitudes and different phases. Figure 5. 24 (c) presents the norm of the unknown vector versus the non-dimensional frequency of vibration. It can be seen that for frequency values near $\omega/\omega_{l_1} \cong 1.1$, the norm of the vector increases. This is due to a super-harmonic resonance, i.e. the excitation frequency becomes one fifth of the third natural frequency, as found in free vibration analysis in sub-section 5. 3. 2. 1. This super-harmonic resonance was not found with the HBM in forced vibration because the fifth harmonic was not included in the Fourier series (4. 22).

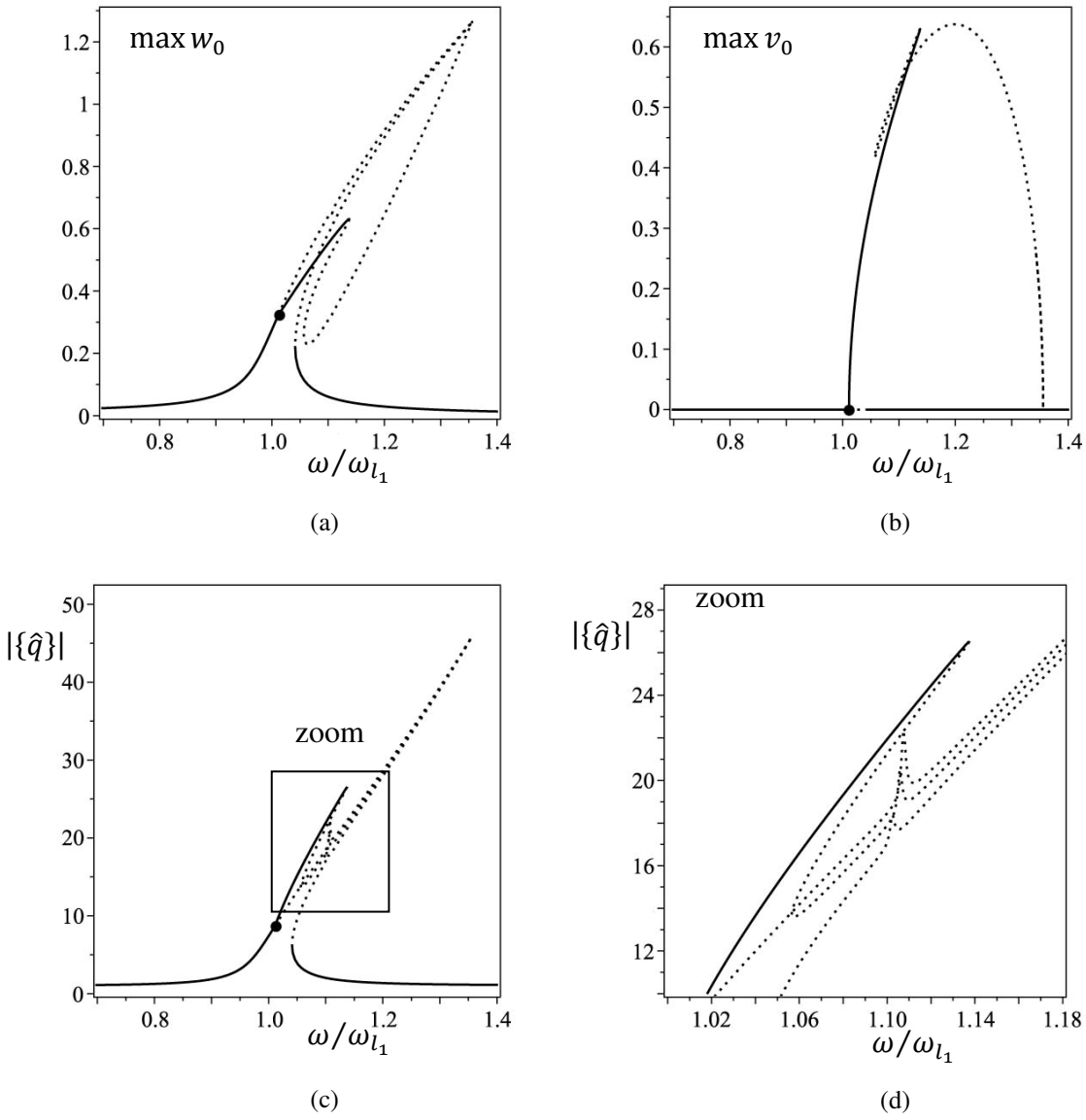

Figure 5. 24. Bifurcation diagrams obtained by AUTO. (a) max value of w_0, (b) max value of v_0, (c) norm of vector $\{\hat{q}\}$, (d) zoomed area of (c).

In the next example, the response curves of beams with different cross sections are compared. The material properties of this numerical study remain equal to the ones assumed in the previous test cases; the length, the width and the applied force are the ones of Figures 5. 16 - 5. 19, i.e., l = 0.58 m and b = 0.02 m. The amplitudes of three different beams with thicknesses h = 0.02 m, h = 0.015 m and h = 0.01 m, as function of the excitation frequency, are compared. Figure 5. 25 presents the first harmonics of the transverse displacements v_0 and w_0 of these three beams. The other harmonics are also excited, but their amplitudes are small and they are not presented here. Increasing the thickness of the beam, it becomes stiffer and vibrates with smaller amplitude. Moreover, the plane of vibration also changes under thickness changes. For the beam with thickness

h = 0.02 m, i.e. square cross section, the linear natural frequencies of bending in both transverse planes are equal and the plane of vibration - a plane inclined with respect to plane *xz* - does not change with the excitation frequency. Hence, increasing the excitation frequency, the amplitude of vibration increases until the turning point and decreases after, with a jump phenomenon, but the plane of vibration remains always the same. The opposite can be noticed in the other beams, particularly in the thinnest. The latter beam, where h = 0.002 m, mainly vibrates on plane *xz* for a wide range of frequencies, specifically till $\omega/\omega_{l_1} = 1.74$. Then, due to a jump phenomenon, the vibration amplitude decreases significantly. Continuing increasing the frequency, the amplitude of vibration increases but now it is mainly in plane *xy*. The torsional response of the beam with square cross section is symmetric, i.e. only the first and the third harmonics are excited. The constant term and the second harmonic of the transverse displacements v_0 and w_0 of the same beam are excited but with much smaller amplitude than in the beams with thinner thickness. Decreasing the thickness of the beam, the constant terms and the second harmonics become more important and the response is more markedly not symmetric. This is shown on Figure 5. 26 where phase plots for the three beams with different thicknesses are shown for points of the bifurcation diagrams where the transverse amplitudes v_0 are with similar amplitudes.

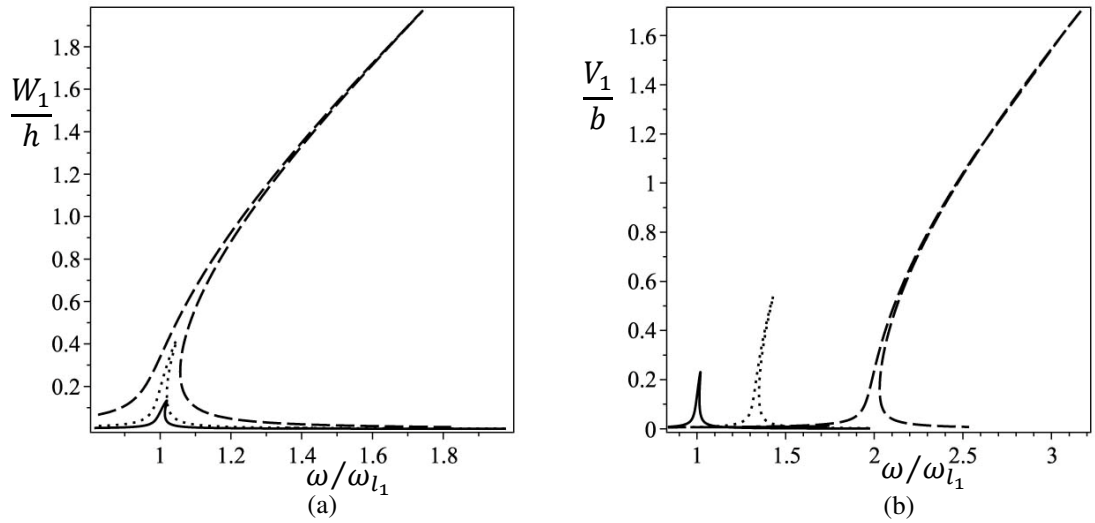

Figure 5. 25. (a) Frequency response curves of first harmonic of w_0 for force amplitude 50 N, ξ = 0; (b) Frequency response curves of first harmonic of v_0 for force amplitude 50 N, ξ = 0; Different cross sections: --- h = 0.01 m, b = 0.02 m, ··· h = 0.015 m, b = 0.02 m, —— h = 0.02 m, b = 0.02 m.

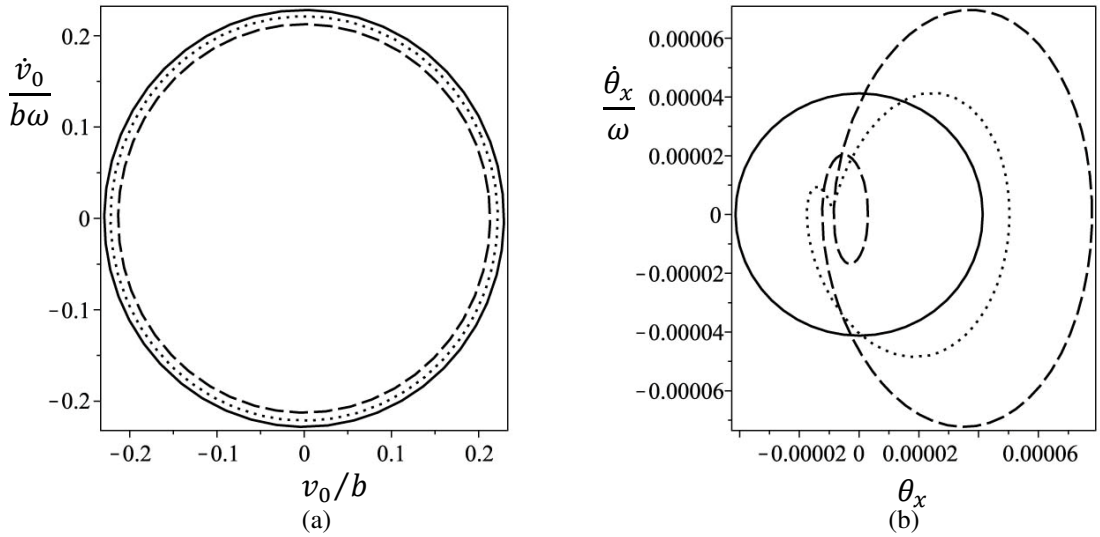

Figure 5. 26. Phase plots of (a) transverse displacement v_0; (b) torsion θ_x; --- h = 0.01 m, $\omega/\omega_{l_1} = 1.02$; ··· h = 0.015 m, $\omega/\omega_{l_1} = 1.34$; ── h=0.02 m, $\omega/\omega_{l_1} = 2.0$.

To finish the numerical tests, stability of the solutions is studied for the beam of the first example, presented in Figures 5. 16 – 5. 18, with the external force applied in the same direction, but with the amplitude increased to 100 N. The goal of this last test is to further demonstrate the efficiency of the procedure suggested in [5. 14] to improve the stability determination. Figure 5. 27 compares the maximum real part of all $2(2H+1)$N eigenvalues of problem (4. 52) with the maximum real part of the selected 2N eigenvalues that correspond to the most symmetric eigenvectors. The maximum eigenvalues are presented as functions of the excitation frequency. It can be seen from Figure 5. 27, that the unstable region starts earlier when all eigenvalues are considered for the stability determination. The response curves of the first harmonics of both transverse displacements v_0 and w_0 are presented on Figure 5. 28, with stability status defined using either all eigenvalues or the selected 2N eigenvalues. Two complex conjugate eigenvalues which satisfy (4. 56) appear as a solution of the eigenvalue problem (4. 52) for $\omega/\omega_{l_1} = 1.15$. This would correspond to a so called secondary Hopf or Neimark bifurcation [5. 11]. If stability is determined using a selection of 2N eigenvalues, the complex conjugate eigenvalues are not among the selected 2N eigenvalues and a Neimark bifurcation is not found. A pair of complex conjugate eigenvalues also appears as a solution of the eigenvalue problem at $\omega/\omega_{l_1} = 1.56$ when the transverse displacement v_0 is in resonance and these complex conjugate eigenvalues do not enter into the selected 2N eigenvalues. Furthermore, the solution that is supposed to be unstable due to the Neimark bifurcation determined by all eigenvalues can be

obtained as a periodic solution using Newmark's [5. 15] time domain integration method. This means that the solution is indeed stable. The numerical integration solution is also presented on Figure 5. 28. The numerical solution obtained by Newmark time integration method does not coincide with the HBM and continuation method data shown in this figure, because only the first harmonics of v_0 and w_0 from HBM are shown, whilst from Newmark's method the total displacement is shown. The latter includes the other harmonics.

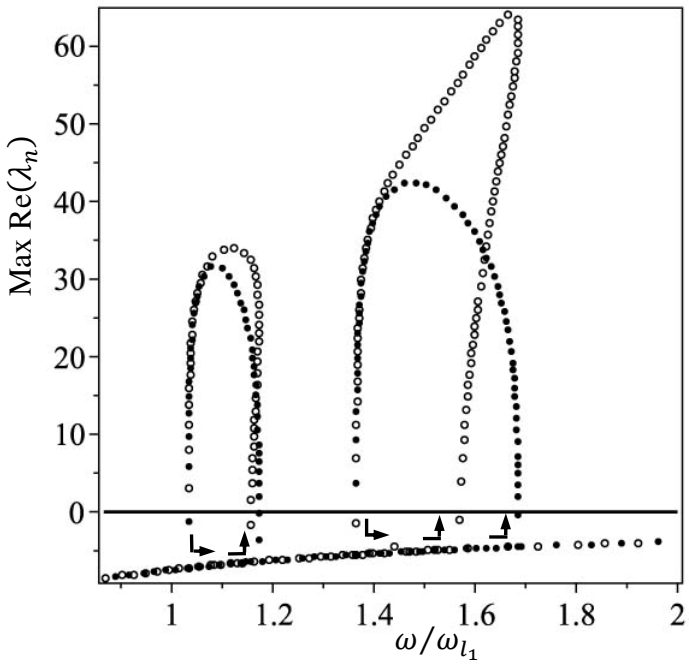

Figure 5. 27. Maximum real part of the eigenvalues as function of the excitation frequency; ○ – maximum eigenvalue among all 2(2H+1)N eigenvalues of the system (4. 52); ● – maximum eigenvalue among selected 2N eigenvalues which correspond to the most symmetric eigenvectors; ─ stability limit.

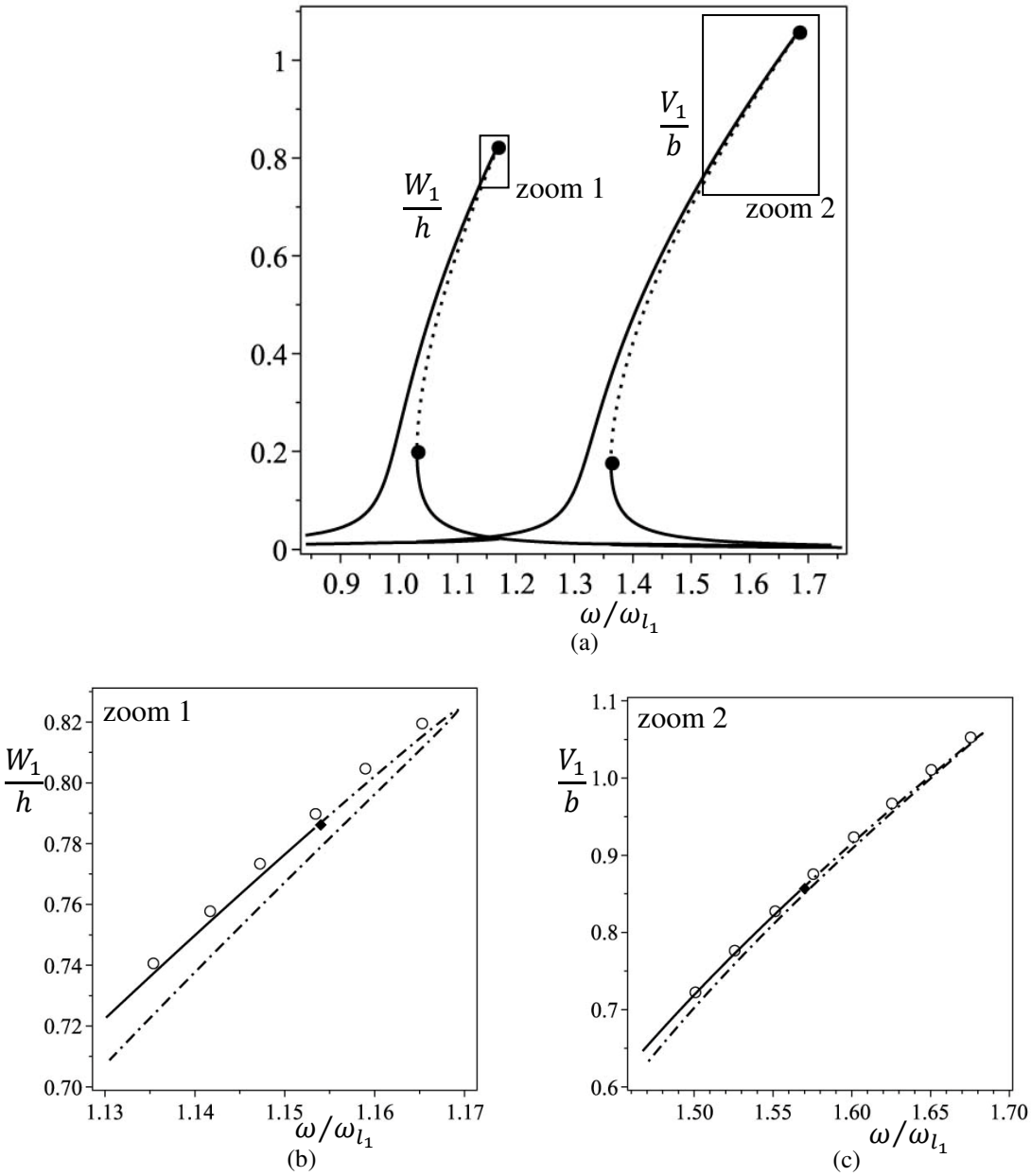

Figure 5. 28. Frequency response curves of first harmonics of w_0 and v_0 for force amplitude 100 N, $\xi = 0$. (a) first harmonics of w_0 and v_0, —— stable solution due to the selected 2N eigenvalues, ··· unstable solution due to the selected 2N eigenvalues, ● saddle node bifurcation due to the selected 2N eigenvalues; (b) zoomed area of the first harmonic of w_0, —— stable solution due to all eigenvalues, — · — · — unstable solution due to all eigenvalues, ♦ Neimark bifurcation found using all eigenvalues, ○ solution obtained by Newmark's time integration method; (c) zoomed area of the first harmonic of v_0, the same meaning of the symbols as in (b)

The method to determine the stability is an approximated method and therefore the stability results obtained by using all eigenvalues of (4. 52) might be not correct. The approximation consists in truncating what should be an infinite sum to a finite number of harmonics in equations (4. 22) and (4. 44). The procedure suggested in reference [5. 14], where only some of the eigenvalues λ_n are considered, appears to provide a way to correctly determine the Floquet exponents, here validated via numerical integration.

5. 5. Conclusion

Free and forced vibrations in a plane and in space of beams with rectangular cross sections were analysed. The model employed took into account geometrical nonlinearity, and is based on Timoshenko's theory for bending and Saint-Venant's for torsion, including a warping function. Periodic oscillations were of interest and the harmonic balance method was employed. Stability was investigated by Floquet's theory.

The evolution with the vibration amplitude of the first mode of free vibration in bending was investigated and several bifurcation points were presented. In what concerns planar vibrations, results previously published using Bernoulli-Euler models were replicated by the present Timoshenko based model. In addition, it was verified that the even harmonics can also be important when the nonlinearity is cubic. In fact, secondary branches were presented where all the harmonics, even and odd, were excited. This result should not really be considered as a surprise, since the appearance of even harmonics is due to symmetry breaking bifurcations. However, oscillations of this type have been very often overlooked in studies on vibrations of beams.

The more important study of this chapter regarded the non-planar oscillations. It was demonstrated that, due to the internal resonance between modes in different transverse planes, secondary branches exist and they relate the nonlinear mode of vibration in one plane to the vibration mode in another plane. In the secondary branch bending actually occurs in space and is coupled with torsion. In the main branches the vibrations are plane bending and longitudinal, without torsion. The longitudinal displacements are coupled with bending and torsion, due to the geometrical nonlinearity.

It was demonstrated in forced vibration analysis that due to variations in the excitation frequency, a beam with a cross section that is not square may vibrate in a variety of planes without changing the direction or the amplitude of the external force.

A beam with square cross section and force applied in one plane was also analysed. Due to 1:1 internal resonance between both transverse frequencies, a supercritical symmetry-breaking bifurcation occurs which leads to two stable asymmetric solutions in space and one unstable symmetric solution which remain in one plane. The finite number of harmonics used in the model can give an accurate solution, but originate an error in the stability study. A procedure to select the exponents appears to solve the later problem.

References

[5. 1] R. Lewandowski, Non-linear free vibration of beams by the finite element and continuation methods, *Journal of Sound and Vibration* 170 (1994) 539-593.

[5. 2] P. Ribeiro, M. Petyt, Non-linear vibration of beams with internal resonance by the hierarchical finite-element method, *Journal of Sound and Vibration* 224 (1999) 591-624.

[5. 3] P. Ribeiro, M. Petyt, Non-linear free vibration of isotropic plates with internal resonance, *International Journal of Non-Linear Mechanics* 35 (2000) 263-278.

[5. 4] M. Crisfield, A fast incremental/iterative solution procedure that handles "snap-through", *Computers & Structures* 13 (1981) 55-62.

[5. 5] E. Riks, An incremental approach to the solution of snapping and buckling problems, *International Journal of Solids and Structures* 15 (1979) 529-551.

[5. 6] R. Seydel, *Practical Bifurcation and Stability Analysis*, Springer-Verlag, New York, 1994.

[5. 7] A. Nayfeh, D. Mook, *Nonlinear Oscillations*, John Wiley & Sons, Inc., New York, 1995.

[5. 8] P. Ribeiro, Asymmetric solutions in large amplitude free periodic vibrations of plates, *Journal of Sound and Vibration* 322 (2009) 8-14.

[5. 9] H. Wolfe, *An Experimental Investigation of Nonlinear Behaviour of Beams and Plates Excited to High Levels of Dynamic Response*, PhD thesis, University of Southampton, 1995.

[5. 10] P. Ribeiro, Non-linear forced vibrations of thin/thick beams and plates by the finite element and shooting methods, *Computers & Structures* 82 (2004) 1413-1423.

[5. 11] A. Nayfeh, B. Balachandran, *Applied Nonlinear Dynamics: Analytical, Computational and Experimental Methods*, New York, 1995.

[5. 12] O. Thomas, A. Lazarus, C. Touzé, A harmonic-based method for computing the stability of periodic oscillations of non-linear structural systems, *Proceedings of the ASME 2010 International Design Engineering Technical Conferences & Computers and Information in Engineering Conference*, August 15-18, 2010, Montreal, Canada.

[5. 13] E. Doedel, *AUTO-07P: Continuation and Bifurcation Software for Ordinary Differential Equations*, Concordia University, Montreal, Canada, 2008.

[5. 14] A. Lazarus, O. Thomas, A harmonic-based method for computing the stability of periodic solutions of dynamical systems, *Comptes Rendus Mecanique* 338 (2010) 510–517.

[5. 15] K. Bathe, *Finite Element Procedures,* Prentice-Hall, New Jersey, 1996.

6

Equations of Motion of Beams with Non-symmetrical Cross Sections

6. 1. Introduction

In this chapter, a model of 3D beams with non-symmetrical cross sections and including geometrical type of nonlinearities is presented. The beam model is based on the assumptions made in Chapter 2. 2, i.e. it follows Timoshenko's theory for flexure and considers that the cross section rotates as a rigid body under bending, but may warp in the longitudinal direction, as in Saint-Venants's theory for torsion. Furthermore, the implementations given in Chapter 2. 2 and shown to be reasonable in Chapter 3, are also adopted here, i.e.: the trigonometric terms are linearized in the expressions of strains, the longitudinal strains of second order in Green's strain are neglected, the third-order terms in the direct strain are also neglected and the warping function is included. An analytical expression for the warping function is not available when the cross section is not symmetric, thus the warping function is calculated numerically by the boundary element method (BEM) [6. 1].

First, the equation of motion of 3D beams with non-symmetrical cross sections is derived. Due to non-symmetrical properties of the cross section, more terms appear in the equation of motion; some of these terms introduce bending-torsional coupling even in linear analysis. Then, the numerical method used to calculate the warping function is presented.

6. 2. Beam equations of motion in time domain

Beams with arbitrary cross sections, constant along the length, in elastic and isotropic materials are considered (Figure 6. 1). Let *u*, *v* and *w*, represent longitudinal, transverse along *y* and transverse along *z* displacement components with respect to the centre of twist of the cross section. The twist centre of the cross-section is the point which does not undergo any displacement during the rotation of the cross section [6. 1]. The displacements are functions of time and of the space coordinates, and are based on Timoshenko's theory for flexure [6. 2] and Saint-Venant's theory for torsion [6. 3]:

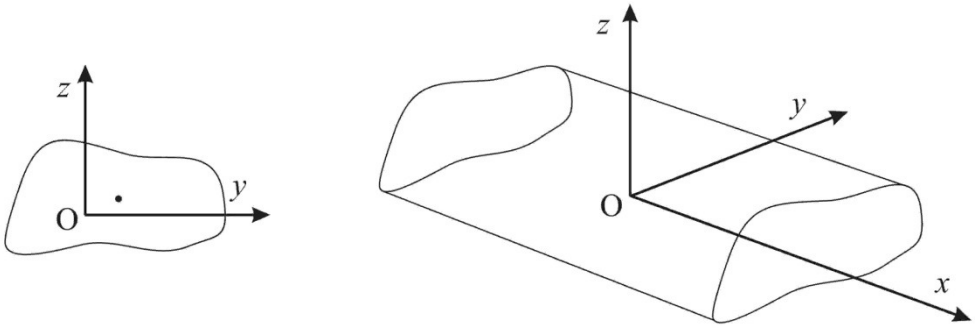

Figure 6. 1. Beam with arbitrary cross section. O - twist centre of intermediate cross section, ● - centroid.

$$u(x,y,z,t) = u_0(x,t) - (y-y_c)\,\phi_z(x,t) + (z-z_c)\,\phi_y(x,t) +$$
$$+\psi(y,z)\,\frac{\partial\theta_x}{\partial x}(x,t),$$
$$v(x,y,z,t) = v_0(x,t) + y\cos\big(\theta_x(x,t)\big) - y - z\sin\big(\theta_x(x,t)\big), \qquad (6.\ 1)$$
$$w(x,y,z,t) = w_0(x,t) + y\sin\big(\theta_x(x,t)\big) + z\cos\big(\theta_x(x,t)\big) - z,$$

where the subscript "0" represents axis *x* (axis where *y* = 0, *z* = 0; *x* contains the twist centres of the undeformed beam cross sections and will be often designated as reference line) and *t* represents time. u_0, v_0 and w_0 are, in this order, the displacements along *x*, *y* and *z* of points on the reference line; θ_x is the rotation of the cross section about the longitudinal axis *x* with respect to the twist centre; ϕ_y and ϕ_z denote rotations of the cross section due to bending with respect to its centroid, $\psi(y,z)$ is the warping function

defined with respect to the centre of twist and $(y_c,\ z_c)$ is the position of the centroid of the cross section.

One can note that the same displacement field as in equation (6. 1), but for Bernoulli-Euler beams, was used in several works, for example [6. 4]-[6. 5], but the centre of the cross section, point O, was placed at the shear centre. Even though the shear and twist centres locate different points on the cross section and generally are dependent on the longitudinal coordinate axis [6. 6]-[6. 8], under the assumptions considered in this work, i.e. that the cross section rotates as a rigid body and may deform only in longitudinal direction due to warping, the shear and the twist centres coincide [6. 8], [6. 9]. The rotation of the cross section about the longitudinal axis was expressed with respect to the unmovable point due to rotation in equation (2. 2), i.e. with respect to the twist centre. Thus, the centre of twist will be preferred in this work to locate the *x* axis.

The warping function must satisfy the following Laplace equation with Neumann boundary conditions [6. 10]:

$$\begin{aligned} &\nabla^2\psi = 0 \quad \text{in } \Omega, \\ &\frac{\partial\psi}{\partial n} = z\,n_y - y\,n_z \quad \text{on } \Gamma, \end{aligned} \tag{6. 2}$$

where Ω is the cross sectional area and Γ is the contour of the cross section. In this work, the warping function is obtained numerically using the boundary element method [6. 1]; details are given in the next section.

Geometrically nonlinear deformation is considered and the axial and shear strains are derived from Green's strain tensor. Considering the results obtained in Chapter 3 the longitudinal terms of second order are neglected (2. 6), linearization of the trigonometric terms is applied in the strain expressions and the third-order terms in the direct strain are neglected:

$$\varepsilon_x = \frac{\partial u}{\partial x} + \frac{1}{2}\left(\frac{\partial v}{\partial x}\right)^2 + \frac{1}{2}\left(\frac{\partial w}{\partial x}\right)^2 =$$

$$= \frac{\partial u_0}{\partial x} - (y - y_c)\frac{\partial \phi_z}{\partial x} + (z - z_c)\frac{\partial \phi_y}{\partial x} + \psi\frac{\partial^2 \theta_x}{\partial x^2} + \frac{1}{2}\left(\frac{\partial v_0}{\partial x}\right)^2 + \frac{1}{2}z^2\left(\frac{\partial \theta_x}{\partial x}\right)^2 + \tag{6. 3}$$

$$+ \frac{1}{2}\left(\frac{\partial w_0}{\partial x}\right)^2 + \frac{1}{2}y^2\left(\frac{\partial \theta_x}{\partial x}\right)^2 - z\frac{\partial v_0}{\partial x}\frac{\partial \theta_x}{\partial x} + y\frac{\partial w_0}{\partial x}\frac{\partial \theta_x}{\partial x},$$

$$\gamma_{zx} = \frac{\partial w}{\partial x} + \frac{\partial u}{\partial z} + \frac{\partial v}{\partial z}\frac{\partial v}{\partial x} + \frac{\partial w}{\partial z}\frac{\partial w}{\partial x} =$$

$$= \left(\frac{\partial \psi}{\partial z} + y\right)\frac{\partial \theta_x}{\partial x} + \sqrt{\lambda}\frac{\partial w_0}{\partial x} + \sqrt{\lambda}\phi_y - \sqrt{\lambda}\frac{\partial v_0}{\partial x}\theta_x, \tag{6. 4}$$

$$\gamma_{xy} = \frac{\partial u}{\partial y} + \frac{\partial v}{\partial x} + \frac{\partial v}{\partial x}\frac{\partial v}{\partial y} + \frac{\partial w}{\partial x}\frac{\partial w}{\partial y} =$$

$$= \left(\frac{\partial \psi}{\partial y} - z\right)\frac{\partial \theta_x}{\partial x} + \sqrt{\lambda}\frac{\partial v_0}{\partial x} - \sqrt{\lambda}\phi_z + \sqrt{\lambda}\frac{\partial w_0}{\partial x}\theta_x, \tag{6. 5}$$

where a square root of the shear correction factor is applied solely to the bending terms of the shear strains. In the case of non-symmetrical cross section, a shear correction factor equal to 5/6 is used.

The stresses are related with the strains by Hooke's law (2. 27). The strains, the stresses and the accelerations are functions of the displacement components *u*, *v* and *w* and their derivatives. These displacement components are functions of displacements on the reference line and rotations of the cross section, as defined in (6. 1). The latter displacements and cross sectional rotations are expressed by means of shape functions and generalised coordinates (2. 13) in local coordinate system. The shape functions used in this chapter are the ones defined in (2. 18) – (2. 20), plus additional shape functions, as Hermite cubics [6. 11], if beams with simply supported or free boundary conditions are investigated. The equation of motion is obtained by applying the principle of virtual work (2. 22) and has the form of (2. 29). In the following subsections, the mass and the stiffness matrices, which include more terms than before, due to the non-symmetrical cross section, are presented.

6. 2. 1. Stiffness matrix

The strains (6. 3) – (6. 5) may be divided in linear and nonlinear strains, as in Chapter 2. The stiffness matrix has the form of (2. 38), i.e. it has matrix of constant terms, which is called linear stiffness matrix and it has matrices that depend linearly and quadraticaly on the vector of generalised displacements, which are called nonlinear stiffness matrices.

6. 2. 1. 1. Linear stiffness matrix [K1]

The linear stiffness matrix [K1] is still defined by equation (2. 39), which involves the linear strains and their virtual variations. These strains and virtual strains are expressed by shape functions and generalized coordinated in a way similar to (2. 40) – (2. 45), but considering the linear strains from (6. 3) – (6. 5). Therefore, the linear stiffness matrix has the following form:

$$[\mathrm{K1}] = \begin{bmatrix} \mathbf{K1_{11}} & \mathbf{0} & \mathbf{0} & \mathbf{K1_{14}} & \mathbf{K1_{15}} & \mathbf{K1_{16}} \\ \mathbf{0} & \mathbf{K1_{22}} & \mathbf{0} & \mathbf{K1_{24}} & \mathbf{0} & \mathbf{K1_{26}} \\ \mathbf{0} & \mathbf{0} & \mathbf{K1_{33}} & \mathbf{K1_{34}} & \mathbf{K1_{35}} & \mathbf{0} \\ \mathbf{K1_{14}^{\mathrm{T}}} & \mathbf{K1_{24}^{\mathrm{T}}} & \mathbf{K1_{34}^{\mathrm{T}}} & \mathbf{K1_{44}} & \mathbf{K1_{45}} & \mathbf{K1_{46}} \\ \mathbf{K1_{15}^{\mathrm{T}}} & \mathbf{0} & \mathbf{K1_{35}^{\mathrm{T}}} & \mathbf{K1_{45}^{\mathrm{T}}} & \mathbf{K1_{55}} & \mathbf{K1_{56}} \\ \mathbf{K1_{16}^{\mathrm{T}}} & \mathbf{K1_{26}^{\mathrm{T}}} & \mathbf{0} & \mathbf{K1_{46}^{\mathrm{T}}} & \mathbf{K1_{56}^{\mathrm{T}}} & \mathbf{K1_{66}} \end{bmatrix}, \tag{6. 6}$$

where

$$\mathbf{K1_{11}} = E\int_V \frac{d\lfloor N^u \rfloor^{\mathrm{T}}}{dx}\frac{d\lfloor N^u \rfloor}{dx}dV, \tag{6. 7a}$$

$$\mathbf{K1_{14}} = E\int_V \psi\frac{d\lfloor N^u \rfloor^{T}}{dx}\frac{d^2\lfloor N^{\theta_x} \rfloor}{dx^2}dV, \tag{6. 7b}$$

$$\mathbf{K1_{15}} = E\int_V (z-z_c)\frac{d\lfloor N^u \rfloor^{T}}{dx}\frac{d\lfloor N^{\phi_y} \rfloor}{dx}dV, \tag{6. 7c}$$

$$\mathbf{K1_{16}} = -E\int_V (y-y_c)\frac{d\lfloor N^u \rfloor^{T}}{dx}\frac{d\lfloor N^{\phi_z} \rfloor}{dx}dV, \tag{6. 7d}$$

$$\mathbf{K1_{22}} = \lambda G\int_V \frac{d\lfloor N^v \rfloor^{\mathrm{T}}}{dx}\frac{d\lfloor N^v \rfloor}{dx}dV, \tag{6. 7e}$$

$$\mathbf{K1_{24}} = \sqrt{\lambda}\, G \int_V \left(\frac{\partial \psi}{\partial y} - z\right) \frac{d\lfloor N^v \rfloor^T}{dx} \frac{d\lfloor N^{\theta_x} \rfloor}{dx} dV, \tag{6. 7f}$$

$$\mathbf{K1_{26}} = -\lambda G \int_V \frac{d\lfloor N^v \rfloor^{\mathrm{T}}}{dx} \lfloor N^{\phi_z} \rfloor dV, \tag{6. 7g}$$

$$\mathbf{K1_{33}} = \lambda G \int_V \frac{d\lfloor N^w \rfloor^{\mathrm{T}}}{dx} \frac{d\lfloor N^w \rfloor}{dx} dV, \tag{6. 7h}$$

$$\mathbf{K1_{34}} = \sqrt{\lambda}\, G \int_V \left(\frac{\partial \psi}{\partial z} + y\right) \frac{d\lfloor N^w \rfloor^T}{dx} \frac{d\lfloor N^{\theta_x} \rfloor}{dx} dV, \tag{6. 7i}$$

$$\mathbf{K1_{35}} = \lambda G \int_V \frac{d\lfloor N^w \rfloor^{\mathrm{T}}}{dx} \lfloor N^{\phi_y} \rfloor dV, \tag{6. 7j}$$

$$\mathbf{K1_{44}} = \int_V \left(E\psi^2 \frac{d^2\lfloor N^{\theta_x} \rfloor^{\mathrm{T}}}{dx^2} \frac{d^2\lfloor N^{\theta_x} \rfloor}{dx^2} + G\left(\frac{\partial \psi}{\partial z} + y\right)^2 \frac{d\lfloor N^{\theta_x} \rfloor^{\mathrm{T}}}{dx} \frac{d\lfloor N^{\theta_x} \rfloor}{dx} + \right. \tag{6. 7k}$$

$$\left. + G\left(\frac{\partial \psi}{\partial y} - z\right)^2 \frac{d\lfloor N^{\theta_x} \rfloor^{\mathrm{T}}}{dx} \frac{d\lfloor N^{\theta_x} \rfloor}{dx} \right) dV,$$

$$\mathbf{K1_{45}} = E \int_V (z - z_c)\, \psi \frac{d^2\lfloor N^{\theta_x} \rfloor^T}{dx^2} \frac{d\lfloor N^{\phi_y} \rfloor}{dx} dV + \tag{6. 7l}$$

$$+ \sqrt{\lambda}\, G \int_V \left(\frac{\partial \psi}{\partial z} + y\right) \frac{d\lfloor N^{\theta_x} \rfloor^T}{dx} \lfloor N^{\phi_y} \rfloor dV,$$

$$\mathbf{K1_{46}} = -E \int_V (y - y_c)\, \psi \frac{d^2\lfloor N^{\theta_x} \rfloor^T}{dx^2} \frac{d\lfloor N^{\phi_z} \rfloor}{dx} dV - \tag{6. 7m}$$

$$- \sqrt{\lambda}\, G \int_V \left(\frac{\partial \psi}{\partial y} - z\right) \frac{d\lfloor N^{\theta_x} \rfloor^T}{dx} \lfloor N^{\phi_z} \rfloor dV,$$

$$\mathbf{K1_{55}} = \int_V \left((z - z_c)^2 E \frac{d\lfloor N^{\phi_y} \rfloor^T}{dx} \frac{d\lfloor N^{\phi_y} \rfloor}{dx} + \lambda G \lfloor N^{\phi_y} \rfloor^T \lfloor N^{\phi_y} \rfloor \right) dV, \tag{6. 7n}$$

$$\mathbf{K1_{56}} = -E \int_V (y - y_c)(z - z_c) \frac{d\lfloor N^{\phi_y} \rfloor^T}{dx} \frac{d\lfloor N^{\phi_z} \rfloor}{dx} dV, \tag{6. 7o}$$

$$\mathbf{K1_{66}} = \int_V \left((y - y_c)^2 E \frac{d\lfloor N^{\phi_z} \rfloor^T}{dx} \frac{d\lfloor N^{\phi_z} \rfloor}{dx} + \lambda G \lfloor N^{\phi_z} \rfloor^T \lfloor N^{\phi_z} \rfloor \right) dV. \tag{6. 7p}$$

The linear stiffness matrix for 3D beams with non-symmetrical cross section has more terms than the linear stiffness matrix for 3D beams with symmetrical cross section with respect to the *y* and *z* axes presented in (2. 46). The integrals over the cross section, which are zero in the presence of symmetry of the cross section with respect to *y* and *z*, are different from zero for non-symmetrical cross sections. These integrals introduce the bending-torsional coupling in linear problems.

6. 2. 1. 2. Nonlinear stiffness matrices [K2] and [K3]

Matrix [K2], which is linearly dependent on the vector of generalized displacements $\{q(t)\}$, results from the integral (2. 48), where the variations of the linear strains and the nonlinear strains are expressed by shape functions and generalized displacements in a similar way as (2. 43) – (2. 45) and (2. 49) – (2. 51) but considering the strains from (6. 3) – (6. 5). Matrix [K2] has the following form:

$$[\mathrm{K2}(\{q\})] = \begin{bmatrix} \mathbf{0} & \mathbf{K2_{12}} & \mathbf{K2_{13}} & \mathbf{K2_{14}} & \mathbf{0} & \mathbf{0} \\ \mathbf{0} & \mathbf{0} & \mathbf{K2_{23}} & \mathbf{K2_{24}} & \mathbf{0} & \mathbf{0} \\ \mathbf{0} & \mathbf{K2_{32}} & \mathbf{0} & \mathbf{K2_{34}} & \mathbf{0} & \mathbf{0} \\ \mathbf{0} & \mathbf{K2_{42}} & \mathbf{K2_{43}} & \mathbf{K2_{44}} & \mathbf{0} & \mathbf{0} \\ \mathbf{0} & \mathbf{K2_{52}} & \mathbf{K2_{53}} & \mathbf{K2_{54}} & \mathbf{0} & \mathbf{0} \\ \mathbf{0} & \mathbf{K2_{62}} & \mathbf{K2_{63}} & \mathbf{K2_{64}} & \mathbf{0} & \mathbf{0} \end{bmatrix}, \tag{6. 8}$$

where

$$\mathbf{K2_{12}}(\boldsymbol{q_v}, \boldsymbol{q_{\theta_x}}) = \frac{1}{2} E \int_V \frac{d\lfloor N^u \rfloor^{\mathrm{T}}}{dx} \frac{d\lfloor N^v \rfloor}{dx} \frac{\partial v_0}{\partial x} dV - \tag{6. 9a}$$

$$- \frac{1}{2} E \int_V z \frac{d\lfloor N^u \rfloor^{\mathrm{T}}}{dx} \frac{d\lfloor N^v \rfloor}{dx} \frac{\partial \theta_x}{\partial x} dV,$$

$$\mathbf{K2_{13}}(\boldsymbol{q_w}, \boldsymbol{q_{\theta_x}}) = \frac{1}{2} E \int_V \frac{d\lfloor N^u \rfloor^{\mathrm{T}}}{dx} \frac{d\lfloor N^w \rfloor}{dx} \frac{\partial w_0}{\partial x} dV + \tag{6. 9b}$$

$$+ \frac{1}{2} E \int_V y \frac{d\lfloor N^u \rfloor^{\mathrm{T}}}{dx} \frac{d\lfloor N^w \rfloor}{dx} \frac{\partial \theta_x}{\partial x} dV,$$

$$\mathbf{K2_{14}}(\boldsymbol{q_v}, \boldsymbol{q_w}, \boldsymbol{q_{\theta_x}}) = \frac{1}{2}E\int_V (y^2+z^2)\frac{d\lfloor N^u\rfloor^{\mathrm{T}}}{dx}\frac{d\lfloor N^{\theta_x}\rfloor}{dx}\frac{\partial\theta_x}{\partial x}dV -$$

$$-\frac{1}{2}E\int_V z\,\frac{d\lfloor N^u\rfloor^{\mathrm{T}}}{dx}\frac{d\lfloor N^{\theta_x}\rfloor}{dx}\frac{\partial v_0}{\partial x}dV + \frac{1}{2}E\int_V y\,\frac{d\lfloor N^u\rfloor^{\mathrm{T}}}{dx}\frac{d\lfloor N^{\theta_x}\rfloor}{dx}\frac{\partial w_0}{\partial x}dV, \tag{6. 9c}$$

$$\mathbf{K2_{23}}(\boldsymbol{q_{\theta_x}}) = \frac{1}{2}\lambda G\int_V \frac{d\lfloor N^v\rfloor^{\mathrm{T}}}{dx}\frac{d\lfloor N^w\rfloor}{dx}\theta_x\,dV, \tag{6. 9d}$$

$$\mathbf{K2_{24}}(\boldsymbol{q_w}) = \frac{1}{2}\lambda G\int_V \frac{d\lfloor N^v\rfloor^{\mathrm{T}}}{dx}\lfloor N^{\theta_x}\rfloor\frac{\partial w_0}{\partial x}dV, \tag{6. 9e}$$

$$\mathbf{K2_{32}}(\boldsymbol{q_{\theta_x}}) = -\frac{1}{2}\lambda G\int_V \frac{d\lfloor N^w\rfloor^{\mathrm{T}}}{dx}\frac{d\lfloor N^v\rfloor}{dx}\theta_x\,dV, \tag{6. 9f}$$

$$\mathbf{K2_{34}}(\boldsymbol{q_v}) = -\frac{1}{2}\lambda G\int_V \frac{d\lfloor N^w\rfloor^{\mathrm{T}}}{dx}\lfloor N^{\theta_x}\rfloor\frac{\partial v_0}{\partial x}dV, \tag{6. 9g}$$

$$\mathbf{K2_{42}}(\boldsymbol{q_v}, \boldsymbol{q_{\theta_x}}) = \frac{1}{2}E\int_V \psi\frac{d^2\lfloor N^{\theta_x}\rfloor^{\mathrm{T}}}{dx^2}\frac{d\lfloor N^v\rfloor}{dx}\frac{\partial v_0}{\partial x}dV -$$

$$-\frac{1}{2}E\int_V z\psi\frac{d^2\lfloor N^{\theta_x}\rfloor^{\mathrm{T}}}{dx^2}\frac{d\lfloor N^v\rfloor}{dx}\frac{\partial\theta_x}{\partial x}dV - \tag{6. 9h}$$

$$-\frac{1}{2}\sqrt{\lambda}G\int_V \left(\frac{\partial\psi}{\partial z}+y\right)\frac{d\lfloor N^{\theta_x}\rfloor^{\mathrm{T}}}{dx}\frac{d\lfloor N^v\rfloor}{dx}\theta_x dV,$$

$$\mathbf{K2_{43}}(\boldsymbol{q_w}, \boldsymbol{q_{\theta_x}}) = \frac{1}{2}E\int_V \psi\frac{d^2\lfloor N^{\theta_x}\rfloor^{\mathrm{T}}}{dx^2}\frac{d\lfloor N^w\rfloor}{dx}\frac{\partial w_0}{\partial x}dV +$$

$$+\frac{1}{2}E\int_V y\psi\frac{d^2\lfloor N^{\theta_x}\rfloor^{\mathrm{T}}}{dx^2}\frac{d\lfloor N^w\rfloor}{dx}\frac{\partial\theta_x}{\partial x}dV + \tag{6. 9i}$$

$$+\frac{1}{2}\sqrt{\lambda}G\int_V \left(\frac{\partial\psi}{\partial y}-z\right)\frac{d\lfloor N^{\theta_x}\rfloor^{\mathrm{T}}}{dx}\frac{d\lfloor N^w\rfloor}{dx}\theta_x dV,$$

$$\mathbf{K2_{44}}(\boldsymbol{q_v}, \boldsymbol{q_w}, \boldsymbol{q_{\theta_x}}) = \frac{1}{2}E\int_V (y^2+z^2)\psi \frac{d^2\lfloor N^{\theta_x}\rfloor^{\mathrm{T}}}{dx^2}\frac{d\lfloor N^{\theta_x}\rfloor}{dx}\frac{\partial\theta_x}{\partial x}dV -$$

$$-\frac{1}{2}E\int_V z\psi \frac{d^2\lfloor N^{\theta_x}\rfloor^{\mathrm{T}}}{dx^2}\frac{d\lfloor N^{\theta_x}\rfloor}{dx}\frac{\partial v_0}{\partial x}dV + \frac{1}{2}E\int_V y\psi \frac{d^2\lfloor N^{\theta_x}\rfloor^{\mathrm{T}}}{dx^2}\frac{d\lfloor N^{\theta_x}\rfloor}{dx}\frac{\partial w_0}{\partial x}dV -$$

$$-\frac{1}{2}\sqrt{\lambda}G\int_V \left(\frac{\partial\psi}{\partial z}+y\right)\frac{d\lfloor N^{\theta_x}\rfloor^{\mathrm{T}}}{dx}\lfloor N^{\theta_x}\rfloor\frac{\partial v_0}{\partial x}dV + \tag{6. 9j}$$

$$+\frac{1}{2}\sqrt{\lambda}G\int_V \left(\frac{\partial\psi}{\partial y}-z\right)\frac{d\lfloor N^{\theta_x}\rfloor^{\mathrm{T}}}{dx}\lfloor N^{\theta_x}\rfloor\frac{\partial w_0}{\partial x}dV,$$

$$\mathbf{K2_{52}}(\boldsymbol{q_v}, \boldsymbol{q_{\theta_x}}) = \frac{1}{2}E\int_V (z-z_c)\frac{d\lfloor N^{\phi_y}\rfloor^{\mathrm{T}}}{dx}\frac{d\lfloor N^{v}\rfloor}{dx}\frac{\partial v_0}{\partial x}dV - \tag{6. 9k}$$

$$-\frac{1}{2}E\int_V z(z-z_c)\frac{d\lfloor N^{\phi_y}\rfloor^{\mathrm{T}}}{dx}\frac{d\lfloor N^{v}\rfloor}{dx}\frac{\partial\theta_x}{\partial x}dV - \frac{1}{2}\lambda G\int_V \lfloor N^{\phi_y}\rfloor^{\mathrm{T}}\frac{d\lfloor N^{v}\rfloor}{dx}\theta_x\,dV,$$

$$\mathbf{K2_{53}}(\boldsymbol{q_w}, \boldsymbol{q_{\theta_x}}) = \frac{1}{2}E\int_V (z-z_c)\frac{d\lfloor N^{\phi_y}\rfloor^{\mathrm{T}}}{dx}\frac{d\lfloor N^{w}\rfloor}{dx}\frac{\partial w_0}{\partial x}dV + \tag{6. 9l}$$

$$+\frac{1}{2}E\int_V y(z-z_c)\frac{d\lfloor N^{\phi_y}\rfloor^{\mathrm{T}}}{dx}\frac{d\lfloor N^{w}\rfloor}{dx}\frac{\partial\theta_x}{\partial x}dV,$$

$$\mathbf{K2_{54}}(\boldsymbol{q_v}, \boldsymbol{q_w}, \boldsymbol{q_{\theta_x}}) = \frac{1}{2}E\int_V (z-z_c)(y^2+z^2)\frac{d\lfloor N^{\phi_y}\rfloor^{\mathrm{T}}}{dx}\frac{d\lfloor N^{\theta_x}\rfloor}{dx}\frac{\partial\theta_x}{\partial x}dV -$$

$$-\frac{1}{2}E\int_V z(z-z_c)\frac{d\lfloor N^{\phi_y}\rfloor^{\mathrm{T}}}{dx}\frac{d\lfloor N^{\theta_x}\rfloor}{dx}\frac{\partial v_0}{\partial x}dV + \tag{6. 9m}$$

$$+\frac{1}{2}E\int_V y(z-z_c)\frac{d\lfloor N^{\phi_y}\rfloor^{\mathrm{T}}}{dx}\frac{d\lfloor N^{\theta_x}\rfloor}{dx}\frac{\partial w_0}{\partial x}dV - \frac{1}{2}\lambda G\int_V \lfloor N^{\phi_y}\rfloor^{\mathrm{T}}\lfloor N^{\theta_x}\rfloor\frac{\partial v_0}{\partial x}dV,$$

$$\mathbf{K2_{62}}(\boldsymbol{q_v}, \boldsymbol{q_{\theta_x}}) = -\frac{1}{2}E\int_V (y-y_c)\frac{d\lfloor N^{\phi_z}\rfloor^{\mathrm{T}}}{dx}\frac{d\lfloor N^{v_0}\rfloor}{dx}\frac{\partial v_0}{\partial x}dV + \\ +\frac{1}{2}E\int_V (y-y_c)z\frac{d\lfloor N^{\phi_z}\rfloor^{\mathrm{T}}}{dx}\frac{d\lfloor N^{v_0}\rfloor}{dx}\frac{\partial \theta_x}{\partial x}dV, \tag{6. 9n}$$

$$\mathbf{K2_{63}}(\boldsymbol{q_w}, \boldsymbol{q_{\theta_x}}) = -\frac{1}{2}E\int_V (y-y_c)\frac{d\lfloor N^{\phi_z}\rfloor^{\mathrm{T}}}{dx}\frac{d\lfloor N^{w}\rfloor}{dx}\frac{\partial w_0}{\partial x}dV - \\ -\frac{1}{2}E\int_V y(y-y_c)\frac{d\lfloor N^{\phi_z}\rfloor^{\mathrm{T}}}{dx}\frac{d\lfloor N^{w}\rfloor}{dx}\frac{\partial \theta_x}{\partial x}dV - \frac{1}{2}\lambda G\int_V \lfloor N^{\phi_z}\rfloor^{\mathrm{T}}\frac{d\lfloor N^{w}\rfloor}{dx}\theta_x\, dV, \tag{6. 9o}$$

$$\mathbf{K2_{64}}(\boldsymbol{q_v}, \boldsymbol{q_w}, \boldsymbol{q_{\theta_x}}) = -\frac{1}{2}E\int_V (y-y_c)(y^2+z^2)\frac{d\lfloor N^{\phi_z}\rfloor^{\mathrm{T}}}{dx}\frac{d\lfloor N^{\theta_x}\rfloor}{dx}\frac{\partial \theta_x}{\partial x}dV + \\ +\frac{1}{2}E\int_V (y-y_c)z\frac{d\lfloor N^{\phi_z}\rfloor^{\mathrm{T}}}{dx}\frac{d\lfloor N^{\theta_x}\rfloor}{dx}\frac{\partial v_0}{\partial x}dV - \\ -\frac{1}{2}E\int_V y(y-y_c)\frac{d\lfloor N^{\phi_z}\rfloor^{\mathrm{T}}}{dx}\frac{d\lfloor N^{\theta_x}\rfloor}{dx}\frac{\partial w_0}{\partial x}dV - \frac{1}{2}\lambda G\int_V \lfloor N^{\phi_z}\rfloor^{\mathrm{T}}\lfloor N^{\theta_x}\rfloor\frac{\partial w_0}{\partial x}dV. \tag{6. 9p}$$

The nonlinear matrix [K3] is defined from the integral (2. 54), relation (2. 58) remains true and will be used.

6. 2. 1. 3. Nonlinear stiffness matrix [K4]

The nonlinear matrix [K4] is defined from integral (2. 61). Here again the nonlinear strains and their variations (the part of "virtual strains" that results from the nonlinear strains) are expressed by shape functions and generalized displacements as in Chapter 2 but considering the strains from equations (6. 3) – (6. 5). The nonlinear matrix [K4] has the following form:

$$[\mathrm{K}_4(\{q\})] = \begin{bmatrix} \mathbf{0} & \mathbf{0} & \mathbf{0} & \mathbf{0} & \mathbf{0} & \mathbf{0} \\ \mathbf{0} & \mathbf{K4_{22}} & \mathbf{0} & \mathbf{K4_{24}} & \mathbf{0} & \mathbf{0} \\ \mathbf{0} & \mathbf{0} & \mathbf{K4_{33}} & \mathbf{K4_{34}} & \mathbf{0} & \mathbf{0} \\ \mathbf{0} & \mathbf{K4_{24}}^{\mathbf{T}} & \mathbf{K4_{34}}^{\mathbf{T}} & \mathbf{K4_{44}} & \mathbf{0} & \mathbf{0} \\ \mathbf{0} & \mathbf{0} & \mathbf{0} & \mathbf{0} & \mathbf{0} & \mathbf{0} \\ \mathbf{0} & \mathbf{0} & \mathbf{0} & \mathbf{0} & \mathbf{0} & \mathbf{0} \end{bmatrix}, \tag{6. 10}$$

where

$$\begin{aligned} \mathbf{K4_{22}}(\boldsymbol{q_v}, \boldsymbol{q_w}, \boldsymbol{q_{\theta_x}}) &= \frac{1}{2}E\int_V \frac{d\lfloor N^v\rfloor^{\mathrm{T}}}{dx}\frac{d\lfloor N^v\rfloor}{dx}\left(\frac{\partial v_0}{\partial x}\right)^2 dV + \\ &+\frac{1}{2}E\int_V \frac{d\lfloor N^v\rfloor^{\mathrm{T}}}{dx}\frac{d\lfloor N^v\rfloor}{dx}\left(\frac{\partial w_0}{\partial x}\right)^2 dV + \\ &+\frac{1}{2}E\int_V (y^2+z^2)\frac{d\lfloor N^v\rfloor^{\mathrm{T}}}{dx}\frac{d\lfloor N^v\rfloor}{dx}\left(\frac{\partial \theta_x}{\partial x}\right)^2 dV - \\ &-E\int_V z\frac{d\lfloor N^v\rfloor^{\mathrm{T}}}{dx}\frac{d\lfloor N^v\rfloor}{dx}\frac{\partial v_0}{\partial x}\frac{\partial \theta_x}{\partial x}dV + E\int_L y\frac{d\lfloor N^v\rfloor^{\mathrm{T}}}{dx}\frac{d\lfloor N^v\rfloor}{dx}\frac{\partial w_0}{\partial x}\frac{\partial \theta_x}{\partial x}dV, \end{aligned} \tag{6. 11a}$$

$$\begin{aligned} \mathbf{K4_{24}}(\boldsymbol{q_v}, \boldsymbol{q_w}, \boldsymbol{q_{\theta_x}}) &= E\int_V z^2\frac{d\lfloor N^v\rfloor^{\mathrm{T}}}{dx}\frac{d\lfloor N^{\theta_x}\rfloor}{dx}\frac{\partial v_0}{\partial x}\frac{\partial \theta_x}{\partial x}dV - \\ &-\frac{1}{2}E\int_V z\frac{d\lfloor N^v\rfloor^{\mathrm{T}}}{dx}\frac{d\lfloor N^{\theta_x}\rfloor}{dx}\left(\frac{\partial v_0}{\partial x}\right)^2 dV - \frac{1}{2}E\int_V z\frac{d\lfloor N^v\rfloor^{\mathrm{T}}}{dx}\frac{d\lfloor N^{\theta_x}\rfloor}{dx}\left(\frac{\partial w_0}{\partial x}\right)^2 dV - \\ &-\frac{1}{2}E\int_V z(y^2+z^2)\frac{d\lfloor N^v\rfloor^{\mathrm{T}}}{dx}\frac{d\lfloor N^{\theta_x}\rfloor}{dx}\left(\frac{\partial \theta_x}{\partial x}\right)^2 dV - \\ &-E\int_V yz\frac{d\lfloor N^v\rfloor^{\mathrm{T}}}{dx}\frac{d\lfloor N^{\theta_x}\rfloor}{dx}\frac{\partial w_0}{\partial x}\frac{\partial \theta_x}{\partial x}dV + \lambda G\int_V \frac{d\lfloor N^v\rfloor^{\mathrm{T}}}{dx}\lfloor N^{\theta_x}\rfloor\frac{\partial v_0}{\partial x}\theta_x\, dV, \end{aligned} \tag{6. 11b}$$

$$\mathbf{K4_{33}}(\boldsymbol{q_v}, \boldsymbol{q_w}, \boldsymbol{q_{\theta_x}}) = \frac{1}{2}E\int_V \frac{d\lfloor N^w\rfloor^{\mathrm{T}}}{dx}\frac{d\lfloor N^w\rfloor}{dx}\left(\frac{\partial v_0}{\partial x}\right)^2 dV +$$

$$+\frac{1}{2}E\int_V \frac{d\lfloor N^w\rfloor^{\mathrm{T}}}{dx}\frac{d\lfloor N^w\rfloor}{dx}\left(\frac{\partial w_0}{\partial x}\right)^2 dV +$$

$$+\frac{1}{2}E\int_V (y^2+z^2)\frac{d\lfloor N^w\rfloor^{\mathrm{T}}}{dx}\frac{d\lfloor N^w\rfloor}{dx}\left(\frac{\partial \theta_x}{\partial x}\right)^2 dV -$$

$$-E\int_V z\frac{d\lfloor N^w\rfloor^{\mathrm{T}}}{dx}\frac{d\lfloor N^w\rfloor}{dx}\frac{\partial v_0}{\partial x}\frac{\partial \theta_x}{\partial x}dV + E\int_V y\frac{d\lfloor N^w\rfloor^{\mathrm{T}}}{dx}\frac{d\lfloor N^w\rfloor}{dx}\frac{\partial w_0}{\partial x}\frac{\partial \theta_x}{\partial x}dV, \tag{6. 11c}$$

$$\mathbf{K4_{34}}(\boldsymbol{q_v}, \boldsymbol{q_w}, \boldsymbol{q_{\theta_x}}) = E\int_V y^2\frac{d\lfloor N^w\rfloor^{\mathrm{T}}}{dx}\frac{d\lfloor N^{\theta_x}\rfloor}{dx}\frac{\partial w_0}{\partial x}\frac{\partial \theta_x}{\partial x}dV +$$

$$+\frac{1}{2}E\int_V y\frac{d\lfloor N^w\rfloor^{\mathrm{T}}}{dx}\frac{d\lfloor N^{\theta_x}\rfloor}{dx}\left(\frac{\partial v_0}{\partial x}\right)^2 dV + \frac{1}{2}E\int_V y\frac{d\lfloor N^w\rfloor^{\mathrm{T}}}{dx}\frac{d\lfloor N^{\theta_x}\rfloor}{dx}\left(\frac{\partial w_0}{\partial x}\right)^2 dV$$

$$+\frac{1}{2}E\int_L y(y^2+z^2)\frac{d\lfloor N^w\rfloor^{\mathrm{T}}}{dx}\frac{d\lfloor N^{\theta_x}\rfloor}{dx}\left(\frac{\partial \theta_x}{\partial x}\right)^2 dV - \tag{6. 11d}$$

$$-E\int_V yz\frac{d\lfloor N^w\rfloor^{\mathrm{T}}}{dx}\frac{d\lfloor N^{\theta_x}\rfloor}{dx}\frac{\partial v_0}{\partial x}\frac{\partial \theta_x}{\partial x}dV + \lambda G\int_V \frac{d\lfloor N^w\rfloor^{\mathrm{T}}}{dx}\lfloor N^{\theta_x}\rfloor\frac{\partial w_0}{\partial x}\theta_x\, dV,$$

$$\mathbf{K4_{44}}(\boldsymbol{q_v}, \boldsymbol{q_w}, \boldsymbol{q_{\theta_x}}) = \frac{1}{2}E\int_V (y^2+z^2)^2\frac{d\lfloor N^{\theta_x}\rfloor^{\mathrm{T}}}{dx}\frac{d\lfloor N^{\theta_x}\rfloor}{dx}\left(\frac{\partial \theta_x}{\partial x}\right)^2 dV +$$

$$+\frac{1}{2}E\int_V (y^2+z^2)\frac{d\lfloor N^{\theta_x}\rfloor^{\mathrm{T}}}{dx}\frac{d\lfloor N^{\theta_x}\rfloor}{dx}\left(\frac{\partial v_0}{\partial x}\right)^2 dV +$$

$$+\frac{1}{2}E\int_V (y^2+z^2)\frac{d\lfloor N^{\theta_x}\rfloor^{\mathrm{T}}}{dx}\frac{d\lfloor N^{\theta_x}\rfloor}{dx}\left(\frac{\partial w_0}{\partial x}\right)^2 dV - \tag{6. 11e}$$

$$-E\int_L z(y^2+z^2)\frac{d\lfloor N^{\theta_x}\rfloor^{\mathrm{T}}}{dx}\frac{d\lfloor N^{\theta_x}\rfloor}{dx}\frac{\partial v_0}{\partial x}\frac{\partial \theta_x}{\partial x}dV +$$

$$+E\int_V y(y^2+z^2)\frac{d\lfloor N^{\theta_x}\rfloor^{\mathrm{T}}}{dx}\frac{d\lfloor N^{\theta_x}\rfloor}{dx}\frac{\partial w_0}{\partial x}\frac{\partial \theta_x}{\partial x}dV.$$

6. 2. 2. Mass matrix

The mass matrix is derived from integral (2. 64). The virtual displacements and the accelerations are derived from equation (6. 1). The mass matrix has the following form:

$$[\mathrm{M}] = \begin{bmatrix} \mathbf{M_{11}} & \mathbf{0} & \mathbf{0} & \mathbf{M_{14}} & \mathbf{M_{15}} & \mathbf{M_{16}} \\ \mathbf{0} & \mathbf{M_{22}} & \mathbf{0} & \mathbf{M_{24}} & \mathbf{0} & \mathbf{0} \\ \mathbf{0} & \mathbf{0} & \mathbf{M_{33}} & \mathbf{M_{34}} & \mathbf{0} & \mathbf{0} \\ \mathbf{M_{14}^{\mathrm{T}}} & \mathbf{M_{24}^{\mathrm{T}}} & \mathbf{M_{34}^{\mathrm{T}}} & \mathbf{M_{44}} & \mathbf{M_{45}} & \mathbf{M_{46}} \\ \mathbf{M_{15}^{\mathrm{T}}} & \mathbf{0} & \mathbf{0} & \mathbf{M_{45}^{\mathrm{T}}} & \mathbf{M_{55}} & \mathbf{M_{56}} \\ \mathbf{M_{16}^{\mathrm{T}}} & \mathbf{0} & \mathbf{0} & \mathbf{M_{46}^{\mathrm{T}}} & \mathbf{M_{56}^{\mathrm{T}}} & \mathbf{M_{66}} \end{bmatrix}, \tag{6. 12}$$

where

$$\mathbf{M_{11}} = \rho \int_V \lfloor N^u \rfloor^{\mathrm{T}} \lfloor N^u \rfloor dV, \tag{6. 13a}$$

$$\mathbf{M_{14}} = \rho \int_V \psi \lfloor N^u \rfloor^T \frac{d\left\lfloor N^{\theta_x} \right\rfloor}{dx} dV, \tag{6. 13b}$$

$$\mathbf{M_{15}} = \rho \int_V (z - z_c) \lfloor N^u \rfloor^T \left\lfloor N^{\phi_y} \right\rfloor dV, \tag{6. 13c}$$

$$\mathbf{M_{16}} = -\rho \int_V (y - y_c) \lfloor N^u \rfloor^T \left\lfloor N^{\phi_z} \right\rfloor dV, \tag{6. 13d}$$

$$\mathbf{M_{22}} = \rho \int_V \lfloor N^v \rfloor^{\mathrm{T}} \lfloor N^v \rfloor dV, \tag{6. 13e}$$

$$\mathbf{M_{24}} = -\rho \int_V z \lfloor N^v \rfloor^T \left\lfloor N^{\theta_x} \right\rfloor dV, \tag{6. 13f}$$

$$\mathbf{M_{33}} = \rho \int_V \lfloor N^w \rfloor^{\mathrm{T}} \lfloor N^w \rfloor dV, \tag{6. 13g}$$

$$\mathbf{M_{34}} = \rho \int_V y \lfloor N^w \rfloor^T \left\lfloor N^{\theta_x} \right\rfloor dV, \tag{6. 13h}$$

$$\mathbf{M_{44}} = \rho \int_V \left(\psi^2 \frac{d\left\lfloor N^{\theta_x} \right\rfloor^{\mathrm{T}}}{dx} \frac{d\left\lfloor N^{\theta_x} \right\rfloor}{dx} + (y^2 + z^2) \left\lfloor N^{\theta_x} \right\rfloor^{\mathrm{T}} \left\lfloor N^{\theta_x} \right\rfloor \right) dV, \tag{6. 13i}$$

$$\mathbf{M_{45}} = \rho \int_V (z - z_c)\, \psi\, \frac{d\left[N^{\theta_x}\right]^T}{dx} \left[N^{\phi_y}\right] dV, \tag{6. 13j}$$

$$\mathbf{M_{46}} = -\rho \int_V (y - y_c)\, \psi \frac{d\left[N^{\theta_x}\right]^T}{dx} \left[N^{\phi_z}\right] dV, \tag{6. 13k}$$

$$\mathbf{M_{55}} = \rho \int_V (z - z_c)^2 \left[N^{\phi_y}\right]^{\mathrm{T}} \left[N^{\phi_y}\right] dV, \tag{6. 13l}$$

$$\mathbf{M_{56}} = -\rho \int_V (y - y_c)(z - z_c) \left[N^{\phi_y}\right]^T \left[N^{\phi_z}\right] dV, \tag{6. 13m}$$

$$\mathbf{M_{66}} = \rho \int_V (y - y_c)^2 \left[N^{\phi_z}\right]^{\mathrm{T}} \left[N^{\phi_z}\right] dV. \tag{6. 13n}$$

It is recalled again that the integrals which define the mass and the stiffness matrices are separated into integration over the cross sectional area and integration over the length of the element. Due to the non-symmetrical cross section, integrals like $\int_\Omega y d\Omega$, $\int_\Omega z d\Omega$, $\int_\Omega yz d\Omega$ or $\int_\Omega (y - y_c)\, \psi d\Omega$ are not zero and are included in the presentation of the matrices. These integrals introduce bending-bending-torsional coupling in linear analysis.

6. 3. Numerical solution for the warping function

The warping function $\psi(y, z)$ must satisfy the Laplace equation with Neumann boundary conditions given in (6. 2). For simple cross sections, like elliptical, rectangular or triangular, the warping function can be determined analytically [6. 10]. However, for beams with complex cross section, the warping function, most often, has to be obtained numerically by solving equation (6. 2).

The function $\psi(y, z)$ is determined exactly apart from an arbitrary constant, i.e. $\psi(y, z) + c$ is also solution of (6. 2), where c is a constant. This constant c is obtained by defining a constraint of the displacement u at the twist centre, i.e. $u = 0$ at the twist centre.

Equation (6. 2) is solved numerically by the boundary element method [6. 1]. The boundary Γ of the cross section Ω is divided into a finite number of segments (boundary

elements), not necessarily equal. With this approach, two approximations are made, one is about the geometry of the boundary and the other is about the variation of the warping function along the element on the boundary. In this work constant boundary elements are used. The boundary is approximated by straight lines, and the quantity of the warping function is assumed to be constant along the straight line and equal to the value of the middle point on the line – Figure 6. 2. The lengths of the elements are not necessarily equal.

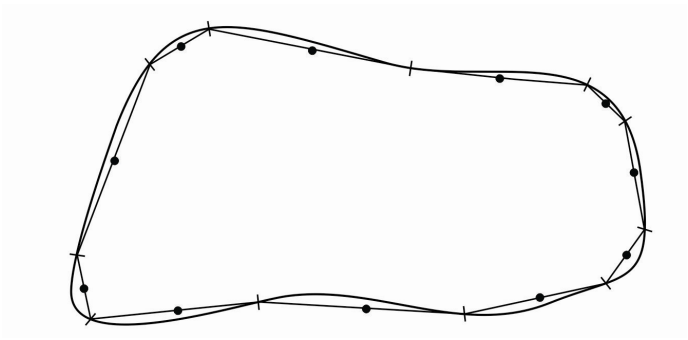

Figure 6. 2. Boundary element method with constant elements, ● – node.

Let's consider the equation:

$$\nabla^2 v(y,z) = \delta(y - y_0, z - z_0), \tag{6. 14}$$

where $\delta(y,z)$ denotes the Dirac delta function. For an arbitrary function $f(y,z)$, which is continuous in Ω and $(y_0, z_0) \in \Omega$, it follows that:

$$\int_{\Omega} \delta(y - y_0, z - z_0)\, f(y,z) d\Omega = f(y_0, z_0), \tag{6. 15}$$

A singular particular solution of (6. 14) is called fundamental solution. The fundamental solution has the form:

$$v(y,z) = \frac{1}{2\pi} \ln r, \tag{6. 16}$$

where

$$r = \sqrt{(y - y_0)^2 + (z - z_0)^2} \tag{6. 17}$$

is the distance between points (y_0, z_0) and (y,z). In fluid dynamics and aerodynamics, the fundamental solution is recognized as a velocity potential of a source located at (y_0, z_0) with unit strength.

The Green's second identity for functions $\psi(y,z)$ and $\upsilon(y,z)$, which are twice continuously differentiable in Ω and once on Γ is:

$$\int_{\Omega} (\upsilon \nabla^2\psi - \psi \nabla^2\upsilon)d\Omega = \int_{\Gamma} \left(\upsilon \frac{\partial\psi}{\partial n} - \psi \frac{\partial\upsilon}{\partial n}\right) d\Gamma. \tag{6. 18}$$

Considering equations (6. 2) and (6. 14), equation (6. 18) becomes:

$$-\int_{\Omega} \psi\, \delta(y-y_0, z-z_0)d\Omega = \int_{\Gamma} \left(\upsilon \frac{\partial\psi}{\partial n} - \psi \frac{\partial\upsilon}{\partial n}\right) d\Gamma. \tag{6. 19}$$

Taking into account (6. 15):

$$\psi(y_0,z_0) = -\int_{\Gamma} \left(\upsilon \frac{\partial\psi}{\partial n} - \psi \frac{\partial\upsilon}{\partial n}\right) d\Gamma, \qquad (y_0,z_0) \in \Omega. \tag{6. 20}$$

The function $\upsilon(y,z)$ is given in (6. 16) and $\frac{\partial\upsilon(y,z)}{\partial n}$ is [6. 11]:

$$\frac{\partial\upsilon(y,z)}{\partial n} = \frac{1}{2}\frac{\cos(\varphi)}{r}, \tag{6. 21}$$

where φ is the angle between vectors $\vec{r}$ and $\vec{n}$, $\vec{r} = \begin{Bmatrix} y-y_0 \\ z-z_0 \end{Bmatrix}$, $\vec{n}$ is the normal vector of the contour at point (y,z) and $\vec{r}$ is the vector between points (y_0,z_0) and (y,z) - Figure 6. 3.

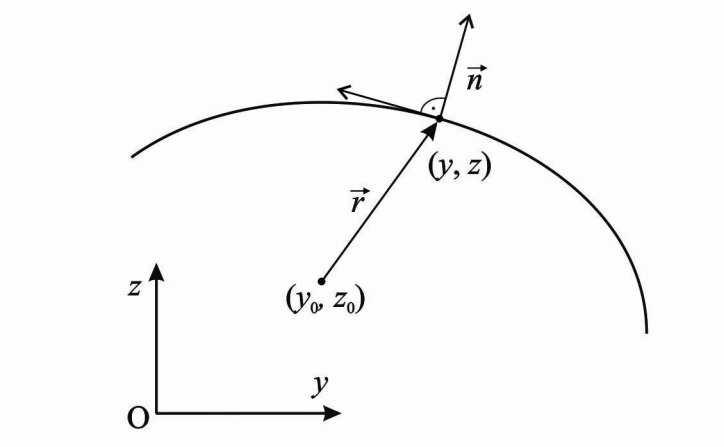

Figure 6. 3. Geometry of the cross section.

So the expression (6. 20) is the solution of (6. 2) at any point (y_0,z_0) inside the cross section Ω in terms of the boundary values of ψ and $\frac{\partial\psi}{\partial n}$. The boundary conditions of

equation (6. 2) specify only the values of $\frac{\partial \psi}{\partial n}$ on the boundary. Consequently, the solution of (6. 2) from the integral representation (6. 20) is still not determined.

It can be shown that for a point (y_0, z_0) on a smooth boundary Γ the following equation holds [6. 1]:

$$\frac{1}{2}\psi(y_0, z_0) = -\int_{\Gamma} \left(v\frac{\partial \psi}{\partial n} - \psi\frac{\partial v}{\partial n}\right) d\Gamma, \quad (y_0, z_0) \in \Gamma. \tag{6. 22}$$

Thus, taking into account that the values of $\frac{\partial \psi}{\partial n}$ are specified in the boundary condition of (6. 2), v is given at (6. 16) and $\frac{\partial v}{\partial n}$ is given at (6. 21), ψ can be obtained for each point on the boundary Γ from equation (6. 22). Then, from equation (6. 20), the value of ψ of each point inside the cross section Ω can be evaluated.

For that purpose, the boundary Γ is divided into *n* elements. Constant values are considered for the warping function ψ and its normal derivative $\frac{\partial \psi}{\partial n}$ along each element and equal to the value at the middle of the element. For a given point (y_i, z_i) located on the middle of the *i*-th element on the boundary Γ, equation (6. 22) becomes:

$$\frac{1}{2}\psi(y_i, z_i) = -\sum_{j=1}^{n}\int_{\Gamma_j} v^i\frac{\partial \psi}{\partial n} d\Gamma + \sum_{j=1}^{n}\int_{\Gamma_j} \psi\frac{\partial v^i}{\partial n} d\Gamma, \quad (y_i, z_i) \in \Gamma, \tag{6. 23}$$

where Γ_j is the boundary of the *j*-th element (straight line) and

$$v^i(y, z) = \frac{1}{2\pi}\ln\sqrt{(y - y_i)^2 + (z - z_i)^2}. \tag{6. 24}$$

is the fundamental solution of

$$\nabla^2 v^i(y, z) = \delta(y - y_i, z - z_i). \tag{6. 25}$$

Considering that ψ and $\frac{\partial \psi}{\partial n}$ are constant along each element, equation (6. 23) may be written as:

$$-\frac{1}{2}\psi^i + \sum_{j=1}^{n}\left(\int_{\Gamma_j}\frac{\partial v^i}{\partial n} ds\right)\psi^j = \sum_{j=1}^{n}\left(\int_{\Gamma_j} v^i ds\right)\psi_n^j, \tag{6. 26}$$

where $\psi^j = \psi(y_j, z_j)$ and $\psi_n^j = \frac{\partial \psi(y_j, z_j)}{\partial n}$.

Let's set:

$$\mathbf{\hat{H}_{ij}} = \int_{\Gamma_j} \frac{\partial v^i}{\partial n} ds \tag{6. 27}$$

$$\mathbf{H_{ij}} = \mathbf{\hat{H}_{ij}} - \frac{1}{2}\delta_{ij}, \tag{6. 28}$$

$$\mathbf{G_{ij}} = \int_{\Gamma_j} v^i ds, \tag{6. 29}$$

where δ_{ij} is the Kronecker delta. Then equation (6. 26) becomes:

$$[\mathrm{H}]\{\psi\} = [\mathrm{G}]\{\psi_n\}, \tag{6. 30}$$

where $\{\psi\}$ and $\{\psi_n\}$ are the vectors which contain the values of ψ and its normal derivative at points on the middle of the elements. The normal derivatives $\{\psi_n\}$ are defined in the boundary conditions, so equation (6. 30) approximates the values of ψ on the nodes of the boundary elements - $\{\psi\}$.

Once the values of ψ on the boundaries are known, its value at each point (y_i, z_i) inside the cross sectional area can be calculated by (6. 20). Equation (6. 20) may be written as:

$$\psi^i = \psi(y_i, z_i) = \sum_{j=1}^{n} \mathbf{\hat{H}_{ij}}\, \psi^j - \sum_{j=1}^{n} \mathbf{G_{ij}}\, \psi_n^j, \tag{6. 31}$$

where ψ_n^j are the values of the normal derivatives of ψ at the middle of each element defined from the boundary conditions, ψ^j are the values of ψ at the middle of each element obtained from (6. 30), $\mathbf{\hat{H}_{ij}}$ and $\mathbf{G_{ij}}$ are defined in (6. 27) and (6. 29) where the point (y_i, z_i) used for the definition of the fundamental solution is an inner point, not on the boundary. The coefficients of the matrices $[\hat{\mathrm{H}}]$ and $[\mathrm{G}]$, which represent integrals over a straight line, are calculated using four Gauss integration points [6. 12]. Equation (6. 31) is used to define the value of any internal point of the warping function by the values of the warping function and its normal derivative on the boundary.

6. 4. Determination of the twist centre

In this sub-section a numerical procedure for defining the centre of twist is presented. For that purpose, the displacement field (6. 1) is written with respect to an arbitrary point O and the twist centre is defined to occupy unknown position (y_0, z_0) with respect to point O. Taking into account only torsion and applying linear approximation of the trigonometric terms, equation (6. 1) becomes:

$$\begin{aligned} u(x,y,z,t) &= \psi(y,z)\,\frac{\partial \theta_x}{\partial x}(x,t), \\ v(x,y,z,t) &= -(z-z_0)\,\theta_x(x,t), \\ w(x,y,z,t) &= (y-y_0)\,\theta_x(x,t). \end{aligned} \tag{6. 32}$$

Calculating the strains and stresses from equation (6. 32), the equilibrium equations with the traction free boundary conditions on the surface of the beam define the following system for the warping function:

$$\begin{aligned} &\nabla^2\psi = 0 \quad \text{in } \Omega, \\ &\frac{\partial \psi}{\partial n} = (z-z_0)\,n_y - (y-y_0)n_z \quad \text{on } \Gamma. \end{aligned} \tag{6. 33}$$

The system (6. 33) can be written as:

$$\begin{aligned} &\nabla^2\psi^* = 0 \quad \text{in } \Omega, \\ &\frac{\partial \psi^*}{\partial n} = z\,n_y - y\,n_z \quad \text{on } \Gamma, \end{aligned} \tag{6. 34}$$

where

$$\psi^* = \psi + y\,z_0 - z\,y_0 + c, \tag{6. 35}$$

and *c* is a constant due to integration.

The position of the twist centre and the integration constant are obtained from the minimization of the strain energy produced by axial normal warping stresses [6. 1]:

$$\Pi(y_0, z_0, c) = \frac{1}{2} E \int_L \left(\frac{\partial \theta_x}{\partial x}\right)^2 dL \int_\Omega \psi^2 \, d\Omega = \tag{6. 36}$$

$$= \frac{1}{2} E \int_L \left(\frac{\partial \theta_x}{\partial x}\right)^2 dL \int_\Omega (\psi^* - y\, z_0 + z\, y_0 - c)^2 \, d\Omega.$$

The minimization conditions require:

$$\frac{\partial \Pi}{\partial y_0} = 0,$$

$$\frac{\partial \Pi}{\partial z_0} = 0, \tag{6. 37}$$

$$\frac{\partial \Pi}{\partial c} = 0.$$

Equations (6. 37) are differentiated and the following linear system for y_0, z_0 and c is obtained:

$$I_y\, y_0 - I_{yz}\, z_0 - S_y\, c = -I_1 \,,$$

$$I_{yz}\, y_0 - I_z\, z_0 - S_z\, c = -I_2 \,, \tag{6. 38}$$

$$S_y\, y_0 - S_z\, z_0 - A\, c = -I_3 \,,$$

where

$$I_y = \int_\Omega z^2 \, d\Omega, \tag{6. 39a}$$

$$I_z = \int_\Omega y^2 \, d\Omega, \tag{6. 39b}$$

$$I_{yz} = \int_\Omega yz \, d\Omega, \tag{6. 39c}$$

$$S_y = \int_\Omega z \, d\Omega, \tag{6. 39d}$$

$$S_z = \int_\Omega y \, d\Omega, \tag{6. 39e}$$

$$A = \int_\Omega d\Omega, \tag{6. 39f}$$

$$I_1 = \int_\Omega z\,\psi^*\,d\Omega, \tag{6. 39g}$$

$$I_2 = \int_\Omega y\,\psi^*\,d\Omega, \tag{6. 39h}$$

$$I_3 = \int_\Omega \psi^*\,d\Omega. \tag{6. 39i}$$

The solution of the linear system (6. 38) gives the position of the twist centre. The equation of motion is derived from the displacement fields (6. 1) with respect to the twist centre. Thus, first an additional procedure is required to obtain the position of the twist centre and then the equations of motion are derived and the warping function is calculated. The numerical solution of the warping function of the system (6. 2) is obtained up to a constant value, which is determined by the constraint condition that the warping function must be zero at the twist centre.

6. 5. Numerical calculation of the integrals over the cross sectional area which appear in the equation of motion

The mass and the stiffness matrices are defined in terms of integrals over the volume of the beam. The functions inside the integrals are products of shape functions and functions of space coordinates *y* and *z*. In the nonlinear stiffness matrices functions of time also appear. Thus, the integral may be divided into an integral over the length of the beam, which includes the shape functions, another integral over the cross section, which includes the functions of *y* and *z*, and the functions of time, which are the generalized coordinates and can be excluded from the integral. For example, the sub-matrix $\mathbf{M_{24}}$ of the mass matrix, defined in equation (6. 13f), can be written as:

$$\mathbf{M_{24}} = -\rho \int_V z \left[N^v\right]^T \left[N^{\theta_x}\right] dV = -\rho \int_L \left[N^v\right]^T \left[N^{\theta_x}\right] dL \int_\Omega z d\Omega, \tag{6. 40}$$

so the integrals over the length and over the cross section can be calculated separately. Sub-matrix $\mathbf{M_{24}}$ is zero in the case of beams with rectangular cross sections because the integral over the cross section vanishes. For beams with non-symmetrical cross sections, this integral is not zero and it introduces bending-torsional coupling. In some cases, as for example L shaped or I shaped beams, the integrals over the cross section which involve functions of *y* and *z*, but do not involve the warping function may be calculated

exactly. If the geometry of the cross section does not allow exact evaluation of the integral over the cross section, Gauss points may be used to evaluate the integral numerically [6. 12].

The integrals which involve the warping function are obtained numerically by Gauss integration. Equation (6. 31) is used to calculate the warping function at the integration points. Beams with L shaped cross sections are investigated, in this case the cross section can be divided into small squares, nine Gauss points are used for each square which give error of $O(h^6)$, where h is the length of the square [6. 1].

The values of the derivatives of the warping function with respect to y and z are also necessary for some of the integrals like (6. 7f) and (6. 7i). These derivatives are calculated by the central difference formula:

$$\frac{\partial\psi(y,z)}{\partial y} \cong \frac{\psi(y+h,z)-\psi(y-h,z)}{2h},$$
$$\frac{\partial\psi(y,z)}{\partial z} \cong \frac{\psi(y,z+h)-\psi(y,z-h)}{2h}, \tag{6. 41}$$

where a small h is used , for example $h = 10^{-6}$.

The coordinates of the centroid (y_c, z_c) are defined from:

$$y_c = \frac{\int_\Omega y d\Omega}{\Omega}, \tag{6. 42}$$

$$z_c = \frac{\int_\Omega z d\Omega}{\Omega}. \tag{6. 43}$$

Thus, from equations (6. 42) and (6. 43) it follows that:

$$\int_\Omega (y - y_c) d\Omega = \Omega(y_c - y_c) = 0, \tag{6. 44}$$

$$\int_\Omega (z - z_c) d\Omega = \Omega(z_c - z_c) = 0. \tag{6. 45}$$

Since the warping function is derived with respect to the twist centre and it is zero at that point, i.e. $y_0 = 0$, $z_0 = 0$ and $c = 0$, it follows from equations (6. 38), (6. 39g) – (6. 39i) that:

$$\int_\Omega \psi \, d\Omega = 0, \tag{6. 46}$$

$$\int_\Omega y \, \psi \, d\Omega = 0, \tag{6. 47}$$

$$\int_\Omega z \, \psi \, d\Omega = 0. \tag{6. 48}$$

Since these integrals are zero, the linear stiffness sub-matrices $\mathbf{K1_{14}}$, $\mathbf{K1_{15}}$ and $\mathbf{K1_{16}}$ and the mass sub-matrices $\mathbf{M_{14}}$, $\mathbf{M_{15}}$ and $\mathbf{M_{16}}$ vanish and there is no coupling between longitudinal displacement and the bending or torsional displacements in linear analysis. The coupling between both transverse and the torsional modes in the linear analysis remains.

6. 6. Conclusion

In this chapter, a model was presented for isotropic beams with arbitrary cross sections, vibrating in space. The displacement components were based on Timoshenko's theory for bending and Saint-Venant's for torsion, and the derivation of the equation of motion follows the lines of the derivation presented in Chapter 2. The warping function, which cannot be derived analytically for complex cross sections, is obtained numerically by solving the Laplace equation with Neumann boundary conditions, using the boundary element method. The integrals over the cross sectional area are obtained numerically by Gauss integration. The non-symmetrical cross section introduces more terms in the equation of motion and coupling between both transverse and the torsional displacements in linear analysis exists. Nevertheless, the longitudinal displacement does not couple with any other displacement in linear analysis. The non-symmetrical cross section introduces more terms in the nonlinear matrices but the nonlinearity remains quadratic and cubic. Pure bending modes do not exist anymore and the existence of quadratic nonlinear terms will cause presence of even harmonics and constant terms in any mode, unlike the case of planar bending of beams, where only the odd harmonics appear in the main branches.

References

[6. 1] J. T. Katsikadelis, *Boundary Elements. Theory and Applications*, Elsevier, Oxford, 2002.

[6. 2] C. Wang, J. Reddy, K. Lee, *Shear Deformable Beams and Plates*, Elsevier, Oxford, 2000.

[6. 3] G. Wempner, D. Talaslidis, *Mechanics of Solids and Shells. Theory and Application*, CRC Press LLC, Boca Raton, 2003.

[6. 4] F. Mohri, L . Azrar, M. Potier-Ferry, Lateral post-buckling analysis of thin-walled open section beams, *Thin-Walled Structures* 40 (2002) 1013–1036.

[6. 5] E. Sapountzakis, V.Tsipiras, Non-linear elastic non-uniform torsion of bars of arbitrary cross-section by BEM, *International Journal of Non-Linear Mechanics* 45 (2010) 63–74.

[6. 6] J. Kosmatka, General behavior and shear center location of prismatic anisotropic beams vie power series, *International Journal of Solids and Structures* 31 (1994) 417-439.

[6. 7] U. Andreaus, G. Ruta, A review of the problem of the shear centre(s), *Continuum Mechanics and Thermodynamics* 10 (1998) 369–380.

[6. 8] G. Romano, A. Barretta, R. Barretta, On Torsion and Shear of Saint-Venant Beams, *European Journal of Mechanics A/Solids* 35 (2012) 47-60.

[6. 9] E. Sapountzakis, V. Mokos, A BEM solution to transverse shear loading of beams, *Computational Mechanics* 36 (2005) 384–397 2005.

[6. 10] I. Sokolnikoff, *Mathematical Theory of Elasticity*, McGraw-Hill, 1956.

[6. 11] O. C. Zienkiewicz, R. L. Taylor, J. Z. Zhu, *The Finite Element Method: Its Basis and Fundamentals*, Sixth edition, Oxford, 2005.

[6. 12] M. Abramowitz, I. A. Stegun (Editors), *Handbook of Mathematical Functions With Formulas, Graphs, and Mathematical Tables*, National Bureau of Standards Applied Mathematics Series 55, 1972.

7

Free and Forced Vibration Analysis in the Frequency Domain of Beams with Non-symmetrical Cross Sections

7. 1. Introduction

In this chapter, nonlinear dynamics of 3D beams with non-symmetrical cross sections are investigated. An L shaped cross section is used as an example of non-symmetrical cross section. First, the twist centre is calculated and then the equation of motion with respect to the twist centre, as presented in Chapter 6, is developed. Linear natural frequencies and the corresponding modes of vibration are presented and compared with results computed using Ansys [7. 1]. Because the cross section is non-symmetric, the linear modes present coupling between transverse and torsional displacements. Free and forced vibrations in the frequency domain are studied by the HBM given in Chapter 4 and by a continuation method [7. 2], [7. 3]. Internal resonances are found and presented and the corresponding multi-modal responses are investigated. A stability study, using the method given in Chapter 4, is also presented.

7. 2. Validation of the twist centre

The twist centres of different L shaped cross sectional beams are calculated by the method presented in Chapter 6 and compared with the shear centre calculated by Ansys. As mentioned in Chapter 6, under the considerations of the beam model adopted here, the shear and the twist centres coincide [7. 4], [7. 5]. Furthermore, Ansys finds the shear centre as a property of the cross section and it is not dependent on the longitudinal coordinate axis. Thus, it is appropriate to compare the shear centre calculated by the

method presented in Chapter 6 with the shear centre calculated by Ansys. Initially, the centre of the coordinate system is chosen to be the left down corner of the L shaped cross section – Figure 7. 1. The twist and shear centres are calculated with respect to that point. The results are presented in Table 7. 1 and they are in very good agreement with the ones from Ansys for shear centre.

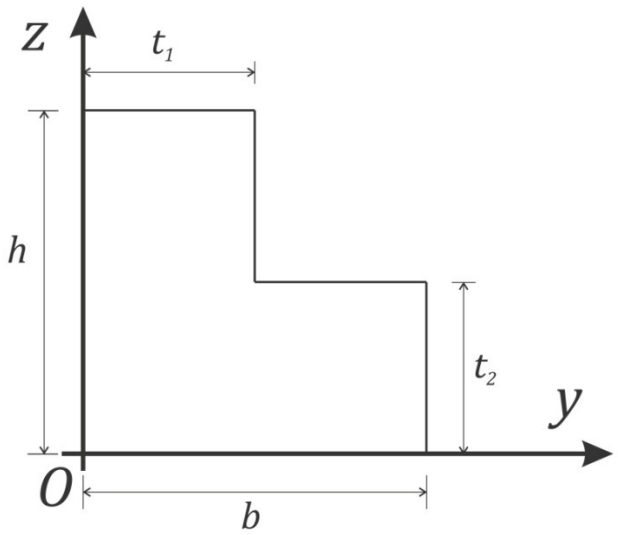

Fig. 7. 1. L shaped cross section.

Table 7. 1. Comparison of twist and shear centres obtained by current model and Ansys. The coordinates are with respect to point O from Figure 7. 1.

L shaped cross sectional dimensions (m)	Twist centre (current model)	Ansys shear centre
$h = 0.02$, $b = 0.02$, $t_1 = 0.01$, $t_2 = 0.01$	(0.006470, 0.006470)	(0.006477, 0.006477)
$h = 0.02$, $b = 0.02$, $t_1 = 0.005$, $t_2 = 0.005$	(0.002887, 0.002887)	(0.002891, 0.002891)
$h = 0.02$, $b = 0.02$, $t_1 = 0.002$, $t_2 = 0.002$	(0.001059, 0.001059)	(0.001061, 0.001061)

7. 3. Linear natural frequencies and mode shapes

In this sub-section, the linear modes of vibration of beams with L shaped cross sections are presented and the linear natural frequencies are compared with Ansys. It is remembered at the outset that the displacements on the transverse directions and torsion are coupled in linear analysis, due to the non-symmetrical cross section. Mathematically, this coupling comes from the structure of linear stiffness and mass matrices given in Chapter 6 – equations (6. 6) and (6. 12).

The linear eigenvalue problem, for L shaped cross sectional beam with dimensions of the cross section h = 0.02 m, b = 0.02 m, t_1 = 0.01 m and t_2 = 0.01 m, length l = 2.0 m and isotropic, homogeneous and elastic material as in previous chapters (aluminium), is solved and the natural frequencies are presented in Table 7. 2. The beam is considered to be clamped-clamped. As discussed in Chapter 6, there is no coupling between the longitudinal and the other displacement components, so the longitudinal displacement can be extracted from the eigenvalue problem, or if it is included, it does not influence the natural frequencies and the mode shapes of vibration. 7 shape functions are used for each displacement component. The linear natural frequencies are in very good agreement with the results obtained by Ansys.

Table 7. 2. Linear natural frequencies (rad/s) of L shaped cross sectional beam, h = 0.02 m, b = 0.02 m, t_1 = 0.01 m and t_2 = 0.01 m, l = 2.0 m.

Mode	Current model	Ansys BEAM189	Error %
1	123.7604	123.7478	0.010
2	181.0561	181.0166	0.022
3	341.0159	340.8992	0.034
4	498.5936	498.2298	0.073
5	668.0120	667.7301	0.042
6	975.4972	974.6398	0.088

The first linear mode, presents both transverse displacements v_0 and w_0 with equal amplitudes and shapes similar to the first mode of transverse vibrations of beams in one plane (that will be designated as 2D beams). Torsion does not appear in this linear mode. The second linear mode is similar to the first linear mode and the transverse displacements v_0 and w_0 have the same shapes, but opposite signs. Torsion appears in this mode and with a shape similar to the first torsional linear mode of a beam with symmetric cross section, i.e. a shape that occurs when the torsional mode is uncoupled from the transverse modes. The mode shapes of the first and second linear modes are presented in Figures 7. 2 and 7. 3.

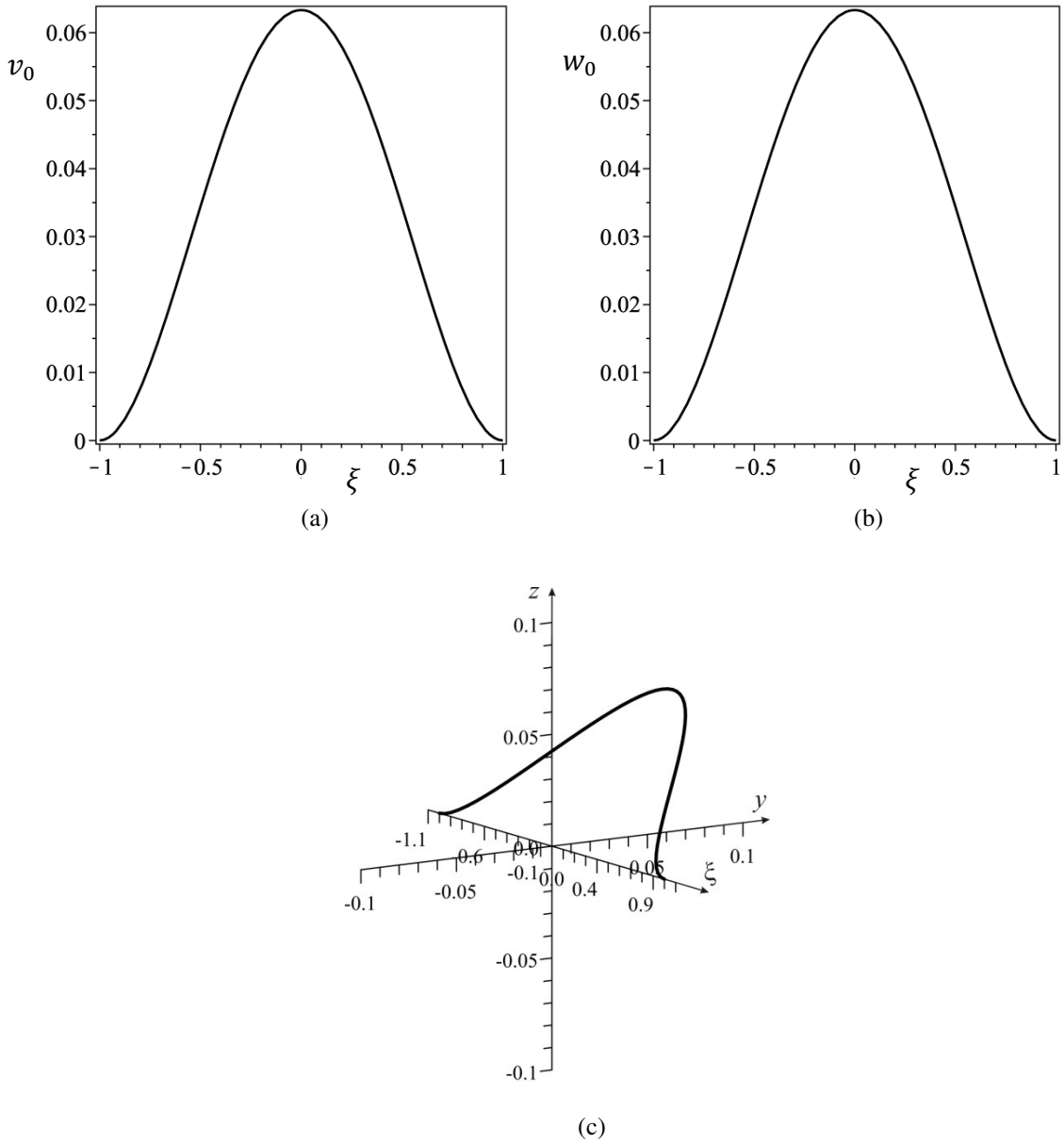

Figure 7. 2. First linear mode of L shaped cross sectional beam. (a) component of transverse displacement v_0, (b) component of transverse displacement w_0, (c) 3D plot.

The third and fourth linear modes, are similar to the second mode of 2D beams, i.e. the projections of the transverse displacements into planes O*xz* and O*xy* are similar to the second linear mode of 2D beams. In both cases, these projections have the same amplitude, but in the fourth linear mode they have opposite signs. There is no torsion in the third linear mode, while in the fourth liner mode there is torsion similar to the second linear torsional mode of a beam with symmetrical cross section. These modes are presented on Figures 7. 4 and 7. 5.

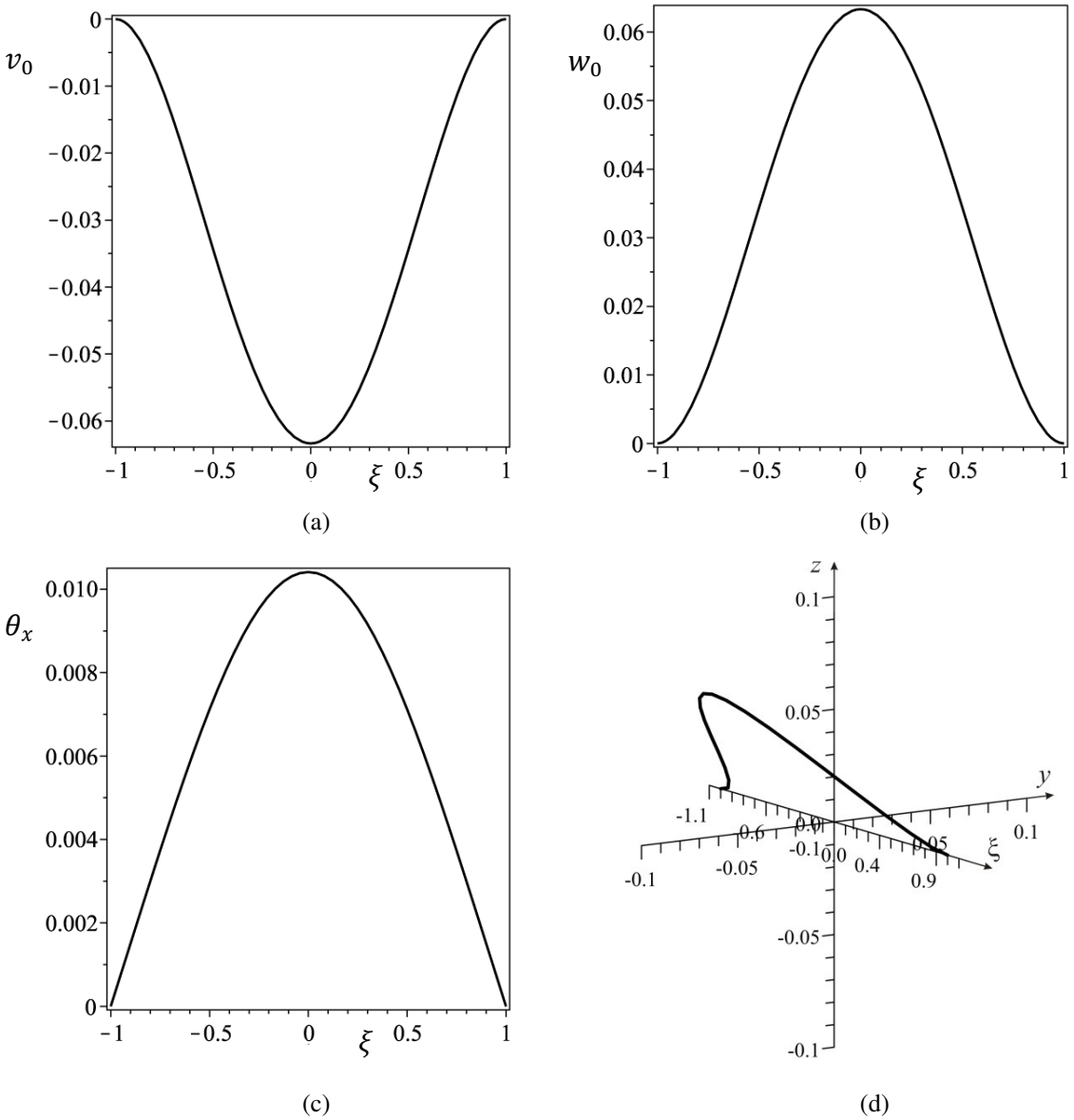

Figure 7. 3. Second linear mode of L shaped cross sectional beam. (a) component of transverse displacement v_0, (b) component of transverse displacement w_0, (c) Torsional component θ_x, (d) 3D plot.

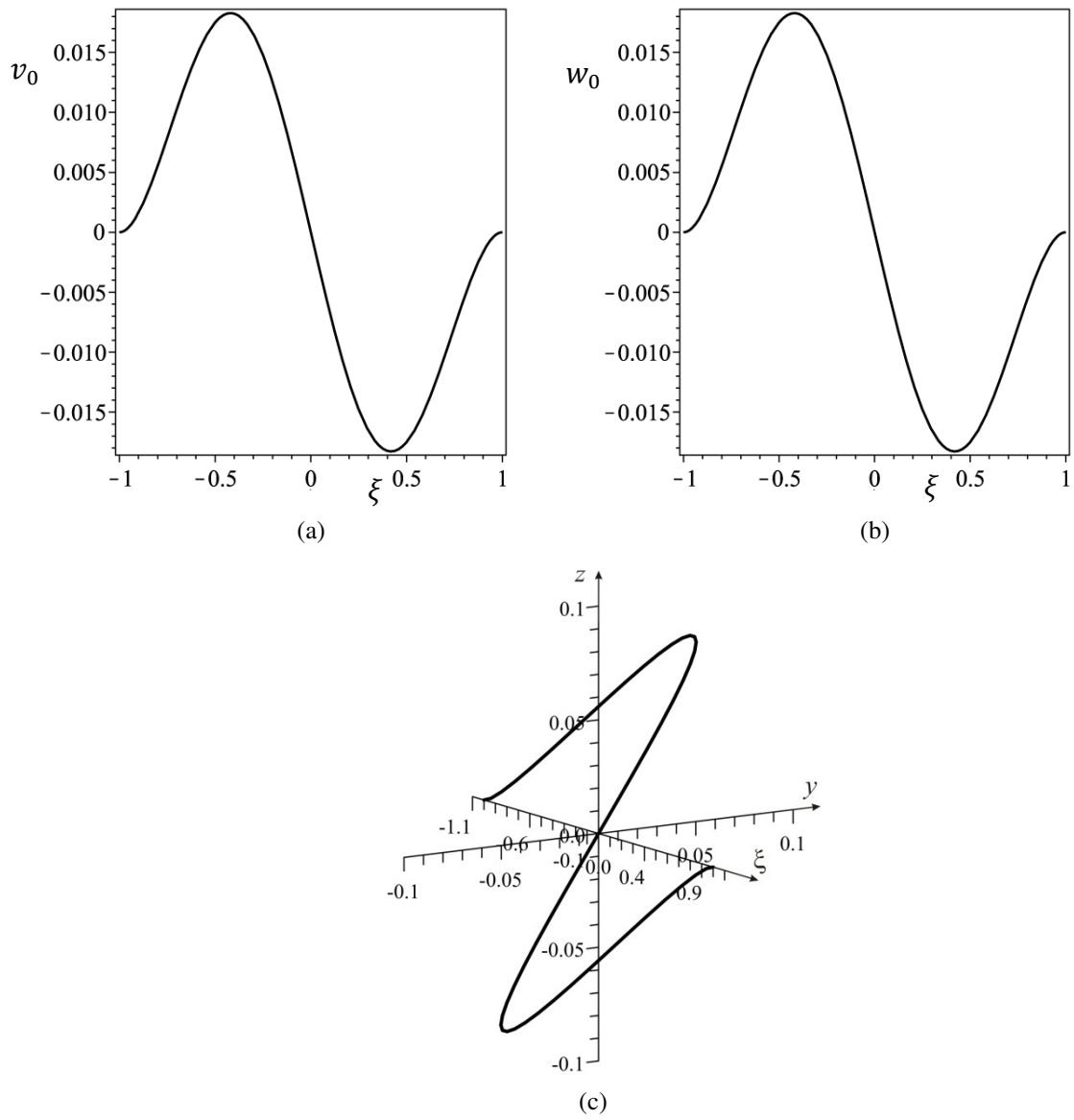

Figure 7. 4. Third linear mode of L shaped cross sectional beam. (a) component of transverse displacement v_0, (b) component of transverse displacement w_0, (c) 3D plot.

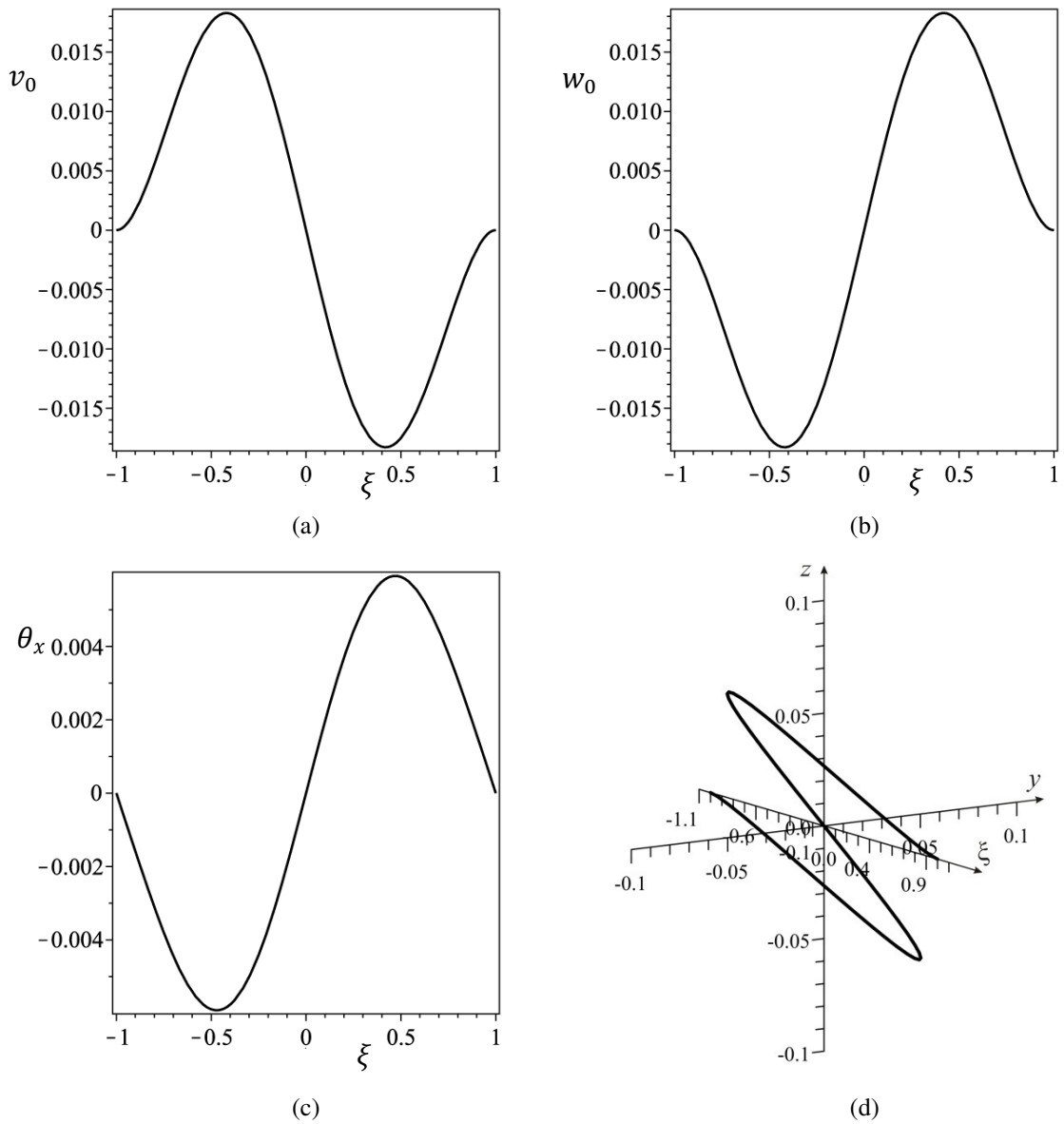

Figure 7. 5. Fourth linear mode of L shaped cross sectional beam. (a) component of transverse displacement v_0, (b) component of transverse displacement w_0, (c) Torsional component θ_x, (d) 3D plot.

7. 4. Free vibration analysis

In this sub-section the nonlinear free vibrations of first mode of a beam with L shaped cross section are investigated and presented. The beam is clamped-clamped, with length l = 2.0 m and dimensions of the cross section h = 0.02 m, b = 0.02 m, t_1 = 0.01 m and t_2 = 0.01 m. The material properties are the same as in the previous chapters, i.e. properties typical of aluminium. 10 shape functions for the longitudinal displacement and 7 shape functions for each of the other displacement components are used in the model. Harmonics up to third order are considered in the Fourier series, and only the cosine terms are used, because in free vibration, there is no damping and velocity related

with it. The continuation method is used to obtain the results in frequency domain [7. 2], [7. 3].

The first harmonic of the bifurcation diagram of the transverse displacement w_0, obtained from the first linear mode is presented on Figure 7. 6. Because both transverse displacements v_0 and w_0 are equally presented in the first linear mode, the bifurcation diagram of the first harmonic of the transverse displacement v_0 is exactly the same, thus it is not given here. Two bifurcation points are found for the frequency range studied. The first one occurs at $\omega/\omega_{l_1} \cong 1.44$ and it is due to a 1:3 internal resonance between the first and the fourth modes. The second bifurcation point occurs at $\omega/\omega_{l_1} \cong 1.68$ and it is due internal resonance which involves more than two harmonics, i.e. all the harmonics are excited in the secondary branch that starts from this bifurcation point. A similar bifurcation point was found for beams with symmetric cross sections, i.e. bifurcation point 5 from Figure 5. 3.

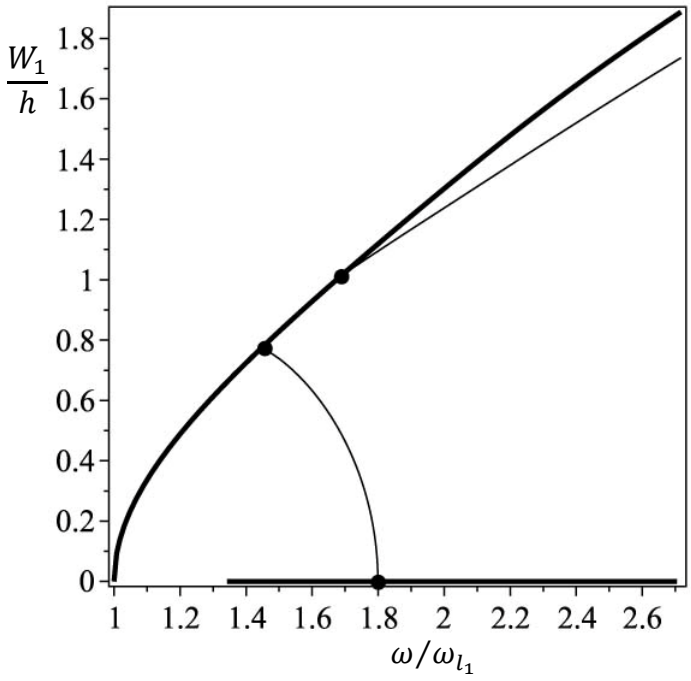

Figure 7. 6. Bifurcation diagram of first harmonic of transverse displacement w_0 of free vibration of L shaped cross sectional beam, started from the first linear mode, ▬ main branch, —— secondary branch, ● bifurcation point.

The mode shape of the first main branch remains similar to the first linear mode, i.e. the beam vibrates in space involving both transverse displacements with equal amplitudes, and with shapes similar to the first linear mode of a 2D beam. The third harmonic

appears in the response and it becomes more important for vibrations with larger amplitudes, as demonstrated in Chapter 5 and in [7. 6] for 2D beams.

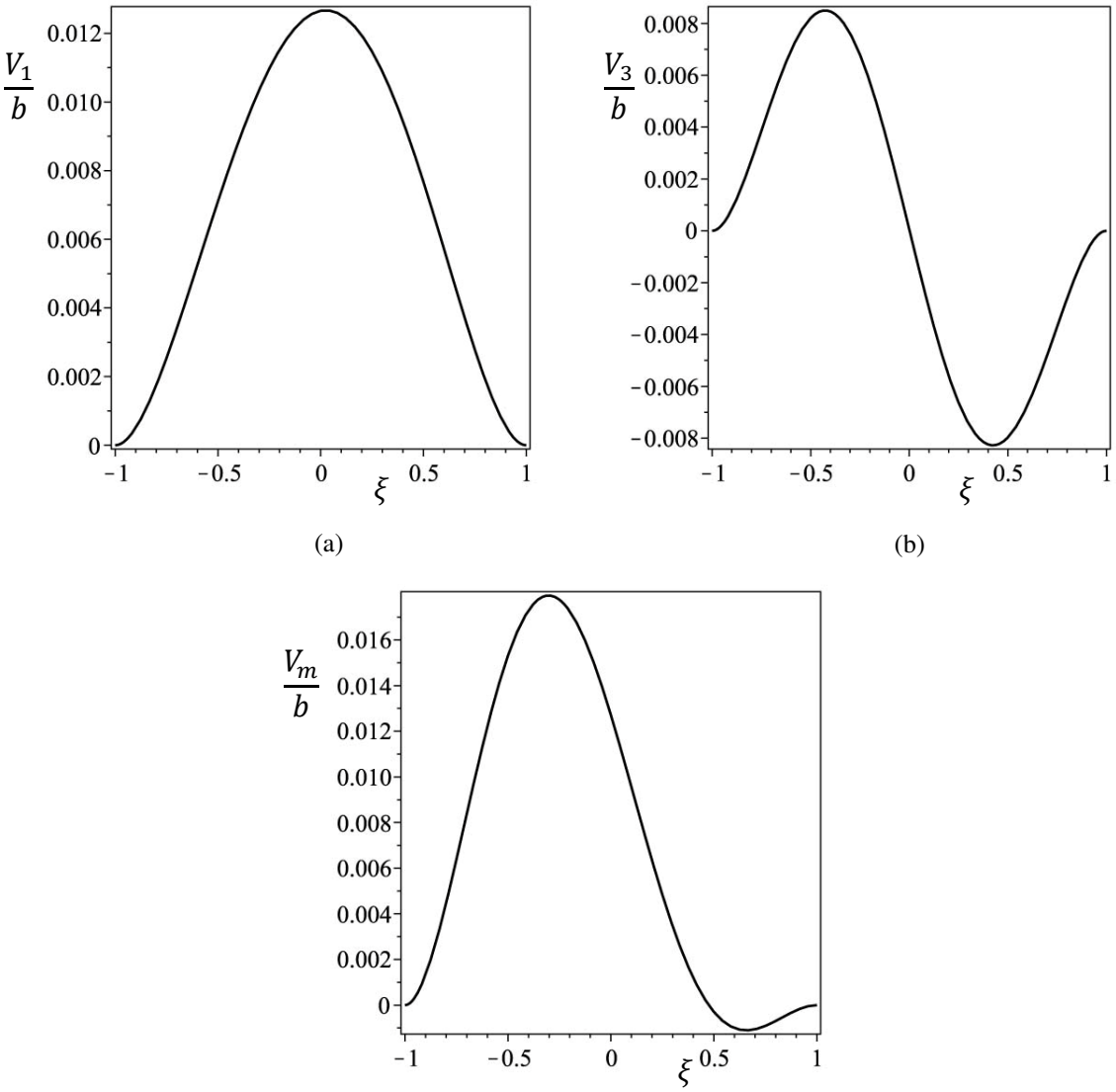

Figure 7. 7. Shapes of transverse displacement v_0 for point $\omega/\omega_{l_1} \cong 1.6$ from the first secondary branch. (a) first harmonic of v_0, (b) third harmonic of v_0, (c) total shape at $t = 0$ s.

It is important to note that unlike in beams with symmetric cross sections or 2D beams, the second harmonic and the constant terms are excited also in the first main branch, but with very small amplitudes. This excitation comes from the quadratic nonlinear terms in the equation of motion. In the case of a 3D beam with symmetric cross section, the quadratic nonlinear terms vanish, because they involve coupling between both transverse displacements or between transverse displacement and torsion, and in the main branch of 3D beams with symmetric cross sections only one transverse displacement is excited. In

the case of beams with non-symmetrical cross section, the displacement components are coupled in the linear analysis and they introduce quadratic nonlinearity in the system.

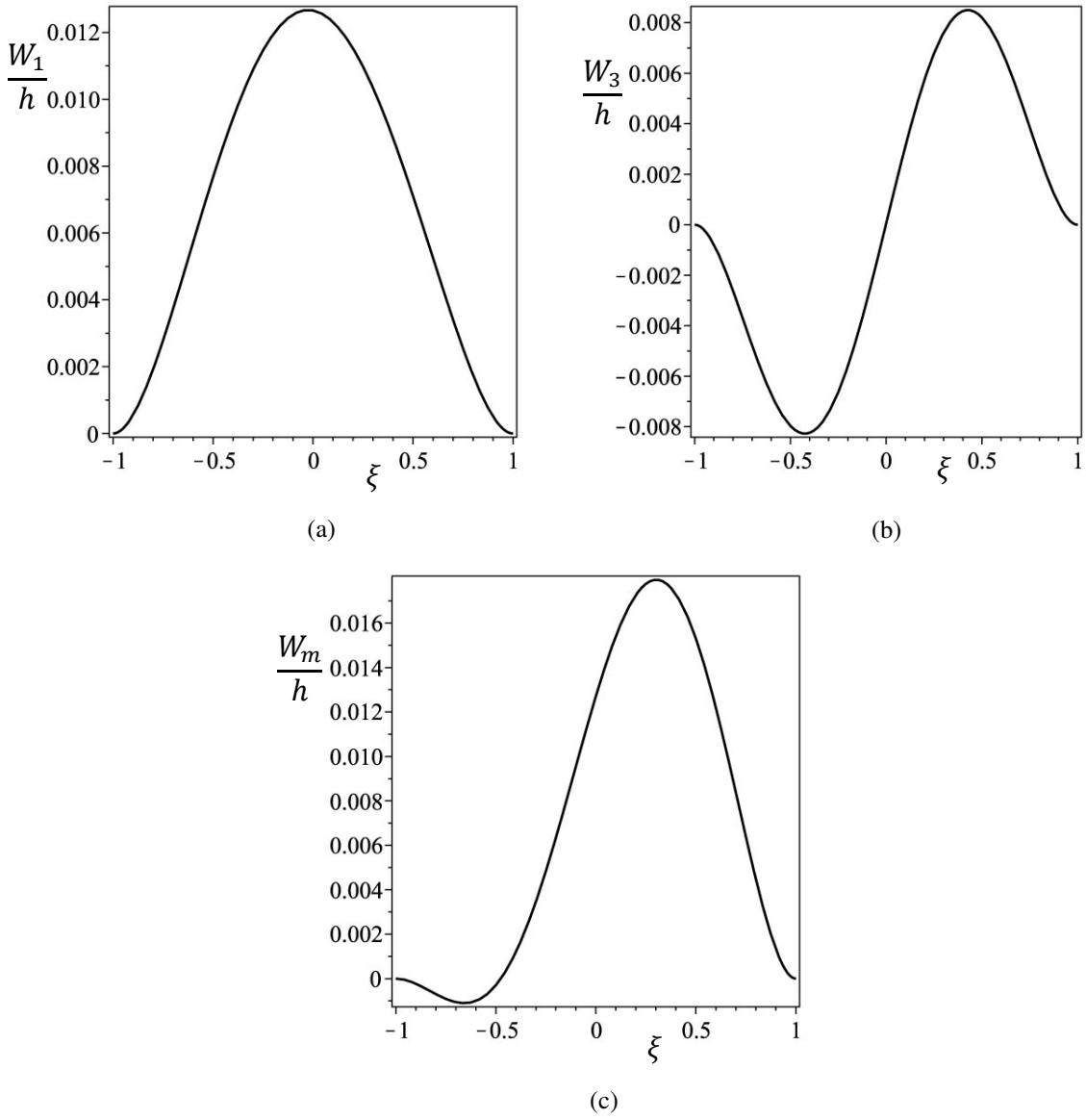

Figure 7. 8. Shapes of transverse displacement w_0 for point $\omega/\omega_{l_1} \cong 1.6$ from the first secondary branch. (a) first harmonic of w_0, (b) third harmonic of w_0, (c) total shape at $t = 0$ s.

Figures 7. 7 and 7. 8 present the mode shapes associated with the first and third harmonics and the total displacement of both transverse displacements for point $\omega/\omega_{l_1} \cong 1.6$ from first secondary branch. Torsion is also excited in the secondary branch; mainly it is represented by the third harmonic in a shape similar to the second linear torsional mode. The constant term and the second harmonic are also excited in the secondary branch, but their amplitudes are significantly smaller than the amplitudes of the first and third harmonics and are not presented.

The secondary branch goes to a bifurcation point which relates it with a second main branch. The vibrations in the second main branch are related with the third harmonic and have shape similar to the fourth linear mode, presented in Figure 7. 5. The constant term is different from zero in the second main branch, but the second harmonic remains zero, because of the quadratic nonlinear terms which appear in the equation of motion due to the mode shape which is in space, i.e. both transverse displacements and torsion are excited.

Finally, the mode shape of point corresponding to frequency $\omega/\omega_{l_1} \cong 2.2$ from the second secondary branch is given on Figure 7. 9. The bifurcation point is due to internal resonance which excites all harmonics included in the model. Like in the first main branch, the shapes of the harmonics of both transverse displacements are equal, i.e. the response remains in the same plane – the plane which is inclined on 45^{o} with respect to planes O*xy* and O*xz*. Thus, only the shapes of the harmonics of transverse displacement v_0 are represented.

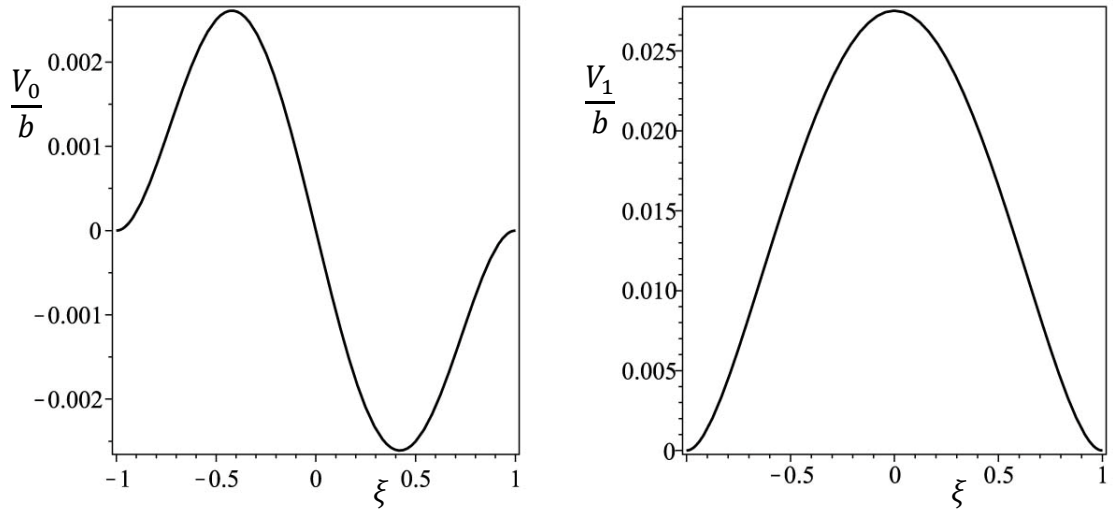

(a) (b)

Figure 7. 9. Continues on the next page.

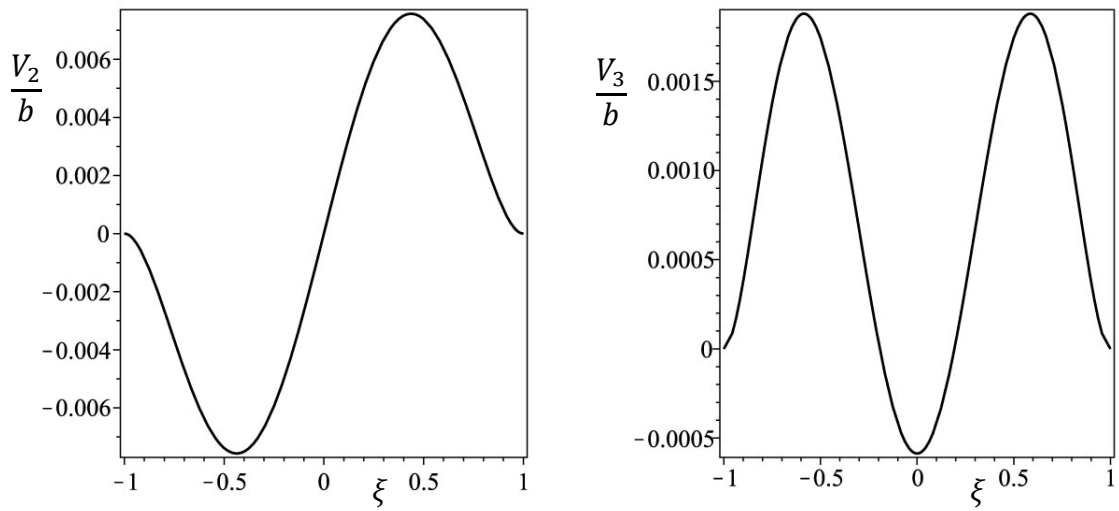

(c)

(d)

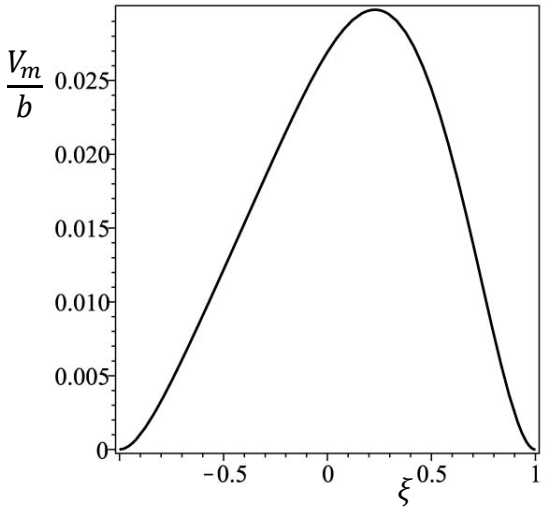

(e)

Figure 7. 9. Mode shapes of transverse displacement v_0 for point $\omega/\omega_{l_1} \cong 2.2$ from the second secondary branch. (a) constant term of v_0, (b) first harmonic of v_0, (c) second harmonic of v_0 (d) third harmonic of v_0, (e) total shape at $t = 0$ s.

7. 5. Forced vibration analysis

An external harmonic force at the twist centre, on the middle of the beam ($x = 0$), is applied in order to excite the first mode and to investigate the forced vibrations. The applied external force is represented on Figure 7. 10, where $F_y = F_z = 5\cos(\omega t)$ N. Mass proportional damping matrix is included in the model, calculated by equation (4. 21), with $\alpha = 0.01$. Harmonics up to third order are considered and the sine terms of the Fourier series are also included. The stability of the solutions is investigated by selecting the eigenvalues as proposed in [7. 7] and described in Chapter 4.

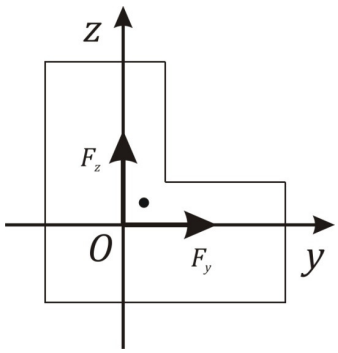

Figure 7. 10. L shaped cross section and the applied excitation. The centre of the coordinate system is chosen to be the twist centre of the cross section, ● – centroid of the cross section.

The bifurcation diagrams of all components of the transverse displacement w_0, calculated at the middle of the beam, are represented on Figure 7. 11. The main branch looses stability at point $\omega/\omega_{l_1} \cong 1.66$ due to a real Floquet exponent which becomes greater than zero, i.e. a bifurcation point is found. The same bifurcation point was found in free vibration in the previous section due to internal resonance. Two stable branches separate from the main branch at that point. These two stable branches can be best seen from the bifurcation diagram for the cosine term of the first harmonic, i.e. W_{c_1}. The bifurcation diagrams for the components of the transverse displacement v_0 are the same as the ones for w_0, thus they are not given here. They are the same because the transverse force is equal in both transverse directions and the bending properties of the L shaped cross sectional area are also the same in both transverse directions. The difference is on the secondary branches, despite the fact that the complete secondary branches coincide. Let's follow the secondary branch from the bifurcation point, which increases with the frequency of vibration (see Figure 7. 12), i.e. W_{c_1} increases with the frequency of vibration. The corresponding component of transverse vibration v_0 - V_{c_1} decreases, i.e. it follows the other stable branch from Figure 7. 12. And the opposite is true, if one follows the secondary branch on which W_{c_1} decreases with the frequency of vibration, the corresponding branch on the plot of V_{c_1} is the one where the amplitude increases from the bifurcation point. The total amplitude of the first harmonics of both transverse displacements is the same, the bifurcation plot of W_1 is given on Figure 7. 11 (b). The difference of the secondary branch comes from the phases of vibration, which are defined from the coefficients of the sine and cosine terms. Thus, the total amplitude of vibration of both stable branches, which separate from the first main branch, is equal, but the phases of vibration are different, in this way introducing two different vibration

modes. The same discussion is valid for the cosine and sine components of the second and third harmonics.

The vibration of a point on the first main branch is in a 2D fixed plane - the plane that is inclined on 45^{o} with respect to planes O*xy* and O*xz*. The response leaves this plane for points from the secondary branch due to the different phases which the harmonics of the transverse vibrations possess, i.e. symmetry with respect to that plane is broken and the response is in 3D space and cannot be fixed anymore in any plane. The bifurcation point is a supercritical symmetry-breaking bifurcation point [7. 8].

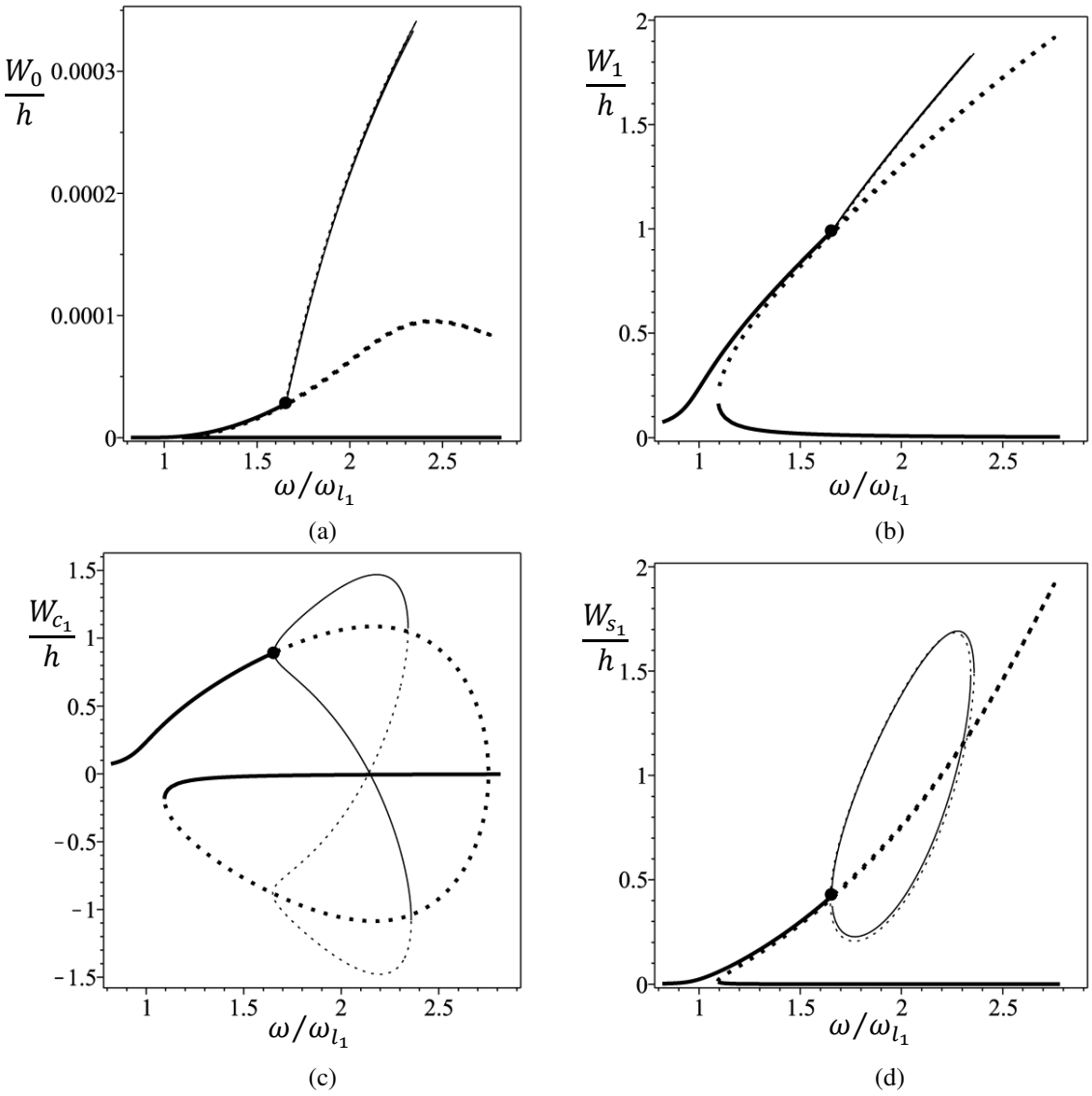

Figure 7. 11. Continues on the next page.

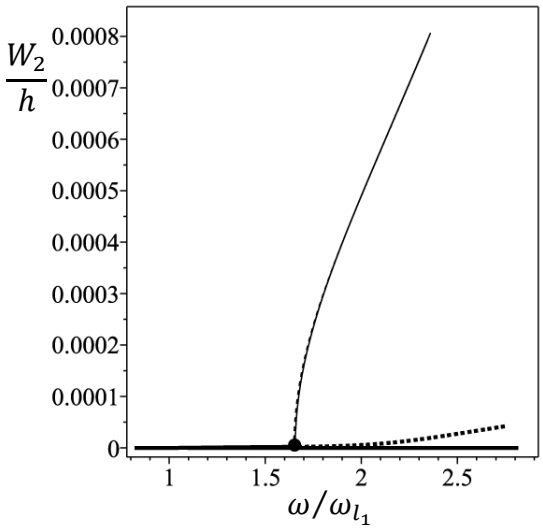

(e)

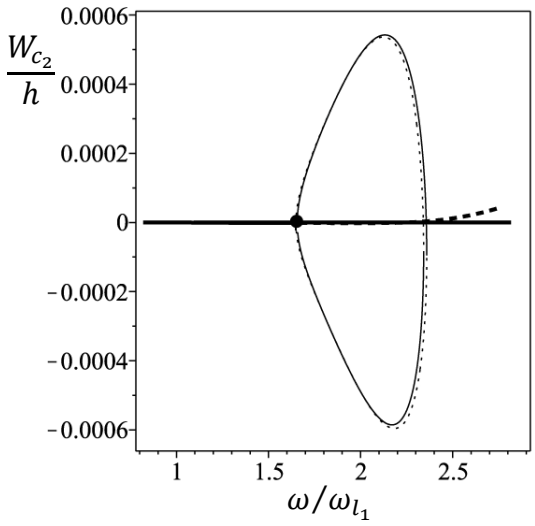

(f)

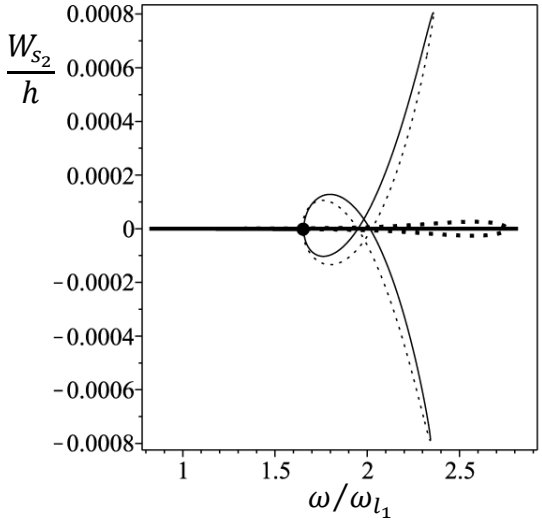

(g)

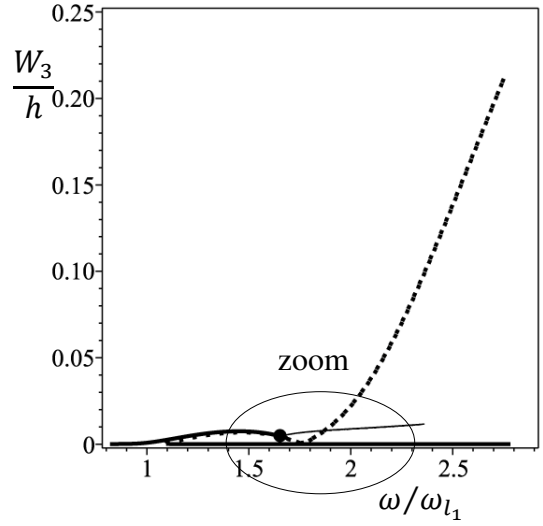

(h)

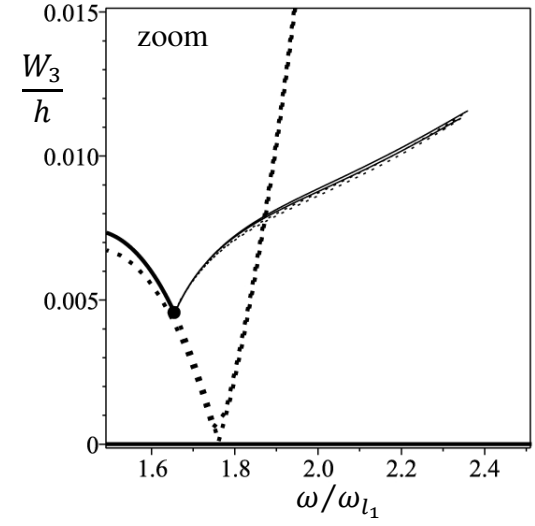

(i)

Figure 7. 11. Continues on the next page.

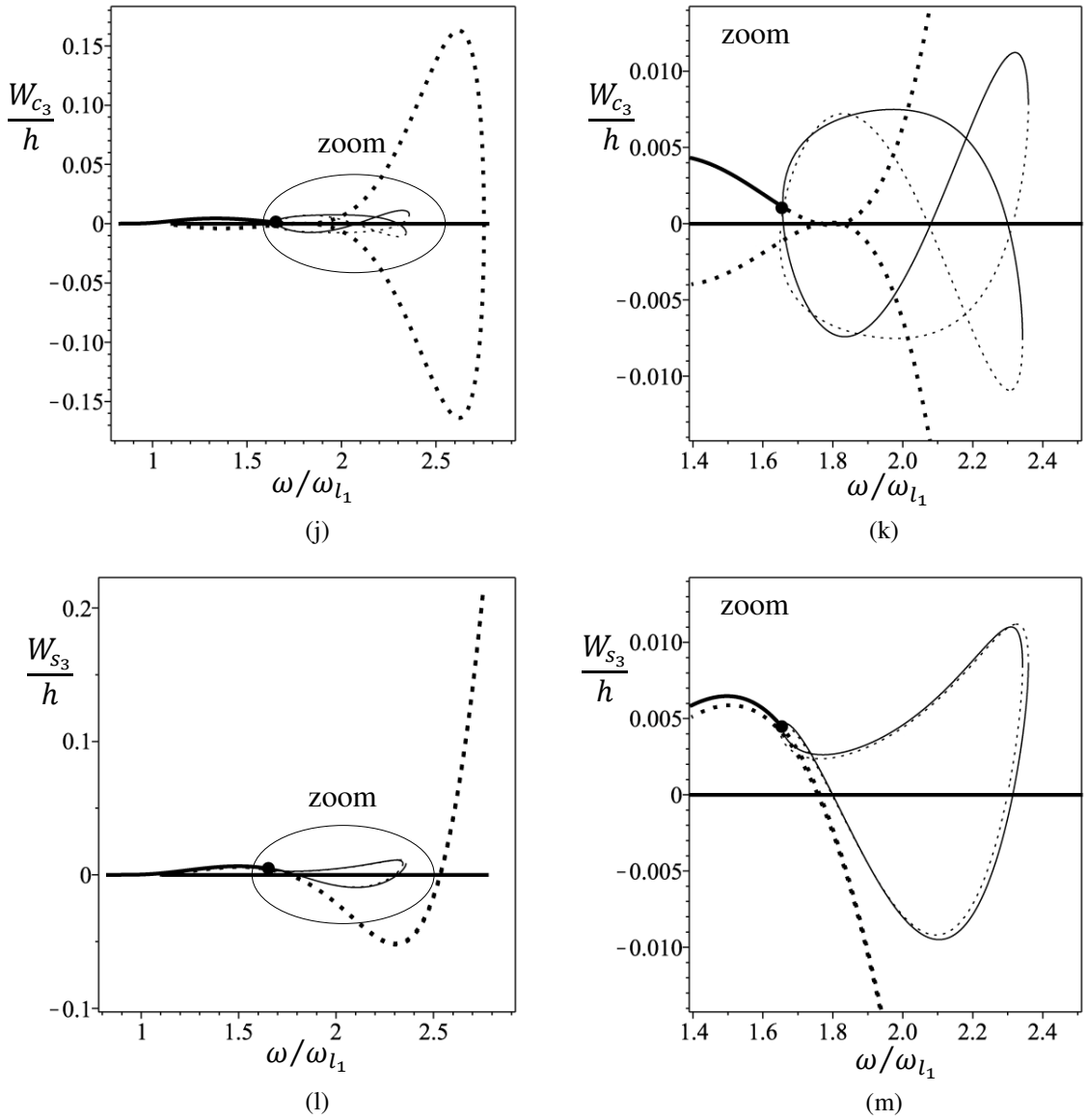

Figure 7. 11. Bifurcation diagrams of the components of transverse displacement w_0, ▬ stable part of first main branch, —— stable part of secondary branch, ▪▪▪ unstable part of first main branch, ····· unstable part of secondary branch, ● bifurcation point. Non-dimensional amplitude of (a) constant term, (b) first harmonic, (c) cosine of first harmonic, (d) sine of first harmonic, (e) second harmonic, (f) cosine of second harmonic, (g) sine of second harmonic, (h) third harmonic, (i) zoomed area of third harmonic, (j) cosine of third harmonic, (k) zoomed area of cosine of third harmonic, (l) sine of third harmonic, (m) zoomed area of sine of third harmonic.

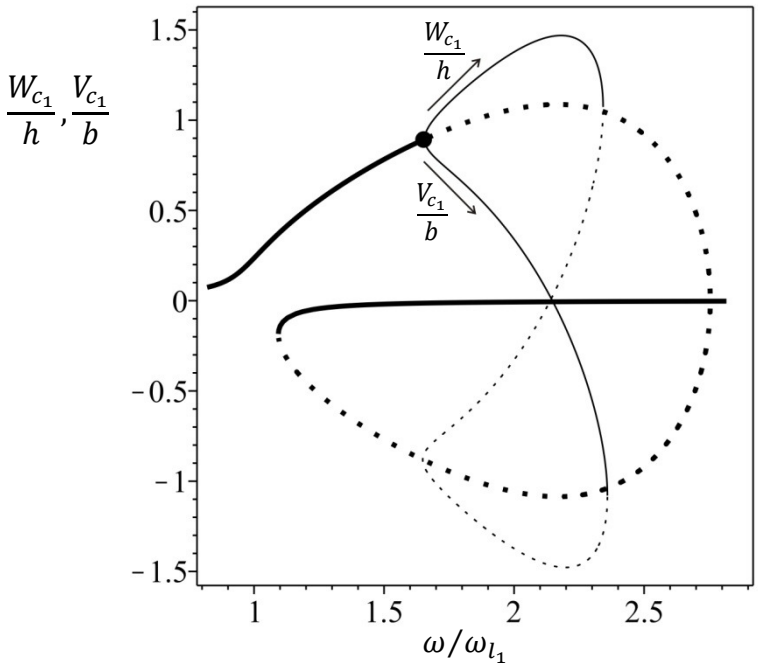

Figure 7. 12. Bifurcation diagrams of cosine components of first harmonic of transverse displacements v_0 and w_0, ▬▬ stable part of first main branch, —— stable part of secondary branch, ▪▪▪▪ unstable part of first main branch, ····· unstable part of secondary branch, ● bifurcation point.

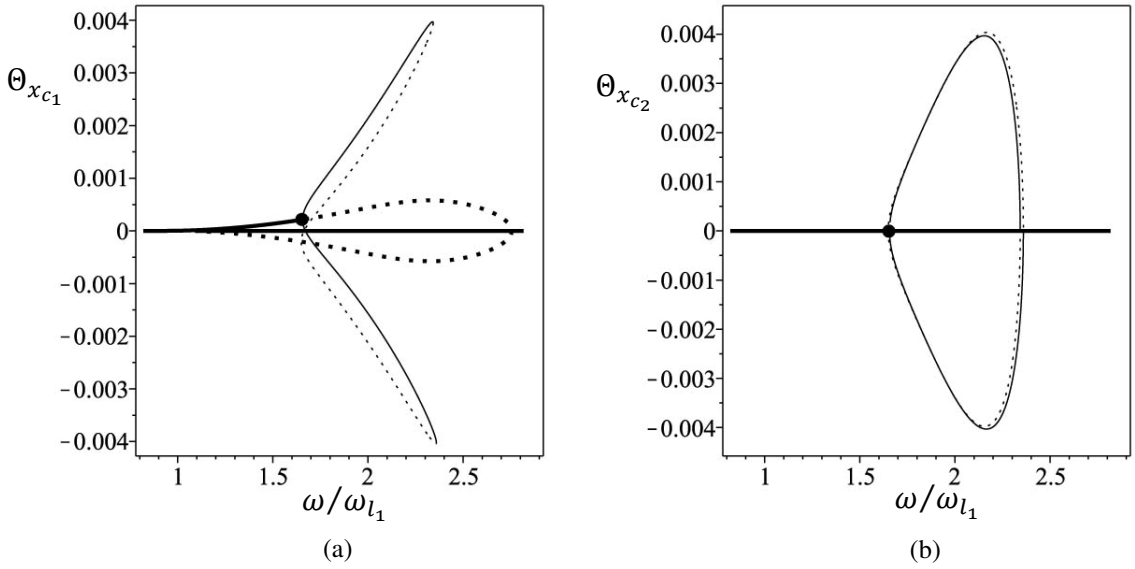

Figure 7. 13. Bifurcation diagrams of cosine components of first and second harmonic of torsion θ_x, ▬▬ stable part of first main branch, —— stable part of secondary branch, ▪▪▪▪ unstable part of first main branch, ····· unstable part of secondary branch, ● bifurcation point.

Torsion appears in the first main branch with small amplitude. The torsional amplitude increases in the secondary branch, but it still remains small. An example of the bifurcation diagrams obtained by depicting the amplitudes of the cosine terms of the first and second harmonics of torsion are presented on Figure 7. 13. The remaining torsional amplitudes are much smaller, thus are not shown.

7. 6. Conclusion

In this chapter, free and forced nonlinear vibrations of beams with non-symmetrical cross section were investigated. First, the position of the twist centre was validated and compared with the position of the shear centre given from Ansys. The linear natural frequencies and the corresponding modes of vibration were presented and the coupling between both transverse displacements and torsion, due to non-symmetrical cross section, was demonstrated.

Nonlinear free vibrations were investigated in the frequency domain. The computations were started on the first linear mode of vibration. Bifurcation points, secondary branches and the corresponding mode shapes were presented. It was pointed out that for beams with non-symmetrical cross sections, the quadratic terms do not vanish for points of the main branches and the constant term and the even harmonics appear in the response.

An external harmonic force, with equal amplitudes on both transverse directions, was applied, in order to excite the first mode and to investigate the nonlinear forced responses. The bifurcation diagrams of all components of transverse displacement w_0 were presented. A supercritical symmetry-breaking bifurcation point was found. The response on the first main branch is in a 2D plane, but it does not coincide with any of the coordinate planes. On the other hand, due to a bifurcation, the stable branches of the response cannot anymore be restricted to one plane and the response is in 3D space.

References

[7. 1] ANSYS Workbench User's Guide, 2009.

[7. 2] E. Riks, An incremental approach to the solution of snapping and buckling problems, *International Journal of Solids and Structures* 15 (1979) 529-551.

[7. 3] M. Crisfield, A fast incremental/iterative solution procedure that handles "snap-through", *Computers & Structures* 13 (1981) 55-62.

[7. 4] G. Romano, A. Barretta, R. Barretta, On Torsion and Shear of Saint-Venant Beams, *European Journal of Mechanics A/Solids* 35 (2012) 47-60.

[7. 5] E. Sapountzakis, V. Mokos, A BEM solution to transverse shear loading of beams, *Computational Mechanics* 36 (2005) 384–397.

[7. 6] P. Ribeiro, M. Petyt, Non-linear vibration of beams with internal resonance by the hierarchical finite-element method, *Journal of Sound and Vibration* 224 (1999) 591-624.

[7. 7] A. Lazarus, O. Thomas, A harmonic-based method for computing the stability of periodic solutions of dynamical systems, *Comptes Rendus Mecanique* 338 (2010) 510–517.

[7. 8] A. Nayfeh, B. Balachandran, *Applied Nonlinear Dynamics: Analytical, Computational and Experimental Methods*, New York, 1995.

8

Equations of Motion of Rotating Beams

8. 1. Introduction

In this chapter a model of rotating 3D beams about a fixed axis is presented. The beam model derived in Chapter 2. 2 is used, but the effect of large rotations is now taken into account in the inertia forces. Rotations of the cross section about the transverse axes are also included in the model and should be distinguished from the rotation of the beam, like a rigid body motion, about a fixed axis The absolute acceleration, which is used to define the inertia forces, is written as a sum of relative, transport and Coriolis accelerations and included in the equation of motion by the principle of virtual work.

8. 2. Mathematical model of rotating 3D beam

Beams with rectangular cross section, uniform thickness and in elastic, homogeneous and isotropic materials are considered. As in Chapter 2, the length is represented by the letter l, the width by b and the thickness by h. In order to express the displacements of a rotating beam, two coordinate systems are considered. The first one (OXYZ) is unmovable; it will be called "fixed coordinate system" and denote it by S_0. The second coordinate system (Oxyz), rotates around the Z axis of the fixed coordinate system and represents the rotational motion of the beam. We will call it "transport coordinate system" or system S_1. The origins of both coordinate systems coincide and the Z axis of the fixed coordinate system coincides with the z axis of the transport system. It will not be considered that the transport coordinate system necessarily rotates with a constant speed, i.e. the speed of rotation can change in time. Let the transport coordinate system at time t be rotated by $\vartheta(t)$ rad in relation to the fixed system (as presented in Figure 8. 1),

then $\dot{\vartheta}(t)$ is the speed of rotation (rad/s), or angular speed, and $\ddot{\vartheta}(t)$ is the angular acceleration (rad/s^2).

Displacement, velocity and acceleration vectors of the beam are written in the transport coordinate system S_1. The displacement field presented in Chapter 2 by equation (2. 1), from which the equation of motion (2. 29) was derived, is used here. It can be expressed by the relative displacement components u_R, v_R and w_R which are functions of time and space coordinates. u_R denotes the longitudinal displacement with respect to coordinate system S_1 and v_R and w_R denote the transverse displacements along *y* and *z*, respectively, written in S_1. The displacement field is based on Timoshenko's theory [8. 1] for flexure and Saint-Venant's theory for torsion [8. 2], and for completeness it is written here again:

$$\begin{aligned} u_R(x,y,z,t) &= u_0(x,t) - y\,\phi_z(x,t) + z\,\phi_y(x,t) + \psi(y,z)\,\frac{\partial\theta_x}{\partial x}(x,t), \\ v_R(x,y,z,t) &= v_0(x,t) + y\cos\big(\theta_x(x,t)\big) - y - z\sin\big(\theta_x(x,t)\big), \\ w_R(x,y,z,t) &= w_0(x,t) + y\sin\big(\theta_x(x,t)\big) + z\cos\big(\theta_x(x,t)\big) - z, \end{aligned} \tag{8. 1}$$

where v_0 and w_0 are the transverse displacements on the middle line – line constituted by points on the centroidal axis – of the beam in the *y* and *z* directions respectively, u_0 is the longitudinal displacement on the middle line, θ_x is the rotation of the cross section about the longitudinal axis *x*, ϕ_y and ϕ_z denote rotations of the cross section about axes *y* and *z*, respectively and $\psi(y,z)$ is the warping function [8. 3] defined in equation (2. 5). The common linearization of the trigonometric terms related with torsion, linearization that is true for small angles of rotation of the cross section, will be done later because, as shown in Chapter 3, more accurate results are achieved in this way.

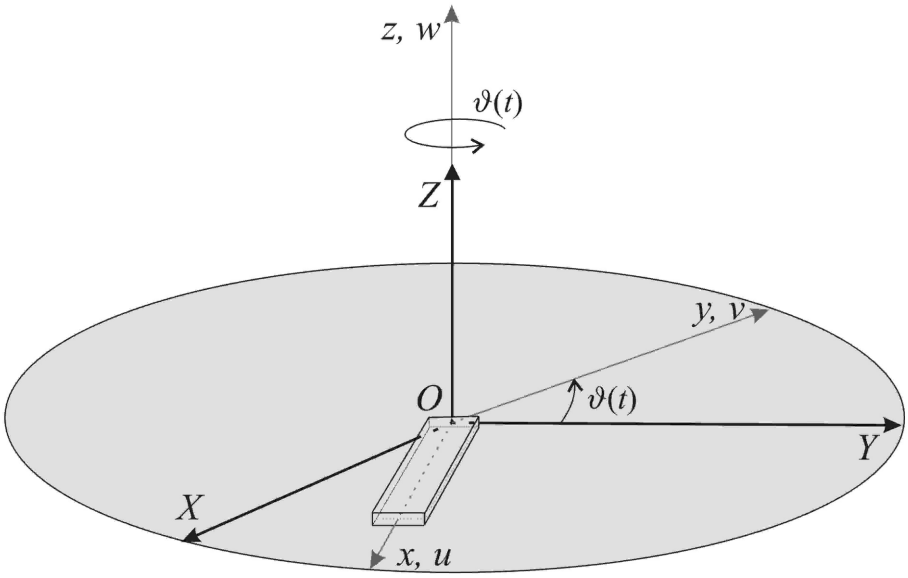

Figure 8. 1. Axes and displacements of the rotating beam model.

The relative displacements of the beam – due to bending, due to torsion and due to extension/compression of the centroidal axis – are expressed in the transport coordinate system, but the rotation of this coordinate system influences the absolute displacements. Let P be an arbitrary point of the beam, which in the transport coordinate system occupies position (x_P, y_P, z_P) before deformation. The position of P depends on time and considering the relative displacement of a general beam point, given by equations (8. 1), P can be written as:

$$P = \begin{Bmatrix} x_P + u_R(x_P, y_P, z_P, t) \\ y_P + v_R(x_P, y_P, z_P, t) \\ z_P + w_R(x_P, y_P, z_P, t) \end{Bmatrix}. \tag{8. 2}$$

In order to express the virtual work of the inertial forces we need an expression for the absolute acceleration – i.e., the acceleration with respect to the fixed coordinate system – of a general point P. This acceleration can be written as the sum of the relative, transport and Coriolis accelerations in the following way [8. 4]:

$$\left\{a_{P_{S_0}}\right\} = \left\{a_{P_{S_1}}\right\} + \{\alpha_{10}\} \times \{OP\} + \{\omega_{10}\} \times (\{\omega_{10}\} \times \{OP\}) + \\ +2\,\{\omega_{10}\} \times \left\{v_{P_{S_1}}\right\}, \tag{8. 3}$$

where $\left\{a_{P_{S_0}}\right\}$ is the absolute acceleration of point P, i.e. the acceleration of point P with respect to S_0, $\left\{v_{P_{S_1}}\right\}$ is the relative velocity of point P, i.e. the velocity of point P with

respect to S_1, given in (8. 4), $\left\{a_{P_{S_1}}\right\}$ is the relative acceleration of point P, i.e. the acceleration of point P with respect to S_1, given in (8. 5), $\{\omega_{10}\}$ is the angular velocity vector of the transport coordinate system (8. 6), $\{\alpha_{10}\}$ is the angular acceleration vector of the transport coordinate system (8. 7) and $\{OP\}$ is the position vector of point P with respect to the origin of S_1 (8. 8).

$$\left\{v_{P_{S_1}}\right\} = \begin{Bmatrix} \dot{u}_0 - y_P\,\dot{\phi}_z + z_P\,\dot{\phi}_y + \psi\dfrac{\partial\dot{\theta}_x}{\partial x} \\ \dot{v}_0 - y_P\sin(\theta_x)\,\dot{\theta}_x - z_P\cos(\theta_x)\,\dot{\theta}_x \\ \dot{w}_0 + y_P\cos(\theta_x)\,\dot{\theta}_x - z_P\sin(\theta_x)\,\dot{\theta}_x \end{Bmatrix}, \tag{8. 4}$$

$$\left\{a_{P_{S_1}}\right\} =$$

$$= \begin{Bmatrix} \ddot{u}_0 - y_P\,\ddot{\phi}_z + z_P\,\ddot{\phi}_y + \psi\dfrac{\partial\ddot{\theta}_x}{\partial x} \\ \ddot{v}_0 - y_P\cos(\theta_x)(\dot{\theta}_x)^2 - y_P\sin(\theta_x)\,\ddot{\theta}_x + z_P\sin(\theta_x)\left(\dot{\theta}_x\right)^2 - z_P\cos(\theta_x)\ddot{\theta}_x \\ \ddot{w}_0 - y_P\sin(\theta_x)(\dot{\theta}_x)^2 + y_P\cos(\theta_x)\,\ddot{\theta}_x - z_P\cos(\theta_x)\left(\dot{\theta}_x\right)^2 - z_P\sin(\theta_x)\ddot{\theta}_x \end{Bmatrix} \tag{8. 5}$$

$$\{\omega_{10}\} = \begin{Bmatrix} 0 \\ 0 \\ \dot{\vartheta}(t) \end{Bmatrix}, \tag{8. 6}$$

$$\{\alpha_{10}\} = \begin{Bmatrix} 0 \\ 0 \\ \ddot{\vartheta}(t) \end{Bmatrix}, \tag{8. 7}$$

$$\{OP\} = \begin{Bmatrix} x_P + u_0 - y_P\,\phi_z + z_P\,\phi_y + \psi\dfrac{\partial\theta_x}{\partial x} \\ y_P + v_0 + y_P\cos(\theta_x) - y_P - z_P\sin(\theta_x) \\ z_P + w_0 + y_P\sin(\theta_x) + z_P\cos(\theta_x) - z_P \end{Bmatrix}. \tag{8. 8}$$

Vectors (8. 4)-(8. 8) are projected in the transport coordinate system S_1, which is the system used to write all the following vectors and second order tensors. We note that

vector $\left\{a_{P_{S_1}}\right\}$ is the acceleration of Chapter 2, where the transport reference system coincided with the absolute one; the slightly different appearance between the terms of (8. 5) and (2. 68) – (2. 70) is due to the fact that in the present chapter it was decided to use subscript *P* to identify the coordinates of this point.

The displacements u_0, v_0 and w_0 and the rotations θ_x, ϕ_y and ϕ_z in the vectors above are functions of time and of the local space coordinate ξ, which are omitted. A dot over a variable represents differentiation with respect to time.

As written before, $\left\{a_{P_{S_1}}\right\}$ represents the relative acceleration; furthermore, $\{\alpha_{10}\} \times \{OP\} + \{\omega_{10}\} \times (\{\omega_{10}\} \times \{OP\})$ is the transport acceleration and $2\,\{\omega_{10}\} \times \left\{v_{P_{S_1}}\right\}$ is the acceleration of Coriolis.

Using the vectors defined in (8. 4) – (8. 8), the following expressions are obtained for each acceleration component:

Relative acceleration

$$\ddot{u}_R = \ddot{u}_0 - y_P\ \ddot{\phi}_z + z_P\ \ddot{\phi}_y + \psi \frac{\partial \ddot{\theta}_x}{\partial x},$$

$$\ddot{v}_R = \ddot{v}_0 - y_P\ \cos(\theta_x)\left(\dot{\theta}_x\right)^2 - y_P\ \sin(\theta_x)\,\ddot{\theta}_x + z_P \sin(\theta_x)\left(\dot{\theta}_x\right)^2 - z_P \cos(\theta_x)\ddot{\theta}_x, \qquad (8.\ 9)$$

$$\ddot{w}_R = \ddot{w}_0 - y_P\ \sin(\theta_x)\left(\dot{\theta}_x\right)^2 + y_P\ \cos(\theta_x)\,\ddot{\theta}_x - z_P \cos(\theta_x)\left(\dot{\theta}_x\right)^2 - z_P \sin(\theta_x)\ddot{\theta}_x.$$

Transport acceleration

$$\ddot{u}_T = -\left(v_0 + y_P \cos(\theta_x) - z_P \sin(\theta_x)\right)\ddot{\vartheta} - \left(x_P + u_0 - y_P\,\phi_z + z_P\,\phi_y + \psi \frac{\partial \theta_x}{\partial x}\right)\dot{\vartheta}^2,$$

$$\ddot{v}_T = \left(x_P + u_0 - y_P\,\phi_z + z_P\,\phi_y + \psi \frac{\partial \theta_x}{\partial x}\right)\ddot{\vartheta} - \left(v_0 + y_P \cos(\theta_x) - z_P \sin(\theta_x)\right)\dot{\vartheta}^2, \qquad (8.\ 10)$$

$$\ddot{w}_T = 0.$$

Acceleration of Coriolis

$$\ddot{u}_C = -2\left(\dot{v}_0 - y_P \sin(\theta_x)\,\dot{\theta}_x - z_P \cos(\theta_x)\,\dot{\theta}_x\right)\dot{\vartheta},$$

$$\ddot{v}_C = 2\left(\dot{u}_0 - y_P\,\dot{\phi}_z + z_P\,\dot{\phi}_y + \psi\frac{\partial\dot{\theta}_x}{\partial x}\right)\dot{\vartheta}, \tag{8. 11}$$

$$\ddot{w}_C = 0.$$

The absolute acceleration might be written as:

$$\left\{a_{P_{S_0}}\right\} = \begin{Bmatrix}\ddot{u}_R + \ddot{u}_T + \ddot{u}_C \\ \ddot{v}_R + \ddot{v}_T + \ddot{v}_C \\ \ddot{w}_R\end{Bmatrix}. \tag{8. 12}$$

The expression for the virtual work of the internal forces remains equal to the one of non-rotating beams. Since this was derived in Chapter 2, here just the main points are remembered. The axial and shear strains result from Green's strain tensor [8. 5], but the longitudinal terms of second order are neglected, because it was shown in Chapter 3 that their influence is small. Hence, the direct and the transverse shear strains are the ones given in equation (2. 6).

The stresses are related with the strains by Hooke's law (2. 27) and a shear correction factor is applied only to the bending terms (2. 21).

The strains, the stresses and the absolute acceleration are functions of the displacement components *u*, *v* and *w* and their derivatives. These displacement components are functions of displacements on the middle line and rotations of the cross section, as defined in (8. 1). The latter displacements and cross section rotations are expressed by means of shape functions and generalised displacements (2. 13). The shape functions used in this work are the ones defined in (2. 18) – (2. 20) plus additional shape function which are required for the clamped-free boundary conditions: a linear shape function which is zero on the clamped end and different from zero on the free end is used for the longitudinal and torsional displacements, Hermite cubic [8. 6] functions are used for the transverse displacements and the corresponding derivatives of the transverse shape functions are used for the rotations about the transverse axes. Since we will analyse straight and homogeneous beams, one *p* element will be used in the numerical examples.

The equation of motion is obtained by applying the principle of virtual work (2. 22). The virtual works of internal, inertia and external forces are defined as:

$$\delta W_V = -\int_V \{\delta\varepsilon\}^{\mathrm{T}}\{\sigma\}dV = -\{\delta q\}^{\mathrm{T}}[\mathrm{K}(\{q(t)\})]\{q(t)\}, \tag{8. 13}$$

$$\begin{aligned}\delta W_{in} &= -\int_V \rho\,\{\delta d\}^{\mathrm{T}}\{a_{P_{S0}}\}dV = \\ &= -\{\delta q\}^{\mathrm{T}}[\mathrm{M}]\{\ddot{q}(t)\} + \{\delta q\}^{\mathrm{T}}\left[\mathrm{CR}\left(\{q(t)\},\dot{\vartheta}\right)\right]\{\dot{q}(t)\} + \\ &+\{\delta q\}^{\mathrm{T}}\left[\mathrm{T}\left(\{q(t)\},\dot{\vartheta},\ddot{\vartheta}\right)\right]\{q(t)\} + \{\delta q\}^{\mathrm{T}}\left\{\mathrm{R}\left(\dot{\vartheta},\ddot{\vartheta}\right)\right\},\end{aligned} \tag{8. 14}$$

$$\delta W_E = \int_V \{\delta d_o\}^{\mathrm{T}}\{\mathrm{F}_0\}dV = \{\delta q\}^{\mathrm{T}}\{\mathrm{F}\}, \tag{8. 15}$$

where $\{\delta\varepsilon\}$ presents the virtual strains, $\{\sigma\}$ the stresses, ρ is the mass density of the beam, and $\{\mathrm{F}_0\}$ is vector of external forces on the middle line, i.e. on the *x* axis ($y = 0$, $z = 0$) in S_1 coordinate system.

Replacing equations (8. 13) – (8. 15) into equation (2. 22), the following equation of motion in the time domain is obtained:

$$\begin{aligned}&[\mathrm{M}]\{\ddot{q}\} + \left[\mathrm{CR}\left(\{q\},\dot{\vartheta}\right)\right]\{\dot{q}\} + [\mathrm{K}(\{q\})]\{q\} + \left[\mathrm{T}\left(\{q\},\dot{\vartheta},\ddot{\vartheta}\right)\right]\{q\} = \\ &= \{\mathrm{F}\} - \left\{\mathrm{R}\left(\dot{\vartheta},\ddot{\vartheta}\right)\right\}.\end{aligned} \tag{8. 16}$$

Three matrices and one vector in equation (8. 16) result from the inertia forces: $[\mathrm{M}]$ is the mass matrix due to relative acceleration; matrix $\left[\mathrm{CR}\left(\{q\},\dot{\vartheta}\right)\right]$ is a consequence of Coriolis acceleration, it depends on the vector of generalized displacements, hence it introduces a nonlinearity in the system, and depends linearly on the speed of rotation; $\left[\mathrm{T}\left(\{q\},\dot{\vartheta},\ddot{\vartheta}\right)\right]$ is a matrix due to the transport acceleration, it depends linearly on the relative generalized displacements $\{q\}$ (also adding nonlinear terms), quadratically on the angular speed and linearly on the angular acceleration; $\left\{\mathrm{R}\left(\dot{\vartheta},\ddot{\vartheta}\right)\right\}$ is a vector that is a consequence of the transport acceleration, it depends quadratically on the speed of rotation and linearly on the angular acceleration, and it is related with the centrifugal forces that act on the beam due to the rotation. The effect of elastic forces is represented

by the stiffness matrix [K({q})], which contains constant terms, terms that depend linearly and terms that depend quadratically on the vector of generalized displacements. {F} is the vector of generalized external forces. The vector of generalized displacements $\{q(t)\}$, the speed of rotation $\dot{\vartheta}(t)$ and the angular acceleration $\ddot{\vartheta}(t)$ depend on time, but argument *t* was omitted in equation (8. 16).

Damping was not added to the equation of motion (8. 16), later a damping proportional to the mass or stiffness matrices will be included in the equation of motion. A damping proportional factor β which may vary from one case to another [8. 7] will be considered.

The mass and the stiffness matrices were presented in Chapter 2, the rest of the terms on the equation of motion (8. 16) are presented here.

8. 3. Additional terms that appear in the equation of motion due to the rotation of the beam

8. 3. 1. Terms of the equation of motion that arise from the transport acceleration

In this sub-chapter, the matrices and the vectors that result from the transport acceleration are presented. The virtual work of inertia forces due to the transport acceleration, which was presented in equation (8. 10), can be written as

$$\delta W_{in}^{transport} = -\int_V \rho\,(\delta u\,\ddot{u}_T + \delta v\,\ddot{v}_T)\,dV. \tag{8. 17}$$

Hence, the transport acceleration results in the following matrix and vector:

$$[\mathrm{T}] = \begin{bmatrix} \mathbf{T_{11}} & \mathbf{T_{12}} & \mathbf{0} & \mathbf{0} & \mathbf{0} & \mathbf{0} \\ \mathbf{T_{21}} & \mathbf{T_{22}} & \mathbf{0} & \mathbf{0} & \mathbf{0} & \mathbf{0} \\ \mathbf{0} & \mathbf{0} & \mathbf{0} & \mathbf{0} & \mathbf{0} & \mathbf{0} \\ \mathbf{0} & \mathbf{0} & \mathbf{0} & \mathbf{T_{44}} & \mathbf{T_{45}} & \mathbf{0} \\ \mathbf{0} & \mathbf{0} & \mathbf{0} & \mathbf{T_{54}} & \mathbf{T_{55}} & \mathbf{0} \\ \mathbf{0} & \mathbf{0} & \mathbf{0} & \mathbf{0} & \mathbf{0} & \mathbf{T_{66}} \end{bmatrix}, \tag{8. 18}$$

$$\{\mathrm{R}\} = \begin{Bmatrix} \mathbf{R_1} \\ \mathbf{R_2} \\ \mathbf{0} \\ \mathbf{0} \\ \mathbf{0} \\ \mathbf{R_6} \end{Bmatrix}, \tag{8. 19}$$

where

$$\mathbf{T_{11}} = -\dot{\vartheta}(t)^2 \, \rho \int_V \lfloor N^u \rfloor^{\mathrm{T}} \lfloor N^u \rfloor \, dV, \tag{8. 20a}$$

$$\mathbf{T_{12}} = -\ddot{\vartheta}(t) \, \rho \int_V \lfloor N^u \rfloor^{\mathrm{T}} \lfloor N^v \rfloor \, dV, \tag{8. 20b}$$

$$\mathbf{T_{21}} = \ddot{\vartheta}(t) \, \rho \int_V \lfloor N^v \rfloor^{\mathrm{T}} \lfloor N^u \rfloor \, dV, \tag{8. 20c}$$

$$\mathbf{T_{22}} = -\dot{\vartheta}(t)^2 \, \rho \int_V \lfloor N^v \rfloor^{\mathrm{T}} \lfloor N^v \rfloor \, dV, \tag{8. 20d}$$

$$\mathbf{T_{44}}\left(\boldsymbol{q}_{\boldsymbol{\phi}_z}\right) =$$

$$= \dot{\vartheta}(t)^2 \, \rho \int_V \left((y^2 - z^2) \left\lfloor N^{\theta_x} \right\rfloor^{\mathrm{T}} \left\lfloor N^{\theta_x} \right\rfloor - \psi^2 \frac{d\left\lfloor N^{\theta_x} \right\rfloor^{\mathrm{T}}}{dx} \frac{d\left\lfloor N^{\theta_x} \right\rfloor}{dx} \right) dV + \tag{8. 20e}$$

$$+\ddot{\vartheta}(t) \, \rho \int_V y^2 \left\lfloor N^{\theta_x} \right\rfloor^{\mathrm{T}} \left\lfloor N^{\theta_x} \right\rfloor \phi_z \, dV,$$

$$\mathbf{T_{45}} = -\ddot{\vartheta}(t) \rho \int_V z^2 \left\lfloor N^{\theta_x} \right\rfloor^{\mathrm{T}} \left\lfloor N^{\phi_y} \right\rfloor dV, \tag{8. 20f}$$

$$\mathbf{T_{54}} = \ddot{\vartheta}(t) \rho \int_V z^2 \left\lfloor N^{\phi_y} \right\rfloor^{\mathrm{T}} \left\lfloor N^{\theta_x} \right\rfloor dV, \tag{8. 20g}$$

$$\mathbf{T_{55}} = -\dot{\vartheta}(t)^2\,\rho \int_V z^2 \left\lfloor N^{\phi_y} \right\rfloor^{\mathrm{T}} \left\lfloor N^{\phi_y} \right\rfloor dV, \tag{8. 20h}$$

$$\mathbf{T_{66}} = -\dot{\vartheta}(t)^2\,\rho \int_V y^2 \left\lfloor N^{\phi_z} \right\rfloor^{\mathrm{T}} \left\lfloor N^{\phi_z} \right\rfloor dV, \tag{8. 20i}$$

$$\mathbf{R_1} = \dot{\vartheta}(t)^2\,\rho \int_V x \left\lfloor N^{u} \right\rfloor^{\mathrm{T}} dV, \tag{8. 21a}$$

$$\mathbf{R_2} = -\ddot{\vartheta}(t)\rho \int_V x \left\lfloor N^{v} \right\rfloor^{\mathrm{T}} dV, \tag{8. 21b}$$

$$\mathbf{R_6} = -\ddot{\vartheta}(t)\rho \int_V y^2 \left\lfloor N^{\phi_z} \right\rfloor^{\mathrm{T}} dV. \tag{8. 21c}$$

It is remarked that approximations $\sin(\theta_x) \cong \theta_x$ and $\cos(\theta_x) \cong 1$ were now adopted. It is also worth noting that the warping function (2. 5) is an odd function in *y* and in *z* and therefore disappears from most of the integrals. Finally, it is noted that matrix $\mathbf{T_{44}}$ depends linearly on the rotation of the cross section ϕ_z and, therefore, introduces nonlinear terms in the equations of motion when the angular acceleration is different from zero.

8. 3. 2. Terms of the equation of motion that arise from the acceleration of Coriolis

In this sub-chapter the matrices that result from acceleration of Coriolis are presented. The acceleration of Coriolis is given in equation (8. 11) and the virtual work of the inertia forces due to this acceleration can be written as

$$\delta W_{in}^{Coriolis} = -\int_V \rho\,(\delta u\,\ddot{u}_C + \delta v\,\ddot{v}_C)\,dV. \tag{8. 22}$$

This virtual work results in the following matrix:

$$[\mathrm{CR}] = \begin{bmatrix} \mathbf{0} & \mathbf{CR_{12}} & \mathbf{0} & \mathbf{0} & \mathbf{0} & \mathbf{0} \\ \mathbf{CR_{21}} & \mathbf{0} & \mathbf{0} & \mathbf{0} & \mathbf{0} & \mathbf{0} \\ \mathbf{0} & \mathbf{0} & \mathbf{0} & \mathbf{0} & \mathbf{0} & \mathbf{0} \\ \mathbf{0} & \mathbf{0} & \mathbf{0} & \mathbf{0} & \mathbf{CR_{45}} & \mathbf{CR_{46}} \\ \mathbf{0} & \mathbf{0} & \mathbf{0} & \mathbf{CR_{54}} & \mathbf{0} & \mathbf{0} \\ \mathbf{0} & \mathbf{0} & \mathbf{0} & \mathbf{CR_{64}} & \mathbf{0} & \mathbf{0} \end{bmatrix}, \tag{8. 23}$$

where

$$\mathbf{CR_{12}} = -2\,\dot{\vartheta}(t)\,\rho \int_V \lfloor N^u \rfloor^{\mathrm{T}} \lfloor N^v \rfloor \, dV, \tag{8. 24a}$$

$$\mathbf{CR_{21}} = 2\,\dot{\vartheta}(t)\,\rho \int_V \lfloor N^v \rfloor^{\mathrm{T}} \lfloor N^u \rfloor \, dV, \tag{8. 24b}$$

$$\mathbf{CR_{45}} = -2\,\dot{\vartheta}(t)\,\rho \int_V z^2 \left\lfloor N^{\theta_x} \right\rfloor^{\mathrm{T}} \left\lfloor N^{\phi_y} \right\rfloor dV, \tag{8. 24c}$$

$$\mathbf{CR_{46}}(\boldsymbol{q}_{\theta_x}) = 2\,\dot{\vartheta}(t)\,\rho \int_V y^2 \left\lfloor N^{\theta_x} \right\rfloor^{\mathrm{T}} \left\lfloor N^{\phi_z} \right\rfloor \theta_x \, dV, \tag{8. 24d}$$

$$\mathbf{CR_{54}} = 2\,\dot{\vartheta}(t)\,\rho \int_V z^2 \left\lfloor N^{\phi_y} \right\rfloor^{\mathrm{T}} \left\lfloor N^{\theta_x} \right\rfloor dV, \tag{8. 24e}$$

$$\mathbf{CR_{64}}(\boldsymbol{q}_{\theta_x}) = -2\,\dot{\vartheta}(t)\,\rho \int_V y^2 \left\lfloor N^{\phi_z} \right\rfloor^{\mathrm{T}} \left\lfloor N^{\theta_x} \right\rfloor \theta_x \, dV. \tag{8. 24f}$$

It should be noted that approximations $\sin(\theta_x) \cong \theta_x$ and $\cos(\theta_x) \cong 1$ were now adopted and that matrices $\mathbf{CR_{46}}$ and $\mathbf{CR_{64}}$ depend linearly on the torsion θ_x. Hence, these two matrices also lead to nonlinear terms in the equations of motion.

8. 4. Conclusion

A *p*-version finite element model for 3D beams that rotate about a fixed axis was presented. In relation to a moving reference frame, the beam may experience relative displacements due to longitudinal, torsional and non-planar bending deformations. The

relative displacement field is based on Timoshenko's theory for bending and Saint-Venant's for torsion presented in Chapter 2. 2. The effects of geometrical nonlinearity are considered in the elastic forces, via a strain displacement relation that can be applied for moderately large vibration amplitudes. The rotational motion of the reference frame is included in the equation of motion via the inertia forces which are written as a sum of the relative, the transport and Coriolis accelerations.

References

[8. 1] C. Wang, J. Reddy, K. Lee, *Shear Deformable Beams and Plates*, Elsevier, Oxford, 2000.

[8. 2] G. Wempner, D. Talaslidis, *Mechanics of Solids and Shells. Theory and Application*, CRC Press, Boca Raton, Florida, 2003.

[8. 3] I. Sokolnikoff, *Mathematical Theory of Elasticity*, McGraw-Hill, New York, 1956.

[8. 4] A. A. Shabana, *Dynamics of Multibody Systems*, Cambridge University Press, Cambridge, 2005.

[8. 5] Y. C. Fung, *Foundations of Solid Mechanics*, Prentice-Hall, Englewood Cliffs, 1965.

[8. 6] O. C. Zienkiewicz, R. L. Taylor, J. Z. Zhu, *The Finite Element Method: Its Basis and Fundamentals*, Sixth edition, Oxford, 2005.

[8. 7] C. F. Beards, *Structural Vibration Analysis: Modelling, Analysis and Damping of Vibrating Structures*, Ellis Horwood, Chichester, 1983.

9

Forced Response of Rotating Beams in the Time Domain

9. 1. Introduction

In this chapter, vibrations of rotating beams are analysed. The influence of the speed of rotation on the linear bending frequencies is presented. Nonlinear forced vibrations of rotating beams are investigated in the time domain using direct integration of the equation of motion and considering constant and non-constant speed of rotation. Impulsive type and harmonic external forces are considered.

9. 2. Solution of the equation of motion of rotating beams

The equation of motion was developed in Chapter 8, assuming Timoshenko's theory for bending and Saint-Venant's theory for torsion and taking into account the effect of the rotational motion of the beam in the inertia terms. It was given in equation (8. 16), where the speed of rotation was included as time dependent, i.e. unlike what occurs in many works in this field, the beam may rotate at non-constant speed and the angular acceleration is taken into account. In this chapter, in section 9. 2. 1, the natural frequencies of rotating beams are presented and its variation with the speed of rotation is investigated. A discussion about the influence of the nonlinear terms in cantilever beams is given in section 9. 2. 2. Then, the forced steady-state response of rotating beams due to harmonic excitation 9. 2. 3, transient response due to non-constant speed of rotation 9. 2. 4 and transient response due to impulsive forces 9. 2. 5 are investigated.

9. 2. 1. Natural frequencies of rotating beams

First, the bending natural frequencies, flapwise and lagwise, for beams rotating with a constant speed are presented and compared with published results. Flapwise is a term that applies to vibrations in a plane parallel to the axis of rotation and lagwise to vibrations in a plane perpendicular to that axis. In this and the following examples, 8 shape functions, as discussed in Chapter 3, are used for each displacement component, i.e. the number of degrees of freedom is 48. The acceleration of Coriolis is neglected, since it is shown in [9. 1] that its effect on the linear natural frequencies is negligible. In these conditions, vector $\{\mathrm{R}(\dot{\vartheta}, \ddot{\vartheta})\}$ depends quadratically on the speed of rotation and represents a longitudinal constant centrifugal force that is applied on the beam, due to the rotation. This vector appeared in equations (8. 14) and (8. 16) and is defined in equations (8. 19) and (8. 21a) – (8. 21c). Because of this constant force, the steady-state solution in free vibration also requires the consideration of a constant term:

$$\{q(t)\} = \{q_0\} + \{q_1\}\cos(\omega\, t) \tag{9. 1}$$

Equation (9. 1) is inserted into the equation of motion (8. 16), without considering damping, Coriolis forces and external forces, and the following two equations are obtained:

$$[\mathrm{KL}]\,\{q_0\} + [\mathrm{T}]\,\{q_0\} = \{\mathrm{R}\}, \tag{9. 2}$$

$$-\omega^2\,[\mathrm{M}]\,\{q_1\} + [\mathrm{K1}]\,\{q_1\} + \,[\mathrm{KNL}(\{q_0\})]\,\{q_1\} + [\mathrm{T}]\,\{q_1\} = \{0\}, \tag{9. 3}$$

where $[\mathrm{KNL}(\{q_0\})] = [\mathrm{K2}(\{q_0\})] + 2[\mathrm{K2}(\{q_0\})]^{\mathrm{T}} + [\mathrm{K4}(\{q_0\})]$. First, equation (9. 2) is solved and the constant solution due to the centrifugal forces is obtained. This constant solution represents a deformation of the beam only in the longitudinal direction. The longitudinal deformation is important for the natural frequencies of rotating beams and the nonlinear terms related with it are used in the eigenvalue problem (9. 3).

The dimensionless flapwise and lagwise natural frequencies are presented in Tables 9. 1 and 9. 2 and they are in a very good agreement with published results. The beam considered is thin (in the computations $h/l = 0.003$), so that the results – with a model that includes transverse shear deformation – can be compared with the Bernoulli-Euler's theory results from references [9. 2] and [9. 6].

Table 9. 1. Dimensionless flapwise frequencies, $\dot{\vartheta}_{ND}$ – dimensionless speed of rotation.

$\dot{\vartheta}_{ND}$		First mode	Second mode	Third mode
0	Current model	3.5160	22.0332	61.6885
	Reference [9. 2]	3.5160153	22.034492	61.697214
	Reference [9. 3]	3.516	22.036	–
	Reference [9. 4]	3.51602	22.0348	61.7049
2	Current model	4.1373	22.6136	62.2645
	Reference [9. 2]	4.1373196	22.614922	62.273184
	Reference [9. 3]	4.137	22.617	–
	Reference [9. 4]	4.13733	22.6153	62.2808
4	Current model	5.5850	24.2721	63.9582
	Reference [9. 2]	5.5850015	24.273349	63.966760
	Reference [9. 3]	5.585	24.275	–
	Reference [9. 4]	5.58503	24.2737	63.9742
8	Current model	9.2568	29.9942	70.2848
	Reference [9. 2]	9.2568376	29.995382	70.292962
	Reference [9. 3]	9.257	29.998	–
	Reference [9. 4]	9.25694	29.9959	70.3002
10	Current model	11.2024	33.6393	74.6415
	Reference [9. 2]	11.202328	33.640366	74.649295
	Reference [9. 3]	11.203	33.643	–
	Reference [9. 4]	11.2025	33.6411	74.5670
12	Current model	13.1703	37.6023	79.6071
	Reference [9. 2]	13.170150	37.603112	79.614478

The dimensionless speed of rotation $\dot{\vartheta}_{ND}$ and the dimensionless frequency ω_{ND} are defined by:

$\dot{\vartheta}_{ND}{}^2 = \frac{\dot{\vartheta}^2}{E\, I_{zz}/\rho\, A\, l^4}$, for the flapwise frequencies and

$\dot{\vartheta}_{ND}{}^2 = \frac{\dot{\vartheta}^2}{E\, I_{yy}/\rho\, A\, l^4}$ for the lagwise frequencies.

The dimensionless frequencies are defined by:

$\omega_{ND} = \frac{\omega_w}{\sqrt{E\, I_{zz}/\rho\, A\, l^4}}$, for the flapwise frequencies and

$\omega_{ND} = \frac{\omega_v}{\sqrt{E\, I_{yy}/\rho\, A\, l^4}}$, for the lagwise frequencies,

where ω_w and ω_v are the flapwise and lagwise frequencies in rad/s. It is recalled that E represents Young's modulus, I_{zz} the second moment of area of the cross section of the beam about the z axis, I_{yy} the second moment of area of the cross section of the beam about the y axis, ρ is the density, l is the length and A is the area of the cross section.

9. 2. 2. Influence of the nonlinear terms in cantilever beams

Even if it is widely accepted that the nonlinear terms are generally not that important in bending of cantilever beams [9. 7], a discussion about the nonlinear terms and its importance is given in this sub-chapter.

Table 9. 2. Dimensionless lagwise frequencies, $\dot{\vartheta}_{ND}$ – dimensionless speed of rotation.

$\dot{\vartheta}_{ND}$		First mode	Second mode	Third mode
0	Current model	3.5160	22.0332	61.6885
	Reference [9. 3]	3.516	22.036	–
	Reference [9. 5]	3.516	22.033	–
2	Current model	3.6218	22.5250	62.2324
	Reference [9. 3]	3.622	22.528	–
	Reference [9. 5]	3.622	22.525	–
	Reference [9. 6]	3.62	–	–
5	Current model	4.0739	24.9487	65.0046
	Reference [9. 3]	4.074	24.952	–
	Reference [9. 5]	4.074	24.949	–
10	Current model	5.0492	32.1187	73.9687
	Reference [9. 3]	5.050	32.123	–
	Reference [9. 5]	5.049	32.118	–
	Reference [9. 6]	5.05	–	–

From equations (2. 1) and (2. 6), considering only deformation in one plane, i.e. plane bending, the non-zero strains are:

$$\varepsilon_x = \frac{\partial u_0}{\partial x} + z\frac{\partial \phi_y}{\partial x} + \frac{1}{2}\left(\frac{\partial w_0}{\partial x}\right)^2$$
$$\gamma_{zx} = \frac{\partial w_0}{\partial x} + \phi_y \tag{9. 4}$$

Two cases are now considered: including and neglecting the nonlinear term in ε_x. A static transverse force F_z, i.e. a force only in the transverse direction z, is applied in the free end of the beam and the beam is not rotating. The beam analysed has the following material properties (aluminium): $E = 7.0^{10}$ N m^{-2}, $\rho = 2778$ kg m^{-3}, $\nu = 0.34$; the dimensions considered are l = 0.58 m, b = 0.02 m and h = 0.002 m. The results of both cases are presented in Table 9. 3 and they are compared with Ansys software [9. 8] using BEAM189 element which is suitable for large displacements and large rotations.

Table 9. 3. Transverse and longitudinal displacements on the free end (in meters) of cantilever beam with a static transverse force applied on the same point.

F_z (N)	Nonlinear Model		Linear model		Ansys nonlinear model BEAM 189	
	w_0	u_0	w_0	u_0	w_0	u_0
0.2	0.013937	-0.000201	0.013937	0.0	0.013929	-0.000201
0.4	0.027873	-0.000804	0.027873	0.0	0.027818	-0.000801
0.6	0.041810	-0.001808	0.041810	0.0	0.037021	-0.001798
0.8	0.055747	-0.003215	0.055747	0.0	0.055394	-0.003184
1.0	0.069683	-0.005023	0.069683	0.0	0.068677	-0.004903

The table shows that if the nonlinear term in ε_x is considered, the transverse and the longitudinal displacements are coupled and the displacements u_0 are negative. In the linear model, those displacements are uncoupled and the longitudinal displacement remains zero. Curiously, the inclusion of term $(\partial w_0/\partial x)^2/2$ in the longitudinal strain does not decrease the transverse displacement of the nonlinear beam, as happens in beams with longitudinally fixed ends. Moreover, in spite of the negative longitudinal displacement u_0 of the nonlinear model, the transverse displacement values of the linear and nonlinear models are equal. In the case of the linear model, the only term in the longitudinal strain different from zero is $z\,\partial\phi_y/\partial x$, while in the case of nonlinear model all the three terms are different from zero. What happens is that in the nonlinear model

terms $\partial u_0/\partial x$ and $(\partial w_0/\partial x)^2/2$ of the longitudinal strain have equal amplitudes but opposite signs, making the longitudinal strains equal to $z\,\partial\phi_y/\partial x$ as occurs in the linear model. As an example, the functions $\partial u_0/\partial x$ and $(\partial w_0/\partial x)^2/2$ from the nonlinear model are presented in Figure 9. 1, for the case where a transverse force of amplitude 1 N is applied on the free end of the beam.

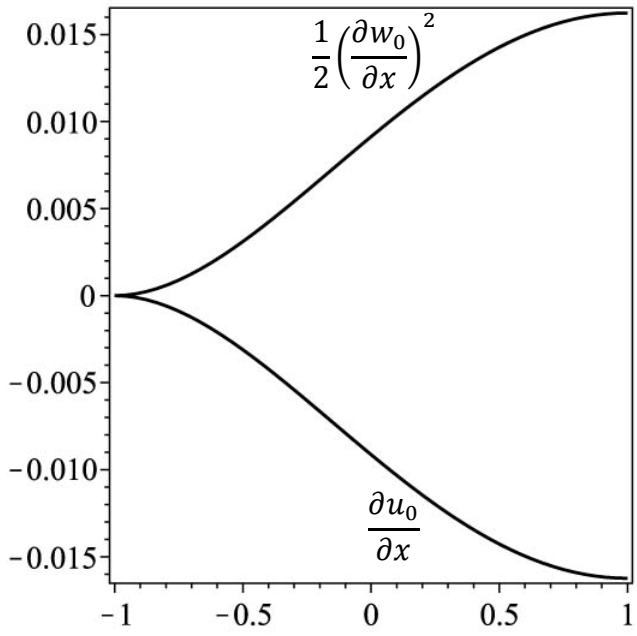

Figure 9. 1. $\frac{\partial u_0(\xi)}{\partial x}$ and $\frac{1}{2}\left(\frac{\partial w_0(\xi)}{\partial x}\right)^2$ components of the axial strain presented as functions of the local coordinate ξ. The amplitude of the force applied on the free end of the cantilever beam is 1 N.

We then conclude that in free end conditions, the length of the middle line of the beam does not change; the beam behaves in a so called "inextensional" fashion [9. 7], [9. 9]. This conclusion results from first principles: inextensionality was not imposed in the model and it is not always true, as we will see in the next examples.

In fact, the beam is not "inextensional" and the nonlinear term $(\partial w_0/\partial x)^2/2$ is not cancelled by $\partial u_0/\partial x$, when a longitudinal force is applied together with the transverse force. The longitudinal force makes $\partial u_0/\partial x$ and $(\partial w_0/\partial x)^2/2$ different in amplitude. If the longitudinal force is positive, the nonlinear model leads to results where the amplitudes of w_0 are smaller, as expected, and if it is negative, the transverse displacements are bigger, because compression leads to a stiffness reduction. This is shown in Table 9. 4, which portrays results with a transverse force of amplitude 1 N and different longitudinal forces F_x.

Table 9. 4. Transverse and longitudinal displacements on the free end (in meters) of cantilever beam with a static transverse force of 1N applied on the same point and different longitudinal forces.

F_x (N)	Nonlinear Model		Linear Model		Ansys nonlinear model BEAM 189	
	w_0	u_0	w_0	u_0	w_0	u_0
0.0	0.069683	-0.005023	0.069683	0.0	0.068677	-0.004903
1.0	0.060916	-0.003826	0.069683	$2.0714\ 10^{-7}$	0.060269	-0.003759
2.0	0.054128	-0.003011	0.069683	$4.1429\ 10^{-7}$	0.053771	-0.00298
3.0	0.048716	-0.002431	0.069683	$6.2143\ 10^{-7}$	0.048403	-0.002405
-1.0	0.081446	-0.006887	0.069683	$-2.0714\ 10^{-7}$	0.07976	-0.006648
-2.0	0.098058	-0.010019	0.069683	$-4.1429\ 10^{-7}$	0.09498	-0.00949

Table 9. 4 shows the disadvantages of the linear model when the force is combined, transverse and longitudinal. Keeping the transverse force constant and changing the longitudinal force, causes not only different longitudinal displacements, but also different transverse displacements, due to the coupling introduced by the geometrical nonlinearity. The linear model gives constant - wrong - results for the transverse displacement and very small longitudinal displacements, which are also wrong. Finally, the nonlinear terms are important for cantilever rotating beams, because of the centrifugal forces which act as longitudinal forces due to the rotation of the beam.

It is important to stress that the results of this *p*-version based model, which employs strain-displacement relations (2. 6), are very close to the ones provided by Ansys. The maximum error is about 3%, and this occurs with a very large tip displacement (about 50 times the beam thickness, i.e., about 0.17 times the beam length; last row of Table 9. 4). The comparisons carried out indicate that the present *p*-version model works well for moderately large displacement amplitudes. Taking into account the validation analysis, and for the sake of safety, the maximum displacement amplitude of the following numerical tests will be kept below $w_0/h = 20$.

9. 2. 3. Forced response of rotating beams

In this section, the speed of rotation is considered to be constant and inclined forces are applied on the beam edge in order to excite displacements in both transverse directions

and torsion. The influence of the speed of rotation on the displacements and torsion is analysed.

The beam analysed has dimensions $0.02 \times 0.002 \times 0.58$ m and material properties as in the section above. A damping matrix equal to 0.0001 times the linear stiffness matrix is used. First, a non-rotating beam is analysed and then different rotational speeds are applied. The transverse force $F = 3\cos(192.7353\, t)$ N is applied at the free end of the beam, inclined 30 degrees with respect to the y axis and perpendicular to the x axis. This force is equivalent to two transverse forces and a moment applied on the middle point of the free end. In reality, the amplitude of the moment that this force causes about the centroidal axis changes under torsion because of the variation of the distance between the force line of action and that axis. However, in our applications small rotations of the cross section about x occur and this effect is neglected. The excitation frequency is close to the second natural frequency of the non-rotating beam, but as the speed of rotation increases the beam becomes stiffer, due to the centrifugal forces, which act on the longitudinal direction. Thus, the fundamental frequency of the rotating beam increases and approaches the excitation frequency.

Figure 9. 2 presents phase plots of the flapwise displacement w_0. It can be seen from the figure that, without changing the amplitude or the excitation frequency of the applied force, the amplitude of vibration first decreases with the speed of rotation and after starts to increase. The initial decreasing of the displacement is due to the stiffening that accompanies the increasing rotational speed, while the increase of the displacement afterwards occurs because the fundamental frequency of the rotating beam becomes closer to the excitation frequency. At a rotational speed of about 183 rad/s the excitation and the fundamental natural frequencies become equal and at that speed the vibration amplitude reaches its maximum. Then, increasing the speed of rotation, the amplitude starts to decrease again due to the increased stiffness of the beam. The variations of the first three natural frequencies of the beam with the rotation speed are presented in Table 9. 5. It can be seen from Table 9. 5 that at rotational speed of about 85 rad/s, the excitation frequency is between the first and second natural frequencies of the system, defining the critical value of rotational speed at which the displacement stops decreasing and starts to increase.

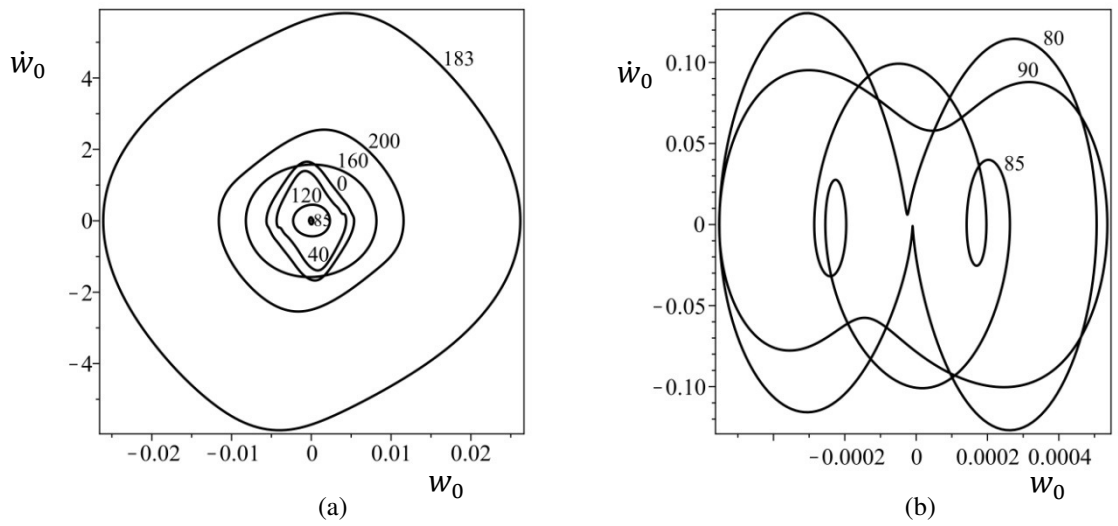

Figure 9. 2. Phase plots of flapwise displacement $w_0(l,t)$ of the beam under harmonic excitation $F = 3\cos(192.7353\,t)$ N for different rotation speeds.

Table 9. 5. Natural frequencies of flapwise displacement w_0 for beam 0.02 × 0.002 × 0.58 m rotating with different speeds.

Speed (rad/s)	0	40	80	85	90	120	183	200
$\omega_{w_{l_1}}$ (rad/s)	30.3	52.8	90.5	95.4	100.3	129.9	192.6	209.6
$\omega_{w_{l_2}}$ (rad/s)	189.8	215.4	278.2	287.6	297.2	358.7	499.3	538.7
Middle of $\omega_{w_{l_1}}$ and $\omega_{w_{l_2}}$	110.1	134.1	184.4	191.5	198.8	244.3	346.0	374.1

The inclined force also excites torsion and the other transverse displacement – i.e. lagwise. The fundamental lagwise frequency of the non-rotating beam is 304.18 rad/s and it changes slightly with the speed of rotation, which was varied from 0 to 200 rad/s. For example, the fundamental lagwise frequency at speed 200 rad/s is 314.70 rad/s. Thus, the beam becomes only a little stiffer in the lagwise direction and as the speed of rotation increases, the displacement in this direction (generally) decreases slightly, Figure 9. 3. Exceptionally, at rotational speed 183 rad/s the lagwise displacement is bigger than at 0 rad/s, which is explained by the fact the other transverse displacement is much bigger at that rotational speed and, due to coupling of both transverse displacements, the lagwise displacement also increases. The coupling is due to the geometrical nonlinear terms considered in the model. It is also noteworthy that at rotational speed 183 rad/s the second harmonic appears in the response of the lagwise displacement.

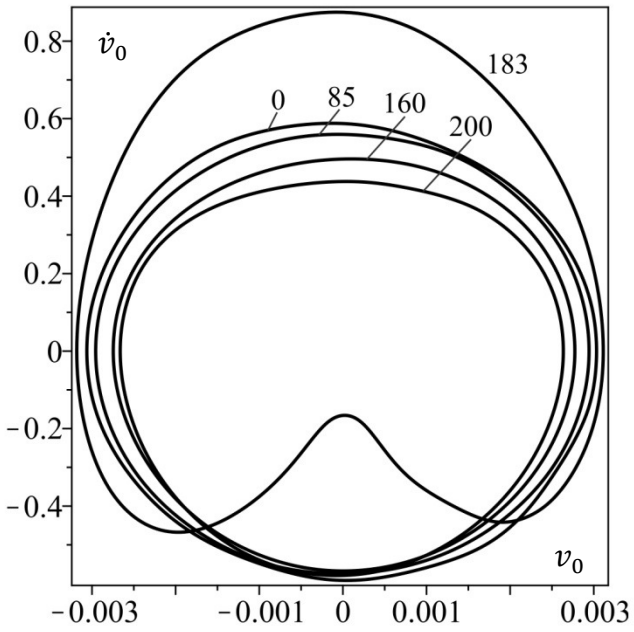

Figure 9. 3. Phase plots of lagwise displacement $v_0(l,\ t)$ of the beam under harmonic excitation $F = 3\cos(192.7353\ t)$ N for different rotation speeds.

As can be seen in Figure 9. 4, the maximum value of torsion remains small, because the moment about the centroidal axis is not large but the torsional stiffness is. However, while for both transverse displacements, the response mainly involves the first harmonic (but not only, at some rotation speeds the second and third harmonics are also significant), in the torsional response that is not true. On the contrary, the constant term and higher harmonics are generally very important in the torsional response. Moreover, the amplitudes of each harmonic change significantly with the speed of rotation, and, thus, the phase plots and the time responses are quite different from one rotational speed to another. This behaviour is a result of bending-torsional coupling, here expressed by the nonlinear terms in the strain-displacement relations.

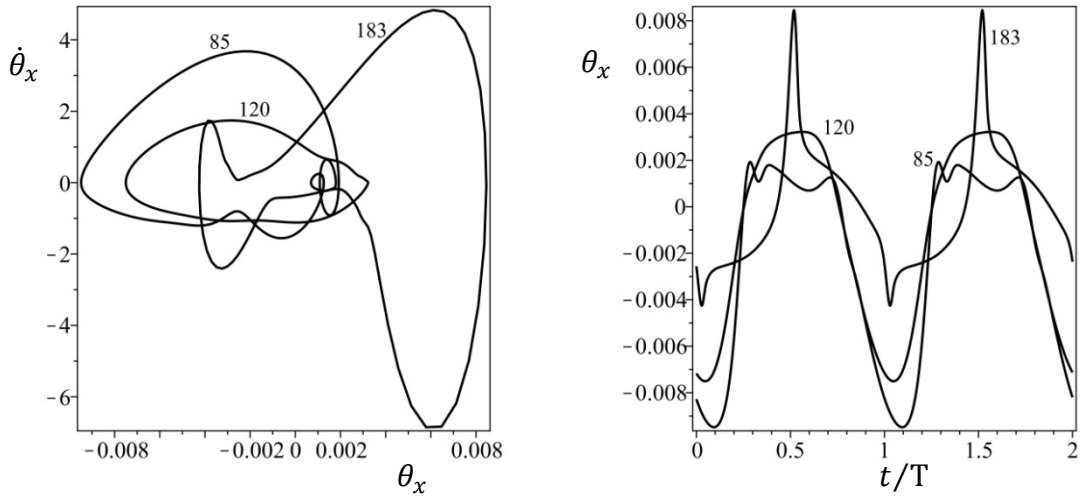

(a) (b)

Figure 9. 4. (a) Phase plots and (b) time responses of torsional displacement $\theta_x(t)$ for beam rotating with speeds 85 rad/s, 120 rad/s and 183 rad/s under harmonic excitation F = 3 cos(192.7353 t) N, t – time, T – period of vibration.

9. 2. 4. Transient response with non-constant speed of rotation

Since acceleration is unavoidable in any rotating system that is starting up or shutting down, in this section the influence of different accelerations are compared and the transient responses of the beam are presented.

The beam analysed here has the properties given in the previous section, but the speed of rotation increases linearly till a limit of 85 rad/s is reached. The applied external force is also the same: F = 3 cos(192.7353 t) N inclined on 30^0 with respect to y axis. Three different accelerations are applied to the model: an acceleration of 42.5 rad/s^2 applied during the initial 2 seconds, 85 rad/s^2 applied during the first second and 170 rad/s^2 applied during the first 0.5 s. In these examples, the acceleration $\ddot{\vartheta}(t)$ is constant and positive in the initial period and then it is zero. Therefore, the speed of rotation is increasing linearly in the initial period and then remains constant at 85 rad/s. The speed functions for these three accelerations are represented in Figure 9. 5.

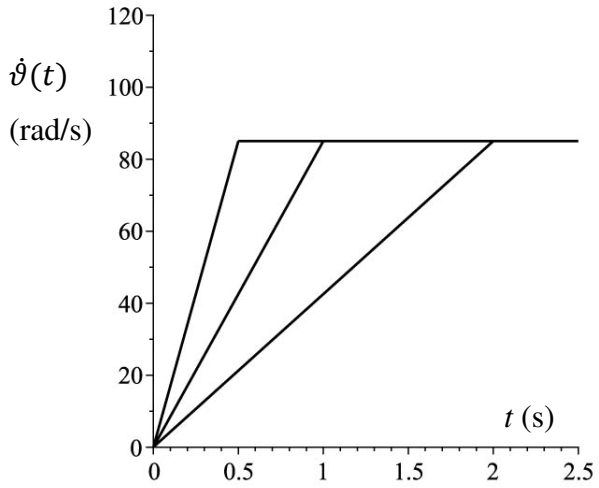

Figure 9. 5. Non-constant speed of rotation as function of time.

The transient responses of the flapwise displacement $w_0(l,t)$ for the three different accelerations are presented on Figure 9. 6, for the initial two seconds. It can be seen from the figure that when the beam accelerates faster till the limited rotational speed of 85 rad/s, it reaches faster its steady state response. In the present case, larger accelerations imply that centrifugal forces become constant sooner, so the behaviour portrayed in Figure 9. 6 is expectable. The faster decrease of the amplitude of vibration when the acceleration is bigger is explained by the fact that the speed of rotation increases faster and the longitudinal forces due to the centrifugal forces increase faster. Then the beam becomes stiffer due to the coupling of the longitudinal and transverse displacements and as a result the transverse displacement decreases, i.e. any variation of the centrifugal force directly affects the transverse displacement.

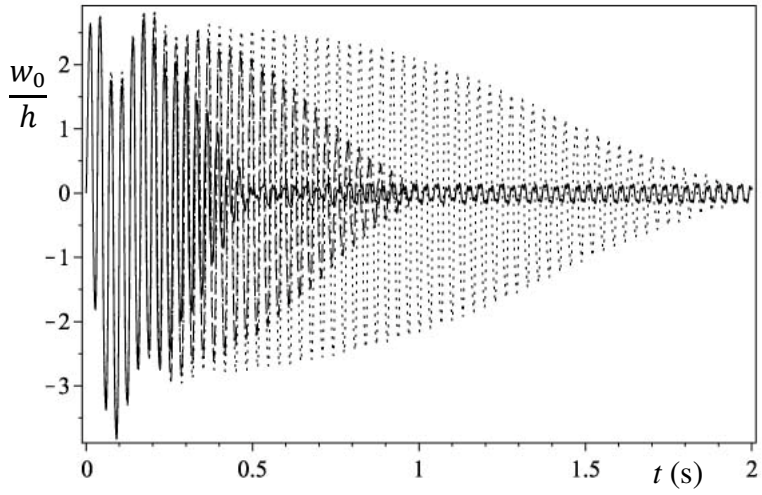

Figure 9. 6. Dimensionless time responses of flapwise displacement $w_0(l,t)$ of beam under harmonic excitation F = 3 cos(192.7353 t) N rotating at non-constant speed: —— $\dot{\vartheta}(t) = 170\ t$ rad/s for $t \in$ [0, 0.5] s and $\dot{\vartheta}(t) = 85$ rad/s for $t >$ 0.5 s; ----- $\dot{\vartheta}(t) = 85\ t$ rad/s for $t \in$ [0, 1] s and $\dot{\vartheta}(t) = 85$ rad/s for $t >$ 1s; ····· $\dot{\vartheta}(t) = 42.5\ t$ rad/s for $t \in$ [0, 2] s, t – time, h – thickness.

The maximum amplitude of relative displacement component w_0 at the beam tip is 3.65 when the acceleration is 42.5 rad/s^2, 3.73 when the acceleration is 85 rad/s^2 and 3.82 when it is 170 rad/s^2 (the amplitude is non-dimensional). It is noticeable that, due to the acceleration, somewhat large relative displacement amplitudes are attained in the transient phase, advising the use of a nonlinear structural model.

As shown in the previous section, the amplitude of vibration can increase with the speed of rotation if the natural frequency of the system approaches the excitation frequency, which was the case for a rotational speed of 183 rad/s. To demonstrate that this effect also occurs when the rotation speed is not constant, the speed limit is increased from 0 to 200 rad/s, and accelerations of 50 rad/s^2, 100 rad/s^2 and 200 rad/s^2 are considered till the speed limit is reached. The results for the flapwise displacement are shown in Figure 9. 7. In the beginning the transverse displacement decreases with time, till the rotational speed becomes about 85 rad/s and then it starts to increase till rotational speed becomes about 183 rad/s. As shown in the previous section, these critical rotational speeds are related with the natural frequencies of the rotating beam. After the system passes the rotational speed of 183 rad/s, the amplitude of vibration slightly decreases, and when the speed of rotation remains constant and equal to 200 rad/s the system begins to approach its steady-state response. In these cases, not only larger accelerations result in faster reaching the steady state response, but also the system experiences big vibration amplitude changes for shorter time spans.

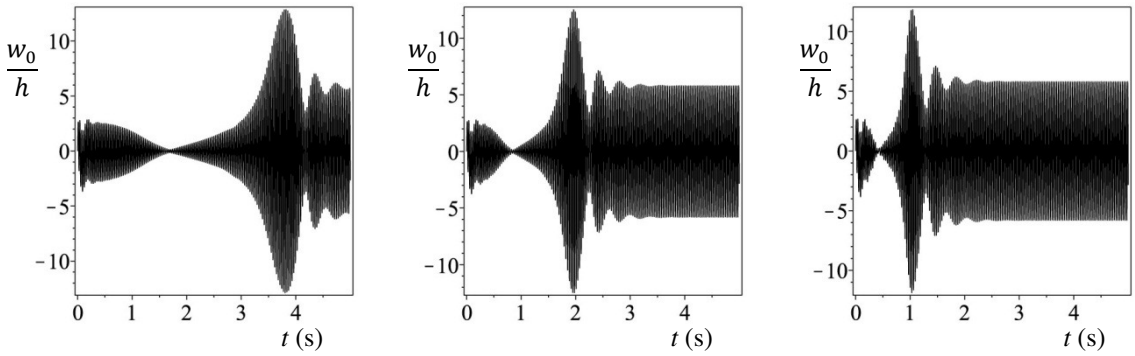

Figure 9. 7. Dimensionless time responses of flapwise displacement $w_0(l,t)$ of beam under harmonic excitation F = 3 cos(192.7353 t) rotating at non-constant speed: (a) $\dot{\vartheta}(t) = 50\ t$ rad/s for $t \in$ [0, 4] s and $\dot{\vartheta}(t) = 200$ rad/s for $t >$ 4 s; (b) $\dot{\vartheta}(t) = 100\ t$ rad/s for $t \in$ [0, 2] s and $\dot{\vartheta}(t) = 200$ rad/s for $t >$ 2 s ; (c) $\dot{\vartheta}(t) = 200\ t$ rad/s for $t \in$ [0, 1] s and $\dot{\vartheta}(t) = 200$ rad/s for $t >$ 1 s.

A similar change of the vibration amplitude appears when the beam is decelerating, i.e. the rotational speed is decreasing. The next example considers that the beam is initially rotating with a constant speed of 85 rad/s and vibrates in its steady state regime due to the external force F = 3 cos(192.7353 t) that is parallel to plane yz and inclined 30^0 with respect to y axis. Then, three different negative accelerations are applied till the rotational speed becomes zero: an acceleration of -42.5 rad/s^2 for a period of 2 seconds, -85 rad/s^2 for a period of 1 second and -170 rad/s^2 for a period of 0.5 s. Thus, in these examples, the acceleration $\ddot{\vartheta}(t)$ is constant and negative in the specified period and the speed of rotation decreases. Finally, both the acceleration and the speed of rotation become zero but the external force is still applied. The results are presented on Figure 9. 8. In accordance with the example of Figure 9. 6 for positive acceleration, it can again be noticed here that bigger deceleration leads to faster change of the amplitude. However, unlike what occurred in Figure 9. 6, the vibration amplitude is not much larger in the variable rotation speed stage than in the constant rotation speed stage.

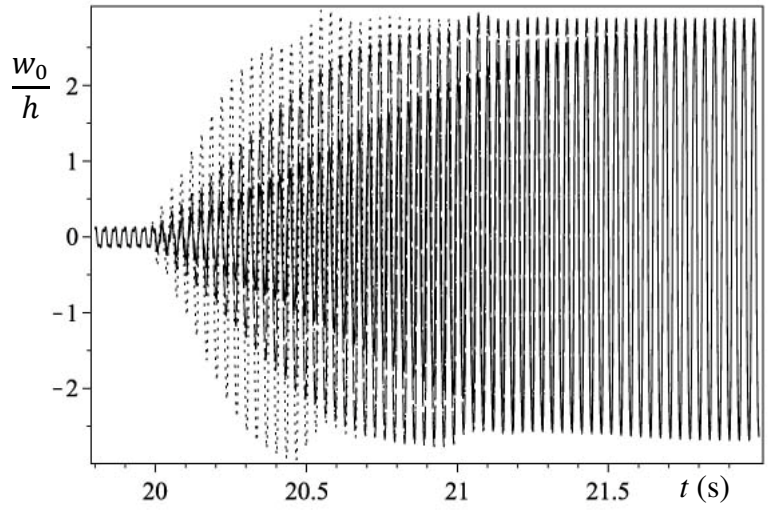

Figure 9. 8. Dimensionless time responses of flapwise displacement $w_0(l,t)$ of beam under harmonic excitation F = 3 cos(192.7353 t) N rotating at non-constant decreasing speed: ····· $\ddot{\vartheta}(t) = -170$ rad/s; ----- $\ddot{\vartheta}(t) = -85$ rad/s; —— $\ddot{\vartheta}(t) = -42.5$ rad/s.

As another example, included here in order to better show the importance of using a 3D rotational beam model instead of a 2D, a beam with the same properties except the thickness, which is increased to h = 0.0075 m, is now analysed. The external force is applied only in transverse direction z, i.e. F_z = 3 cos(192.7353 t) N and displacement component w_0 is directly excited. The acceleration and the speed of rotation are as in Figure 9. 5. We should mention that increasing the thickness, the flapwise natural frequencies are also increased and the fundamental flapwise frequency for rotating beam with constant speed of 85 rad/s becomes 146.51 rad/s, i.e. still smaller than, but closer to, the applied excitation frequency. The transient response of the lagwise displacement v_0 for the three different accelerations is presented on Figure 9. 9. This displacement is computed at the beam tip.

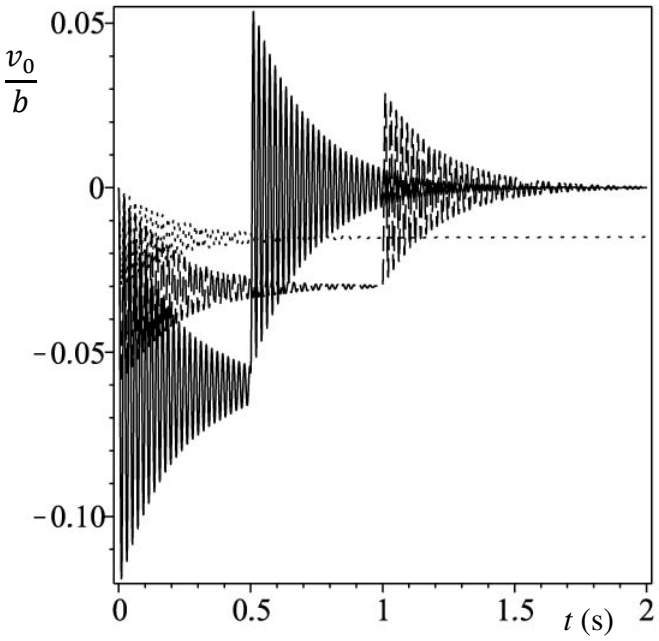

Figure 9. 9. Dimensionless time responses of lagwise displacement $v_0(l,t)$ of beam under transverse harmonic excitation F_z = 3 cos(192.7353 t) N rotating at non-constant speed: —— $\dot{\vartheta}(t) = 170\,t$ for $t \in$ [0, 0.5] s and $\dot{\vartheta}(t) = 85$ for $t >$ 0.5; ----- $\dot{\vartheta}(t) = 85\,t$ for $t \in$ [0, 1] s and $\dot{\vartheta}(t) = 85$ for $t >$ 1; ····· $\dot{\vartheta}(t) = 42.5\,t$ for $t \in$ [0, 2] s; t – time, b – width.

Even though the applied external force does not excite directly the lagwise displacement, this displacement is different from zero due to its couplings with the longitudinal displacement. These couplings are induced by the rotational inertia. Furthermore, in the beginning when the acceleration is positive and the speed is varying, the lagwise displacement is negative due to the force $\mathbf{R_2}$ (given in equation (8. 21b)), which acts on negative lagwise direction, this force depends linearly on the acceleration and results from the transport acceleration. The lagwise displacement decreases with time due to the stiffening of beam, under the increasing action of centrifugal force at larger speeds. The $\mathbf{R_2}$ force will stop acting on the beam when the speed of rotation becomes constant, but the beam will still have lagwise displacement due to coupling between longitudinal and lagwise displacements due to acceleration of Coriolis, which is represented by matrices $\mathbf{CR_{12}}$ and $\mathbf{CR_{21}}$ given in equations (8. 24a) – (8. 24b).

9. 2. 5. Impulsive forces

In this sub-section the effect that an impulsive force has on the response of the rotating blade is analysed. Impulsive forces may, for example, occur due to impact between the rotating blade and a bird, or a rotating blade and a piece of material coming from damage

elsewhere in a machine. Since this chapter focus on time domain analyses, it is particularly appropriate to carry out this last study.

The blade under analysis is the same as in section 9. 2. 3 and it is considered that it rotates with a constant speed of 85 rad/s. To facilitate the comparison with section 9. 2. 3 the blade is in a steady state regime of vibration under the action of an external harmonic force as in that section, i.e. $F = 3\cos(192.7353\,t)$ N, inclined on 30^0 with respect to the y axis. The impulsive force has a duration equal to a quarter of the period of the harmonic force, it is applied together with the harmonic force but only in z direction and at moment t = 19.955 s. The impulsive, harmonic and total (i.e. the sum) forces are represented on Figure 9. 10. Impulsive forces with three different amplitudes are considered, as if three different perturbations occur on the harmonic force.

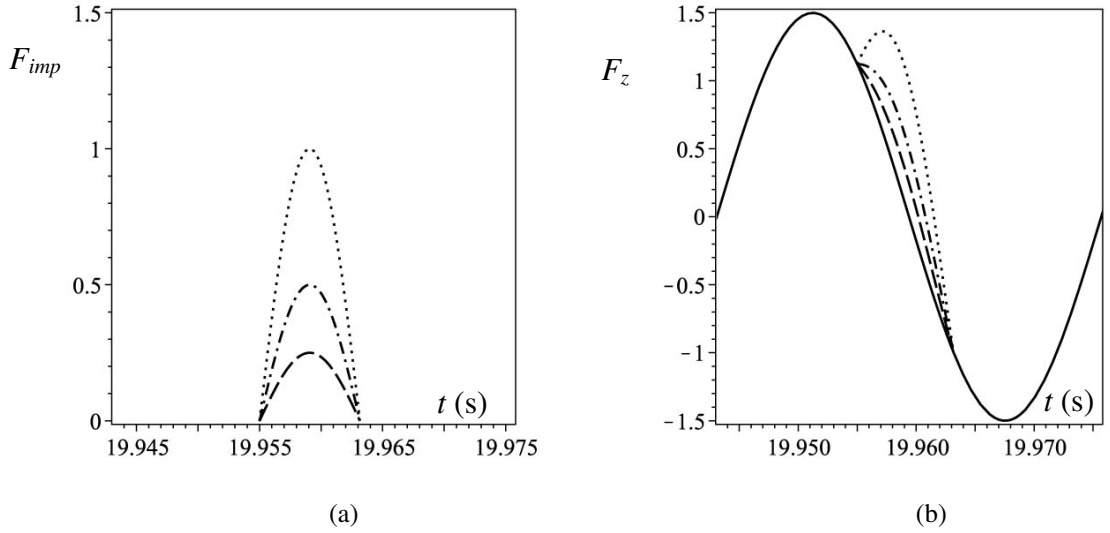

Figure 9. 10. Transverse external force applied on the z direction of the rotating beam (a) impulsive force, F_{imp} (N), (b) total external force, F_z (N), —— purely harmonic , ····· harmonic plus impulse with amplitude 1 N, –·–·–·– harmonic plus impulse with amplitude 0.5 N, – – – – harmonic plus impulse with amplitude 0.25 N.

The response of the beam due to this combined force is shown on Figures 9. 11 and 9. 12. Since the impulsive force is applied only in direction z, it changes mainly the vibration of the beam in xz plane, i.e. the flapwise displacement. But it also influences slightly the lagwise displacement w_0 and the torsion θ_x due to the bending-torsional couplings represented in the present model by nonlinear stiffness terms. Even though the duration of the impulsive force is very short, 0.008 seconds, its effect continues for several seconds till steady state regime is achieved again. It can be noticed that

significantly larger vibration amplitudes in displacement $w_0(l,t)$ are attained due to the impulses.

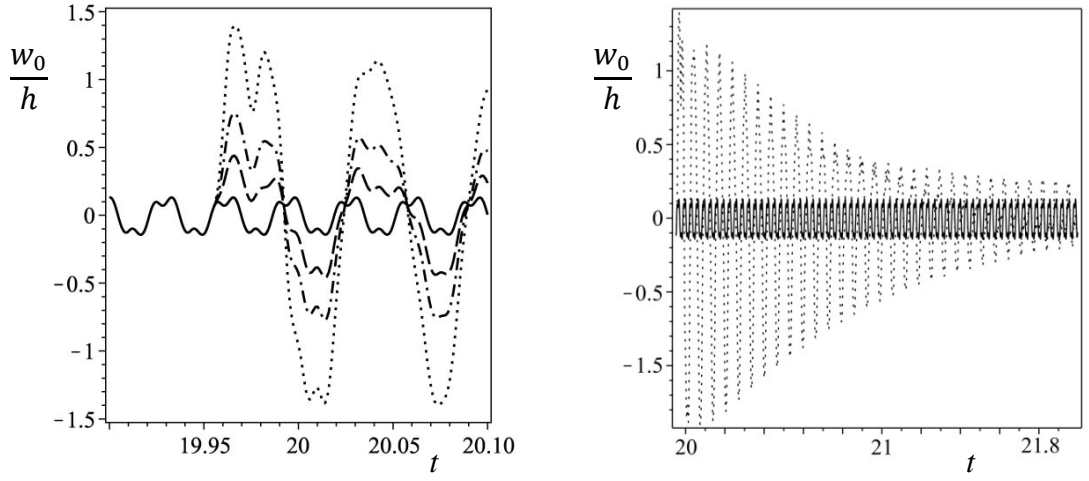

(a) (b)

Figure 9. 11. Response of the flapwise displacement $w_0(l,t)$ due to the impulsive force, —— steady state response without impulsive force, ····· response due to impulsive force with amplitude 1 N, –·–·–·– response due to impulsive force with amplitude 0.5 N, – – – – response due to impulsive force with amplitude 0.25 N, (a) response presented for short time interval, (b) longer time interval.

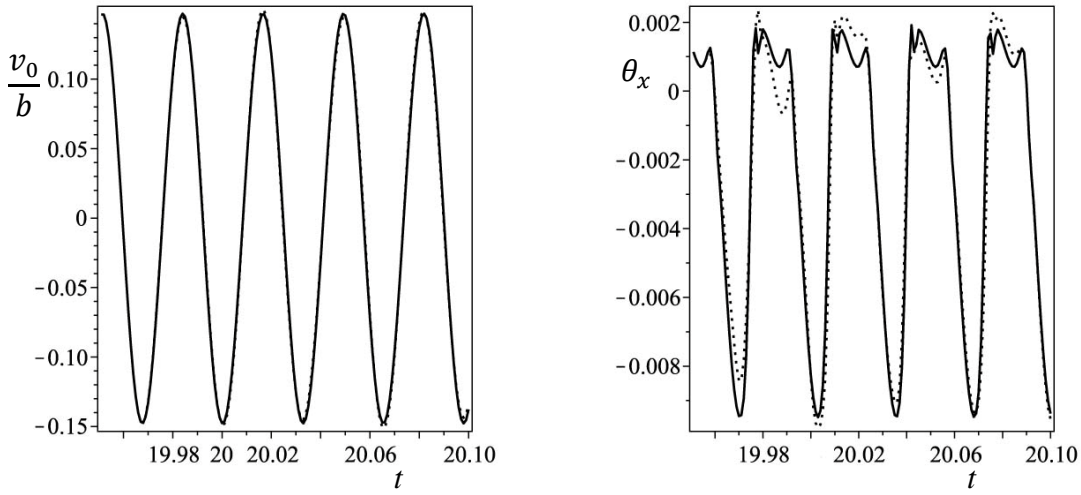

(a) (b)

Figure 9. 12. Response of (a) lagwise displacement $v_0(l,t)$ and (b) torsion $\theta_x(l,t)$ due to the impulsive force, —— steady state response without impulsive force, ····· response due to impulsive force with amplitude 1 N.

9. 3. Conclusion

The *p*-version finite element method for 3D beams that rotate about a fixed axis, which was presented in Chapter 8, is now solved in time domain. As a (necessary) preamble the natural frequencies in the linear regime were computed.

It was demonstrated that the nonlinear terms which appear in the strain-displacement relations can be quite important for cantilever beams when the applied force has a longitudinal component, which is the case of rotating beams due to the centrifugal effects.

Steady-state responses to harmonic external forces were analysed for different rotational speeds and it was shown that the amplitude of vibration may vary significantly with the speed of rotation, i.e. not only with the amplitude or the frequency of the external load. This behaviour is explained by the fact that the natural frequencies change with the speed of rotation and if a frequency becomes close to the excitation frequency, a resonance appears and the amplitude increases.

The effect of different accelerations on the transient responses were also investigated and presented. It was shown that even when the applied force excites only the flapwise displacement, the lagwise displacement is also excited due to the inertia forces of the rotation and longitudinal-lagwise couplings due to the acceleration of Coriolis. In addition, it was verified that large vibration amplitudes can be caused by the acceleration that precedes a constant rotation speed.

Impulsive forces were also applied in a steady-state regime of vibration. It was shown that an impulsive force with very small duration and somewhat small amplitude can disturb the beam vibration from the steady state regime for a long time interval.

References

[9. 1] S. Lin, K. Hsiao, Vibration Analysis of a Rotating Timoshenko Beam, *Journal of Sound and Vibration* 240 (2001) 303-322.

[9. 2] D. Hodges, M. Rutkowski, Free-Vibration Analysis of Rotating Beams by a Variable-Order Finite-Element Method, *AIAA Journal* 19 (1981) 1459-1466.

[9. 3] T. Yokoyama, Free Vibration Characteristics of Rotating Timoshenko Beams, *International Journal of Mechanical Sciences* 30 (1988) 743-755.

[9. 4] A. Bazoune, Y. Khulief, N. Stephen, Further Results for Modal Characteristics of Rotating Tapered Timoshenko Beams, *Journal of Sound and Vibration* 219 (1999) 157-174.

[9. 5] S. Lin, K. Hsiao, Vibration Analysis of a Rotating Timoshenko Beam, *Journal of Sound and Vibration* 240 (2001) 303-322.

[9. 6] H. Yoo, S. Shin, Vibration analysis or rotating cantilever beams, *Journal of Sound and Vibration* 212 (1998) 807-828.

[9. 7] A. Nayfeh, P. Pai, *Linear and Nonlinear Structural Mechanics*, John Wiley & Sons, Weinheim, 2004.

[9. 8] ANSYS Workbench User's Guide, 2009.

[9. 9] M. R. M. Crespo da Silva, C. C. Glynn, Nonlinear Flexural-Flexural-Torsional Dynamics of Inextensional Beams. I. Equation of Motion, *Journal of Structural Mechanics* 6 (1978) 437-448.

10

Conclusion

10. 1. General conclusion

3D beam structures appear in many engineering applications and are often subjected to large displacements which lead to geometrical nonlinear behaviour. Unlike in linear beam theories, both transverse displacements and torsion are coupled, involving nonlinear terms, and strong interaction between modes may exist. Due to internal resonance, the shape of vibration can change significantly and the planar vibrations can turn into vibrations in space.

In this work, vibrations of 3D beams, rotating about a fixed axes and non-rotating, with symmetrical and with non-symmetrical cross sections, were investigated, in frequency and time domains.

The beam model, which was used to carry out most of the investigations, was based on Timoshenko's theory for bending and it considers that under torsion, the cross section rotates as a rigid body, but might deform in longitudinal direction due to warping, as in Saint-Venant's theory for torsion. The equation of motion was derived by the principle of virtual work and it was transformed into ordinary differential equation by the *p*-version finite element method. Green's strain tensor was used to relate the strains with the displacements and elastic materials were considered by employing Hooke's law.

A model for beams with non-symmetrical cross sections was also developed, following the steps of the model for symmetrical cross sections. The warping function was calculated numerically, by solving the Laplace equation with Neumann boundary conditions, by the boundary element method. Gauss integration points were used to evaluate the integrals over the cross sectional area which appear in the equation of motion.

The equation of motion of beams rotating about a fixed axis, not necessarily with constant speed of rotation, was developed. The rotation was taken into account in the inertia forces. For that purpose, the absolute acceleration, which introduces the acceleration of Coriolis, centrifugal forces and additional bending-longitudinal-torsional coupling into the equation of motion, was used in the virtual work of inertia forces.

The system of nonlinear ordinary differential equations was solved in time domain and frequency domain. For the time domain solutions, the Newmark method, which assumes that the acceleration is linear within the time step, was used to transform the system of nonlinear ordinary differential equations into a system of algebraic nonlinear equations. The last was solved by Newton's method.

The results in frequency domain were obtained by assuming periodic solutions, so the unknown vector of generalized coordinates was expressed in Fourier series and the harmonic balance method was implemented. With this assumption, the system of ordinary differential equations was transformed into a system of algebraic equations with an additional unknown – the frequency of vibration. The arc-length continuation method was used to solve the nonlinear system and obtain the solutions in frequency-amplitude diagrams. Stability of the solutions was studied by Floquet's theory.

Several comparisons of different models were carried out in order to choose the most appropriate model, in terms of accuracy and degrees of freedom, for the rest of the investigations in the current work. The importance of the warping function on the torsional modes; the influence of the linearization of the trigonometric functions related with the twist angle on the torsional displacements; the direct approximation of the rotations of the cross section about the transverse axes by derivatives of the transverse displacements, assumption used in Bernoulli-Euler's theory; the influence of the longitudinal terms of second order in strain-displacement relations were studied for different beams and the following numerical investigations were continued with the model based on these comparisons.

Free vibrations of beams with rectangular, therefore symmetrical, cross sections, were studied in frequency domain. Several bifurcation points were found and the corresponding secondary branches were presented and investigated. The vibrations of some of the secondary branches remained in one plane, i.e. the plane of vibration of the linear mode used to start the continuation, while some secondary branches led to

oscillations in space. It was shown that, due to a bifurcation point, even harmonics could also be excited, even when the nonlinearity is cubic. It was demonstrated that it is meaningful to neglect the longitudinal inertia and exclude the longitudinal displacement from the equation of motion. With this step, the longitudinal displacement became a quadratic function of the other displacements, and after the implementation of the harmonic balance method, it was expressed with twice more harmonics than the other displacements.

Forced vibrations due to harmonic excitations and stability of beams with rectangular cross sections were also studied in the frequency domain. A beam with square cross section was investigated because the frequencies of bending in both transverse planes are equal, and the modes may interact due to 1:1 internal resonance. A super-critical symmetry breaking bifurcation point was found near the linear natural frequency. Two stable and one unstable branches arose from that point. The stable branches were in three-dimensional space, in spite of the fact that the external force remained in one plane. A recent method to determine the stability of the solutions, based on Floquet's theory and on an appropriate selection of the eigenvalues, when harmonic balance method was adopted, was demonstrated to be efficient by validating the stable solutions with time integration method. It was also shown that by changing the excitation frequency, the plane of vibration can also change significantly.

The work was continued by investigating free and forced vibrations of beams with non-symmetrical cross sections in the frequency domain, using an L shaped cross section, as an example. The linear modes of vibration were presented and it was shown that both bending displacements and torsion were coupled even in linear analysis. Thus, in nonlinear analysis, the vibration is in space, or it can be fixed in a plane, which is not any of the planes defined by the coordinate axes. Due to a bifurcation point, which was found, the symmetry with respect to that plane was broken and the response of the beam became a motion in space. Even in the main branch, the system possesses cubic plus quadratic nonlinearity, which lead to even harmonics in the response, unlike in beams with symmetrical cross sections.

Finally, forced vibrations of rotating beams in the time domain were also investigated. The influence of the speed of rotation on the linear natural frequencies and on the steady-state responses was shown. By increasing the speed of rotation, the beam become stiffer due to the centrifugal forces which acts in longitudinal direction, thus the natural

frequencies become higher and consequently the displacements generally become smaller. But it was shown that the displacements did not always decrease; they may increase if the natural frequency becomes closer to the excitation frequency. It was shown that when the beam rotates with non-constant speed, additional forces act on the beam and their influence on the beam's response was presented. The response due to impact forces was also investigated.

10. 2. Future work

The current work can be continued in several ways. Here are given some suggestions.

With small changes, a model for fibre reinforced composite beams can be obtained and the influence of the orientation of the laminates on the dynamic behaviour of 3D beams can be studied. Furthermore, beams in composite materials with variable stiffness can also be studied, which require more significant changes of the model for deriving the equation of motion.

In what concern the geometry of the beam, models for 3D tapered beams can be easily developed. Beams with more complex cross sections can also be obtained by the proposed model. To facilitate the process, in the cases of complex cross sections, the constants of integration over the cross sectional area, which involve the warping function, can be calculated by additional finite element software.

A rigid hub radius can be introduced in the rotating beam model and the influence of its length on the nonlinear modes can be studied. A setting angle – an angle which inclines the cross section to the plane of rotation, i.e. between z and Z axes, can also be included, and its influence on the dynamic behaviour can be investigated.

A significant modification of the current work can be achieved by adopting the model for large rotations of the cross section about the transverse axes. These displacements occur in cantilever beams and introduce nonlinear inertia. The nonlinear terms of the equation of motion will not be anymore quadratic and cubic, thus the harmonic balance method can be burdensome for implementation. Other methods should be considered, for solving the system of nonlinear differential equations, such as shooting method or perturbation methods. Some modes of cantilever beams may experience softening behaviour, but this behaviour can transform into hardening due to the speed of rotation of the beam. Such

investigations, of 3D cantilever beams, rotating in a fixed plane, which may perform large displacements and large rotations of the cross section about the transverse axes, seems an interesting and important continuation of the current work.

Finally, the knowledge of the nonlinear normal modes is essential in the design of structures, and its investigations cannot be limited to beam structures. While the simple structures are good for investigating and understanding the dynamics and the nonlinear phenomenon which structures may exhibit, the real engineering applications, like aircrafts, require modelling of complex structures which result in systems with enormous degrees of freedom. Such structures can be discretized into a finite system of ordinary differential equations by finite element software and can be solved by numerical methods. The computations of such systems require solving of systems of linear equations on iterative steps (the nonlinear solution is obtained by several linear solutions, as in Newton's method used in this work), for that purpose, advanced numerical methods for solving systems of linear equations with huge number of degrees of freedom can be used, as well.

Appendix A

In this Appendix, the sub-matrices of the quadratically dependent on components of the harmonics matrix $\mathbf{K4_{33}^{HBM}(Q_w)}$ given in equation (4. 16), which results after application of the HBM in free vibration analysis, is given. The structure of the matrix is rewritten again:

$$\mathbf{K4_{33}^{HBM}(Q_w)} = \frac{1}{4}\begin{bmatrix} \mathbf{A_{11}} & \mathbf{A_{12}} & \mathbf{A_{13}} & \mathbf{A_{14}} & \mathbf{A_{15}} & \mathbf{A_{16}} \\ \mathbf{A_{12}}^{\mathrm{T}} & \mathbf{A_{22}} & \mathbf{A_{23}} & \mathbf{A_{24}} & \mathbf{A_{25}} & \mathbf{A_{26}} \\ \mathbf{A_{13}}^{\mathrm{T}} & \mathbf{A_{23}}^{\mathrm{T}} & \mathbf{A_{33}} & \mathbf{A_{34}} & \mathbf{A_{35}} & \mathbf{A_{36}} \\ \mathbf{A_{14}}^{\mathrm{T}} & \mathbf{A_{24}}^{\mathrm{T}} & \mathbf{A_{34}}^{\mathrm{T}} & \mathbf{A_{44}} & \mathbf{A_{45}} & \mathbf{A_{46}} \\ \mathbf{A_{15}}^{\mathrm{T}} & \mathbf{A_{25}}^{\mathrm{T}} & \mathbf{A_{35}}^{\mathrm{T}} & \mathbf{A_{45}}^{\mathrm{T}} & \mathbf{A_{55}} & \mathbf{A_{56}} \\ \mathbf{A_{16}}^{\mathrm{T}} & \mathbf{A_{26}}^{\mathrm{T}} & \mathbf{A_{36}}^{\mathrm{T}} & \mathbf{A_{46}}^{\mathrm{T}} & \mathbf{A_{56}}^{\mathrm{T}} & \mathbf{A_{66}} \end{bmatrix}, \tag{A1}$$

where the sub-matrices $\mathbf{A_{ij}}$ are defined as:

$$\begin{aligned} \mathbf{A_{11}} = \frac{1}{2}\,&\mathbf{K4_{33}(Q_{w_0}, Q_{w_0})} + \mathbf{K4_{33}(Q_{w_1}, Q_{w_1})} + \mathbf{K4_{33}(Q_{w_2}, Q_{w_2})} + \\ &+\mathbf{K4_{33}(Q_{w_3}, Q_{w_3})} + \mathbf{K4_{33}(Q_{w_4}, Q_{w_4})} + \mathbf{K4_{33}(Q_{w_5}, Q_{w_5})} \end{aligned} \tag{A2-1}$$

$$\begin{aligned} \mathbf{A_{12}} = &\mathbf{K4_{33}(Q_{w_0}, Q_{w_1})} + \mathbf{K4_{33}(Q_{w_1}, Q_{w_0})} + \mathbf{K4_{33}(Q_{w_1}, Q_{w_2})} + \\ &+\mathbf{K4_{33}(Q_{w_2}, Q_{w_1})} + \mathbf{K4_{33}(Q_{w_2}, Q_{w_3})} + \mathbf{K4_{33}(Q_{w_3}, Q_{w_2})} + \\ &+\mathbf{K4_{33}(Q_{w_3}, Q_{w_4})} + \mathbf{K4_{33}(Q_{w_4}, Q_{w_3})} + \mathbf{K4_{33}(Q_{w_4}, Q_{w_5})} + \mathbf{K4_{33}(Q_{w_5}, Q_{w_4})} \end{aligned} \tag{A2-2}$$

$$\begin{aligned} \mathbf{A_{13}} = &\mathbf{K4_{33}(Q_{w_4}, Q_{w_2})} + \mathbf{K4_{33}(Q_{w_1}, Q_{w_3})} + \mathbf{K4_{33}(Q_{w_5}, Q_{w_3})} + \\ &+\mathbf{K4_{33}(Q_{w_2}, Q_{w_4})} + \mathbf{K4_{33}(Q_{w_0}, Q_{w_2})} + \mathbf{K4_{33}(Q_{w_2}, Q_{w_0})} + \\ &+\mathbf{K4_{33}(Q_{w_3}, Q_{w_1})} + \mathbf{K4_{33}(Q_{w_1}, Q_{w_1})} + \mathbf{K4_{33}(Q_{w_3}, Q_{w_5})} \end{aligned} \tag{A2-3}$$

$$\begin{aligned} \mathbf{A_{14}} = &\mathbf{K4_{33}(Q_{w_3}, Q_{w_0})} + \mathbf{K4_{33}(Q_{w_4}, Q_{w_1})} + \mathbf{K4_{33}(Q_{w_2}, Q_{w_1})} + \\ &+\mathbf{K4_{33}(Q_{w_1}, Q_{w_2})} + \mathbf{K4_{33}(Q_{w_1}, Q_{w_4})} + \mathbf{K4_{33}(Q_{w_5}, Q_{w_2})} + \mathbf{K4_{33}(Q_{w_0}, Q_{w_3})} + \\ &+\mathbf{K4_{33}(Q_{w_2}, Q_{w_5})} \end{aligned} \tag{A2-4}$$

$$\begin{aligned} \mathbf{A_{15}} = &\mathbf{K4_{33}(Q_{w_2}, Q_{w_2})} + \mathbf{K4_{33}(Q_{w_5}, Q_{w_1})} + \mathbf{K4_{33}(Q_{w_0}, Q_{w_4})} + \\ &+\mathbf{K4_{33}(Q_{w_1}, Q_{w_5})} + \mathbf{K4_{33}(Q_{w_3}, Q_{w_1})} + \mathbf{K4_{33}(Q_{w_4}, Q_{w_0})} + \mathbf{K4_{33}(Q_{w_1}, Q_{w_3})} \end{aligned} \tag{A2-5}$$

$$\mathbf{A_{16}} = \mathbf{K4_{33}}(\mathbf{Q_{w_3}}, \mathbf{Q_{w_2}}) + \mathbf{K4_{33}}(\mathbf{Q_{w_0}}, \mathbf{Q_{w_5}}) + \mathbf{K4_{33}}(\mathbf{Q_{w_1}}, \mathbf{Q_{w_4}}) + \\ + \mathbf{K4_{33}}(\mathbf{Q_{w_2}}, \mathbf{Q_{w_3}}) + \mathbf{K4_{33}}(\mathbf{Q_{w_4}}, \mathbf{Q_{w_1}}) + \mathbf{K4_{33}}(\mathbf{Q_{w_5}}, \mathbf{Q_{w_0}}) \quad \text{(A2-6)}$$

$$\mathbf{A_{22}} = \mathbf{K4_{33}}(\mathbf{Q_{w_0}}, \mathbf{Q_{w_0}}) + \mathbf{K4_{33}}(\mathbf{Q_{w_0}}, \mathbf{Q_{w_2}}) + \mathbf{K4_{33}}(\mathbf{Q_{w_2}}, \mathbf{Q_{w_0}}) + \\ + 3\,\mathbf{K4_{33}}(\mathbf{Q_{w_1}}, \mathbf{Q_{w_1}}) + \mathbf{K4_{33}}(\mathbf{Q_{w_1}}, \mathbf{Q_{w_3}}) + \mathbf{K4_{33}}(\mathbf{Q_{w_3}}, \mathbf{Q_{w_1}}) + \\ + 2\,\mathbf{K4_{33}}(\mathbf{Q_{w_2}}, \mathbf{Q_{w_2}}) + \mathbf{K4_{33}}(\mathbf{Q_{w_2}}, \mathbf{Q_{w_4}}) + \\ + \mathbf{K4_{33}}(\mathbf{Q_{w_4}}, \mathbf{Q_{w_2}}) + 2\,\mathbf{K4_{33}}(\mathbf{Q_{w_3}}, \mathbf{Q_{w_3}}) + \mathbf{K4_{33}}(\mathbf{Q_{w_3}}, \mathbf{Q_{w_5}}) + \mathbf{K4_{33}}(\mathbf{Q_{w_5}}, \mathbf{Q_{w_3}}) + \\ + 2\,\mathbf{K4_{33}}(\mathbf{Q_{w_4}}, \mathbf{Q_{w_4}}) + 2\,\mathbf{K4_{33}}(\mathbf{Q_{w_5}}, \mathbf{Q_{w_5}}) \quad \text{(A2-7)}$$

$$\mathbf{A_{23}} = \mathbf{K4_{33}}(\mathbf{Q_{w_1}}, \mathbf{Q_{w_0}}) + \mathbf{K4_{33}}(\mathbf{Q_{w_0}}, \mathbf{Q_{w_3}}) + 2\,\mathbf{K4_{33}}(\mathbf{Q_{w_2}}, \mathbf{Q_{w_1}}) + \\ + \mathbf{K4_{33}}(\mathbf{Q_{w_2}}, \mathbf{Q_{w_5}}) + \mathbf{K4_{33}}(\mathbf{Q_{w_3}}, \mathbf{Q_{w_0}}) + \mathbf{K4_{33}}(\mathbf{Q_{w_2}}, \mathbf{Q_{w_3}}) + \\ + \mathbf{K4_{33}}(\mathbf{Q_{w_3}}, \mathbf{Q_{w_2}}) + \mathbf{K4_{33}}(\mathbf{Q_{w_3}}, \mathbf{Q_{w_4}}) + \mathbf{K4_{33}}(\mathbf{Q_{w_4}}, \mathbf{Q_{w_1}}) + \mathbf{K4_{33}}(\mathbf{Q_{w_4}}, \mathbf{Q_{w_3}}) + \\ + \mathbf{K4_{33}}(\mathbf{Q_{w_4}}, \mathbf{Q_{w_5}}) + \mathbf{K4_{33}}(\mathbf{Q_{w_5}}, \mathbf{Q_{w_2}}) + \mathbf{K4_{33}}(\mathbf{Q_{w_1}}, \mathbf{Q_{w_4}}) + \mathbf{K4_{33}}(\mathbf{Q_{w_0}}, \mathbf{Q_{w_1}}) + \\ + \mathbf{K4_{33}}(\mathbf{Q_{w_5}}, \mathbf{Q_{w_4}}) + 2\,\mathbf{K4_{33}}(\mathbf{Q_{w_1}}, \mathbf{Q_{w_2}}) \quad \text{(A2-8)}$$

$$\mathbf{A_{24}} = \mathbf{K4_{33}}(\mathbf{Q_{w_5}}, \mathbf{Q_{w_1}}) + \mathbf{K4_{33}}(\mathbf{Q_{w_3}}, \mathbf{Q_{w_5}}) + \mathbf{K4_{33}}(\mathbf{Q_{w_2}}, \mathbf{Q_{w_0}}) + \\ + \mathbf{K4_{33}}(\mathbf{Q_{w_4}}, \mathbf{Q_{w_0}}) + \mathbf{K4_{33}}(\mathbf{Q_{w_0}}, \mathbf{Q_{w_2}}) + \mathbf{K4_{33}}(\mathbf{Q_{w_0}}, \mathbf{Q_{w_4}}) + \mathbf{K4_{33}}(\mathbf{Q_{w_1}}, \mathbf{Q_{w_5}}) + \\ + 2\,\mathbf{K4_{33}}(\mathbf{Q_{w_3}}, \mathbf{Q_{w_1}}) + \mathbf{K4_{33}}(\mathbf{Q_{w_1}}, \mathbf{Q_{w_1}}) + \mathbf{2\,K4_{33}}(\mathbf{Q_{w_1}}, \mathbf{Q_{w_3}}) + \\ + \mathbf{K4_{33}}(\mathbf{Q_{w_2}}, \mathbf{Q_{w_2}}) + \mathbf{K4_{33}}(\mathbf{Q_{w_2}}, \mathbf{Q_{w_4}}) + \mathbf{K4_{33}}(\mathbf{Q_{w_5}}, \mathbf{Q_{w_3}}) + \mathbf{K4_{33}}(\mathbf{Q_{w_4}}, \mathbf{Q_{w_2}}) \quad \text{(A2-9)}$$

$$\mathbf{A_{25}} = \mathbf{K4_{33}}(\mathbf{Q_{w_1}}, \mathbf{Q_{w_2}}) + \mathbf{K4_{33}}(\mathbf{Q_{w_3}}, \mathbf{Q_{w_0}}) + \mathbf{K4_{33}}(\mathbf{Q_{w_2}}, \mathbf{Q_{w_1}}) + \\ + \mathbf{K4_{33}}(\mathbf{Q_{w_0}}, \mathbf{Q_{w_5}}) + \mathbf{K4_{33}}(\mathbf{Q_{w_2}}, \mathbf{Q_{w_5}}) + \mathbf{K4_{33}}(\mathbf{Q_{w_3}}, \mathbf{Q_{w_2}}) + 2\,\mathbf{K4_{33}}(\mathbf{Q_{w_4}}, \mathbf{Q_{w_1}}) + \\ + \mathbf{K4_{33}}(\mathbf{Q_{w_2}}, \mathbf{Q_{w_3}}) + 2\,\mathbf{K4_{33}}(\mathbf{Q_{w_1}}, \mathbf{Q_{w_4}}) + \mathbf{K4_{33}}(\mathbf{Q_{w_5}}, \mathbf{Q_{w_2}}) + \\ + \mathbf{K4_{33}}(\mathbf{Q_{w_0}}, \mathbf{Q_{w_3}}) + \mathbf{K4_{33}}(\mathbf{Q_{w_5}}, \mathbf{Q_{w_0}}) \quad \text{(A2-10)}$$

$$\mathbf{A_{26}} = \mathbf{K4_{33}}(\mathbf{Q_{w_3}}, \mathbf{Q_{w_3}}) + 2\,\mathbf{K4_{33}}(\mathbf{Q_{w_5}}, \mathbf{Q_{w_1}}) + \mathbf{K4_{33}}(\mathbf{Q_{w_4}}, \mathbf{Q_{w_2}}) + \\ + \mathbf{K4_{33}}(\mathbf{Q_{w_1}}, \mathbf{Q_{w_3}}) + \mathbf{K4_{33}}(\mathbf{Q_{w_2}}, \mathbf{Q_{w_4}}) + \mathbf{K4_{33}}(\mathbf{Q_{w_0}}, \mathbf{Q_{w_4}}) + \\ + 2\,\mathbf{K4_{33}}(\mathbf{Q_{w_1}}, \mathbf{Q_{w_5}}) + \mathbf{K4_{33}}(\mathbf{Q_{w_3}}, \mathbf{Q_{w_1}}) + \mathbf{K4_{33}}(\mathbf{Q_{w_2}}, \mathbf{Q_{w_2}}) + \mathbf{K4_{33}}(\mathbf{Q_{w_4}}, \mathbf{Q_{w_0}}) \quad \text{(A2-11)}$$

$$\mathbf{A_{33}} = \mathbf{K4_{33}}(\mathbf{Q_{w_1}}, \mathbf{Q_{w_3}}) + 3\,\mathbf{K4_{33}}(\mathbf{Q_{w_2}}, \mathbf{Q_{w_2}}) + \mathbf{K4_{33}}(\mathbf{Q_{w_4}}, \mathbf{Q_{w_0}}) + \\ + 2\,\mathbf{K4_{33}}(\mathbf{Q_{w_4}}, \mathbf{Q_{w_4}}) + \mathbf{K4_{33}}(\mathbf{Q_{w_5}}, \mathbf{Q_{w_1}}) + \mathbf{K4_{33}}(\mathbf{Q_{w_0}}, \mathbf{Q_{w_4}}) + \\ + \mathbf{K4_{33}}(\mathbf{Q_{w_0}}, \mathbf{Q_{w_0}}) + 2\,\mathbf{K4_{33}}(\mathbf{Q_{w_3}}, \mathbf{Q_{w_3}}) + \mathbf{K4_{33}}(\mathbf{Q_{w_1}}, \mathbf{Q_{w_5}}) + \\ + 2\,\mathbf{K4_{33}}(\mathbf{Q_{w_1}}, \mathbf{Q_{w_1}}) + \mathbf{K4_{33}}(\mathbf{Q_{w_3}}, \mathbf{Q_{w_1}}) + 2\,\mathbf{K4_{33}}(\mathbf{Q_{w_5}}, \mathbf{Q_{w_5}}) \quad \text{(A2-12)}$$

$$\mathbf{A_{34}} = \mathbf{K4_{33}}(\mathbf{Q_{w_1}}, \mathbf{Q_{w_4}}) + \mathbf{K4_{33}}(\mathbf{Q_{w_1}}, \mathbf{Q_{w_2}}) + \mathbf{K4_{33}}(\mathbf{Q_{w_4}}, \mathbf{Q_{w_1}}) + \\ + \mathbf{K4_{33}}(\mathbf{Q_{w_0}}, \mathbf{Q_{w_5}}) + \mathbf{K4_{33}}(\mathbf{Q_{w_4}}, \mathbf{Q_{w_3}}) + \mathbf{K4_{33}}(\mathbf{Q_{w_3}}, \mathbf{Q_{w_4}}) + 2\,\mathbf{K4_{33}}(\mathbf{Q_{w_2}}, \mathbf{Q_{w_3}}) + \\ + \mathbf{K4_{33}}(\mathbf{Q_{w_1}}, \mathbf{Q_{w_0}}) + 2\,\mathbf{K4_{33}}(\mathbf{Q_{w_3}}, \mathbf{Q_{w_2}}) + \mathbf{K4_{33}}(\mathbf{Q_{w_0}}, \mathbf{Q_{w_1}}) + \mathbf{K4_{33}}(\mathbf{Q_{w_4}}, \mathbf{Q_{w_5}}) + \\ + \mathbf{K4_{33}}(\mathbf{Q_{w_5}}, \mathbf{Q_{w_0}}) + \mathbf{K4_{33}}(\mathbf{Q_{w_5}}, \mathbf{Q_{w_4}}) + \mathbf{K4_{33}}(\mathbf{Q_{w_2}}, \mathbf{Q_{w_1}}) \tag{A2-13}$$

$$\mathbf{A_{35}} = \mathbf{K4_{33}}(\mathbf{Q_{w_5}}, \mathbf{Q_{w_1}}) + \mathbf{K4_{33}}(\mathbf{Q_{w_1}}, \mathbf{Q_{w_5}}) + \mathbf{K4_{33}}(\mathbf{Q_{w_5}}, \mathbf{Q_{w_3}}) + \\ + 2\,\mathbf{K4_{33}}(\mathbf{Q_{w_2}}, \mathbf{Q_{w_4}}) + \mathbf{K4_{33}}(\mathbf{Q_{w_0}}, \mathbf{Q_{w_2}}) + \mathbf{K4_{33}}(\mathbf{Q_{w_3}}, \mathbf{Q_{w_1}}) + \\ + \mathbf{K4_{33}}(\mathbf{Q_{w_1}}, \mathbf{Q_{w_1}}) + \mathbf{K4_{33}}(\mathbf{Q_{w_2}}, \mathbf{Q_{w_0}}) + \mathbf{K4_{33}}(\mathbf{Q_{w_1}}, \mathbf{Q_{w_3}}) + \mathbf{K4_{33}}(\mathbf{Q_{w_3}}, \mathbf{Q_{w_3}}) + \\ + \mathbf{K4_{33}}(\mathbf{Q_{w_3}}, \mathbf{Q_{w_5}}) + 2\,\mathbf{K4_{33}}(\mathbf{Q_{w_4}}, \mathbf{Q_{w_2}}) \tag{A2-14}$$

$$\mathbf{A_{36}} = \mathbf{K4_{33}}(\mathbf{Q_{w_4}}, \mathbf{Q_{w_1}}) + \mathbf{K4_{33}}(\mathbf{Q_{w_1}}, \mathbf{Q_{w_2}}) + \mathbf{K4_{33}}(\mathbf{Q_{w_3}}, \mathbf{Q_{w_4}}) + \\ + 2\,\mathbf{K4_{33}}(\mathbf{Q_{w_5}}, \mathbf{Q_{w_2}}) + \mathbf{K4_{33}}(\mathbf{Q_{w_3}}, \mathbf{Q_{w_0}}) + \mathbf{K4_{33}}(\mathbf{Q_{w_4}}, \mathbf{Q_{w_3}}) + \\ + \mathbf{K4_{33}}(\mathbf{Q_{w_2}}, \mathbf{Q_{w_1}}) + \mathbf{K4_{33}}(\mathbf{Q_{w_0}}, \mathbf{Q_{w_3}}) + 2\,\mathbf{K4_{33}}(\mathbf{Q_{w_2}}, \mathbf{Q_{w_5}}) + \mathbf{K4_{33}}(\mathbf{Q_{w_1}}, \mathbf{Q_{w_4}}) \tag{A2-15}$$

$$\mathbf{A_{44}} = \mathbf{K4_{33}}(\mathbf{Q_{w_5}}, \mathbf{Q_{w_1}}) + 3\,\mathbf{K4_{33}}(\mathbf{Q_{w_3}}, \mathbf{Q_{w_3}}) + \mathbf{K4_{33}}(\mathbf{Q_{w_0}}, \mathbf{Q_{w_0}}) + \\ + 2\,\mathbf{K4_{33}}(\mathbf{Q_{w_4}}, \mathbf{Q_{w_4}}) + 2\,\mathbf{K4_{33}}(\mathbf{Q_{w_5}}, \mathbf{Q_{w_5}}) + \mathbf{K4_{33}}(\mathbf{Q_{w_1}}, \mathbf{Q_{w_5}}) + \\ + 2\,\mathbf{K4_{33}}(\mathbf{Q_{w_1}}, \mathbf{Q_{w_1}}) + 2\,\mathbf{K4_{33}}(\mathbf{Q_{w_2}}, \mathbf{Q_{w_2}}) + \mathbf{K4_{33}}(\mathbf{Q_{w_2}}, \mathbf{Q_{w_4}}) + \mathbf{K4_{33}}(\mathbf{Q_{w_4}}, \mathbf{Q_{w_2}}) \tag{A2-16}$$

$$\mathbf{A_{45}} = \mathbf{K4_{33}}(\mathbf{Q_{w_1}}, \mathbf{Q_{w_2}}) + \mathbf{K4_{33}}(\mathbf{Q_{w_2}}, \mathbf{Q_{w_1}}) + \mathbf{K4_{33}}(\mathbf{Q_{w_0}}, \mathbf{Q_{w_1}}) + \\ + \mathbf{K4_{33}}(\mathbf{Q_{w_4}}, \mathbf{Q_{w_5}}) + 2\,\mathbf{K4_{33}}(\mathbf{Q_{w_4}}, \mathbf{Q_{w_3}}) + 2\,\mathbf{K4_{33}}(\mathbf{Q_{w_3}}, \mathbf{Q_{w_4}}) + \\ + \mathbf{K4_{33}}(\mathbf{Q_{w_5}}, \mathbf{Q_{w_4}}) + \mathbf{K4_{33}}(\mathbf{Q_{w_1}}, \mathbf{Q_{w_0}}) + \mathbf{K4_{33}}(\mathbf{Q_{w_2}}, \mathbf{Q_{w_5}}) + \mathbf{K4_{33}}(\mathbf{Q_{w_3}}, \mathbf{Q_{w_2}}) + \\ + \mathbf{K4_{33}}(\mathbf{Q_{w_2}}, \mathbf{Q_{w_3}}) + \mathbf{K4_{33}}(\mathbf{Q_{w_5}}, \mathbf{Q_{w_2}}) \tag{A2-17}$$

$$\mathbf{A_{46}} = \mathbf{K4_{33}}(\mathbf{Q_{w_4}}, \mathbf{Q_{w_2}}) + \mathbf{K4_{33}}(\mathbf{Q_{w_1}}, \mathbf{Q_{w_3}}) + \mathbf{K4_{33}}(\mathbf{Q_{w_2}}, \mathbf{Q_{w_0}}) + \\ + \mathbf{K4_{33}}(\mathbf{Q_{w_0}}, \mathbf{Q_{w_2}}) + 2\,\mathbf{K4_{33}}(\mathbf{Q_{w_3}}, \mathbf{Q_{w_5}}) + 2\,\mathbf{K4_{33}}(\mathbf{Q_{w_5}}, \mathbf{Q_{w_3}}) + \\ + \mathbf{K4_{33}}(\mathbf{Q_{w_4}}, \mathbf{Q_{w_4}}) + \mathbf{K4_{33}}(\mathbf{Q_{w_1}}, \mathbf{Q_{w_1}}) + \mathbf{K4_{33}}(\mathbf{Q_{w_2}}, \mathbf{Q_{w_4}}) + \mathbf{K4_{33}}(\mathbf{Q_{w_3}}, \mathbf{Q_{w_1}}) \tag{A2-18}$$

$$\mathbf{A_{55}} = 2\,\mathbf{K4_{33}}(\mathbf{Q_{w_3}}, \mathbf{Q_{w_3}}) + \mathbf{K4_{33}}(\mathbf{Q_{w_3}}, \mathbf{Q_{w_5}}) + 2\,\mathbf{K4_{33}}(\mathbf{Q_{w_1}}, \mathbf{Q_{w_1}}) + \\ + \mathbf{K4_{33}}(\mathbf{Q_{w_5}}, \mathbf{Q_{w_3}}) + \mathbf{K4_{33}}(\mathbf{Q_{w_0}}, \mathbf{Q_{w_0}}) + 3\,\mathbf{K4_{33}}(\mathbf{Q_{w_4}}, \mathbf{Q_{w_4}}) + \\ + 2\,\mathbf{K4_{33}}(\mathbf{Q_{w_5}}, \mathbf{Q_{w_5}}) + 2\,\mathbf{K4_{33}}(\mathbf{Q_{w_2}}, \mathbf{Q_{w_2}}) \tag{A2-19}$$

$$\mathbf{A_{56}} = \mathbf{K4_{33}}(\mathbf{Q_{w_3}}, \mathbf{Q_{w_4}}) + 2\,\mathbf{K4_{33}}(\mathbf{Q_{w_5}}, \mathbf{Q_{w_4}}) + \mathbf{K4_{33}}(\mathbf{Q_{w_1}}, \mathbf{Q_{w_0}}) + \\ + \mathbf{K4_{33}}(\mathbf{Q_{w_1}}, \mathbf{Q_{w_2}}) + 2\,\mathbf{K4_{33}}(\mathbf{Q_{w_4}}, \mathbf{Q_{w_5}}) + \mathbf{K4_{33}}(\mathbf{Q_{w_2}}, \mathbf{Q_{w_1}}) + \mathbf{K4_{33}}(\mathbf{Q_{w_0}}, \mathbf{Q_{w_1}}) + \\ + \mathbf{K4_{33}}(\mathbf{Q_{w_4}}, \mathbf{Q_{w_3}}) + \mathbf{K4_{33}}(\mathbf{Q_{w_3}}, \mathbf{Q_{w_2}}) \tag{A2-20}$$

$$\mathbf{A_{66}} = 3\,\mathbf{K4_{33}}\left(\mathbf{Q_{w_5}}, \mathbf{Q_{w_5}}\right) + 2\,\mathbf{K4_{33}}\left(\mathbf{Q_{w_4}}, \mathbf{Q_{w_4}}\right) + 2\,\mathbf{K4_{33}}\left(\mathbf{Q_{w_2}}, \mathbf{Q_{w_2}}\right) + \\ +2\,\mathbf{K4_{33}}\left(\mathbf{Q_{w_1}}, \mathbf{Q_{w_1}}\right) + 2\,\mathbf{K4_{33}}\left(\mathbf{Q_{w_3}}, \mathbf{Q_{w_3}}\right) + \mathbf{K4_{33}}\left(\mathbf{Q_{w_0}}, \mathbf{Q_{w_0}}\right) \tag{A2-21}$$

The matrices $\mathbf{K4_{33}}\left(\mathbf{Q_{w_i}}, \mathbf{Q_{w_j}}\right)$, used to define $\mathbf{K4_{33}^{HBM}}(\mathbf{Q_w})$, are given in equation (2. 63c), where only the terms which depend on $\{q_w\}$ are used, but now these terms depend on the coefficients of the harmonics of $\{q_w\}$ - $\mathbf{Q_{w_i}}$ and $\mathbf{Q_{w_j}}$:

$$\mathbf{K4_{33}}\left(\mathbf{Q_{w_i}}, \mathbf{Q_{w_j}}\right) = \frac{1}{2}E\int_V \frac{d\lfloor N^w\rfloor^{\mathrm{T}}}{dx}\frac{d\lfloor N^w\rfloor}{dx}\left(\frac{d\lfloor N^w\rfloor}{dx}\{\mathrm{Q_{w_i}}\}\frac{d\lfloor N^w\rfloor}{dx}\{\mathrm{Q_{w_j}}\}\right)dV. \tag{A3}$$

In equation (A3), one should note that $\frac{d\lfloor N^w\rfloor}{dx}\{\mathrm{Q_{w_i}}\}$ is a scalar. The sub-matrices $\mathbf{K4_{33}^{HBM}}(\mathbf{Q_v})$ and $\mathbf{K4_{33}^{HBM}}\left(\mathbf{Q_{\theta_x}}\right)$ from equation (4. 15) are defined on the same way, like in equation (A1), but using the coefficients of harmonics of $\{q_v\}$ and $\{q_{\theta_x}\}$ instead of the coefficient of the harmonics of $\{q_w\}$.

The sub-matrix $\mathbf{K4_{33}^{HBM^*}}(\mathbf{Q_w})$ is also defined like in equation (A1), but the matrices $\mathbf{K4_{33}}\left(\mathbf{Q_{w_i}}, \mathbf{Q_{w_j}}\right)$ should be replaced by $\mathbf{K2_{13}}\left(\mathbf{Q_{w_i}}\right)^{\mathrm{T}}\mathbf{K1_{11}}^{-1}\mathbf{K2_{13}}\left(\mathbf{Q_{w_j}}\right)$. This formulation comes from equation (4. 4) which is result of neglecting the longitudinal inertia. Furthermore:

$$\mathbf{K2_{13}}\left(\mathbf{Q_{w_i}}\right) = \frac{1}{2}E\int_V \frac{d\lfloor N^u\rfloor^{\mathrm{T}}}{dx}\frac{d\lfloor N^w\rfloor}{dx}\left(\frac{d\lfloor N^w\rfloor}{dx}\{\mathrm{Q_{w_i}}\}\right)dV \tag{A4}$$

is defined in equation (2. 53b) but here the coefficients of the harmonics are used.

Appendix B

In this Appendix, the sub-matrices of the quadratically dependent on components of the harmonics matrix $\mathbf{K4_{33}^{HBM}(Q_w)}$ given in equation (6. 31), which results after application of the HBM in forced vibration analysis, is given. The structure of the matrix is rewritten again:

$$\mathbf{K4_{33}^{HBM}(Q_w)} = \frac{1}{4}\begin{bmatrix} \mathbf{A_{11}} & \mathbf{A_{12}} & \mathbf{A_{13}} & \mathbf{A_{14}} & \mathbf{A_{15}} & \mathbf{A_{16}} & \mathbf{A_{17}} \\ \mathbf{A_{12}}^{\mathrm{T}} & \mathbf{A_{22}} & \mathbf{A_{23}} & \mathbf{A_{24}} & \mathbf{A_{25}} & \mathbf{A_{26}} & \mathbf{A_{27}} \\ \mathbf{A_{13}}^{\mathrm{T}} & \mathbf{A_{23}}^{\mathrm{T}} & \mathbf{A_{33}} & \mathbf{A_{34}} & \mathbf{A_{35}} & \mathbf{A_{36}} & \mathbf{A_{37}} \\ \mathbf{A_{14}}^{\mathrm{T}} & \mathbf{A_{24}}^{\mathrm{T}} & \mathbf{A_{34}}^{\mathrm{T}} & \mathbf{A_{44}} & \mathbf{A_{45}} & \mathbf{A_{46}} & \mathbf{A_{47}} \\ \mathbf{A_{15}}^{\mathrm{T}} & \mathbf{A_{25}}^{\mathrm{T}} & \mathbf{A_{35}}^{\mathrm{T}} & \mathbf{A_{45}}^{\mathrm{T}} & \mathbf{A_{55}} & \mathbf{A_{56}} & \mathbf{A_{57}} \\ \mathbf{A_{16}}^{\mathrm{T}} & \mathbf{A_{26}}^{\mathrm{T}} & \mathbf{A_{36}}^{\mathrm{T}} & \mathbf{A_{46}}^{\mathrm{T}} & \mathbf{A_{56}}^{\mathrm{T}} & \mathbf{A_{66}} & \mathbf{A_{67}} \\ \mathbf{A_{17}}^{\mathrm{T}} & \mathbf{A_{27}}^{\mathrm{T}} & \mathbf{A_{37}}^{\mathrm{T}} & \mathbf{A_{47}}^{\mathrm{T}} & \mathbf{A_{57}}^{\mathrm{T}} & \mathbf{A_{67}}^{\mathrm{T}} & \mathbf{A_{77}} \end{bmatrix}, \tag{B1}$$

where the sub-matrices $\mathbf{A_{ij}}$ are defined as:

$$\begin{aligned} \mathbf{A_{11}} = \frac{\mathbf{1}}{\mathbf{2}}\,&\mathbf{K4_{33}(Q_{w_0}, Q_{w_0})} + \mathbf{K4_{33}(Q_{w_1}, Q_{w_1})} + \mathbf{K4_{33}(Q_{w_2}, Q_{w_2})} + \\ &+\mathbf{K4_{33}(Q_{w_3}, Q_{w_3})} + \mathbf{K4_{33}(Q_{w_4}, Q_{w_4})} + \mathbf{K4_{33}(Q_{w_5}, Q_{w_5})} + \mathbf{K4_{33}(Q_{w_6}, Q_{w_6})} \end{aligned} \tag{B2-1}$$

$$\begin{aligned} \mathbf{A_{12}} = \,&\mathbf{K4_{33}(Q_{w_4}, Q_{w_2})} + \mathbf{K4_{33}(Q_{w_4}, Q_{w_6})} + \mathbf{K4_{33}(Q_{w_3}, Q_{w_5})} + \\ &+\mathbf{K4_{33}(Q_{w_3}, Q_{w_1})} + \mathbf{K4_{33}(Q_{w_2}, Q_{w_4})} + \mathbf{K4_{33}(Q_{w_1}, Q_{w_0})} + \mathbf{K4_{33}(Q_{w_6}, Q_{w_4})} + \\ &+\mathbf{K4_{33}(Q_{w_0}, Q_{w_1})} + \mathbf{K4_{33}(Q_{w_1}, Q_{w_3})} + \mathbf{K4_{33}(Q_{w_5}, Q_{w_3})} \end{aligned} \tag{B2-2}$$

$$\begin{aligned} \mathbf{A_{13}} = \,&-\mathbf{K4_{33}(Q_{w_2}, Q_{w_3})} - \mathbf{K4_{33}(Q_{w_5}, Q_{w_4})} + \mathbf{K4_{33}(Q_{w_3}, Q_{w_6})} + \\ &+\mathbf{K4_{33}(Q_{w_0}, Q_{w_2})} + \mathbf{K4_{33}(Q_{w_1}, Q_{w_4})} - \mathbf{K4_{33}(Q_{w_3}, Q_{w_2})} + \mathbf{K4_{33}(Q_{w_2}, Q_{w_0})} - \\ &-\mathbf{K4_{33}(Q_{w_4}, Q_{w_5})} + \mathbf{K4_{33}(Q_{w_6}, Q_{w_3})} + \mathbf{K4_{33}(Q_{w_4}, Q_{w_1})} \end{aligned} \tag{B2-3}$$

$$\begin{aligned} \mathbf{A_{14}} = \,&\mathbf{K4_{33}(Q_{w_2}, Q_{w_6})} + \mathbf{K4_{33}(Q_{w_1}, Q_{w_1})} + \mathbf{K4_{33}(Q_{w_0}, Q_{w_3})} - \\ &-\mathbf{K4_{33}(Q_{w_2}, Q_{w_2})} + \mathbf{K4_{33}(Q_{w_1}, Q_{w_5})} + \mathbf{K4_{33}(Q_{w_5}, Q_{w_1})} + \mathbf{K4_{33}(Q_{w_3}, Q_{w_0})} + \\ &+\mathbf{K4_{33}(Q_{w_6}, Q_{w_2})} \end{aligned} \tag{B2-4}$$

$$\begin{aligned} \mathbf{A_{15}} = \,&\mathbf{K4_{33}(Q_{w_6}, Q_{w_1})} + \mathbf{K4_{33}(Q_{w_2}, Q_{w_1})} + \mathbf{K4_{33}(Q_{w_1}, Q_{w_2})} - \\ &-\mathbf{K4_{33}(Q_{w_2}, Q_{w_5})} - \mathbf{K4_{33}(Q_{w_5}, Q_{w_2})} + \mathbf{K4_{33}(Q_{w_0}, Q_{w_4})} + \mathbf{K4_{33}(Q_{w_1}, Q_{w_6})} + \\ &+\mathbf{K4_{33}(Q_{w_4}, Q_{w_0})} \end{aligned} \tag{B2-5}$$

$$\mathbf{A_{16}} = \mathbf{K4_{33}}(\mathbf{Q_{w_1}}, \mathbf{Q_{w_3}}) + \mathbf{K4_{33}}(\mathbf{Q_{w_3}}, \mathbf{Q_{w_1}}) - \mathbf{K4_{33}}(\mathbf{Q_{w_4}}, \mathbf{Q_{w_2}}) + \\ + \mathbf{K4_{33}}(\mathbf{Q_{w_5}}, \mathbf{Q_{w_0}}) + \mathbf{K4_{33}}(\mathbf{Q_{w_0}}, \mathbf{Q_{w_5}}) - \mathbf{K4_{33}}(\mathbf{Q_{w_2}}, \mathbf{Q_{w_4}}) \quad \text{(B2-6)}$$

$$\mathbf{A_{17}} = \mathbf{K4_{33}}(\mathbf{Q_{w_6}}, \mathbf{Q_{w_0}}) + \mathbf{K4_{33}}(\mathbf{Q_{w_0}}, \mathbf{Q_{w_6}}) + \mathbf{K4_{33}}(\mathbf{Q_{w_4}}, \mathbf{Q_{w_1}}) + \\ + \mathbf{K4_{33}}(\mathbf{Q_{w_2}}, \mathbf{Q_{w_3}}) + \mathbf{K4_{33}}(\mathbf{Q_{w_3}}, \mathbf{Q_{w_2}}) + \mathbf{K4_{33}}(\mathbf{Q_{w_1}}, \mathbf{Q_{w_4}}) \quad \text{(B2-7)}$$

$$\mathbf{A_{22}} = \mathbf{K4_{33}}(\mathbf{Q_{w_0}}, \mathbf{Q_{w_3}}) + \mathbf{K4_{33}}(\mathbf{Q_{w_0}}, \mathbf{Q_{w_0}}) + 3\,\mathbf{K4_{33}}(\mathbf{Q_{w_1}}, \mathbf{Q_{w_1}}) + \\ + \mathbf{K4_{33}}(\mathbf{Q_{w_1}}, \mathbf{Q_{w_5}}) + \mathbf{K4_{33}}(\mathbf{Q_{w_5}}, \mathbf{Q_{w_1}}) + 2\,\mathbf{K4_{33}}(\mathbf{Q_{w_3}}, \mathbf{Q_{w_3}}) + \mathbf{K4_{33}}(\mathbf{Q_{w_6}}, \mathbf{Q_{w_2}}) + \\ + 2\,\mathbf{K4_{33}}(\mathbf{Q_{w_6}}, \mathbf{Q_{w_6}}) + 2\,\mathbf{K4_{33}}(\mathbf{Q_{w_4}}, \mathbf{Q_{w_4}}) + 2\,\mathbf{K4_{33}}(\mathbf{Q_{w_5}}, \mathbf{Q_{w_5}}) + \\ + \mathbf{K4_{33}}(\mathbf{Q_{w_2}}, \mathbf{Q_{w_6}}) + \mathbf{K4_{33}}(\mathbf{Q_{w_2}}, \mathbf{Q_{w_2}}) + \mathbf{K4_{33}}(\mathbf{Q_{w_3}}, \mathbf{Q_{w_0}}) \quad \text{(B2-8)}$$

$$\mathbf{A_{23}} = \mathbf{K4_{33}}(\mathbf{Q_{w_1}}, \mathbf{Q_{w_2}}) + \mathbf{K4_{33}}(\mathbf{Q_{w_6}}, \mathbf{Q_{w_1}}) + \mathbf{K4_{33}}(\mathbf{Q_{w_0}}, \mathbf{Q_{w_4}}) - \\ - \mathbf{K4_{33}}(\mathbf{Q_{w_2}}, \mathbf{Q_{w_5}}) + \mathbf{K4_{33}}(\mathbf{Q_{w_1}}, \mathbf{Q_{w_6}}) + \mathbf{K4_{33}}(\mathbf{Q_{w_2}}, \mathbf{Q_{w_1}}) + \mathbf{K4_{33}}(\mathbf{Q_{w_4}}, \mathbf{Q_{w_0}}) - \\ - \mathbf{K4_{33}}(\mathbf{Q_{w_5}}, \mathbf{Q_{w_2}}) \quad \text{(B2-9)}$$

$$\mathbf{A_{24}} = 2\,\mathbf{K4_{33}}(\mathbf{Q_{w_3}}, \mathbf{Q_{w_1}}) + \mathbf{K4_{33}}(\mathbf{Q_{w_3}}, \mathbf{Q_{w_5}}) + \mathbf{K4_{33}}(\mathbf{Q_{w_1}}, \mathbf{Q_{w_0}}) + \\ + \mathbf{K4_{33}}(\mathbf{Q_{w_6}}, \mathbf{Q_{w_4}}) + \mathbf{K4_{33}}(\mathbf{Q_{w_5}}, \mathbf{Q_{w_3}}) + \mathbf{K4_{33}}(\mathbf{Q_{w_0}}, \mathbf{Q_{w_1}}) + \mathbf{K4_{33}}(\mathbf{Q_{w_4}}, \mathbf{Q_{w_6}}) + \\ + \mathbf{K4_{33}}(\mathbf{Q_{w_5}}, \mathbf{Q_{w_0}}) + \mathbf{K4_{33}}(\mathbf{Q_{w_0}}, \mathbf{Q_{w_5}}) + 2\,\mathbf{K4_{33}}(\mathbf{Q_{w_1}}, \mathbf{Q_{w_3}}) \quad \text{(B2-10)}$$

$$\mathbf{A_{25}} = \mathbf{K4_{33}}(\mathbf{Q_{w_3}}, \mathbf{Q_{w_6}}) + 2\,\mathbf{K4_{33}}(\mathbf{Q_{w_4}}, \mathbf{Q_{w_1}}) + \mathbf{K4_{33}}(\mathbf{Q_{w_0}}, \mathbf{Q_{w_6}}) + \\ + 2\,\mathbf{K4_{33}}(\mathbf{Q_{w_1}}, \mathbf{Q_{w_4}}) + \mathbf{K4_{33}}(\mathbf{Q_{w_2}}, \mathbf{Q_{w_0}}) - \mathbf{K4_{33}}(\mathbf{Q_{w_4}}, \mathbf{Q_{w_5}}) + \mathbf{K4_{33}}(\mathbf{Q_{w_6}}, \mathbf{Q_{w_0}}) - \\ - \mathbf{K4_{33}}(\mathbf{Q_{w_5}}, \mathbf{Q_{w_4}}) + \mathbf{K4_{33}}(\mathbf{Q_{w_0}}, \mathbf{Q_{w_2}}) + \mathbf{K4_{33}}(\mathbf{Q_{w_6}}, \mathbf{Q_{w_3}}) \quad \text{(B2-11)}$$

$$\mathbf{A_{26}} = \mathbf{K4_{33}}(\mathbf{Q_{w_3}}, \mathbf{Q_{w_0}}) + \mathbf{K4_{33}}(\mathbf{Q_{w_1}}, \mathbf{Q_{w_1}}) + \mathbf{K4_{33}}(\mathbf{Q_{w_3}}, \mathbf{Q_{w_3}}) - \\ - \mathbf{K4_{33}}(\mathbf{Q_{w_2}}, \mathbf{Q_{w_2}}) + \mathbf{2}\,\mathbf{K4_{33}}(\mathbf{Q_{w_5}}, \mathbf{Q_{w_1}}) + 2\,\mathbf{K4_{33}}(\mathbf{Q_{w_1}}, \mathbf{Q_{w_5}}) - \\ - \mathbf{K4_{33}}(\mathbf{Q_{w_4}}, \mathbf{Q_{w_4}}) + \mathbf{K4_{33}}(\mathbf{Q_{w_0}}, \mathbf{Q_{w_3}}) \quad \text{(B2-12)}$$

$$\mathbf{A_{27}} = \mathbf{K4_{33}}(\mathbf{Q_{w_1}}, \mathbf{Q_{w_2}}) + \mathbf{K4_{33}}(\mathbf{Q_{w_4}}, \mathbf{Q_{w_0}}) + \mathbf{K4_{33}}(\mathbf{Q_{w_4}}, \mathbf{Q_{w_3}}) + \\ + \mathbf{K4_{33}}(\mathbf{Q_{w_3}}, \mathbf{Q_{w_4}}) + 2\,\mathbf{K4_{33}}(\mathbf{Q_{w_6}}, \mathbf{Q_{w_1}}) + 2\,\mathbf{K4_{33}}(\mathbf{Q_{w_1}}, \mathbf{Q_{w_6}}) + \\ + \mathbf{K4_{33}}(\mathbf{Q_{w_2}}, \mathbf{Q_{w_1}}) + \mathbf{K4_{33}}(\mathbf{Q_{w_0}}, \mathbf{Q_{w_4}}) \quad \text{(B2-13)}$$

$$\mathbf{A_{33}} = 3\,\mathbf{K4_{33}}(\mathbf{Q_{w_2}}, \mathbf{Q_{w_2}}) - \mathbf{K4_{33}}(\mathbf{Q_{w_1}}, \mathbf{Q_{w_5}}) + 2\,\mathbf{K4_{33}}(\mathbf{Q_{w_6}}, \mathbf{Q_{w_6}}) + \\ + \mathbf{K4_{33}}(\mathbf{Q_{w_0}}, \mathbf{Q_{w_0}}) + 2\,\mathbf{K4_{33}}(\mathbf{Q_{w_3}}, \mathbf{Q_{w_3}}) - \mathbf{K4_{33}}(\mathbf{Q_{w_6}}, \mathbf{Q_{w_2}}) + \mathbf{K4_{33}}(\mathbf{Q_{w_1}}, \mathbf{Q_{w_1}}) - \\ - \mathbf{K4_{33}}(\mathbf{Q_{w_0}}, \mathbf{Q_{w_3}}) - \mathbf{K4_{33}}(\mathbf{Q_{w_2}}, \mathbf{Q_{w_6}}) - \mathbf{K4_{33}}(\mathbf{Q_{w_5}}, \mathbf{Q_{w_1}}) + 2\,\mathbf{K4_{33}}(\mathbf{Q_{w_5}}, \mathbf{Q_{w_5}}) + \\ + 2\,\mathbf{K4_{33}}(\mathbf{Q_{w_4}}, \mathbf{Q_{w_4}}) - \mathbf{K4_{33}}(\mathbf{Q_{w_3}}, \mathbf{Q_{w_0}}) \quad \text{(B2-14)}$$

$$\mathbf{A_{34}} = -\mathbf{K4_{33}}(\mathbf{Q_{w_3}}, \mathbf{Q_{w_6}}) + \mathbf{K4_{33}}(\mathbf{Q_{w_6}}, \mathbf{Q_{w_0}}) + \mathbf{K4_{33}}(\mathbf{Q_{w_4}}, \mathbf{Q_{w_5}}) - \\ -\mathbf{K4_{33}}(\mathbf{Q_{w_0}}, \mathbf{Q_{w_2}}) + 2\,\mathbf{K4_{33}}(\mathbf{Q_{w_3}}, \mathbf{Q_{w_2}}) + \mathbf{K4_{33}}(\mathbf{Q_{w_0}}, \mathbf{Q_{w_6}}) - \mathbf{K4_{33}}(\mathbf{Q_{w_2}}, \mathbf{Q_{w_0}}) - \\ -\mathbf{K4_{33}}(\mathbf{Q_{w_6}}, \mathbf{Q_{w_3}}) + 2\,\mathbf{K4_{33}}(\mathbf{Q_{w_2}}, \mathbf{Q_{w_3}}) + \mathbf{K4_{33}}(\mathbf{Q_{w_5}}, \mathbf{Q_{w_4}}) \quad \text{(B2-15)}$$

$$\mathbf{A_{35}} = \mathbf{K4_{33}}(\mathbf{Q_{w_4}}, \mathbf{Q_{w_6}}) + \mathbf{K4_{33}}(\mathbf{Q_{w_6}}, \mathbf{Q_{w_4}}) - \mathbf{K4_{33}}(\mathbf{Q_{w_0}}, \mathbf{Q_{w_5}}) + \\ +\mathbf{K4_{33}}(\mathbf{Q_{w_0}}, \mathbf{Q_{w_1}}) - \mathbf{K4_{33}}(\mathbf{Q_{w_5}}, \mathbf{Q_{w_0}}) + 2\,\mathbf{K4_{33}}(\mathbf{Q_{w_2}}, \mathbf{Q_{w_4}}) + \mathbf{K4_{33}}(\mathbf{Q_{w_3}}, \mathbf{Q_{w_5}}) + \\ +2\,\mathbf{K4_{33}}(\mathbf{Q_{w_4}}, \mathbf{Q_{w_2}}) + \mathbf{K4_{33}}(\mathbf{Q_{w_1}}, \mathbf{Q_{w_0}}) + \mathbf{K4_{33}}(\mathbf{Q_{w_5}}, \mathbf{Q_{w_3}}) \quad \text{(B2-16)}$$

$$\mathbf{A_{36}} = \mathbf{K4_{33}}(\mathbf{Q_{w_3}}, \mathbf{Q_{w_4}}) + 2\,\mathbf{K4_{33}}(\mathbf{Q_{w_5}}, \mathbf{Q_{w_2}}) - \mathbf{K4_{33}}(\mathbf{Q_{w_1}}, \mathbf{Q_{w_2}}) - \\ -\mathbf{K4_{33}}(\mathbf{Q_{w_2}}, \mathbf{Q_{w_1}}) - \mathbf{K4_{33}}(\mathbf{Q_{w_4}}, \mathbf{Q_{w_0}}) + \mathbf{K4_{33}}(\mathbf{Q_{w_4}}, \mathbf{Q_{w_3}}) + 2\,\mathbf{K4_{33}}(\mathbf{Q_{w_2}}, \mathbf{Q_{w_5}}) - \\ -\mathbf{K4_{33}}(\mathbf{Q_{w_0}}, \mathbf{Q_{w_4}}) \quad \text{(B2-17)}$$

$$\mathbf{A_{37}} = \mathbf{K4_{33}}(\mathbf{Q_{w_4}}, \mathbf{Q_{w_4}}) - 2\,\mathbf{K4_{33}}(\mathbf{Q_{w_3}}, \mathbf{Q_{w_3}}) + 2\,\mathbf{K4_{33}}(\mathbf{Q_{w_6}}, \mathbf{Q_{w_2}}) + \\ +\mathbf{K4_{33}}(\mathbf{Q_{w_3}}, \mathbf{Q_{w_0}}) - \mathbf{K4_{33}}(\mathbf{Q_{w_2}}, \mathbf{Q_{w_2}}) + 2\,\mathbf{K4_{33}}(\mathbf{Q_{w_2}}, \mathbf{Q_{w_6}}) + \mathbf{K4_{33}}(\mathbf{Q_{w_1}}, \mathbf{Q_{w_1}}) + \\ +\mathbf{K4_{33}}(\mathbf{Q_{w_0}}, \mathbf{Q_{w_3}}) \quad \text{(B2-18)}$$

$$\mathbf{A_{44}} = -\mathbf{K4_{33}}(\mathbf{Q_{w_2}}, \mathbf{Q_{w_6}}) - \mathbf{K4_{33}}(\mathbf{Q_{w_6}}, \mathbf{Q_{w_2}}) + 2\,\mathbf{K4_{33}}(\mathbf{Q_{w_1}}, \mathbf{Q_{w_1}}) + \\ +\mathbf{K4_{33}}(\mathbf{Q_{w_4}}, \mathbf{Q_{w_4}}) + 3\,\mathbf{K4_{33}}(\mathbf{Q_{w_3}}, \mathbf{Q_{w_3}}) + \mathbf{K4_{33}}(\mathbf{Q_{w_0}}, \mathbf{Q_{w_0}}) + \\ +2\,\mathbf{K4_{33}}(\mathbf{Q_{w_6}}, \mathbf{Q_{w_6}}) + \mathbf{K4_{33}}(\mathbf{Q_{w_1}}, \mathbf{Q_{w_5}}) + 2\,\mathbf{K4_{33}}(\mathbf{Q_{w_5}}, \mathbf{Q_{w_5}}) + \\ +\mathbf{K4_{33}}(\mathbf{Q_{w_5}}, \mathbf{Q_{w_1}}) + 2\,\mathbf{K4_{33}}(\mathbf{Q_{w_2}}, \mathbf{Q_{w_2}}) \quad \text{(B2-19)}$$

$$\mathbf{A_{45}} = \mathbf{K4_{33}}(\mathbf{Q_{w_6}}, \mathbf{Q_{w_1}}) + \mathbf{K4_{33}}(\mathbf{Q_{w_5}}, \mathbf{Q_{w_2}}) + \mathbf{K4_{33}}(\mathbf{Q_{w_2}}, \mathbf{Q_{w_5}}) + \\ +\mathbf{K4_{33}}(\mathbf{Q_{w_4}}, \mathbf{Q_{w_3}}) + \mathbf{K4_{33}}(\mathbf{Q_{w_3}}, \mathbf{Q_{w_4}}) + \mathbf{K4_{33}}(\mathbf{Q_{w_1}}, \mathbf{Q_{w_6}}) \quad \text{(B2-20)}$$

$$\mathbf{A_{46}} = \mathbf{K4_{33}}(\mathbf{Q_{w_1}}, \mathbf{Q_{w_3}}) + \mathbf{K4_{33}}(\mathbf{Q_{w_3}}, \mathbf{Q_{w_1}}) + \mathbf{K4_{33}}(\mathbf{Q_{w_4}}, \mathbf{Q_{w_2}}) + \\ +2\,\mathbf{K4_{33}}(\mathbf{Q_{w_3}}, \mathbf{Q_{w_5}}) + \mathbf{K4_{33}}(\mathbf{Q_{w_0}}, \mathbf{Q_{w_1}}) + \mathbf{2}\,\mathbf{K4_{33}}(\mathbf{Q_{w_5}}, \mathbf{Q_{w_3}}) + \\ +\mathbf{K4_{33}}(\mathbf{Q_{w_1}}, \mathbf{Q_{w_0}}) + \mathbf{K4_{33}}(\mathbf{Q_{w_2}}, \mathbf{Q_{w_4}}) \quad \text{(B2-21)}$$

$$\mathbf{A_{47}} = \mathbf{K4_{33}}(\mathbf{Q_{w_4}}, \mathbf{Q_{w_1}}) + \mathbf{K4_{33}}(\mathbf{Q_{w_1}}, \mathbf{Q_{w_4}}) - \mathbf{K4_{33}}(\mathbf{Q_{w_3}}, \mathbf{Q_{w_2}}) - \\ -\mathbf{K4_{33}}(\mathbf{Q_{w_2}}, \mathbf{Q_{w_3}}) + 2\,\mathbf{K4_{33}}(\mathbf{Q_{w_3}}, \mathbf{Q_{w_6}}) + \mathbf{K4_{33}}(\mathbf{Q_{w_2}}, \mathbf{Q_{w_0}}) + \\ +\mathbf{K4_{33}}(\mathbf{Q_{w_0}}, \mathbf{Q_{w_2}}) + 2\,\mathbf{K4_{33}}(\mathbf{Q_{w_6}}, \mathbf{Q_{w_3}}) \quad \text{(B2-22)}$$

$$\mathbf{A_{55}} = 2\,\mathbf{K4_{33}}(\mathbf{Q_{w_1}}, \mathbf{Q_{w_1}}) + 2\,\mathbf{K4_{33}}(\mathbf{Q_{w_5}}, \mathbf{Q_{w_5}}) - \mathbf{K4_{33}}(\mathbf{Q_{w_5}}, \mathbf{Q_{w_1}}) + \\ + \mathbf{K4_{33}}(\mathbf{Q_{w_3}}, \mathbf{Q_{w_3}}) + 2\,\mathbf{K4_{33}}(\mathbf{Q_{w_6}}, \mathbf{Q_{w_6}}) + 2\,\mathbf{K4_{33}}(\mathbf{Q_{w_2}}, \mathbf{Q_{w_2}}) + \\ + 3\,\mathbf{K4_{33}}(\mathbf{Q_{w_4}}, \mathbf{Q_{w_4}}) + \mathbf{K4_{33}}(\mathbf{Q_{w_6}}, \mathbf{Q_{w_2}}) + \mathbf{K4_{33}}(\mathbf{Q_{w_0}}, \mathbf{Q_{w_0}}) - \mathbf{K4_{33}}(\mathbf{Q_{w_1}}, \mathbf{Q_{w_5}}) + \\ + \mathbf{K4_{33}}(\mathbf{Q_{w_2}}, \mathbf{Q_{w_6}}) \tag{B2-23}$$

$$\mathbf{A_{56}} = \mathbf{K4_{33}}(\mathbf{Q_{w_2}}, \mathbf{Q_{w_3}}) + \mathbf{2}\,\mathbf{K4_{33}}(\mathbf{Q_{w_5}}, \mathbf{Q_{w_4}}) - \mathbf{K4_{33}}(\mathbf{Q_{w_2}}, \mathbf{Q_{w_0}}) - \\ - \mathbf{K4_{33}}(\mathbf{Q_{w_4}}, \mathbf{Q_{w_1}}) + 2\,\mathbf{K4_{33}}(\mathbf{Q_{w_4}}, \mathbf{Q_{w_5}}) - \mathbf{K4_{33}}(\mathbf{Q_{w_0}}, \mathbf{Q_{w_2}}) - \\ - \mathbf{K4_{33}}(\mathbf{Q_{w_1}}, \mathbf{Q_{w_4}}) + \mathbf{K4_{33}}(\mathbf{Q_{w_3}}, \mathbf{Q_{w_2}}) \tag{B2-24}$$

$$\mathbf{A_{57}} = \mathbf{K4_{33}}(\mathbf{Q_{w_1}}, \mathbf{Q_{w_3}}) + \mathbf{2}\,\mathbf{K4_{33}}(\mathbf{Q_{w_6}}, \mathbf{Q_{w_4}}) + \mathbf{K4_{33}}(\mathbf{Q_{w_2}}, \mathbf{Q_{w_4}}) + \\ + 2\,\mathbf{K4_{33}}(\mathbf{Q_{w_4}}, \mathbf{Q_{w_6}}) + \mathbf{K4_{33}}(\mathbf{Q_{w_0}}, \mathbf{Q_{w_1}}) + \mathbf{K4_{33}}(\mathbf{Q_{w_1}}, \mathbf{Q_{w_0}}) + \mathbf{K4_{33}}(\mathbf{Q_{w_4}}, \mathbf{Q_{w_2}}) + \\ + \mathbf{K4_{33}}(\mathbf{Q_{w_3}}, \mathbf{Q_{w_1}}) \tag{B2-25}$$

$$\mathbf{A_{66}} = 2\,\mathbf{K4_{33}}(\mathbf{Q_{w_1}}, \mathbf{Q_{w_1}}) + \mathbf{K4_{33}}(\mathbf{Q_{w_0}}, \mathbf{Q_{w_0}}) + 2\,\mathbf{K4_{33}}(\mathbf{Q_{w_3}}, \mathbf{Q_{w_3}}) + \\ + 2\,\mathbf{K4_{33}}(\mathbf{Q_{w_2}}, \mathbf{Q_{w_2}}) + 3\,\mathbf{K4_{33}}(\mathbf{Q_{w_5}}, \mathbf{Q_{w_5}}) + \mathbf{K4_{33}}(\mathbf{Q_{w_6}}, \mathbf{Q_{w_6}}) + 2\,\mathbf{K4_{33}}(\mathbf{Q_{w_4}}, \mathbf{Q_{w_4}}) \tag{B2-26}$$

$$\mathbf{A_{67}} = \mathbf{K4_{33}}(\mathbf{Q_{w_5}}, \mathbf{Q_{w_6}}) + \mathbf{K4_{33}}(\mathbf{Q_{w_6}}, \mathbf{Q_{w_5}}) \tag{B2-27}$$

$$\mathbf{A_{77}} = \mathbf{2}\,\mathbf{K4_{33}}(\mathbf{Q_{w_1}}, \mathbf{Q_{w_1}}) + \mathbf{K4_{33}}(\mathbf{Q_{w_5}}, \mathbf{Q_{w_5}}) + 2\,\mathbf{K4_{33}}(\mathbf{Q_{w_4}}, \mathbf{Q_{w_4}}) + \\ + 2\,\mathbf{K4_{33}}(\mathbf{Q_{w_3}}, \mathbf{Q_{w_3}}) + \mathbf{K4_{33}}(\mathbf{Q_{w_0}}, \mathbf{Q_{w_0}}) + 3\,\mathbf{K4_{33}}(\mathbf{Q_{w_6}}, \mathbf{Q_{w_6}}) + 2\,\mathbf{K4_{33}}(\mathbf{Q_{w_2}}, \mathbf{Q_{w_2}}) \tag{B2-28}$$

The matrices $\mathbf{K4_{33}}\left(\mathbf{Q_{w_i}}, \mathbf{Q_{w_j}}\right)$ are defined as in equation (A3) from Appendix A.

Appendix C

Here are presented the matrices $[\mathbb{M}_0]$, $[\mathbb{M}_1]$ and $[\mathbb{M}_2]$ which are used to define the stability of the periodic solution and were partially defined in equations (6. 47) – (6. 51). The non-written elements are zeros. Matrix $[\mathbb{MNL}_0]$ is symmetric and only half of it is presented.

$$[\mathbb{M}_2] = \begin{bmatrix} 1/2\,[\mathrm{I}] & & & & & & & & & & \\ & [\mathrm{I}] & & & & & & & & & \\ & & [\mathrm{I}] & & & & & & & & \\ & & & [\mathrm{I}] & & & & & & & \\ & & & & [\mathrm{I}] & & & & & & \\ & & & & & [\mathrm{I}] & & & & & \\ & & & & & & [\mathrm{I}] & & & & \\ & & & & & & & [\mathrm{I}] & & & \\ & & & & & & & & [\mathrm{I}] & & \\ & & & & & & & & & [\mathrm{I}] & \\ & & & & & & & & & & [\mathrm{I}] \end{bmatrix}$$

$$[\mathbb{M}_1] =$$

$$= \begin{bmatrix} 1/2\,\beta[\mathrm{I}] & & & & & & & & & & \\ & \beta[\mathrm{I}] & 2\omega[\mathrm{I}] & & & & & & & & \\ & -2\omega[\mathrm{I}] & \beta[\mathrm{I}] & & & & & & & & \\ & & & \beta[\mathrm{I}] & 4\omega[\mathrm{I}] & & & & & & \\ & & & -4\omega[\mathrm{I}] & \beta[\mathrm{I}] & & & & & & \\ & & & & & \beta[\mathrm{I}] & 6\omega[\mathrm{I}] & & & & \\ & & & & & -6\omega[\mathrm{I}] & \beta[\mathrm{I}] & & & & \\ & & & & & & & \beta[\mathrm{I}] & 8\omega[\mathrm{I}] & & \\ & & & & & & & -8\omega[\mathrm{I}] & \beta[\mathrm{I}] & & \\ & & & & & & & & & \beta[\mathrm{I}] & 10\omega[\mathrm{I}] \\ & & & & & & & & & -10\omega[\mathrm{I}] & \beta[\mathrm{I}] \\ & & & & & & & & & & \\ & & & & & & & & & & \beta[\mathrm{I}] & 12\omega[\mathrm{I}] \\ & & & & & & & & & & -12\omega[\mathrm{I}] & \beta[\mathrm{I}] \end{bmatrix}$$

$$[\mathbb{M}\mathbb{L}_0] =$$

$$= \begin{bmatrix}
1/2\left[\omega_j^2\right] & & & & & & & & & & & & \\
 & \left[\omega_j^2\right]-\omega^2[\mathrm{I}] & \beta[\mathrm{I}] & & & & & & & & & & \\
 & -\beta[\mathrm{I}] & \left[\omega_j^2\right]-\omega^2[\mathrm{I}] & & & & & & & & & & \\
 & & & \left[\omega_j^2\right]-4\omega^2[\mathrm{I}] & 2\beta[\mathrm{I}] & & & & & & & & \\
 & & & -2\beta[\mathrm{I}] & \left[\omega_j^2\right]-4\omega^2[\mathrm{I}] & & & & & & & & \\
 & & & & & \left[\omega_j^2\right]-9\omega^2[\mathrm{I}] & 3\beta[\mathrm{I}] & & & & & & \\
 & & & & & -3\beta[\mathrm{I}] & \left[\omega_j^2\right]-9\omega^2[\mathrm{I}] & & & & & & \\
 & & & & & & & \left[\omega_j^2\right]-16\omega^2[\mathrm{I}] & 4\beta[\mathrm{I}] & & & & \\
 & & & & & & & -4\beta[\mathrm{I}] & \left[\omega_j^2\right]-16\omega^2[\mathrm{I}] & & & & \\
 & & & & & & & & & \left[\omega_j^2\right]-25\omega^2[\mathrm{I}] & 5\beta[\mathrm{I}] & & \\
 & & & & & & & & & -5\beta[\mathrm{I}] & \left[\omega_j^2\right]-25\omega^2[\mathrm{I}] & & \\
 & & & & & & & & & & & \left[\omega_j^2\right]-36\omega^2[\mathrm{I}] & 6\beta[\mathrm{I}] \\
 & & & & & & & & & & & -6\beta[\mathrm{I}] & \left[\omega_j^2\right]-36\omega^2[\mathrm{I}]
\end{bmatrix}$$

$$[\mathbb{MNL}_0] = \begin{bmatrix}
\frac{1}{2}\mathbf{p}_0 & \frac{1}{2}\mathbf{p}_{c_1} & \frac{1}{2}\mathbf{p}_{s_1} & \frac{1}{2}\mathbf{p}_{c_2} & \frac{1}{2}\mathbf{p}_{s_2} & \frac{1}{2}\mathbf{p}_{c_3} & \frac{1}{2}\mathbf{p}_{s_3} & \frac{1}{2}\mathbf{p}_{c_4} & \frac{1}{2}\mathbf{p}_{s_4} & \frac{1}{2}\mathbf{p}_{c_5} & \frac{1}{2}\mathbf{p}_{s_5} & \frac{1}{2}\mathbf{p}_{c_6} & \frac{1}{2}\mathbf{p}_{s_6} \\
 & \mathbf{p}_0 + \frac{1}{2}\mathbf{p}_{s_1} & \frac{1}{2}\mathbf{p}_{s_2} & \frac{1}{2}\mathbf{p}_{c_1} + \frac{1}{2}\mathbf{p}_{c_3} & \frac{1}{2}\mathbf{p}_{s_1} + \frac{1}{2}\mathbf{p}_{s_3} & \frac{1}{2}\mathbf{p}_{c_2} + \frac{1}{2}\mathbf{p}_{c_4} & \frac{1}{2}\mathbf{p}_{s_2} + \frac{1}{2}\mathbf{p}_{s_4} & \frac{1}{2}\mathbf{p}_{c_3} + \frac{1}{2}\mathbf{p}_{c_5} & \frac{1}{2}\mathbf{p}_{s_3} + \frac{1}{2}\mathbf{p}_{s_5} & \frac{1}{2}\mathbf{p}_{c_4} + \frac{1}{2}\mathbf{p}_{c_6} & \frac{1}{2}\mathbf{p}_{s_4} + \frac{1}{2}\mathbf{p}_{s_6} & \frac{1}{2}\mathbf{p}_{c_5} & \frac{1}{2}\mathbf{p}_{s_5} \\
 & & \mathbf{p}_0 - \frac{1}{2}\mathbf{p}_{c_2} & -\frac{1}{2}\mathbf{p}_{s_1} + \frac{1}{2}\mathbf{p}_{s_3} & \frac{1}{2}\mathbf{p}_{c_1} - \frac{1}{2}\mathbf{p}_{c_3} & -\frac{1}{2}\mathbf{p}_{s_2} + \frac{1}{2}\mathbf{p}_{s_4} & \frac{1}{2}\mathbf{p}_{c_2} - \frac{1}{2}\mathbf{p}_{c_4} & -\frac{1}{2}\mathbf{p}_{s_3} + \frac{1}{2}\mathbf{p}_{s_5} & \frac{1}{2}\mathbf{p}_{c_3} - \frac{1}{2}\mathbf{p}_{c_5} & -\frac{1}{2}\mathbf{p}_{s_4} + \frac{1}{2}\mathbf{p}_{s_6} & \frac{1}{2}\mathbf{p}_{c_4} - \frac{1}{2}\mathbf{p}_{c_6} & -\frac{1}{2}\mathbf{p}_{s_5} & \frac{1}{2}\mathbf{p}_{c_5} \\
 & & & \mathbf{p}_0 + \frac{1}{2}\mathbf{p}_{c_4} & \frac{1}{2}\mathbf{p}_{s_4} & \frac{1}{2}\mathbf{p}_{c_1} + \frac{1}{2}\mathbf{p}_{c_5} & \frac{1}{2}\mathbf{p}_{s_1} + \frac{1}{2}\mathbf{p}_{s_5} & \frac{1}{2}\mathbf{p}_{c_2} + \frac{1}{2}\mathbf{p}_{c_6} & \frac{1}{2}\mathbf{p}_{s_2} + \frac{1}{2}\mathbf{p}_{12} & \frac{1}{2}\mathbf{p}_{c_3} & \frac{1}{2}\mathbf{p}_{s_3} & \frac{1}{2}\mathbf{p}_{c_4} & \frac{1}{2}\mathbf{p}_{s_4} \\
 & & & & \mathbf{p}_0 - \frac{1}{2}\mathbf{p}_{c_4} & -\frac{1}{2}\mathbf{p}_{s_1} + \frac{1}{2}\mathbf{p}_{s_5} & \frac{1}{2}\mathbf{p}_{c_1} - \frac{1}{2}\mathbf{p}_{c_5} & -\frac{1}{2}\mathbf{p}_{s_2} + \frac{1}{2}\mathbf{p}_{s_6} & \frac{1}{2}\mathbf{p}_{c_2} - \frac{1}{2}\mathbf{p}_{c_6} & -\frac{1}{2}\mathbf{p}_{s_3} & \frac{1}{2}\mathbf{p}_{c_3} & -\frac{1}{2}\mathbf{p}_{s_4} & \frac{1}{2}\mathbf{p}_{c_4} \\
 & & & & & \mathbf{p}_0 + \frac{1}{2}\mathbf{p}_{c_6} & \frac{1}{2}\mathbf{p}_{s_6} & \frac{1}{2}\mathbf{p}_{c_1} & \frac{1}{2}\mathbf{p}_{s_1} & \frac{1}{2}\mathbf{p}_{c_2} & \frac{1}{2}\mathbf{p}_{s_2} & \frac{1}{2}\mathbf{p}_{c_3} & \frac{1}{2}\mathbf{p}_{s_3} \\
 & & & & & & \mathbf{p}_0 - \frac{1}{2}\mathbf{p}_{c_6} & -\frac{1}{2}\mathbf{p}_{s_1} & \frac{1}{2}\mathbf{p}_{c_1} & -\frac{1}{2}\mathbf{p}_{s_2} & \frac{1}{2}\mathbf{p}_{c_2} & -\frac{1}{2}\mathbf{p}_{s_3} & \frac{1}{2}\mathbf{p}_{c_3} \\
 & & & & & & & \mathbf{p}_0 & \mathbf{0} & \frac{1}{2}\mathbf{p}_{c_1} & \frac{1}{2}\mathbf{p}_{s_1} & \frac{1}{2}\mathbf{p}_{c_2} & \frac{1}{2}\mathbf{p}_{s_2} \\
 & & & & \text{SYM} & & & & \mathbf{p}_0 & -\frac{1}{2}\mathbf{p}_{s_1} & \frac{1}{2}\mathbf{p}_{c_1} & \frac{1}{2}\mathbf{p}_{s_2} & \frac{1}{2}\mathbf{p}_{c_2} \\
 & & & & & & & & & \mathbf{p}_0 & \mathbf{0} & \frac{1}{2}\mathbf{p}_{c_1} & \frac{1}{2}\mathbf{p}_{s_1} \\
 & & & & & & & & & & \mathbf{p}_0 & -\frac{1}{2}\mathbf{p}_{s_1} & \frac{1}{2}\mathbf{p}_{c_1} \\
 & & & & & & & & & & & \mathbf{p}_0 & \mathbf{0} \\
 & & & & & & & & & & & & \mathbf{p}_0
\end{bmatrix}$$